**Technische Universität München**

Fakultät für Medizin

# *Myeloid cells require the ribonuclease Regnase-3 for immune homeostasis and balanced interferon responses in vivo*

*Matthias von Gamm*

Vollständiger Abdruck der von der Fakultät für Medizin der Technischen Universität München zur Erlangung des akademischen Grades eines

**Doktors der Naturwissenschaften (Dr. rer. nat.)**

genehmigten Dissertation.

| | |
|---|---|
| **Vorsitzender** | Prof. Dr. Heiko Lickert |
| **Prüfer der Dissertation** | 1. Prof. Dr. Matthias Tschöp |
| | 2. Prof. Dr. Martin Hrabě de Angelis |
| | 3. Prof. Dr. Ingo Bechmann |

Die Dissertation wurde am 04.07.2019 bei der Technischen Universität München eingereicht und durch die Fakultät für Medizin am 11.02.2020 angenommen.

## ABSTRACT

Pathogens and foreign or defective cellular components can initiate protective immune responses in mammals. Sufficient resolution of inflammation, however, is required to prevent tissue damage and autoimmunity. Several post-transcriptional factors, such as Regnase-1, protect the organism from such overwhelming immunity. Regnase-1 belongs to a family comprising 4 members and its capacity to bind and degrade RNA has been intensively studied *in vitro* and *in vivo*. However, only little is known about the biological roles of its family members.

Herein, physiological, cell-biological and molecular functions of Regnase-3 have been thoroughly studied. *Regnase-3* deficiency in mice provoked lymphadenopathy and shifted proportions of various immune cell populations under steady-state conditions. Hypertrophic lymph nodes contain elevated total cell counts of all major immune cell subsets, however B cells in particular were the most numerous. No indications for autoimmunity were found, yet the splenic architecture in *Regnase-3*-deficient mice is disrupted and the formation of germinal centers is impaired. Also the abundance of splenic marginal zone B cells, immature B cells and $CD8^+$ effector memory T cells are increased in the knockout. Further, Regnase-3 was identified to be pivotal for modulating interferon responses *in vivo*. Absence of Regnase-3 leads to elevated IFNγ serum levels and interferon response genes are upregulated locally in hypertrophic lymph nodes and systemically in tissues. In line with this observation, Regnase-3 but not its family member Regnase-1 is induced by a viral RNA mimic and IRF7 was found to be the responsible transcription factor. Conditional deletion of *Regnase-3* in B cells, in T cells and in myeloid cells demonstrated that hypertrophic lymph nodes were not caused by a B cell lymphoma, but instead were provoked by malfunctions in innate immune cells. Pathophysiological manifestations in mice with conditional *Regnase-3* deletion in macrophages and neutrophils resemble those observed in globally deficient mice, while no lymphadenopathy occurs in mice where *Regnase-3* is specifically absent in T or B cells. To reveal further insight into its molecular regulatory pathways, a novel Regnase-3-specific antibody was developed and identified counter expression of Regnase-3 and Regnase-1 in tissues and immune cells. Regnase-3 is particularly highly expressed in macrophages and dendritic cells, but also in some non-lymphoid tissues, suggesting a role in tissue-resident macrophages. Although both members share an overlapping set of molecular patterns, Regnase-3 responds uniquely in the interferon-signaling cascade. In contrast, Regnase-1 expression, but not that of Regnase-3, depends on the transcription factor NF-κB when macrophages were activated with lipopolysaccharide. Taken together, these data suggest that Regnase-3 evolved evolutionary as counterpart to Regnase-1 and has pivotal modulatory functions in macrophages for the control of interferon responses *in vivo*. Of note, a potential for therapeutic approaches involving Regnase-3 is further illustrated by published, genome-wide studies, in which polymorphisms in the human *Regnase-3* gene have been associated with Psoriasis susceptibility.

## KURZFASSUNG

Das Immunsystem bietet dem Organismus Schutz gegenüber pathogenen und anderen externen Einflüssen. Die vom Immunsystem hervorgerufenen Entzündungsreaktionen sind aber in ihrem Ausmaß limitiert, sodass Autoimmunerkrankungen und Gewebeschäden vermieden werden. Dazu tragen auch post-transkriptionelle Prozesse bei, wie etwa der Abbau von mRNA durch Regnase-1. Während für Regnase-1 die Relevanz im Immunsystem klar belegt ist, sind die biologischen Funktionen von drei weiteren Mitgliedern der Regnase-Familie weitestgehend unbekannt.

Diese Arbeit beschreibt nun physiologische, zellbiologische und molekulare Eigenschaften von Regnase-3. In der Maus verursacht die genetische Deaktivierung von Regnase-3 vergrößerte Lymphknoten sowie Verschiebungen diverser Immunzell-Populationen. Die hypertrophen Lymphknoten *Regnase-3*-defizienter Mäuse enthalten deutlich erhöhte Zellzahlen unterschiedlicher Leukozyten, wobei besonders B-Zellen dominieren. Auch die Milz ist morphologisch verändert, zeigt eine reduzierte Bildung von Keimzentren und enthält vermehrt B-Zellen der Randzone, unreife B-Zellen und $CD8^+$ Effektor T-Zellen. Zur Klärung von Ursachen, die zu diesen Symptomen führten, wurden Mausmodelle generiert, in denen *Regnase-3* spezifisch in T-Zellen, in B-Zellen und in myeloiden Zellen entfernt wurde. Während Tiere mit T- und B-Zell-spezifischem Knockout unauffällig blieben, zeigten Tiere mit einer Defizienz in neutrophilen Granulozyten und Makrophagen sehr ähnliche Symptome wie sie auch im vollständig defizienten Tier auftreten. Die Hypertrophie der Lymphknoten ist also nicht auf ein B-Zell Lymphom zurückzuführen, sondern vielmehr auf eine Fehlfunktion im angeborenen Immunsystem. Zudem wurde gezeigt, dass Regnase-3 entscheidend zur Modulation von Interferonen beiträgt: Zum einen zeigt der Knockout signifikant erhöhte IFNγ Serumkonzentrationen und damit einhergehend auch eine gesteigerte Aktivierung von Genen der Interferon-Signatur. Zum anderen vermittelt ein Analogon viraler RNA über den Transkriptionsfaktor IRF7 die Expression von *Regnase-3*, nicht aber die von *Regnase-1*. Zur weiteren Untersuchung von Regnase-3 auf molekularer Ebene wurde ein neuer, Regnase-3-spezifischer monoklonaler Antikörper generiert. Dieser half die entgegen gerichteten Expressionsprofile von Regnase-1 und -3 zu erkennen: Eine hohe Expression von Regnase-3 in Makrophagen und in nicht-lymphatischen Organen deutet auf eine mögliche Funktion in gewebsständigen Makrophagen hin. Zwar werden Regnase-1 und -3 auf molekularer Ebene teils ähnlich reguliert, dennoch reagiert nur Regnase-3 im Interferon-Weg auf artifizielle virale RNA. In Makrophagen hingegen, die mit Lipopolysaccharid aktiviert wurden, beruht die Transkription von *Regnase-1*, nicht aber die von *Regnase-3*, auf der NF-κB Signalkaskade. Zusammen ergibt dies ein Modell, in dem Regnase-3 eine modulierende Aufgabe in Makrophagen zukommt, die zur Regulation der Interferonantwort beiträgt. Ansatzpunkte für Regnase-3 als potentielles therapeutisches Zielmolekül liefern neben den dargelegten Daten auch publizierte Genom-weite Studien, die Polymorphismen im humanen *Regnase-3* Gen mit Psoriasis assoziierten.

# 1 Introduction

## 1.1 Immune responses in mammals

Mammals are under constant exposure to different pathogens, including bacteria, fungi, viruses and parasites such as protozoans and helminths (Murphy and Weaver, 2018). Beginning with the vaccination studies of Edward Jenner in the late 18$^{th}$ century, more than two centuries of research has provided knowledge on how the mammalian immune system protects the organism from pathogens, how it discriminates foreign components from self-antigens and how it destroys pathogens and damaged cells (Murphy and Weaver, 2018; Beutler, 2009a). Defects within the immune system may result in predispositions for infections, autoimmunity or cancer (Murphy and Weaver, 2018).
Due to differences in the recognizing mechanisms, its evolutionary development and the maturation of the involved cell types, the complex immune system is traditionally divided into two branches: the innate immune system and the adaptive or acquired immunity (Beutler, 2009b). Several immune cell types can be mainly assigned to one of the branches, nevertheless there is crucial overlap in their functions and the innate and adaptive immunity affect each other.

### 1.1.1 Cells of the immune system

All blood cells, including erythrocytes, platelets and the leukocytes of the immune system originate from hematopoietic stem cells (HSCs) in the bone marrow. Nevertheless, not all immune cells originate from the bone marrow: In particular some tissue-resident macrophage populations, such as brain microglia, mature during the embryonic development in yolk sac or fetal liver. These cells colonize the embryonic tissues and remain there as a lifelong self-renewing population (Murphy and Weaver, 2018).
HSCs are pluripotent cells and have the ability to differentiate into two main branches: the common myeloid progenitor cells and the common lymphocyte progenitor cells. The myeloid progenitor cells give rise to erythrocytes and megakaryocytes, which produce platelets as well as myeloblasts, the precursor of several leukocytes. The myeloblast can differentiate into key actors of the innate immune response: basophil, eosinophil and neutrophil granulocytes, monocytes, macrophages, myeloid dendritic cells and mast cells. The lymphoid progenitor cell can differentiate into B and T lymphocytes as well as into natural killer (NK) cells. T and B cells are the main actors in the acquired or adaptive immune response, leading to highly specified and long-term immunity (Murphy and Weaver, 2018). Main actors in the immune system with their allocation to the innate or adaptive branch are summarized in Figure 1 and selected cell types are described in more detail in the following chapters.

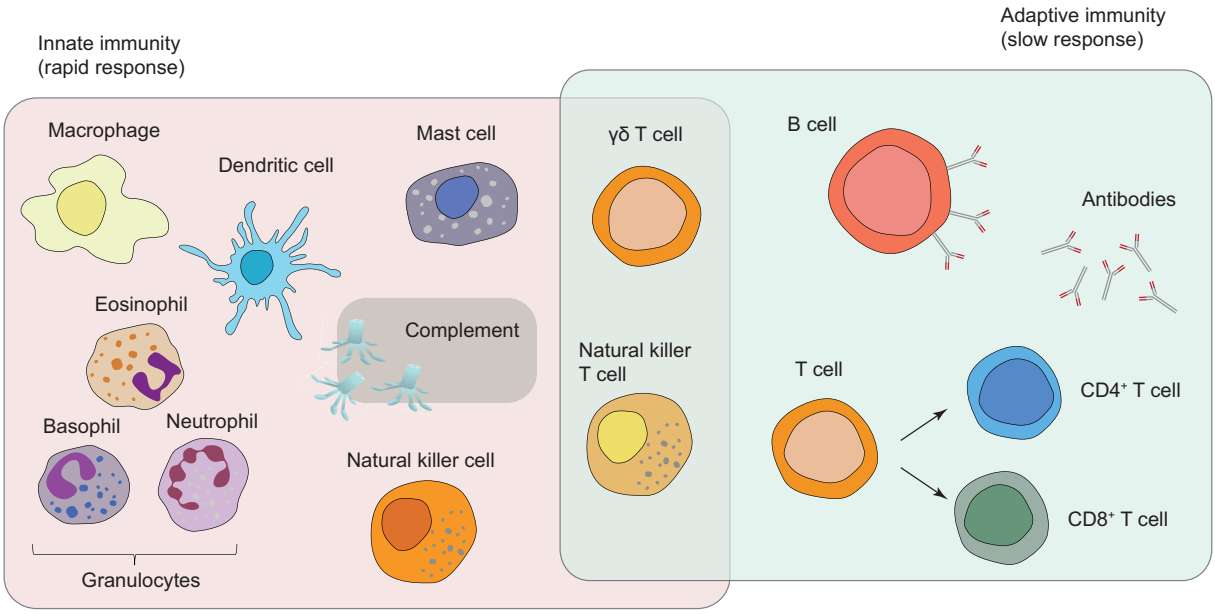


**Figure 1 Schematic representation of innate and adaptive immunity.**

*Left*: The innate immune system responds rapidly upon pathogens and forms a first line defence mechanism. It contains different immune cells including granulocytes (neutrophils, basophils and eosinophils), macrophages, dendritic cells, mast cells and natural killer cells, but also soluble components, such as complement factors. *Right*: The adaptive immune system reacts slowly, but is highly specific in its response mechanisms and allows forming an immunologic memory. It consists of B cells, $CD4^+$ and $CD8^+$ T lymphocytes and of soluble antibodies. Cytotoxic natural killer T cells and γδ T cells have characteristics of both innate and adaptive immunity. Figure adopted and modified from publication (Dranoff, 2004).

### 1.1.2 Innate immunity

The innate immune system is said to be rapid in its response, but rather unspecific (Beutler, 2009a). It is based on germline-encoded receptors that recognize features common to a variety of pathogens. Therefore, the innate immune response is able to respond within minutes after pathogen encounter and only if this first barrier of defense is not sufficient is an adaptive immune response required (Murphy and Weaver, 2018). The first barrier for pathogens is the epithelial surface. If this barrier is broken, the pathogen may replicate and this results in local or global infections. Replicating microorganisms are in most cases promptly recognized by the mononuclear phagocytes (macrophages), which reside in the respective tissues. Neutrophils are a second family of phagocytes, present as short-lived cells in the circulation, but not in normal, healthy tissues (Murphy and Weaver, 2018). The first cells to encounter incoming pathogens are macrophages in the submucosal tissue, followed by rapidly recruited neutrophils in large numbers. Macrophages and neutrophils are able to recognize pathogens with specific receptors, as described in a following section. Linking of several of those receptors by pathogens results in phagocytosis. Macrophages, with their ability to phagocyte, can directly fight pathogens, but also enable antigen presentation to T and B lymphocytes of the adaptive immune system (Murphy and Weaver, 2018). The cooperation of innate and adaptive immunity is also emphasized by the complement system: It includes an organized cluster of blood plasma proteins that interact

with pathogens and mark them to be removed by phagocytes. The opsonization of the complement system can be immunoglobulin-mediated, but can also be independent of the adaptive immune response (Murphy and Weaver, 2018).

### 1.1.3 Macrophages and their functions in the tissue

First descriptions of the macrophage system by Elie Metchnikoff go back to the late 19$^{th}$ century, but his assumption of macrophages being part of an endothelial cell population was later shown to be incorrect (Davies *et al.*, 2013). Macrophages belong to the mononuclear phagocyte system, together with monocytes and dendritic cells (DCs). Monocytes continuously leave the circulation, migrate into tissues and mature there to macrophages. The concept of how macrophages settle the tissues was later extended due to two further well-established observations: First, resident macrophages undergo self-renewal, and second, certain embryonic macrophage populations occur before circulating monocytes emerge. These observations were verified by fate-mapping experiments and led to the conclusion that a huge proportion of tissue residing macrophages do not originate from circulating monocytes, but from neonatal invaded and self-renewing adult macrophages (Varol *et al.*, 2015). Therefore, it is now believed that the majority of macrophages in the healthy tissues are of embryonic origin. While the second origin of macrophages, the infiltration and maturation of blood monocytes is associated with pathological and homeostatic inflammatory reactions (Varol *et al.*, 2015). One notable exception for this general rule is the gastrointestinal tract, which contains primarily bone marrow derived macrophages (Davies *et al.*, 2013). In contrast to macrophages with embryonic origin, monocyte-derived macrophages are believed to generally have a limited life span (Varol *et al.*, 2015).

Tissue-resident macrophages belong to a very heterogeneous group, including populations with highly varying morphologies as well as diverse functions and are often specialized for their tissue residence: Osteoclasts are responsible for bone resorption, lung alveolar macrophages recycle surfactant, microglia cells are indispensable for the central nervous system and splenic red-pulp macrophages obtain heme and iron from senescent erythrocytes (Okabe and Medzhitov, 2016). Thus, macrophages are not only important for pathogen defense, but also play a critical role in the maintenance of tissue homeostasis (Okabe and Medzhitov, 2016).

Macrophages are often broadly classified into two subsets: classically activated (M1-like) and alternatively activated cells (M2-like). The definition and nomenclature of M1 and M2 macrophages is closely connected to the discovery of T cell subsets, known as $T_h1$ and $T_h2$ $CD4^+$ T helper cells (Cherwinski *et al.*, 1987; Coffman, 2006). IFNγ is the major cytokine in the $T_h1$ response, while Interleukin (IL)-4 is central in the $T_h2$ response. First observations were made in different mouse strains, which respond by either intensive IFNγ production

(*C57BL/6* mice) or IL-4 production (Balb/C mice) in response to an infection with the intracellular protozoa *Leishmania* (Heinzel *et al.*, 1989). *C57BL/6* mice were more resistant than Balb/C, which was later explained by the IFNγ-mediated induction of NO production in macrophages, while IL-4-mediated induction of antibody secretion was ineffective against the intracellular infection (Heinzel *et al.*, 1989; Mills, 2015). M1-primed macrophages are characterized by prototypic pro-inflammatory responses and markers (Martinez and Gordon, 2014). The M1-priming stimuli include IFNγ and lipopolysaccharide (LPS) (often in combination) as well as Tumor necrosis factor α (TNFα). M2-primining stimuli originate from the initial IL-4 experiments, but were extended with respect to the ability of specific agonists to antagonize inflammatory responses (Martinez and Gordon, 2014). Thus, differently primed macrophages fulfill diverse tasks in a broad range from killing pathogens to repairing and healing of harmed tissues (Mills, 2015). While the priming of macrophages is caused by surrounding T cell derived cytokines, Charles Dudley Mills in particular emphasized that T cells do not induce the macrophage phenotype, but the opposite is true (Mills, 2015). Mills *et al.* demonstrated that macrophages, which were derived from NOD scid gamma mice that lack mature T and B cells could still produce high amounts of NO, if the mice were on *C57BL/6* background. In contrast, this was not the case if the NOD scid gamma mice were on Balb/C background and therefore it was concluded that the propensity of macrophages to get primed for inflammation (M1) or repair (M2), was independent of T or B cells (Mills *et al.*, 2000). Thus, they concluded that macrophages could drive the T cell reaction into the IFNγ-centered $T_h1$ or IL-4-centred $T_h2$ responses. In summary, macrophages are a very inhomogeneous as well as highly specialized population and fulfill a broad range of tasks, including phagocytosis, antigen presentation, inflammation, healing and several more.

### 1.1.4 Pattern recognition in innate immune cells

The essential attribute of the innate immune system is its capability to promptly recognize conserved structures, which are part of a broad spectrum of pathogens. These components are called pathogen-associated molecular patterns (PAMPs) and can be part of the bacterial cell membrane, such as lipopolysaccharides (LPS) or some nucleic acids. These patterns are recognized by specific receptors, the pattern recognition receptors (PRRs), which include Toll-like receptors (TLRs), retinoic acid-inducible gene (RIG)-I-like receptors (RLRs), nucleotide-binding oligomerization domain (NOD)-like receptors (NLRs), and C-type lectin receptors (CLRs) (Takeuchi and Akira, 2010). TLRs and CLRs are transmembrane proteins and detect extra cellular or phagocytized pathogenic material, while RLRs and NLRs sense cytosolic components (Baccala *et al.*, 2009). Major PRR families and their PAMPs are summarized in Figure 2.

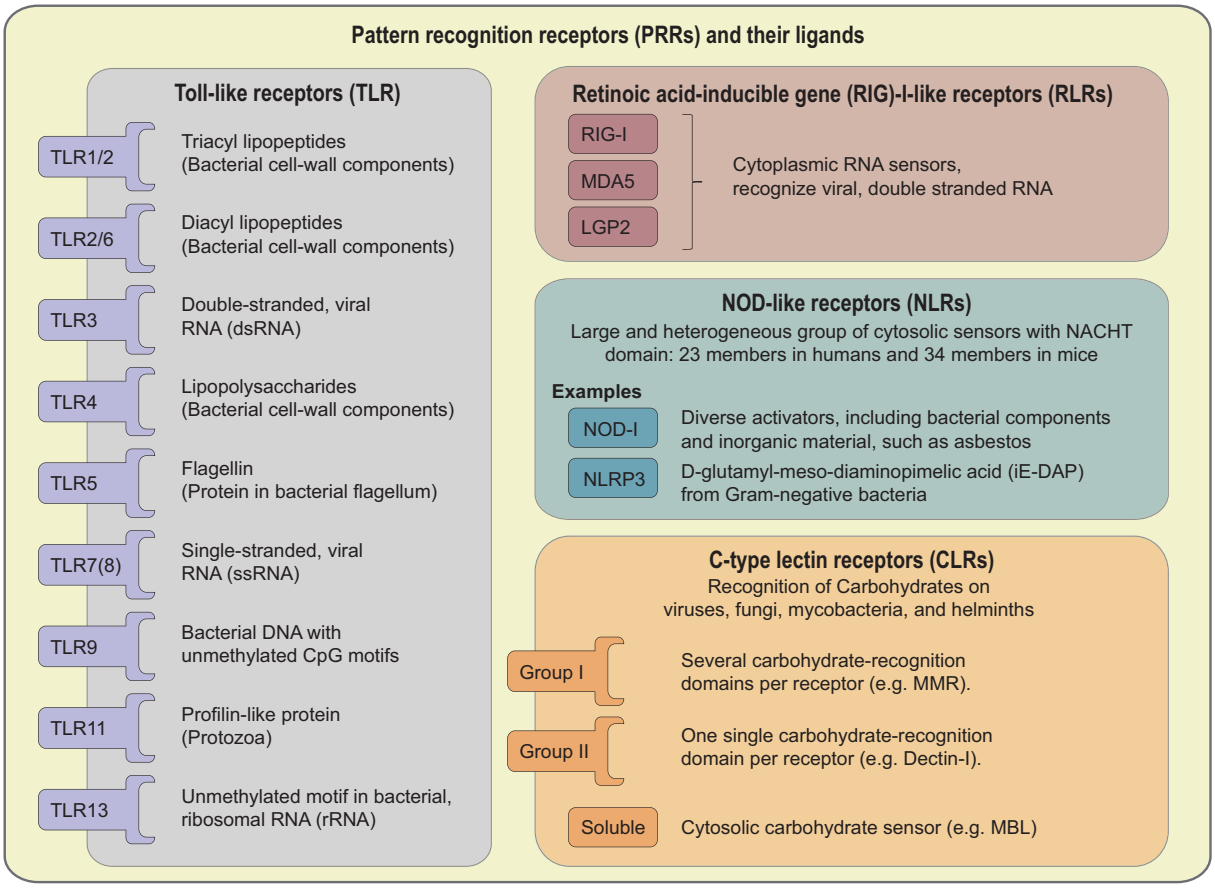


**Figure 2 Pattern recognition receptors in innate immune cells.**

Summary of major pattern recognition receptor (PRR) families and their pathogen-associated molecular patterns (PAMPS). Cell surface receptors are indicated with T-shaped symbols, cytosolic receptors are indicated with square-shaped symbols. For more detailed description see text and review (Takeuchi and Akira, 2010).

In 1997, Medzhitov *et al.* described that a human homologue of the Toll proteins previously identified in *drosophila melanogaster* signals via the nuclear factor κ-light-chain-enhancer of activated B-cells (NF-κB) pathway and induces an immune response with upregulated IL-1, IL-6 and IL-8 gene expression (Medzhitov *et al.*, 1997). Meanwhile, 13 mammalian TLRs have been identified, of which 10 TLRs (TLR1-10) are functional in humans and 11 in mice (TLR1-7, TLR9, TLR11-13) (Baccala *et al.*, 2009). TLRs are homo- or heterodimers of type I transmembrane glycoproteins with a ligand binding ectodomain and a cytoplasmic Toll- / interleukin-1 receptor (TIR) domain (Baccala *et al.*, 2009). TLR1–TLR2 hetero dimers recognize triacyl lipopeptides, TLR2–TLR6 hetero dimers sense diacyl lipopeptides, TLR3 binds double-stranded ribonucleic acids (RNA), TLR4 is activated by LPS, TLR5 recognizes flagellin, TLR7 and in human TLR8 sense single stranded RNA, TLR9 detects deoxyribonucleic acid (DNA) with unmethylated CpG motifs and TLR11 detects protozoan profilin-like protein (Baccala *et al.*, 2009). TLR13 recognizes an unmethylated motif within the large ribosomal subunit of bacterial RNA (23S rRNA) (Signorino *et al.*, 2014). On the cytosolic side of the TLR receptor, two main adaptors are recruited for signal transduction: myeloid differentiation factor 88 (MyD88) and TIR-domain-containing adapter-inducing

interferon-β (TRIF). MyD88 is fundamental for the downstream signaling of most TLRs, with the exception of TLR3, which depends on the adaptor protein TRIF. TLR4 activates both MyD88 as well as TRIF signaling (Takeuchi and Akira, 2010).

While most TLRs are located in the cell surface membrane, TLR3 and TLR7-9 are also found in the membrane of cytoplasmic vesicles. Highest TLR expression is found in classic innate immune cells, such as plasmacytoid dendritic cells, conventional dendritic cells and macrophages, but also on B cells and to a lower extent on most other cell types (Baccala *et al.*, 2009).

The family of RLRs includes three RNA helicases: Retinoic acid-inducible gene I (RIG-I), Melanoma differentiation-associated protein 5 (MDA5) and Laboratory of genetics and physiology 2 (LGP2). RLRs are cytoplasmic RNA sensors, which recognize viral dsRNA and are significantly upregulated in response to type I Interferon (IFN) stimulation or viral infection (Theofilopoulos *et al.*, 2011; Takeuchi and Akira, 2010).

NLRs are cytosolic sensors embracing a heterogeneous set of 23 members in humans and 34 in mice, which were classified into five subfamilies. Most complex and most important for inflammation are caspase activation and recruitment domain (CARD)-containing NLRCs and pyrin domain (PYD)-containing NLRPs (Baccala *et al.*, 2009). Common for NLRs is their central NOD and NACHT-associated domain (NAD), which facilitate nucleotide binding and self-oligomerization as well as a leucine rich repeat domain, used for PAMP recognition (Baccala *et al.*, 2009). The most studied NLRs are NOD1, which recognizes D-glutamyl-meso-diaminopimelic acid (iE-DAP) from the cell membrane of Gram-negative bacteria and NOD2, which senses muramyl dipeptide (MDP), present on Gram-positive and -negative bacteria (Baccala *et al.*, 2009). The most studied NLRP is NLRP3, which is not only activated by bacterial components, but also by inorganic material such as asbestos and can result in the formation of an inflammasome complex with consequent conversion of pro-interleukin (IL)-1β and pro-IL-18 to their mature forms (Baccala *et al.*, 2009).

CLRs are transmembrane receptor proteins with at least one carbohydrate-binding domain (Geijtenbeek and Gringhuis, 2009). CLRs are classified into group I CLRs, which belong to the mannose receptor family and the group II CLRs, which belong to the asialoglycoprotein receptor family. CLRs on dendritic cells recognize mannose, fucose and glucan carbohydrate structures, thereby identifying structures on viruses, fungi, mycobacteria, and helminths (Geijtenbeek and Gringhuis, 2009).

Together, these receptors provide a repertoire of congenital sensors, which can detect a variety of pathogens and initiate an immunologic response. Phagocytosis can be induced when several pattern recognition receptors are linked by pathogens. Molecular downstream activation pathways of two of those PRRs, the bacterial sensor TLR4 and the viral sensor TLR3 will be described in the following two chapters.

### 1.1.5 NF-κB signaling in innate immune cells

Signaling cascades via the transcription factor NF-κB are among the best-studied activation pathways in immune cells. NF-κB plays a vital role for maturation and function of innate as well as adaptive immune cells. Originally, NF-κB members were found to bind to enhancer sequences in genes of the immunoglobulin chains in B cells and were thus named nuclear factor of 'kappa-light-chain-enhancer' of activated B-cells (NF-κB) (Sen and Baltimore, 1986a; Sen and Baltimore, 1986b). Yet, its role is by far not restricted to B cells. A schematic and simplified view of lipopolysaccharide-mediated activation of the NF-κB pathway in macrophages is displayed in Figure 3.

There are five NF-κB members in humans of which p50 and p52 are expressed as p105 and p100 precursors, respectively. All five NF-κB members RelA (p65), RelB, c-Rel, p50 and p52 contain the Rel homology region that enables DNA-binding and the formation of homo- or hetero-dimers (Oeckinghaus and Ghosh, 2009). Under steady-state conditions, NF-κB members are bound to proteins of the inhibitory κB family (IκB), which prevents them from interacting with DNA (Napetschnig and Wu, 2013). Various receptors induce NF-κB downstream signaling, including Toll-like receptor 4 (TLR4), upon activation by its natural ligand lipopolysaccharides (LPS) from Gram-negative bacteria. Ligand binding induces TLR4 oligomerization and recruitment of downstream adaptors via its cytosolic Toll-interleukin-1 receptor (TIR) domain (Lu *et al.*, 2008). Among those adaptors are myeloid differentiation primary response gene 88 (MyD88) and TIR domain-containing adaptor protein (TIRAP), which further recruit and activate proteins of the IL-1 receptor-associated kinase (IRAK) and TNF receptor-associated factor (TRAF) families (Lu *et al.*, 2008). This protein complex further activates transforming growth factor-β-activated kinase 1 (TAK1), which in turn induces the IκB kinase (IKK) complex (Napetschnig and Wu, 2013; Lu *et al.*, 2008). The IKK complex is composed of the two catalytic subunits IKKα and IKKβ and the regulatory subunit NF-κB essential modulator (NEMO) (Napetschnig and Wu, 2013). IKK is responsible to phosphorylate IκB, which gets subsequently polyubiquitinated and degraded via the proteasome (Napetschnig and Wu, 2013). IκB degradation releases NF-κB members, which can then translocate to the nucleus. Here, NF-κB dimers bind to consensus motif sequences in the promoter regions of target genes and initiate transcription of pro-inflammatory factors, such as IL-6 (Oeckinghaus and Ghosh, 2009).

However the NF-κB signaling cascade varies with respect to prevalence for particular adaptor molecules and NF-κB dimers as it is rather ubiquitously expressed in various cell types and can also be activated by quite distinct receptors. However, activation via most pattern recognition receptors in macrophages relies on the adaptor protein MyD88. In macrophages, the activated NF-κB pathway then promotes a very strong cellular response that is primarily characterized by production of inflammatory cytokines.

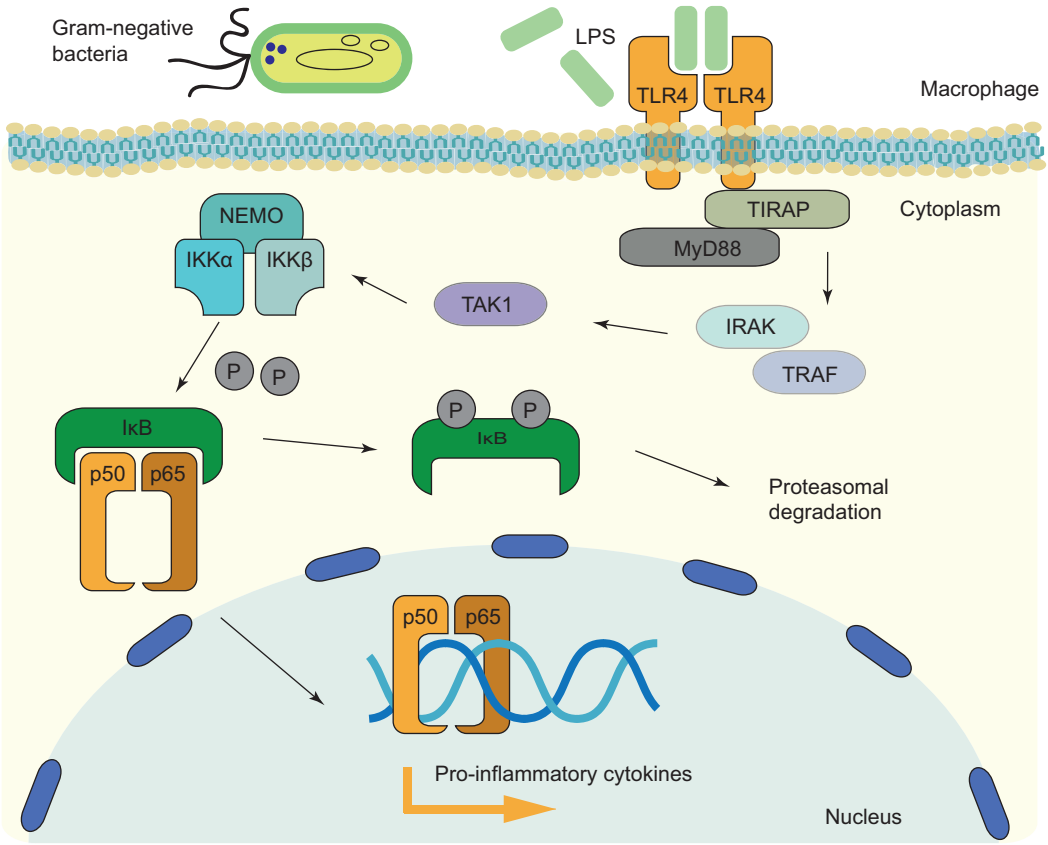


**Figure 3 Simplified, schematic representation for activation of the NF-κB signaling cascade in macrophages upon TLR4 induction.**

LPS from Gram-negative bacteria activate TLR4 on macrophages. Recruited TIR domain-containing adaptor proteins (e.g. TIRAP, MyD88) transfer the signal to TAK1, which activates the IKK complex. The IKK complex, composed of the catalytic IKKα and IKKβ subunits and the regulatory NEMO subunit, phosphorylate the inhibitory IκB proteins and release NF-κB units. NF-κB homo- and hetero-dimers, such as p50/p65 translocate to the nucleus and initiate transcription of pro-inflammatory factors. Figure adopted and modified from publications (Napetschnig and Wu, 2013; Chau *et al.*, 2008; Oeckinghaus and Ghosh, 2009).

### 1.1.6 Interferon signaling upon TLR3 induction

Viral infections can induce strong anti-viral immune-response programs, which are in particular characterized by high IFNα and IFNβ secretion (Chau *et al.*, 2008). Such an interferon response can be initiated when the Toll-like receptor 3 (TLR3) on macrophages recognizes viral, double stranded RNA. Subsequent signal transduction within this cascade is strongly amplified by transcription factors of the interferon regulatory factor (IRF) family (Takeuchi and Akira, 2010). A schematic, simplified overview of the TLR3-mediated signaling cascade is given in Figure 4.

When macrophages incorporate viral RNA via endosomes, TLR3 is activated and the signal is transferred to its cytosolic adaptor proteins. While various TLRs depend on the cytosolic adaptor protein MyD88, only TLR3 depends on TIR-domain-containing adapter-inducing interferon-β (TRIF) (Takeuchi and Akira, 2010). TRAF3 then connects the adaptor protein TRIF to a heterodimer kinase complex, composed of TRAF-family member-associated NF-κB activator (TANK)-binding kinase (TBK1) as well as IκB kinase ε (IKKε) (Chau *et al.*, 2008;

Honda and Taniguchi, 2006). The TBK1-IKKε complex in turn phosphorylates the transcription factors IRF3 and IRF7, resulting in their activation and translocation to the nucleus. Here, IRF3 and IRF7 homo- or hetero-dimers can bind to response elements in the promotor regions of its target genes, in particular type 1 interferons (Chau *et al.*, 2008). In short, activation of TLR3 with double stranded RNA leads to the recruitment of the TBK1-IKKε kinase complex via the adaptor proteins TRIF and TRAF3, which further results in phosphorylation and activation of the transcription factors IRF3 and IRF7. IRF3 and IRF7 dimers then bind to consensus motif sequences in promoter regions of respective response genes on the DNA. Pivotal response factors include the type 1 interferon genes, since secreted IFNα and IFNβ potentiates the anti-viral program by autocrine and paracrine feedback loops. The TLR3-mediated signaling cascade is further refined by activation of various adaptor proteins and substantial crosstalk to further signaling cascades is also possible (Chau *et al.*, 2008). This allows an orchestrated and potent program to eradicate virus-infected cells.

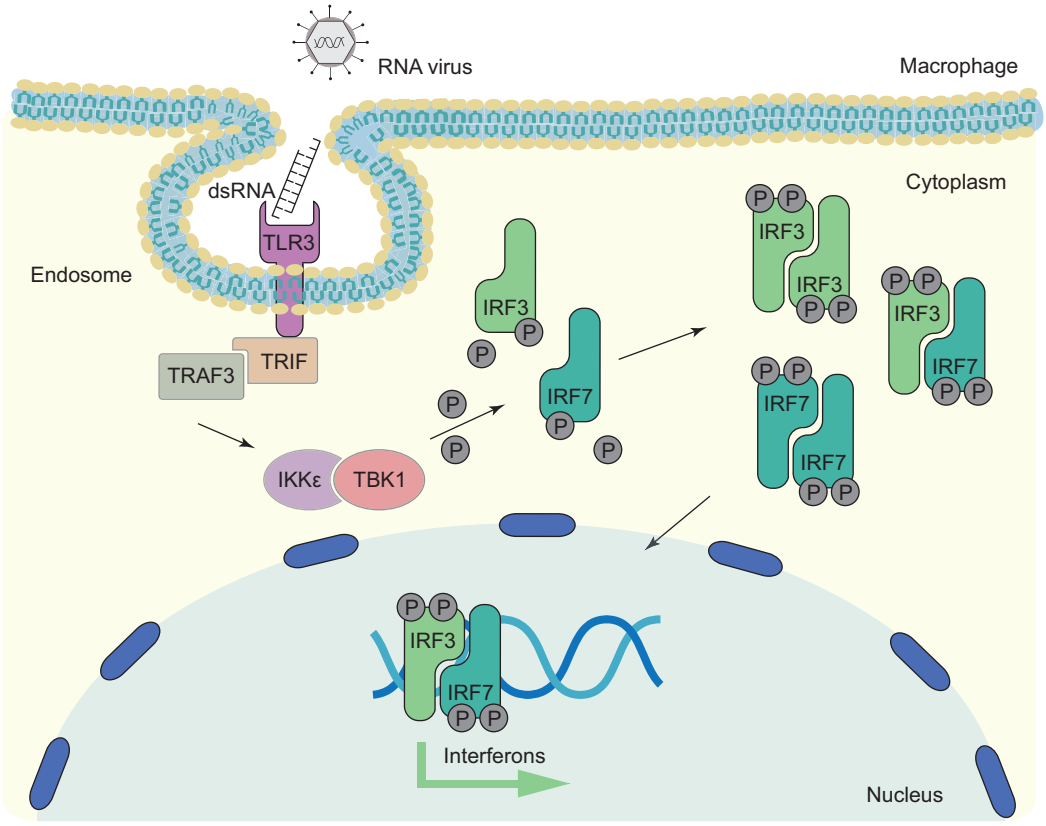


**Figure 4 Simplified, schematic representation for activation of the IRF signaling cascade in macrophages upon TLR3 induction.**

Viral, double stranded RNA (dsRNA) is taken up by macrophages via endocytosis. TLR3 is activated by dsRNA and the signal is transferred to its cytoplasmic domain, causing recruitment of adaptor proteins TRIF and TRAF3. Those adaptor proteins activate a kinase complex containing IKKε and TBK1, which in turn phosphorylate transcription factors IRF3 and IRF7. Phosphorylated IRF3 and IRF7 translocate to the nucleus and form homo- or hetero-dimers, which induce the expression of response genes, such as *Ifnα* and *Ifnβ*. Figure adopted and modified from publication (Honda and Taniguchi, 2006; Chau *et al.*, 2008).

### 1.1.7 The adaptive immune system

While the innate immune system has the benefit of being astonishingly fast in its defense mechanisms, it has poor quality in building an immunological memory and has low specificity. Lymphocytes of the adaptive immune system with their capacity to recognize specific antigens evolved and augmented the innate immune system (Murphy and Weaver, 2018). Both B and T cells produce highly selective receptors to recognize a diversity of pathogenic antigens. In B cells, these receptors are the immunoglobulins (Ig), which can be bound to the B cell surface as receptors, but which can also be secreted as antibodies from terminally differentiated B plasma cells (Murphy and Weaver, 2018). Starting from the common lymphoid progenitor in the bone marrow, B cell differentiate in multiple steps, mainly characterized by the arrangement of the gene loci of the immunoglobulin light and heavy chains. During this arrangement, variable ($V_H$), joining ($J_H$) and diversity ($D_H$) gene segments of the heavy chain and the $V_L$ and $J_L$ gene segments of the light chain are fused together, which forms a B cell repertoire with the potential to recognize $5x10^{13}$ different antigens (Pieper *et al.*, 2013). The maturation and development of B cells subsets is summarized in Figure 5.

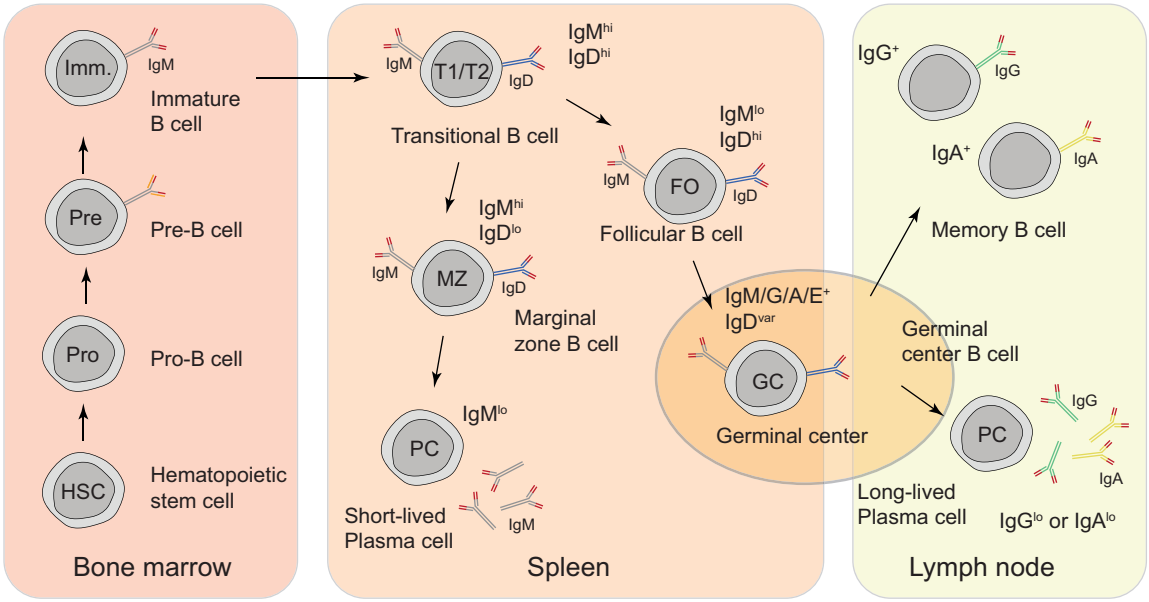


**Figure 5 B cell maturation and B cell subsets.**

Starting from hematopoietic stem cells in the bone marrow, B cells mature in several steps in which, variable ($V_H$), joining ($J_H$) and diversity ($D_H$) gene segments of the heavy chain and the $V_L$ and $J_L$ gene segments of the light chain are rearranged. Depending on this arrangement, three developmental stages are defined: 1) Pro-B cells: Rearrangement of the D and J segments of the heavy chain, followed by a rearrangement to the upstream V region. 2) Pre-B cell: Rearrangement of the V-J segments of the light chain. 3) Immature B cells: Expression of surface bound IgM receptors. Immature B cells leave the bone marrow and enter the spleen as transitional B cells, where they further mature into marginal zone (MZ) of follicular B cells, depending of the specificity of their receptors. Upon antigen encounter, MZ B cells develop into short-lived plasma cells. Follicular B cells mature in spleen or lymph nodes upon antigen encounter into germinal center B cells and further into memory B cells or antigen secreting long-lived plasma B cells. During maturation, B cells undergo class switching and the isotype of their surface receptors and/or secreted antibodies (IgM, IgD, IgG, IgA, IgE) change. Information and figure adopted and modified from publication (Pieper *et al.*, 2013; Murphy and Weaver, 2018).

In contrast to the B cell receptor, the antigen-specific T cell receptor (TCR) is always surface bound and can not be secreted. Also T cells originate from the bone marrow, but most of the relevant maturation steps occur in the thymus. T cell precursors migrate from the bone marrow to the thymus, where they mature and undergo a selection procedure, which allows the elimination of auto-reactive cells. T cells are characterized by their T cell receptor (TCR), which is composed in the vast majority as a heterodimer of one α– and one β-chain (α:β-T cells) or in a small minority as a heterodimer of one γ and one δ-chain (γ:δ-T cells). $CD4^+$ and $CD8^+$ peripheral T cells originate from α:β-T cells. Similar to B cells, also T cells go through a stepwise maturation procedure in which the V (variable), D (diversity), and/or J (joining) regions of the α– and β–chains are rearranged (Actor, 2014). These steps are characterized by the expression of specific markers, in particular the expression patterns of cluster of differentiation 3 (CD3) as well as the TCR co-receptors CD4 and CD8. Major differentiation stages are the CD4-CD8 double negative, CD4-CD8 double positive and CD4 or CD8 single positive stages (Murphy and Weaver, 2018). In the double negative stage, T cells are prepared for the T cell commitment and the arrangement of the β-chain occurs, in which first Dβ–Jβ segments and subsequently the Vβ-DJβ segments are fused. In the end of the double negative stage, the β-chain is fused to a surrogate α-chain, which forms a preliminary TCR that is selected for its reactivity. The next step is termed double positive stage, as one cell expresses both CD4 and CD8 receptors on its surface. The double positive stage is characterized by consecutive arrangements of the TCR α-chain. Within this procedure, the thymocytes are selected with respect to their capability and strength to recognize self-antigens. At the end of this positive selection CD4 single positive 'helper' T cells, CD8 positive 'killer' T cells as well as natural killer T (NK-T) cells are generated. $CD4^+$ cells are positively selected by interaction with Major histocompatibility complex (MHC)-II molecules, $CD8^+$ cells are positively selected with MHC-I molecules. Next, also the CD4 and CD8 single positive cells are further checked in a process called negative selection, orchestrated by specific thymic stromal cells. During the negative selection, T cells with strongly auto-reactive TCRs can be depleted by induction of apoptosis. Alternatively $CD4^+$ T cells can be programmed to get natural tolerogenic regulatory T cells ($nT_{reg}$) (Paul, 2013; Actor, 2014; Murphy and Weaver, 2018). As consequence of antigen encounter and priming, $CD4^+$ T cells differentiate into several subpopulations that secrete different cytokines. $T_h2$ cells typically secrete IL-4, IL-13, IL-5 and IL-6 and are effective against helminthic parasites. $T_h1$ cells mainly produce IFNγ and lymphotoxin and induce the cellular immune response, including induced microbial activity of macrophages and as a consequence an increased lysing efficiency. $T_h17$ cells are named due to their characteristic expression of IL-17 and are important to recruit granulocytes into infections with extracellular bacterial pathogens. $CD4^+$ follicular B helper T ($T_{fh}$) cells are a subset of T cells that enter B cell follicles and support B cells to differentiate into antibody producing cells, antibody class switching and affinity maturation. A small subset of naïve $CD4^+$ T cells may differentiate

into induced regulatory T cells ($iT_{reg}$). While $CD4^+$ T cells mediate several effector functions, by receptor-mediated direct binding to other immune cells as well as by cytokine release, $CD8^+$ T cells can also develop into cytotoxic T lymphocytes capable of lysing target cells (Paul, 2013).

### 1.1.8 Immune homeostasis

Immune defense mechanisms have evolved in all animals, which highlight the importance of immunity for survival in the animal kingdom. In particular the innate immune system responds immediately to pathogens and causes inflammation. The inflammatory reaction is initiated by sensing exogenous and endogenous danger signals caused by mechanically, chemically or biologically induced tissue damage. Consequently, effector cells are recruited and this leads to an orchestrated inflammatory response (Schett and Neurath, 2018). Inflammation ideally results in the elimination of the initial cause of injury, the clearance of necrotic cells and tissue repair (Netea *et al.*, 2017). The initiation of inflammation can be induced by sensing PAMPs, as described in a previous section, or by endogenous stress signals, also known as danger-associated molecular patterns. This induction leads to the release of proinflammatory cytokines and chemokines, such as TNFα and IL-1β, with their main function to activate and recruit further immune cells to the site of infection (Netea *et al.*, 2017). Nevertheless, prolonged or overwhelming and not sufficiently terminated inflammatory processes can cause a broad spectrum of diseases. This includes the septic shock, in which an inflammation is initiated by PAMPs. Unrestrained activation of the complement system and systemic coagulation due to sepsis may cause multi-organ failure, eventually even leading to death. (Schett and Neurath, 2018). But also autoimmune diseases, such as rheumatoid arthritis as well as inflammatory skin diseases like psoriasis are characterized by a prolonged inflammation. Moreover, asthmatic airway diseases, some forms of chronic kidney diseases, neurodegenerative diseases such as Alzheimer's and Parkinson's diseases as well as diabetes mellitus have been associated with malfunctions of the immune system (Netea *et al.*, 2017). Thus, it is highly important that the organism returns to the homeostatic steady state condition due to sufficient resolution of inflammation. This termination is regulated on several levels and is similarly orchestrated as the initiation of the inflammation. The resolution of inflammation includes neutrophil death and in macrophages a shift from pro-inflammatory towards pro-resolving functions (Schett and Neurath, 2018). These cellular changes are widely modulated by changes on the molecular level, such as post-transcriptional regulatory factors, which will be described in the following section.

## 1.2 RNA binding proteins as regulators in the immune response

### 1.2.1 Overview on RNA binding proteins in mice and humans

The resolution of inflammation is not only regulated on the cellular, but also on the subcellular basis, by inducing and limiting the secretion of different cytokines and other factors. Such changes in gene and protein expression can be modulated on multiple regulatory steps: 1) On the transcriptional level, e.g. by transcription factors. 2) On the post-transcriptional level, e.g. through splicing, export of the messenger RNA (mRNA) into the cytosol or mRNA stability 3) On the translational level at the ribosomes or by subcellular mRNA localization and 4) On the post-translational level, e.g. through protein modification and degradation (Piccirillo *et al.*, 2014). A schematic overview on cellular processes by which gene and protein expression is controlled is given in Figure 6.

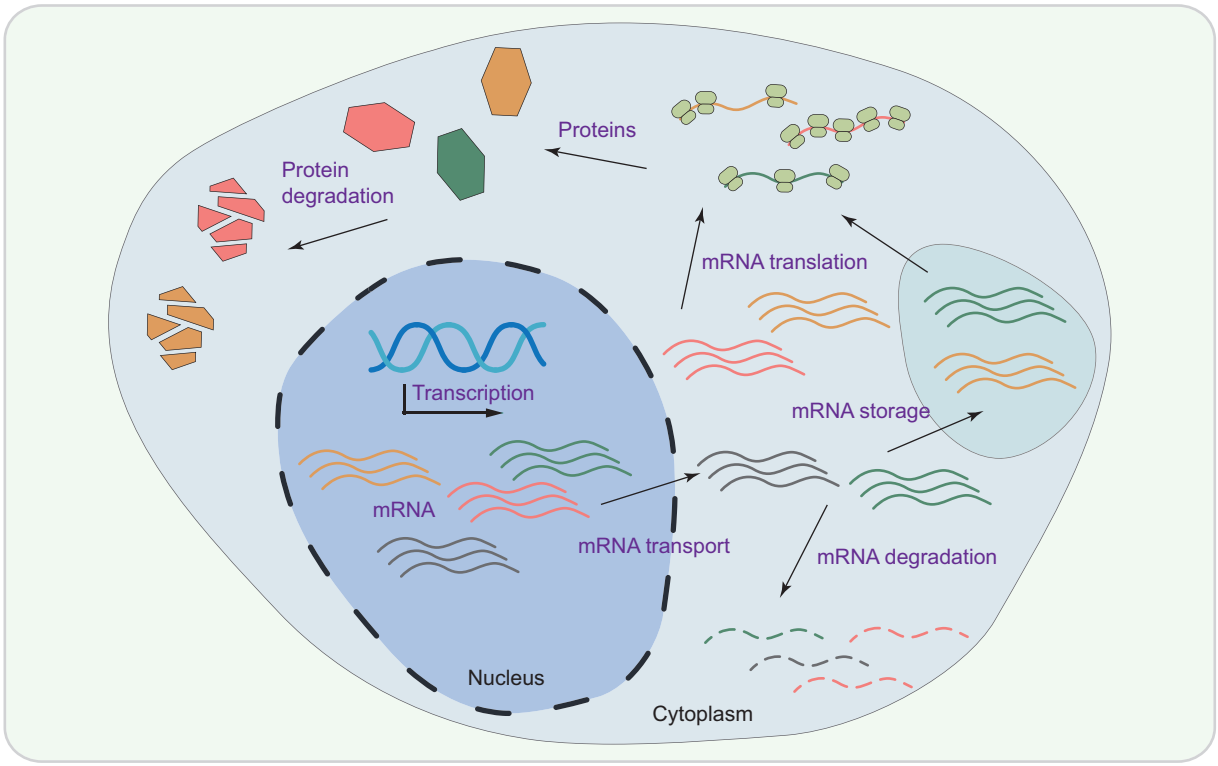


**Figure 6 Schematic representation of cellular regulation on the level of gene and protein expression.**

Transcription generates mRNA, which is transported to the cytoplasm where it might be first stored or directly used for protein translation. Both mRNA transcripts and proteins can be either stabilized or degraded over time. Information and figure adopted and modified from a publication (Piccirillo *et al.*, 2014).

Research over the past decades in particular unveiled the mandatory regulatory role of RNA binding proteins (RBPs) as modulators of the immune response. Gerstberger *et al.* bioinformatically analyzed the human genome and found 1542 out of 20500 protein-coding genes (7.5%) to be potential RBPs (Gerstberger *et al.*, 2014). Huge progress in the understanding of RBPs and their role *in vivo* has been generated by use of global approaches with next generation sequencing techniques, namely crosslinking and immunoprecipitation followed by sequencing (CLIP–seq) and RNA immunoprecipitation and sequencing (RIP-seq) (Gerstberger *et al.*, 2014). In these techniques, protein-RNA complexes are captured by immobilized antibodies and the bound RNA is determined by RNA sequencing analysis. Alternatively, RNA binding activity of proteins can be determined when RNA is extracted together with their bound proteins and protein identity is subsequently revealed by protein mass spectrometry.

Annotated RBPs may detect a variety of RNA molecules: 38% is predicted to bind messenger RNA (mRNA), 12% transfer RNA (tRNA) and 14% ribosomal RNA. Nevertheless, all kinds of RNA, including small nuclear RNAs (snRNAs), small nucleolarRNAs (snoRNAs), microRNAs (miRNAs), PIWI-interacting RNAs (piRNAs) and longnon-coding RNAs (lncRNAs) and even extrinsic RNA such as viral RNA might be targets of RBPs (Gerstberger *et al.*, 2014).

Although RBPs can target a variety of RNA species, RBPs are in particular mandatory for multiple steps during mRNA processing as summarized in Figure 7 and includes 5' capping, splicing, 3' polyadenylation, mRNA export, mRNA stability and protein translation (Sutherland *et al.*, 2015). Starting with the RNA transcription, all of these processes require specific RBPs. The pre-mRNA is first equipped with a 5' cap and introns are removed during splicing. The transcripts are then polyadenylated before exported into the cytoplasm. Here, RBPs may participate in the stabilization of the mRNA, but others promote RNA breakdown by removing 5' cap and 3' poly-(A)-tail and therefore provide access to exonucleases. In addition, some endonucleases may also degrade intact mRNA transcripts by binding to specific recognition motifs. Finally, also the translational machinery is composed of multiple RBPs, which allows translation of the polypeptide chains.

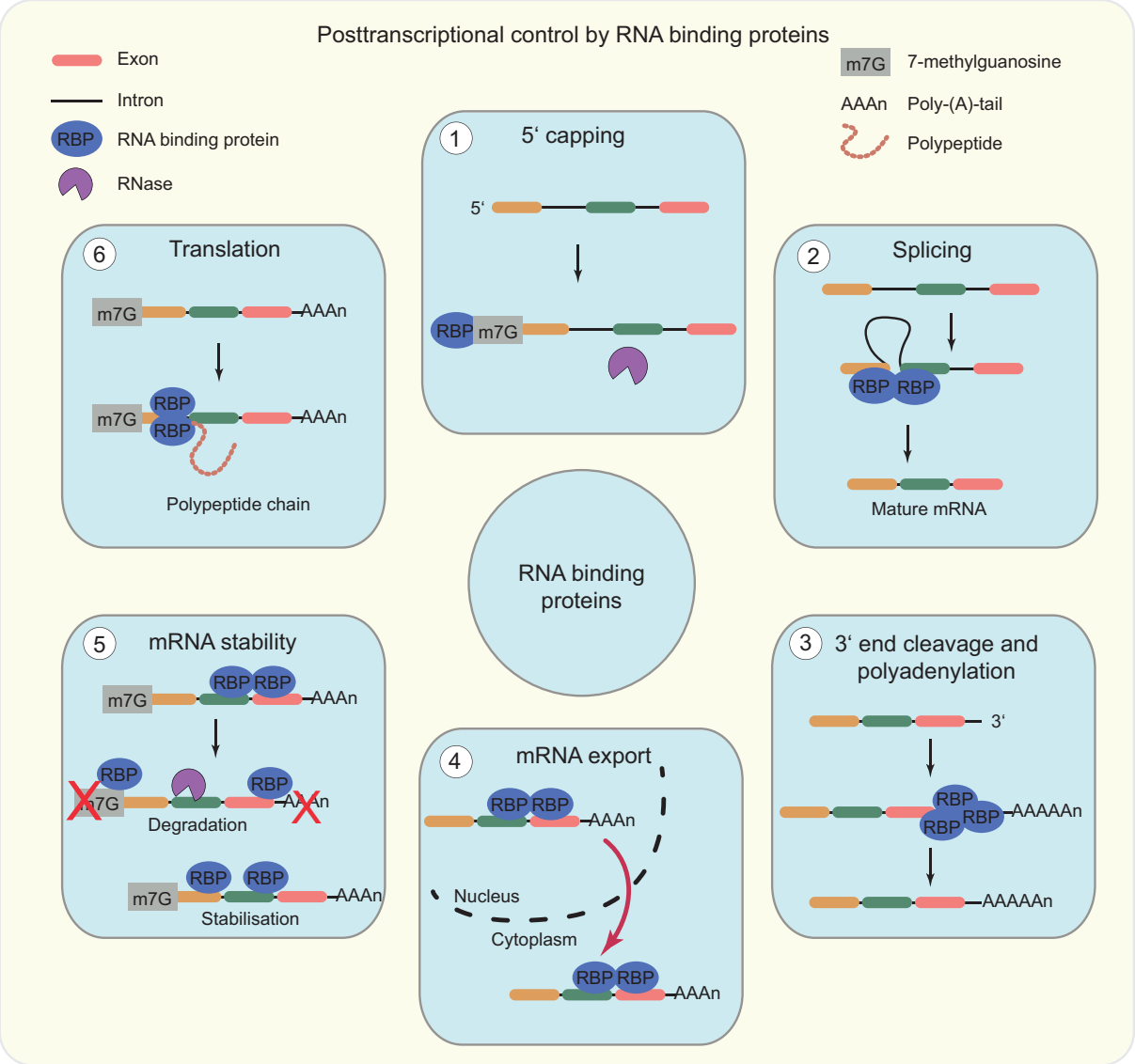


**Figure 7 RNA binding proteins regulate mechanisms of post-transcriptional control.**

1) The nascent mRNA precursor is protected from exoribonuclease activity through addition of 7-methylguanosine to the 5’ end of the pre-mRNA, mediated by the capping enzyme. 2) Subsequent removal of intronic regions within the pre-mRNA during splicing involves the macromolecular spliceosome complex. 3) Several RBPs mediate the cleavage of the nascent mRNA 3’-end and equip the mRNA with a protective poly-(A)-tail. 4) Also the transfer of the mRNA through the nuclear pore requires protein factors associated with the mRNA. 5) Transcripts can be either protected by RBPs, but mRNAs are also destabilized by proteins that remove the 5’ cap and the poly-(A)-tail or are directly digested by endonucleases 6) Also the translational machinery, which generates the polypeptide chain requires multiple RBPs. Figure adopted and modified from publication (Sutherland *et al.*, 2015).

### 1.2.2 CCCH zinc finger proteins in immunologic processes

The very inhomogeneous group of RBPs can be classified with respect to their RNA binding domains. The majority of the proteins that bind messenger RNA contain an RNA recognition motif, a K homology domain, a DEAD motif, a double-stranded RNA-binding motif or a zinc-finger domain (Gerstberger *et al.*, 2014).

Several RBPs with CCCH zinc-finger binding domain are indispensable for the immune system and are involved in maturation, activation and deactivation of immune cells. CCCH zinc finger proteins have at least one CCCH zinc finger domain, containing three cysteines and one histidine, which coordinate a single Zn ion. Currently, 59 and 57 CCCH zinc finger proteins have been identified in mice and humans, respectively. The functions of these CCCH zinc finger proteins are incompletely dissolved, but include diverse RNA regulatory functions, such as deadenylation (e.g. CNOT4), mRNA splicing (e.g. MBNL1), RNA helicase activity (e.g. HELZ), RNA export (e.g. NUPL2), mRNA decay (e.g. ZC3H2) and ribonuclease function (e.g. Regnase-1) (Fu and Blackshear, 2017).

In immune cells, the regulatory function of particularly three RBPs with zinc finger binding motif went into the focus of scientists: Tristetraprolin (TTP; encoded by *Zfp36*), Roquin-1 (encoded by *Rc3h1*) and Monocyte Chemotactic Protein-Induced Protein 1 (MCPIP1 or Regnase-1, encoded by *Zc3h12a*).

TTP can bind directly to AU-rich elements (ARE) in the 3' untranslated region (3'UTR) of *TNFα* mRNA and thereby provoke *TNFα* mRNA instability. AREs are specific nucleotide sequences of usually one or several AUUUA pentamer motives. These AREs are located in the 3'UTR of approximately 8% – 10% of all mRNAs, of which many are key regulatory proteins, such as cytokines, chemokines and growth factors (Lai *et al.*, 1990; Guo *et al.*, 2017). AREs recruit TPP in a complex with other RBPs, which provoke a breakdown of the protective 3' poly-(A)-tail (Guo *et al.*, 2017). Consequently, TTP deficiency causes severe pro-inflammatory symptoms in mice, which could be reduced, when mice were treated with anti-TNFα blocking antibodies (Taylor *et al.*, 1996; Carballo *et al.*, 1997).

The *in vivo* relevance of Roquin-1 has been first described by Vinuesa *et al.* in 2005, where mice with the *sanroque* mutation in the *Roquin* locus (*Roquin*$^{san/san}$) developed a severe T cell-mediated autoimmune phenotype (Vinuesa *et al.*, 2005). Both miRNA-dependent and miRNA-independent concepts have been described for Roquin-mediated RNA breakdown. (Yu *et al.*, 2007; Glasmacher *et al.*, 2010).

In summary, TTP and Roquin are among the best-studied CCCH-domain containing RBPs and have rather distinct molecular and cell-biological functions. Another CCCH-domain containing protein is Regnase-1, which attracted high attention by the scientific community during the last decade and will be described in detail in following sections.

### 1.2.3 The Regnase protein family

In 2006, Zhou *et al.* described a protein that was induced upon stimulation with monocyte chemotactic protein 1 (MCP1) in human peripheral blood monocytes and therefore named the protein monocyte chemotactic protein-induced protein (MCPIP) (Zhou *et al.*, 2006). However, this publication falsely predicted MCPIP to predominantly act as a transcription factor. Liang *et al.* shortly thereafter elucidated that MCPIP belongs to a small family with four members (MCPIP1-4), encoded by genes *Zc3h12a*, *Zc3h12b*, *Zc3h12c* and *Zc3h12d* and predicted an RNA binding activity for this family (Liang *et al.*, 2008). Profound research on family member MCPIP1 was then done by the group of Shizuo Akira, who renamed the protein Regnase-1 (regulatory RNase 1) with respect to its regulatory functions in immune cells (Akira, 2013).

To simplify the nomenclature, the four proteins of the family will be consistently named Regnase-1, -2, -3, and -4 within this publication. Family member Regnase-1 has been intensively studied over the past ten years and major outcomes regarding its *in vivo* as well as *in vitro* functions will be summarized in the following sections. In contrast, little is known about the family members Regnase-2, -3 and -4, which will be discussed in a separate section.

### 1.2.4 Molecular mechanisms of Regnase-1 in the decay of mRNA

*Regnase-1*$^{-/-}$ mice develop a severe form of autoimmunity and upon TLR activation *Regnase-1*-deficient macrophages secreted increased concentrations of IL-6 and IL-12p40, but not TNFα into the supernatant (Matsushita *et al.*, 2009). Increased cytokine secretion also correlated with their respective cellular mRNA expression levels. The analysis of mRNA degradation kinetics in stimulated macrophages and reporter gene assays with 3'UTR fragments of different mRNAs revealed that Regnase-1 is directly involved in 3'UTR-mediated mRNA degradation (Matsushita *et al.*, 2009). Of note, the specificity of Regnase-1 for particular mRNA targets that was observed in cultured cells was abolished in pure *in vitro* RNA degradation assays. An RNase domain in the protein sequence of Regnase-1 was predicted and indeed, a mutant form (D141N) failed to destabilize RNA containing the IL-6 3'UTR (Matsushita *et al.*, 2009).

In parallel, the group of Mingui Fu worked on the mechanism of Regnase-1-mediated immune cell regulation. In clear contrast to the previous mentioned publication, Liang *et al.* did not focus on an RNase activity of Regnase-1, but revealed a deubiquitinating enzyme domain in the Regnase-1 protein that is able to remove ubiquitin moieties from TNF receptor-associated factor (TRAF) 2, TRAF3 and TRAF6 and thereby modifies c-Jun N-terminal kinase (JNK) and NF-κB activity (Liang *et al.*, 2010). This suggests that Regnase-1 controls the immune reaction by multiple mechanisms. Nevertheless, the direct deubiquitinating activity of Regnase-1 was later questioned, when it has been shown, that

Regnase-1 interacts with the deubiquitinase USP10, which reduces NF-κB essential modulator (NEMO) ubiquitionation (Niu *et al.*, 2013; Takeuchi, 2018).

Regnase-1 and also its family members harbor a PilT N-terminus (PIN) like RNase domain, which is responsible for its endoribonuclease activity (Matsushita *et al.*, 2009; Takeuchi, 2018). Also the CCCH-type Zn finger domain is highly conserved among species and other Regnase family members and is, besides the PIN-like RNase domain, able to interact with RNA molecules (Yokogawa *et al.*, 2016). Regnase-1 preferentially binds to the 3'UTR at stem-loop structures that contain a pyrimidine-purine-pyrimidine loop, particularly UAU or UGU (Mino *et al.*, 2015).

In addition to these highly conserved domains, Regnase-1 possesses an N-terminal domain (NTD) and a C-terminal domain (CTD) with less homology to other Regnase family members. The NTD was shown to interact intramolecularly with the PIN-like RNase domain and thereby promote efficient cleavage of RNA molecules, while it does not increase RNA binding activity by Regnase-1 (Yokogawa *et al.*, 2016). The function of the CTD, however, remains elusive (Yokogawa *et al.*, 2016; Takeuchi, 2018).

Inconsistent data have been published regarding the localization as well as common or distinct features of the RNA binding proteins Regnase-1 and Roquin. While it seems uncontroversial that Regnase-1 and Roquin regulate an overlapping set of mRNAs via a common stem-loop structure, the distinct mechanisms are under debate. Mino *et al.* suggested that Regnase-1 localizes to the endoplasmatic reticulum and ribosomes, but not to P-bodies or stress granules, which are both subcellular vesicles involved in storage and/or degradation of RNA (Mino *et al.*, 2015). Consequently, Regnase-1 and Roquin would target the same mRNAs, but are separated by location, time of action and mechanism. Regnase-1 would then tend to control the early phase of inflammation, localize to the endosome and depend on the helicase activity of UPF1. Roquin would control a later phase of the immune response, localize to P-bodies and in contrast to Regnase-1, rely on the Ccr4/Caf1/not deadenylase complex (Mino *et al.*, 2015). However, Jeltsch *et al.* found functional cooperation of Roquin and Regnase-1 and suggested that Roquin provides RNA binding activity and target specificity, while Regnase-1 is indispensable for the nuclease activity (Jeltsch *et al.*, 2014).

Regnase-1 influences the protein expression of several factors, preferentially by repressing their mRNA transcripts. The group of Regnase-1 regulated proteins include IL-6, IL-12, CALCR, IL-2, CD44, ICOS, IL-1β and c-Rel, TNFR2, OX40, NFKBID, NFKBIZ, IRF4, ID1, MAFK, PTGS2, CXCL1, CXCL2, CXCL3, Bcl2L1, Bcl2A1, RelB, BIRC3, Bcl3, IER3 and Regnase-1 itself (Mao *et al.*, 2017). It was also suggested that Regnase-1 suppresses miRNA synthesis by cleavage of loops in precursor miRNAs and thus functionally counteracts Dicer-mediated miRNA generation (Suzuki *et al.*, 2011). However, it is under debate whether this mechanism contributes to a significant level to mRNA stability and consequently to the respective inflammatory response of the cell (Takeuchi, 2018).

### 1.2.5 Regulation of Regnase-1 expression

As described above, Regnase-1 is critical to regulate the expression of key mediators in the innate as well as adaptive immune response. Thus, it appears necessary that Regnase-1 protein expression is also under constant regulation. And indeed, Regnase-1 expression is controlled on several levels.

First, Regnase-1 is rapidly upregulated on the transcriptional level upon an immune response, such as TLR activation and is expressed in temporal correlation together with proinflammatory factors (Matsushita *et al.*, 2009). Relevant transcription factors for *Regnase-1* induction include NF-κB, ETS domain-containing protein (ELK1) and serum response factor (Kasza *et al.*, 2010; Iwasaki *et al.*, 2011).

Next, a direct and intrinsic feedback loop exists in form of a stem-loop structure within the 3'UTR of *Regnase-1* mRNA. This motif is recognized and degraded by the nuclease activity of the Regnase-1 protein itself and therefore destabilizes its own mRNA (Iwasaki *et al.*, 2011).

Further, Regnase-1 is also controlled post-translationaly. The protein sequence contains a DSGxxS motif that is recognized by the Inhibitor of κB (IκB) kinase (IKK) complex. The serine residues within this short sequence can be phosphorylated by the IKK complex, which results in polyubiquitination by the E3 ligase β-transducin repeat-containing protein (β-TrCP) complex and subsequent degradation via the proteasome (Iwasaki *et al.*, 2011). Degradation of Reganse-1 protein is significantly delayed in time and magnitude upon stimulation with the TLR4 agonist LPS, when cells are deficient for the *NF-κB* essential modulator (*NEMO*), which forms the IKK complex together with IKK-α and IKK-β (Iwasaki *et al.*, 2011). The activation of most TLRs and also other receptors initiate the induction of the NF-κB pathway including an activated IKK complex (see previous sections). Thus, the expression of several proinflammatory genes, such as IL-6 and IL-12, is transcriptionally upregulated by the transcription factor NF-κB. Simultaneously, Regnase-1 protein is degraded via the IKK complex and this consequently opens a time frame in which transcription and translation of proinflammatory genes is drastically increased, because their mRNA transcripts are not destabilized by Regnase-1 (Iwasaki *et al.*, 2011). This mechanism has been verified in macrophages for TLR and IL-1 receptor signaling and will be certainly a major regulatory pathway for Regnase-1 in innate immune cells.

In T cells, another counter regulatory mechanism for Regnase-1 via the Mucosa-associated lymphoid tissue lymphoma translocation protein 1 (MALT1) has been revealed. The paracaspase MALT1 is known to form a complex together with BCL10 and CARMA1/3 or CARD9, which enables the activation of the NF-κB pathway in response to stimulation via the T cell and B cell receptors (Jaworski and Thome, 2016). MALT1 contains a protease that is able to directly cleave and inactivate Regnase-1 protein at amino acid residue R111 (Uehata *et al.*, 2013). Similarly to IKK-mediated degradation of Regnase-1 in macrophages, MALT1 protease activity is freeing T cells from Regnase-1-mediated suppression by

Regnase-1. Likewise, paracaspase MALT1 also degrades the RNA binding protein Roquin and accordingly removes negative regulators of the T cell response (Jeltsch *et al.*, 2014).

### 1.2.6 Role of Regnase-1 as regulator in the immune response

The *in vivo* relevance of functional Regnase-1 protein was apparent, when Matsushita *et al.* published the phenotypic description of *Regnase-1*-deficient mice (Matsushita *et al.*, 2009). *Regnase-1*$^{-/-}$ mice developed anemia, splenomegaly, lymphadenopathy, immune cell infiltrations into the lung and most mice died within the first 12 weeks after birth. In addition, *Regnase-1*$^{-/-}$ mice had higher numbers of splenic effector/memory T cells, significantly increased serum immunoglobulin antibodies as well as anti-nuclear and anti-double-stranded DNA autoantibodies (Matsushita *et al.*, 2009). All these pathophysiological manifestations resemble a very severe form of autoimmunity. Liang *et al.* confirmed parts of the phenotypic evaluation with independently generated *Regnase-1*$^{-/-}$ mice (Liang *et al.*, 2010).

Though initial publications described the phenotype of globally *Regnase-1*-deficient mice, *in vitro* assays were centered on the molecular role of Regnase-1 within macrophages. Indeed, Regnase-1 has been demonstrated to be crucial for the degradation of IL-6 and IL-12 mRNA in macrophages in response to different TLR agonists (Matsushita *et al.*, 2009). Also *Regnase-1*-deficient bone marrow derived macrophages secreted higher amounts of TNFα, IL-1β, IL-6, and MCP-1 into the supernatant (Liang *et al.*, 2010). In line with this, *Regnase-1*-deficient mice were extremely susceptible to LPS induced septic shock with overwhelming TNFα secretion and severe lung injuries (Huang *et al.*, 2013). Nevertheless, Regnase-1 expression is not restricted to macrophages, but is also found in a variety of organs and cell types (Matsushita *et al.*, 2009; Iwasaki *et al.*, 2011; Takeuchi, 2018). Remarkably, mice with conditional deletion of *Regnase-1* in T cells (*Regnase-1*$^{fl/fl}$ +CD4-Cre mice) develop an autoimmune phenotype similar to that observed in globally *Regnase-1*-deficient mice (Uehata *et al.*, 2013). The survival rate was slightly prolonged in mice with Regnase-1 deletion in T cells compared to globally deficient mice, but similar deregulated T and B cell subsets as well as anti-nuclear antibodies were detected (Uehata *et al.*, 2013). In T cells, Regnase-1 is critical to degrade targets that are involved in T cell activation, including the NF-κB member c-Rel as well as ICOS, Ox40 and IL-2. Thus, Regnase-1 is believed to control T cell activation and their differentiation into effector T cells. (Uehata *et al.*, 2013; Li *et al.*, 2012). Therefore, autoimmunity in *Regnase-1*$^{-/-}$ mice is caused by a T cell-intrinsic function of Regnase-1 and not indirectly by malfunctioning macrophages.

A recent publication described mice with *Regnase-1* deletion in the myeloid linage using the LysM (lysozyme 2) Cre mice. Regnase-1 deletion in myeloid cells caused pathophysiologic manifestations that were weaker compared to that observed in the global knockout or conditional deletion in T cells. These mice did not die before 5 months of age and at 3 months of age, splenomegaly and lymphadenopathy was not observed (Li *et al.*, 2017).

However, *Regnase-1*$^{fl/fl}$ +LysM-Cre mice developed inflammatory symptoms at 5 months of age or older (Li *et al.*, 2017).

Taken together, Regnase-1 in T cells is indispensable to protect the organism from autoimmunity and myeloid Regnase-1 is crucial for controlled innate immune responses. The role of Regnase-1 in B cells still remains illusive (Takeuchi, 2018). Furthermore, considering its broad expression pattern in a variety of different cell types, Regnase-1 may be involved in many biological functions, not necessarily restricted to a role in the immune system.

### 1.2.7 Biological role of family members Regnase-2, -3 and -4

As mentioned, little data has been published to other Regnase family members, except Regnase-1. Very recently in April 2019, the first study that specifically covers Regnase-2 protein has been published (Wawro *et al.*, 2019). It has been shown that Regnase-2 shares some mRNA targets with Regnase-1 (Wawro *et al.*, 2019). However, *Regnase-2*-deficient mice are still not published. Compared to Regnase-2, Regnase-4 has been investigated in more detail. Also *Regnase-4*-deficient mice have been published under its alternative name transformed follicular lymphoma (TFL) (Minagawa *et al.*, 2014). In contrast to *Regnase-1*-deficient mice, *Regnase-4*$^{-/-}$ mice developed normally and had physiological lymphocyte profiles in blood, spleen and lymph nodes, indicating no interference with steady-state lymphopoiesis (Minagawa *et al.*, 2014). Nevertheless, Regnase-4 is upregulated in activated T cells and its deletion leads to increased T cell proliferation, enhanced secretion of cytokines IL-2, IL-6 and IL-10. In addition, 3'UTRs of *IL-2*, *IL-6*, *IL-10*, *TNFα* and *IL-17* mRNAs were recognized and degraded by Regnase-4 (Zhang *et al.*, 2015; Minagawa *et al.*, 2014). In line with this, *Regnase-4*-deficient mice were more susceptible to experimental autoimmune encephalitis (EAE) experiments and responded with severe paralysis and T cell infiltrations into the central nervous system (Minagawa *et al.*, 2014). Though Regnase-4 has been reported to also modify TLR responses in macrophages, *in vivo* data suggest that Regnase-4 mainly mediates immune signaling in lymphocytes (Huang *et al.*, 2012; Minagawa *et al.*, 2014).

At the beginning of our project, also for Regnase-3 only minimal data was available and the deficient mouse model was not published. However, Regnase-3 has been reported to attenuate the expression of TNFα-induced chemokines and adhesive molecules in human umbilical vein endothelial cells (HUVECs) and a suppressive function on NF-κB has been supposed (Liu *et al.*, 2013). Moreover, Regnase-3 might be involved in the suppression of cell migration and could therefore potentially inhibit tumor metastasis (Suk *et al.*, 2018). Regnase-3 also downregulated *Vimentim* mRNA, but this seemed to be not mediated by the RNase activity, as AU rich elements were not present in the *Vimentim* 3'UTR and an RNase inactive mutant had the same effect (Suk *et al.*, 2018).

Despite the poor data situation on other Regnase family members except Regase-1, it is still reasonable to compare the individual members with respect to their protein and RNA sequence. All family members share the PIN-like RNase domain as well as the CCCH Zn finger domain, but they differ in their C-terminal and N-terminal regions (Figure 8). Regnase-3 has the longest coding sequence with 903 amino acids (aa) and a calculated molecular weight of 101.1 kilodalton (kD), followed by Regnase-2 with 835 aa and 93.9 kD. Regnase-1 has 596 aa with 65.6 kD and Regnase-4 is the shortest member with a length of 533 aa and a predicted molecular weight of 59.1 kD.

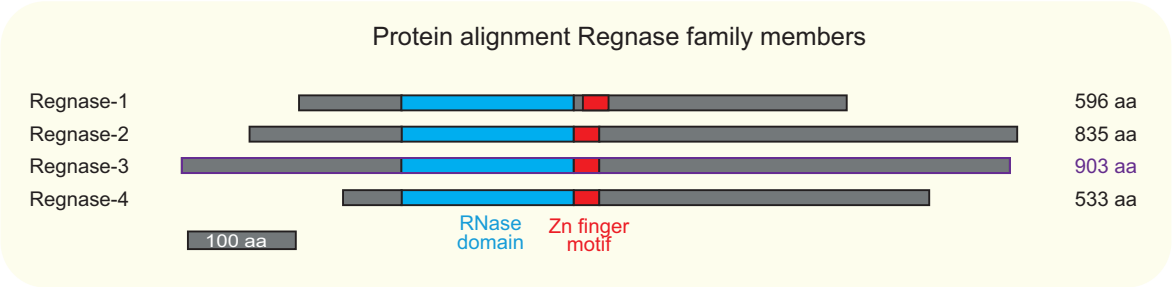


**Figure 8 Protein sequence alignment of Regnase family members.**

Sequences for protein alignment were obtained from NCBI: Regnase-1 (Zc3h12a) NP_694799.1; Regnase-2 (Zc3h12b) NP_001030079.2; Regnase-3 (Zc3h12c) NP_001156393.1; Regnase-4 (Zc3h12d) NP_766373.2. The PIN-like RNase domain is indicated in blue and the zinc finger motif is marked in red, aa = amino acids.

Also, a comparison of the respective 5' and 3'UTRs is useful, but may differ regarding different NCBI accession numbers for the same gene. *Regnase-3* has the longest 3'UTR with a remarkable length of 3.4 kilobases (kb), but no 5'UTR, while *Regnase-2* has a 5'UTR, but no 3'UTR. *Regnase-1* and *Regnase-4* have both a short 5'UTR and a longer 3'UTR (Figure 9).

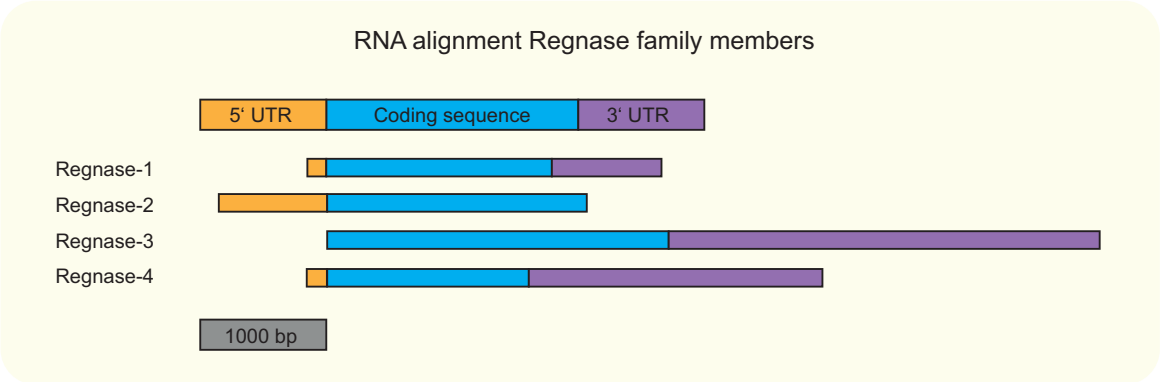


**Figure 9 RNA sequence alignment of Regnase family members.**

Sequences for RNA alignment were obtained from NCBI: *Regnase-1* (*Zc3h12a*) NM_153159_2; *Regnase-2* (*Zc3h12b*) NM_001034907.2; *Regnase-3* (*Zc3h12c*) NM_001162921.1; *Regnase-4* (*Zc3h12d*) NM_172785.3. Annotated 5'UTRs, coding sequences and 3'UTRs are indicated in orange, blue and violet, respectively. Size marker is indicated in grey.

## 1.3 Aim of the study

As described in previous sections, immune cell activation relies on dynamic changes in gene and protein expression. This regulation takes place on multiple levels, including the transcriptional, post-transcriptional, translational and post-translational levels. It is mandatory that the cellular immune response be gently orchestrated to allow sufficient eradication of pathogens on the one hand, but to avoid tissue damage and autoimmunity on the other. Only ten years ago, a novel family of four RNA binding proteins with CCCH Zn finger domain has been described. One of these proteins, the RNase Regnase-1 has been studied intensively since that. Emerging evidence suggests that Regnase-1 is a post-transcriptional regulator that protects the organism from autoimmunity and allows a sufficient termination of an immune response. Though the number of Regnase-1 centered publications on PubMed is permanently rising, little is known regarding the biological role of the other family members. Sequence alignment demonstrates that all members share the RNase domain as well as a CCCH Zn finger moiety, but differ in their C- and N-terminal regions. In addition, Regnase-3 has an exceptionally long 3'UTR, indicating high regulatory potential. Thus, we hypothesize that Regnase-3 is a crucial and unique mediator within immune cells and that loss of Regnase-3 results in altered immune responses *in vivo*. Therefore, we have obtained mice with 'knockout-first' conditional alleles for *Regnase-3* and aimed to analyze effects of the lost Regnase-3 function *in vivo*. Additionally we aimed to reveal molecular mechanisms for Regnase-3.

# 2 Results

## 2.1 Targeting strategy and mating schemes for *Regnase-3*$^{-/-}$ mice

We have obtained mice from EUCOMM with 'knockout-first allele' promoter-driven selection cassette for the *Zc3h12c* gene locus (*Zc3h12c*$^{tm2a(EUCOMM)Hmgu}$ mice) with the objective to analyze the role of Regnase-3 *in vivo* by investigating its loss in mice. These mice carry a targeting vector in which the intronic region between Exon 3 and Exon 4 contains a selection cassette that is flanked by flippase recognition target (FRT) sites, while Exon 4 is flanked by loxP sites. The splice acceptor (SA) together with a poly-A signal leads to a mature and spliced fusion mRNA in which Exon 3 is spliced in frame to the β-galactosidase (lacZ) gene sequence. Thus, a poly-A signal causes a premature transcriptional stop and consequently a truncated gene product (Figure 10 A). Crossbreeding with mice that express FLP recombinase under a general promotor such as ROSA26, generates mice that have lost major parts of the inserted cassette including the premature poly-A signal, but remain two loxP sites within the introns flanking Exon 4 (Figure 10 A, B). These *Regnase-3* floxed mice (*Regnase-3*$^{fl/fl}$) can be further crossbred with mice expressing a site-specific Cre recombinase to obtain conditional deletion of *Regnase-3* (Figure 10 B).

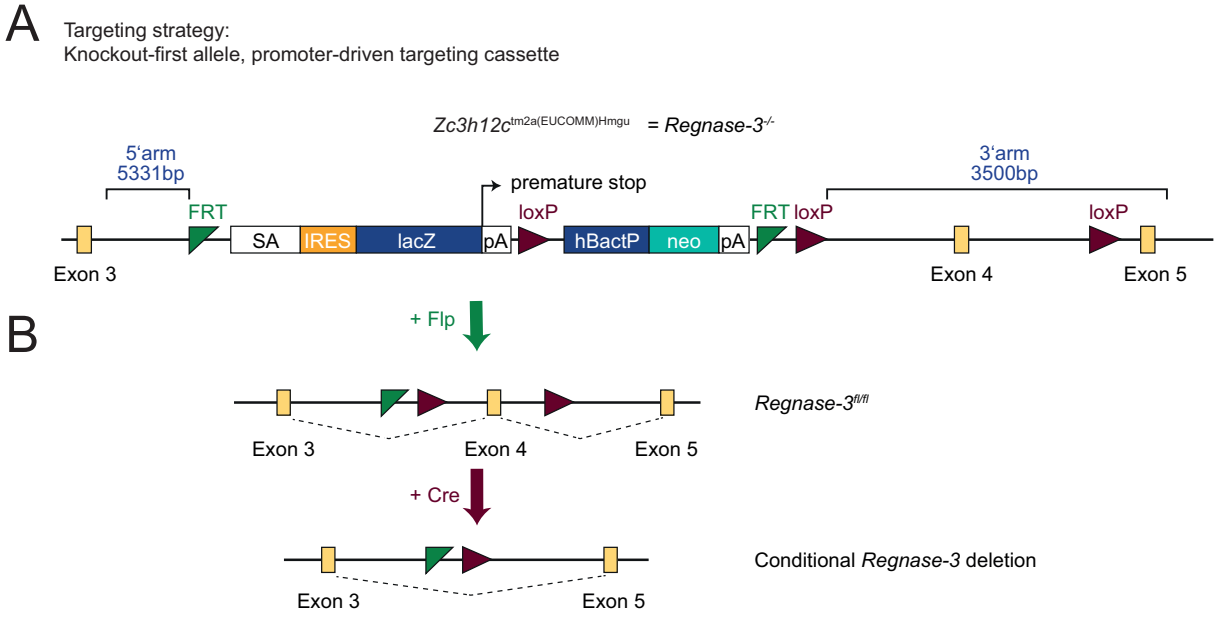


**Figure 10 Schematic representation of the targeting strategy for *Zc3h12c*$^{tm2a(EUCOMM)Hmgu}$ mice (von Gamm *et al.*, 2019).**

(A) Targeting vector for *Zc3h12c*$^{tm2a(EUCOMM)Hmgu}$ mice: FRT: FLP recombinase target, SA: splice acceptor, IRES: internal ribosome entry site, lacZ: β-galactosidase, pA: poly-A, hBactP: promoter, neo: neomycin resistance gene.
(B) Mating strategies with promotor driven FLP and Cre recombinases to first obtain mice with a floxed allele for the *Zc3h12c* (*Regnase-3*) gene and next mice with a conditional deletion of Exon 4 in the *Zc3h12c* gene locus.

The genetic modification in the mice was checked by polymerase chain reaction (PCR) with primers that detect the wildtype allele or the inserted targeting cassette (Figure 11 A). Sufficient gene disruption was further checked by reverse transcription (RT)-PCR of liver samples from wildtype and *Regnase-3*$^{-/-}$ mice. As expected, the *Regnase-3* mRNA levels were massively reduced in *Regnase-3*$^{-/-}$ mice relative to *Regnase-3*$^{+/+}$ mice without remarkable outliers throughout the analyzed individuals (Figure 11 B).

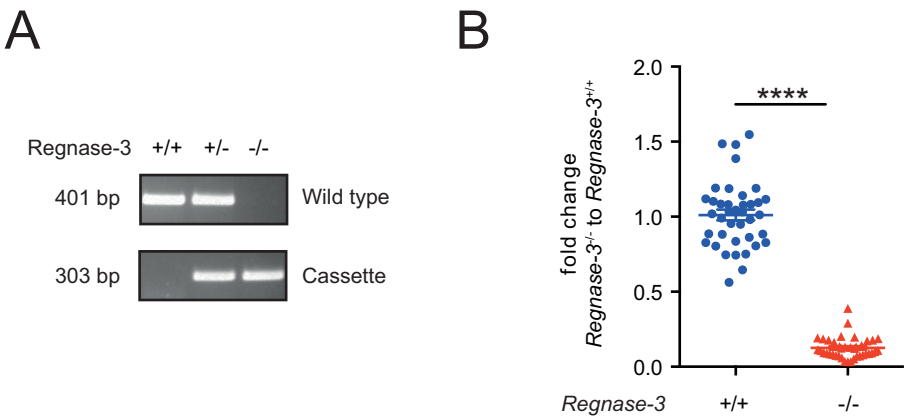


**Figure 11 Characterization of *Zc3h12c*$^{-/-}$ mice (*Zc3h12c*$^{tm2a(EUCOMM)Hmgu}$) (von Gamm *et al.*, 2019).**

(A) Genotyping PCR: Analysis of the mouse ear tissue with primers that identify the cassette in *Zc3h12c*$^{tm2a(EUCOMM)Hmgu}$ mice and primers that recognize the *Zc3h12c* wildtype allele.
(B) Quantitative RT-PCR for the *Zc3h12c* (*Regnase-3*) mRNA in liver tissues from *Regnase-3*$^{+/+}$ and *Regnase-3*$^{-/-}$ mice (n = 39/39). Calculated relative to the expression in *Regnase-3*$^{+/+}$ mice.
Data are represented as mean +/- SEM and were compared by the Mann-Whitney U test (**** p ≤0.0001).

## 2.2 *Regnase-3*$^{-/-}$ mice develop severe lymphadenopathy

### 2.2.1 Lymphadenopathy in *Regnase-3*$^{-/-}$ mice

First, 20 representative litters of *Regnase-3*-deficient mice from matings with two heterozygous parents were analyzed regarding basic statistical expectations. Wildtype, heterozygous and homozygous genotypes of the offspring were distributed according to expected Mendelian ratios (Figure 12 A). In addition, there was no trend towards a specific sex and also the average litter size of 6.95 is comparable to other *C57BL/6* strains (Figure 12 A). Keeping a cohort of 10 *Regnase-3*$^{+/+}$ and 10 *Regnase-3*$^{-/-}$ mice revealed long survival rates of at least 12 months (Figure 12 B). Of note, it has been reported that most *Regnase-1*-deficient mice died within 12 weeks of age (Matsushita *et al.*, 2009)

A

| | |
|---|---|
| Average litter size | 6.95 animals |
| *Regnase-3*$^{+/+}$ | 26.62 % |
| *Regnase-3*$^{-/-}$ | 25.90 % |
| *Regnase-3*$^{+/-}$ | 47.48 % |
| female | 52.52 % |
| male | 47.48 % |

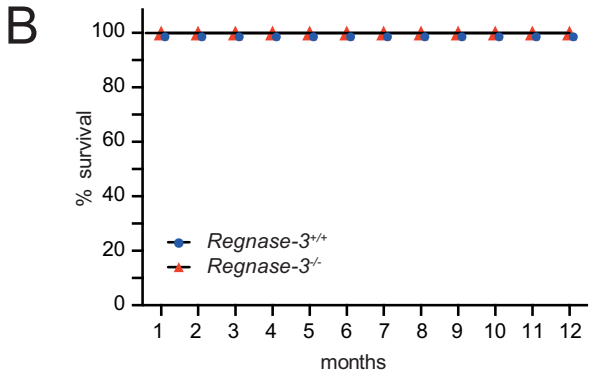


**Figure 12 Characterization of *Zc3h12c*$^{-/-}$ mice: Litters and survival rates (von Gamm *et al.*, 2019).**

(A) *Zc3h12c*$^{+/-}$ x *Zc3h12c*$^{+/-}$ matings (het x het): Average litter sizes and the distributions of sex and genotypes were calculated from 20 representative litters with a total of 139 mice.
(B) Survival rate of *Regnase-3*$^{+/+}$ and *Regnase-3*$^{-/-}$ mice (in a cohort of n = 10/10).

Despite unobtrusive survival rates, more than 80% of *Regnase-3*-deficient mice developed lymphadenopathy in form of hypertrophic lymph nodes after approximately 6 months of age (Figure 13 A). Some *Regnase-3*$^{-/-}$ mice, however, did not respond with lymphadenopathy and had lymph nodes of physiological size, even when analyzed at 5 months of age or older (Figure 13 B). Usually, superficial cervical, axillary, brachial or inguinal skin-draining lymph nodes were affected. Hypertrophic mesenteric lymph nodes, which are located close to the intestine were observed in only few individuals. In addition, only about 10% – 20% of mice with hypertrophic lymph nodes, had all skin-draining lymph nodes systemically affected. The majority (ca. 80% – 90%) of mice with lymphadenopathy had only one or several hypertrophic lymph nodes, while others remained of physiological size. Figure 13 C shows the photography of a *Regnase-3*$^{-/-}$ mouse, in which one of the two inguinal lymph nodes is several times increased in size, while the second one is of physiological size.

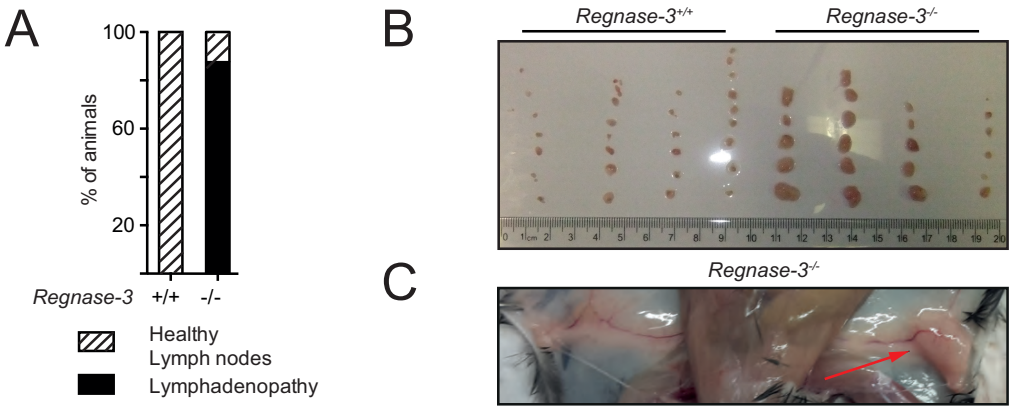


**Figure 13 Hypertrophic lymph nodes in *Regnase-3*$^{-/-}$ mice (von Gamm *et al.*, 2019).**

(A) Lymphadenopathy in *Regnase-3*-deficient mice: Proportion of mice with hypertrophic lymph nodes in a cohort of 24 *Regnase-3*$^{-/-}$ mice and 24 *Regnase-3*$^{+/+}$ littermate controls at 3 to 6.5 months of age.
(B) Photography of dissected skin draining lymph nodes (superficial cervical, axillary, brachial and inguinal) of *Regnase-3*$^{-/-}$ mice and their *Regnase-3*$^{+/+}$ littermate controls at 5 months of age (n = 4/4).
(C) Inguinal lymph nodes in a *Regnase-3*$^{-/-}$ mouse at 5 months of age (representative photography).

### 2.2.2 Pathophysiologic leukocyte distribution in lymph nodes

To further analyze pathophysiologic manifestations within hypertrophic lymph nodes of *Regnase-3*-deficient mice, histological sections were prepared and analyzed by immunohistochemistry. Markers for B cells (B220) and T cells (CD3) help to determine local distributions of these immune cells and thus to discriminate B cell follicles and T cell zones. *Regnase-3*$^{+/+}$ mice have a physiological distribution of T and B cells within their lymph nodes. B cell zones are located distal, close to the subcapsular sinus, while T cells are located central, in proximity to the medulla of the lymph nodes (Figure 14, upper panel). In contrast, lymph nodes of *Regnase-3*$^{-/-}$ mice were not only increased significantly in size, but in addition also their T cell follicles and B cell zones were massively disrupted (Figure 14, lower panel). Though B cells and T cells still partly cluster together, it is not possible to clearly define separate structures. Moreover, the proportion of B cells is clearly increased (Figure 14, B220 panel), which is further described in following sections. In contrast, the proportions of T cells were reduced (Figure 14, CD3 panel).

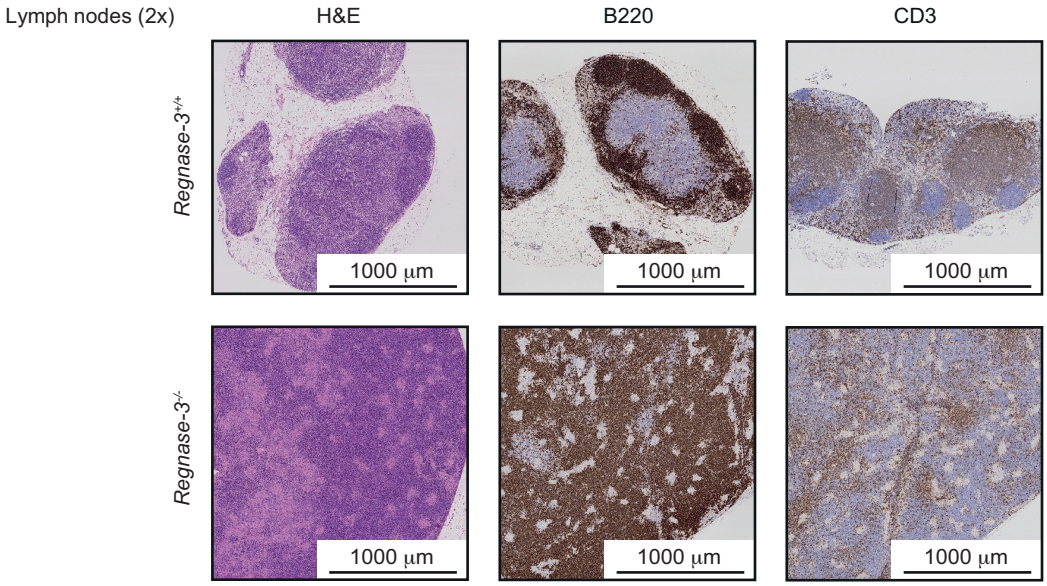


**Figure 14 Histological analyses of lymph nodes in *Regnase-3*$^{-/-}$ mice (von Gamm *et al.*, 2019).**

Tissue sections of lymph nodes from *Regnase-3*$^{-/-}$ mice with lymphadenopathy and their *Regnase-3*$^{+/+}$ littermate controls were stained with H&E or were immunohistochemically analyzed for B cells (B220), T cells (CD3) and macrophages (F4/80) (representative images from n = 3/3). 2 x magnification, bar 1000 µm.

We further analyzed macrophages within lymph nodes of *Regnase-3*$^{-/-}$ mice by immunohistochemistry for the pan-macrophage marker CD68. Visual comparison indicated a decreased proportion of macrophages within hypertrophic lymph nodes from *Regnase-3*$^{-/-}$ mice as compared to their *Regnase-3*$^{+/+}$ littermates (Figure 15 A, *left*). In contrast, lymph nodes of physiological size from the same *Regnase-3*-deficient mouse seemed to have similar numbers of macrophages as compared to wildtype mice (Figure 15 A, *right*). In order

to further validate this observation, histological sections were subjected to a computational analysis and a logarithm determined the amount of CD68 positively stained pixels. This evaluation confirmed the initiate presumption and showed that only hypertrophic lymph nodes in *Regnase-3*-deficient mice had significantly reduced proportions of $CD68^+$ macrophages (Figure 15 B). Moreover, it was observed that the remaining macrophages within hypertrophic lymph nodes were not as evenly distributed as in the wildtype, but were more centered to a specific area. This is in particular seen at 1x magnifications of the respective histological sections (Figure 15 C).

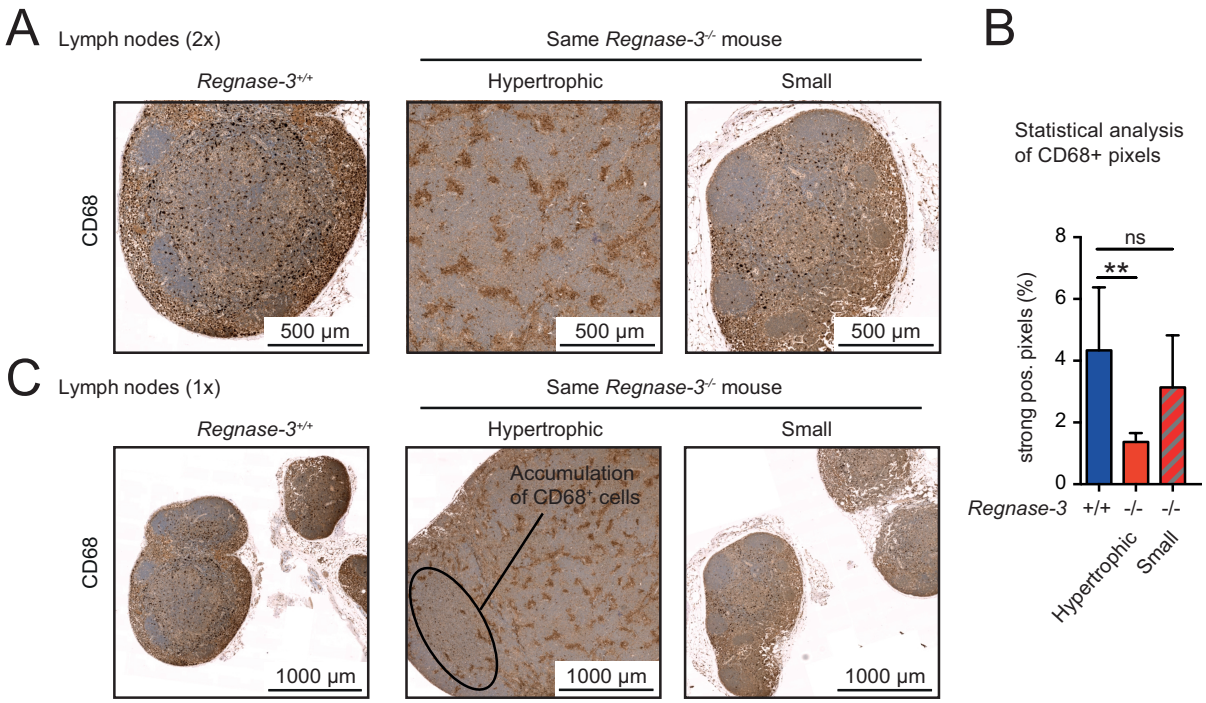


**Figure 15 Histological analysis of macrophages within lymph nodes of *Regnase-3*$^{-/-}$ mice (von Gamm *et al.*, 2019)**

(A) Skin-draining lymph nodes of *Regnase-3*$^{-/-}$ mice with lymphadenopathy and *Regnase-3*$^{+/+}$ littermate controls were stained for the macrophage marker CD68. 2x magnification. Representative images from n = 6/6 mice are shown.
(B) Computational analysis with the Definiens software to determine the amount of macrophages. Proportions for strong CD68 positive pixels in lymph node sections are displayed (n = 6/6).
(C) Representative images as in (A) at 1x magnification show macrophage distribution. Area with higher proportion of $CD68^+$ cells in hypertrophic lymph node of a *Regnase-3*$^{-/-}$ mouse is indicated.
Data are represented as mean +/- SEM and were compared by the Mann-Whitney U test (** $p \leqslant 0.01$, ns not significant).

In summary, immunohistochemistry in lymph nodes of *Regnase-3*$^{+/+}$ and *Regnase-3*$^{-/-}$ mice revealed that hypertrophic lymph nodes in *Regnase-3*$^{-/-}$ mice had disrupted T cell and B cell zones and a decreased proportion of macrophages.

Due to striking pathophysiological manifestations within lymph nodes of *Regnase-3*-deficient mice, major immune cell subsets were additionally analyzed by flow cytometry. B cells were determined with the pan-B cell marker CD19 and total T cells with the pan-T cell marker CD90. T cells were further specified regarding their main subsets, the

CD4⁺ and CD8⁺ T cells. Within hypertrophic lymph nodes of Regnase-3$^{-/-}$ mice, the proportion of B cells (CD19⁺) was increased while the proportion of T cells (CD90⁺) was decreased within both major subsets, the CD4⁺ and CD8⁺ T cells (Figure 16 A, B). This is in line with previous observations from immunohistochemical analyses. Cells from lymph nodes were also analyzed regarding their expression of CD11b, which is expressed on a variety of myeloid cells, such as neutrophils, monocytes and macrophages. The proportion of myeloid cells was increased in *Regnase-3*-deficient mice (Figure 16 B).

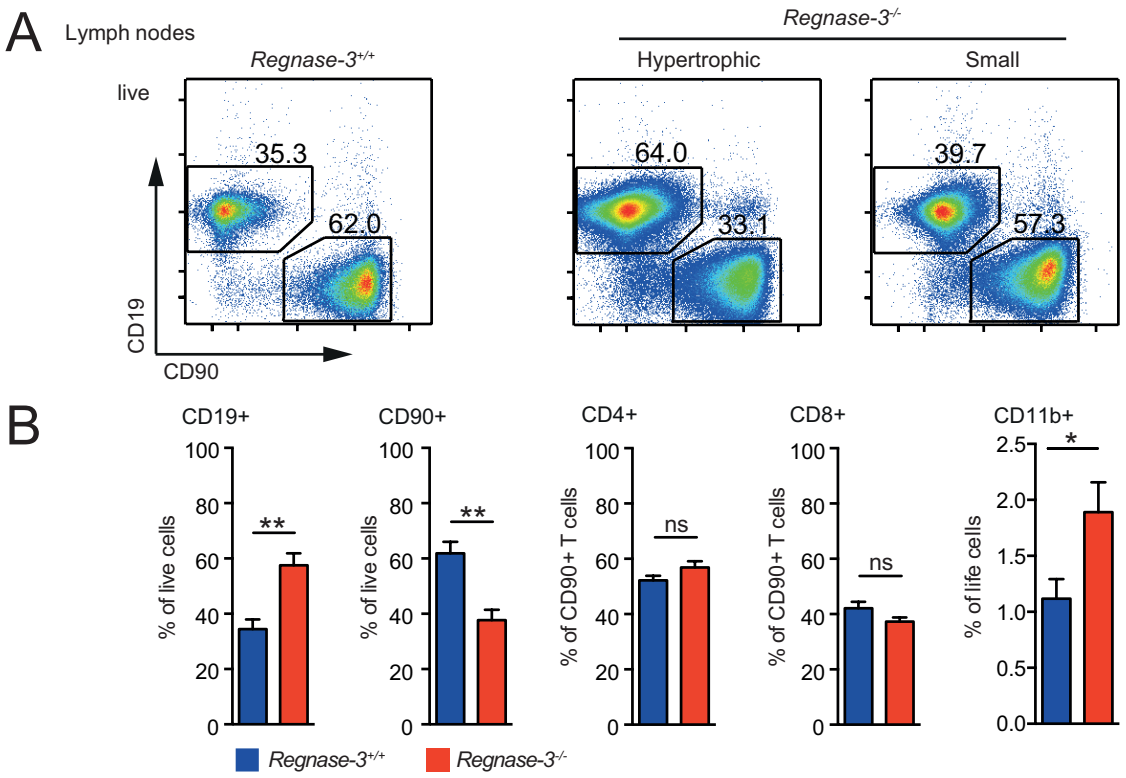


**Figure 16 Flow cytometric analysis in lymph nodes of *Regnase-3*$^{-/-}$ mice (von Gamm *et al.*, 2019).**

(A) Hypertrophic lymph nodes and lymph nodes of physiological size (small) of the same *Regnase-3*$^{-/-}$ mouse as well as from *Regnase-3*$^{+/+}$ littermates were stained for B cells (CD19⁺) and T cells (CD90⁺) and analyzed by flow cytometry. Representative blots of n = 6/6 mice at 6 months of age.
(B) Flow cytometry in lymph nodes: Proportions for B cells (CD19⁺), total T cells (CD90⁺), CD4⁺ and CD8⁺ T cells and myeloid cells (CD11b⁺) in hypertrophic lymph nodes of *Regnase-3*$^{-/-}$ mice and their *Regnase-3*$^{+/+}$ littermate controls at 6 months of age (n = 6/6).
Data are represented as mean +/- SEM and were compared by the Mann-Whitney U test (* $p \leq 0.05$, ** $p \leq 0.01$, ns = not significant).

Considering severely increased lymph nodes sizes in *Regnase-3*$^{-/-}$ mice, it was expected that also the total cell numbers of pooled skin draining lymph nodes were significantly increased in *Regnase-3*-deficient mice (Figure 17 A). While the total cell number of pooled skin draining lymph nodes in wildtype mice was in the range of approximately 10 to 20 million cells, *Regnase-3*-deficient mice could yield numbers of more than 300 million cells in some individuals (Figure 17 A). These highly increased total cell numbers also caused an increase even for total CD4⁺ and CD8⁺ T cell numbers, despite their reduced proportions (Figure 17 B).

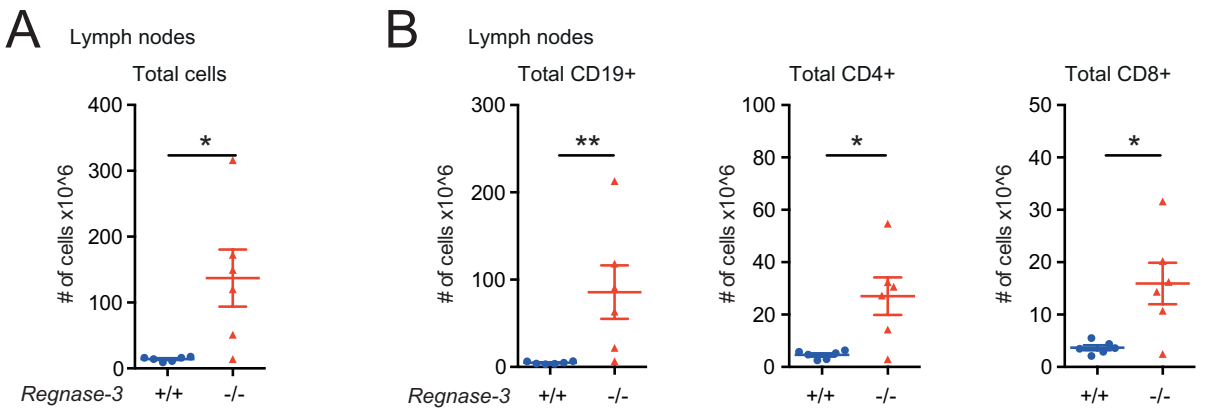


**Figure 17 Absolute cell numbers in lymph nodes of *Regnase-3*$^{-/-}$ mice (von Gamm *et al.*, 2019).**

(A) Total cell numbers in lymph nodes of *Regnase-3*$^{-/-}$ mice and their littermate controls at 6 months of age.
(B) Calculated total B cells (CD19$^{+}$), CD4$^{+}$ and CD8$^{+}$ T cells in lymph nodes of *Regnase-3*$^{-/-}$ mice and their littermate controls at 6 months of age. Numbers were calculated from the analysis of Figure 16 (n = 6/6).
Data are represented as mean +/- SEM and were compared by the Mann-Whitney U test (* $p \leq 0.05$, ** $p \leq 0.01$).

## 2.3 *Regnase-3*$^{-/-}$ mice do not develop systemic autoimmunity

Increased lymph nodes are one typical sign of systemic auto-immunity that is often associated with splenomegaly, such as in the Lupus-like auto-immunity in *MRL/lpr* mice, which have a specific mutation in the Fas gene or in *Roquin*$^{san/san}$ mice with a point mutation in the *Rc3h1* gene (Vinuesa *et al.*, 2005; Andrews *et al.*, 1978; Watanabe-Fukunaga *et al.*, 1992). Also *Regnase-1*-deficient mice develop auto-immunity with lymphadenopathy, splenomegaly, increased serum immunoglobulins and the formation of auto-reactive antibodies (Matsushita *et al.*, 2009). Thus, it was of high relevance to evaluate whether *Regnase-3*$^{-/-}$ mice suffer from auto-immunity. Serum antibody levels are frequently highly increased in different forms of systemic auto-immunity. In contrast, *Regnase-3*-deficient mice had only slightly increased concentrations of serum IgG, IgM or IgA (Figure 18).

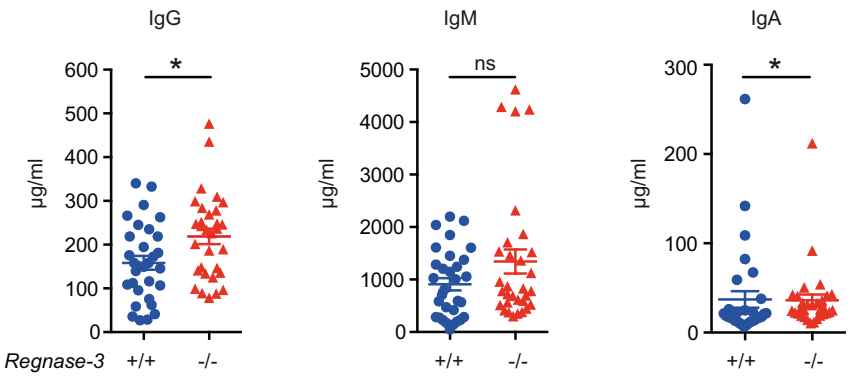


**Figure 18 Serum immunoglobulin titers in *Regnase-3*$^{-/-}$ mice (von Gamm *et al.*, 2019).**

Total IgG, IgM and IgA serum immunoglobulin titers in *Regnase-3*$^{-/-}$ mice and their *Regnase-3*$^{+/+}$ littermate controls, determined by ELISA (n = 31/31).
Data are represented as mean +/- SEM and were compared by the Mann-Whitney U test (* $p \leq 0.05$, ns = not significant).

Though *Regnase-3*$^{-/-}$ mice had lymphadenopathy, they did not develop splenomegaly, in particular also not in mice with significantly increased skin draining lymph nodes (Figure 19 A). Total splenic cell counts in *Regnase-3*$^{-/-}$ mice were rather decreased than increased and both major immune cell subsets in the spleen, the T and B cells were reduced in numbers (Figure 19 B).

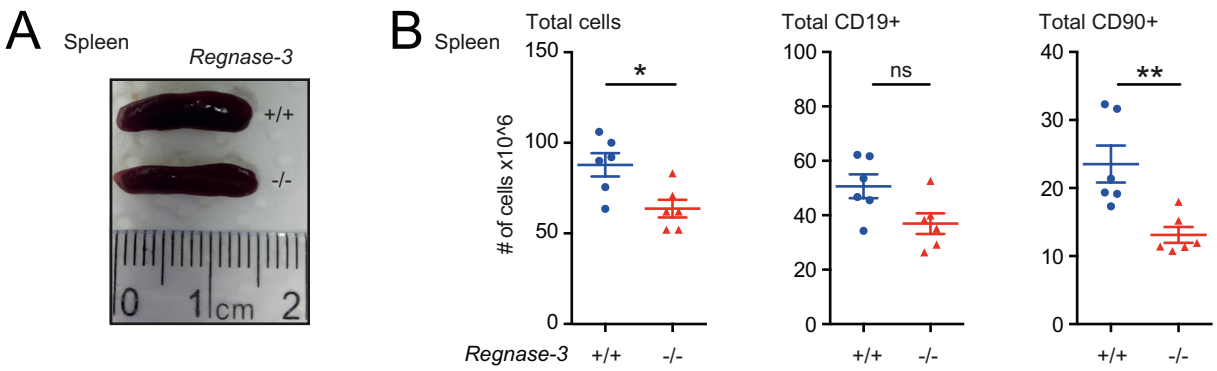


**Figure 19 *Regnase-3*$^{-/-}$ mice do not develop splenomegaly (von Gamm *et al.*, 2019).**

(A) Photography of the spleen of a *Regnase-3*-deficient mouse that was suffering from lymphadenopathy and its *Regnase-3*$^{+/+}$ littermate control.
(B) Total splenic cell numbers and total calculated splenic B cells (CD19$^{+}$) and T cells (CD90$^{+}$) in *Regnase-3*$^{-/-}$ mice and their littermate controls at 6 months of age (n = 6/6), assessed by flow cytometry.
Data are represented as mean +/- SEM and were compared by the Mann-Whitney U test (* $p \leq 0.05$, ** $p \leq 0.01$, ns = not significant).

To further assess whether *Regnase-3* deficiency causes the formation of auto-reactive antibodies, the blood sera were tested in two different assays. The presence of anti-nuclear antibodies (ANA) was evaluated by subjecting the sera to immobilized HEp-2 cells on imaging slides. Bound murine ANA were then visualized with Fluorescein isothiocyanate (FITC)-conjugated anti-mouse-IgG (Figure 20). This test does not only allow detecting ANA, but also a differential diagnostic evaluation of specific diseases and antigens depending on the observed staining patterns is possible. A detailed description of known patterns and their disease associations can be found in the manufacturers instructions for the imaging slides (see material and methods). The fluorescence pattern found for the *MRL/lpr* positive control is typical for reactivity against single or double stranded DNA, nucleosomes and histones (Figure 20). This pattern is frequently observed in systemic lupus erythematosus. However, this assay indicates that ANA are not significantly increased in *Regnase-3*-deficient mice (Figure 20).

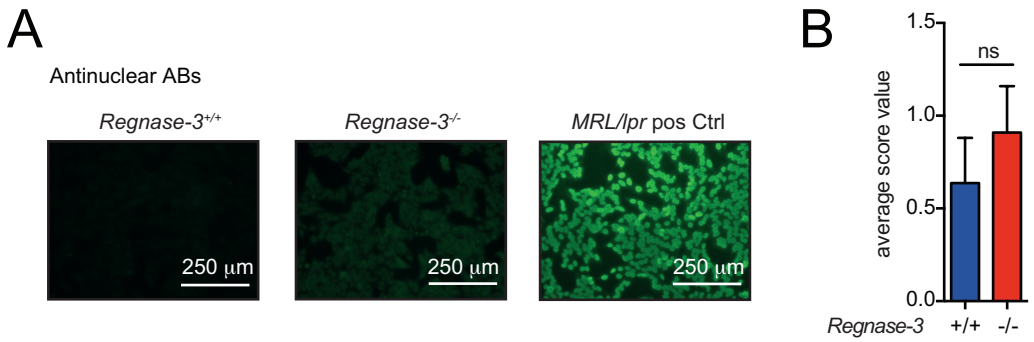


**Figure 20 Analysis of anti-nuclear antibodies (ANA) (von Gamm *et al.*, 2019).**

Immobilized HEp-2 cells were probed with sera from *Regnase-3*$^{+/+}$ and *Regnase-3*$^{-/-}$ mice. Bound serum IgGs were detected with FITC-conjugated anti-mouse IgG on a fluorescence microscope and scored images for each individual were scored as 0 = negative, 1 = weak positive, 2 = strong positive (n = 11/11). Serum from *MRL/lpr* mice was used as positive control. *Left*: Representative images. *Right*: Statistics for scoring values. Data are represented as mean +/- SEM and were compared by the Mann-Whitney U test (ns = not significant).

Next, we also wanted to evaluate, whether *Regnase-3*-deficient mice would develop a systemic form of auto-immunity and secrete antibodies, which are reactive against tissues. Therefore, liver protein lysates from immunodeficient NOD scid gamma mice were subjected to sodium dodecyl sulfate–polyacrylamide gel electrophoresis (SDS-PAGE) and blotted to polyvinylidene difluoride (PVDF) membranes. These membranes were then probed with the blood sera of *Regnase-3*$^{+/+}$ and *Regnase-3*$^{-/-}$ mice and bound tissue reactive antibodies were visualized using anti-mouse horseradish peroxidase (HRP)-conjugated anti-mouse-IgG with chemiluminescence detection on photo films (Figure 21). Also this assay did not provide evidence for the presence of auto-reactive antibodies in *Regnase-3*-deficient mice.

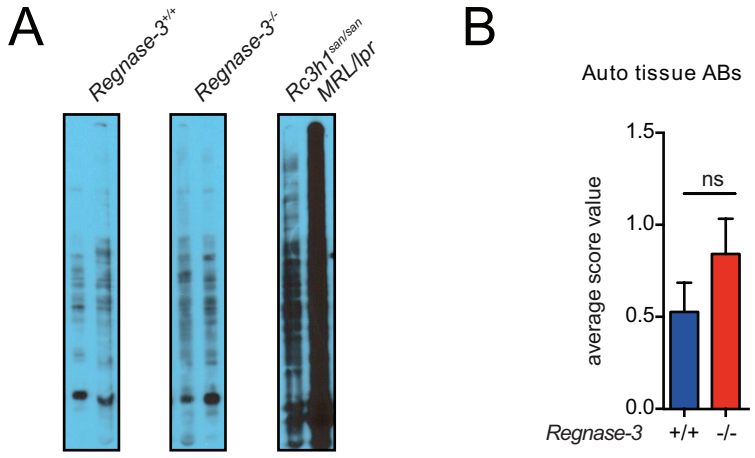


**Figure 21 Test for auto-reactivity of serum antibodies against tissue (von Gamm *et al.*, 2019).**

Protein lysates from the liver of immunodeficient *NOD scid gamma* mice were separated by SDS-PAGE and blotted to PVDF membranes. Membranes were loaded with sera from *Regnase-3*$^{+/+}$ and *Regnase-3*$^{-/-}$ mice and bound antibodies were detected by anti mouse IgG-HRP conjugates. Signal intensities on developed blots for each individual were scored as 0 = negative, 1 = weak positive, 2 = strong positive (n = 19/19). Serum from *Rc3h1*$^{san/san}$ and *MRL/lpr* mice were used as positive control. *Left*: Representative immunoblots. *Right*: Statistics for scoring values. Data are represented as mean +/- SEM and were compared by the Mann-Whitney U test (ns = not significant).

We were also wondering, whether analysis of peripheral blood counts would provide an indication for the presence of auto-immunity or other diseases related to the hematopoietic system. However, peripheral blood counts, such as white blood cells (WBC), red blood cells (RBC), platelets (PLT) and further blood related measurements, such as hematocrit values were comparable in *Regnase-3*$^{+/+}$ and *Regnase-3*$^{-/-}$ mice (Figure 22).

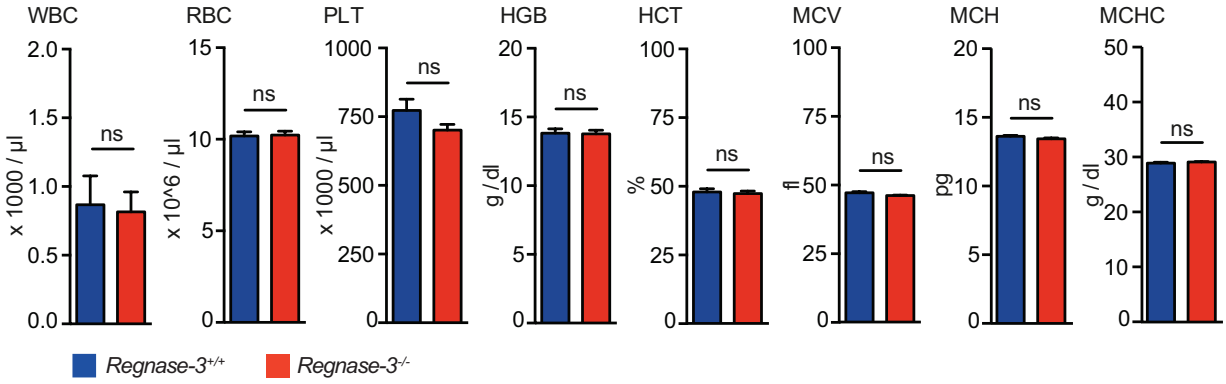


**Figure 22 Peripheral blood counts in *Regnase-3*$^{-/-}$ mice (von Gamm *et al.*, 2019).**

Anti-coagulated blood was taken from *Regnase-3*$^{-/-}$ mice and their *Regnase-3*$^{+/+}$ littermate controls and measured by an automated blood analyzer (n = 6/6). WBC, white blood cells; RBC, red blood cells; PLT, platelets; HGB, haemoglobin; HCT, haematocrit; MCV, mean corpuscular volume; MCH, mean corpuscular haemoglobin; MCHC, mean corpuscular haemoglobin concentration. Data are represented as mean +/- SEM and were compared by the Mann-Whitney U test (ns = not significant).

Under healthy conditions, immune cells are only present at low numbers within non-lymphoid tissues. Thus, infiltration of immune cells into these tissues may indicate signs of diseases, such as inflammation or also some types of systemic auto-immunity. Therefore, immunohistochemistry was performed for B cells (B220), T cells (CD3) and macrophages (F4/80) in the lung, kidney and liver of *Regnase-3*-deficient mice and their littermate controls (Figure 23). Analysis of the tissue sections revealed that immune cells were not increasingly infiltrated into the tissues of *Regnase-3*$^{-/-}$ mice.

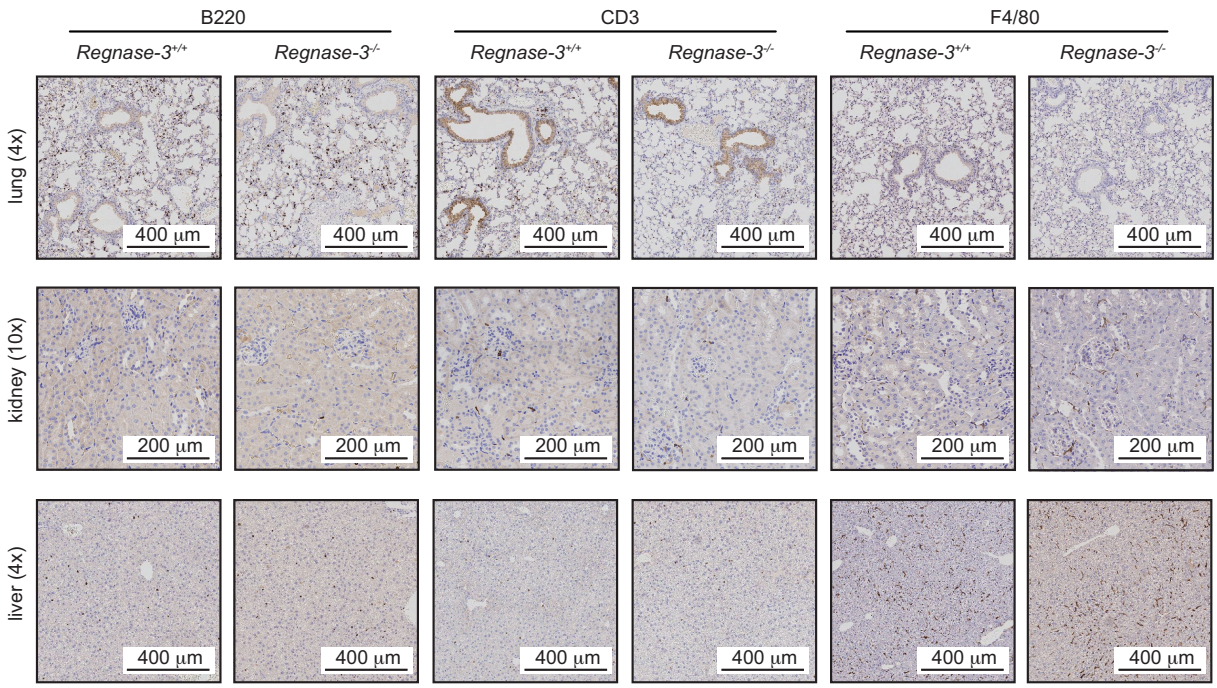


**Figure 23 Immunohistochemical analysis for immune cells in lung, kidney and liver of *Regnase-3*$^{-/-}$ mice (von Gamm *et al.*, 2019).**

Histological sections of lung, kidney and liver from *Regnase-3*$^{-/-}$ mice and *Regnase-3*$^{+/+}$ control mice were stained for B cells (B220), T cells (CD3) and macrophages (F4/80). Representative images from n = 3 *Regnase-3*$^{-/-}$ mice with lymphadenopathy and 3 *Regnase-3*$^{+/+}$ littermate controls at 8 months of age are shown. Magnification of images in brackets.

As germinal centers are necessary for the generation of memory B cells, auto-immune mice frequently have increased numbers of germinal centers in the spleen (Luzina *et al.*, 2001). Thus, the splenic structure of *Regnase-3*$^{-/-}$ mice was analyzed by immunohistochemistry for B cells (B220), T cells (CD3) and macrophages (F4/80) and the proportions of germinal center B cells in spleen and lymph nodes were studied by flow cytometry. Extramedullary hematopoiesis was observed in the spleen of *Regnase-3*$^{-/-}$ mice. Moreover, white pulp areas and marginal zones lost their architecture and the macrophage distribution was altered (Figure 24). An increase in germinal centers was not observed.

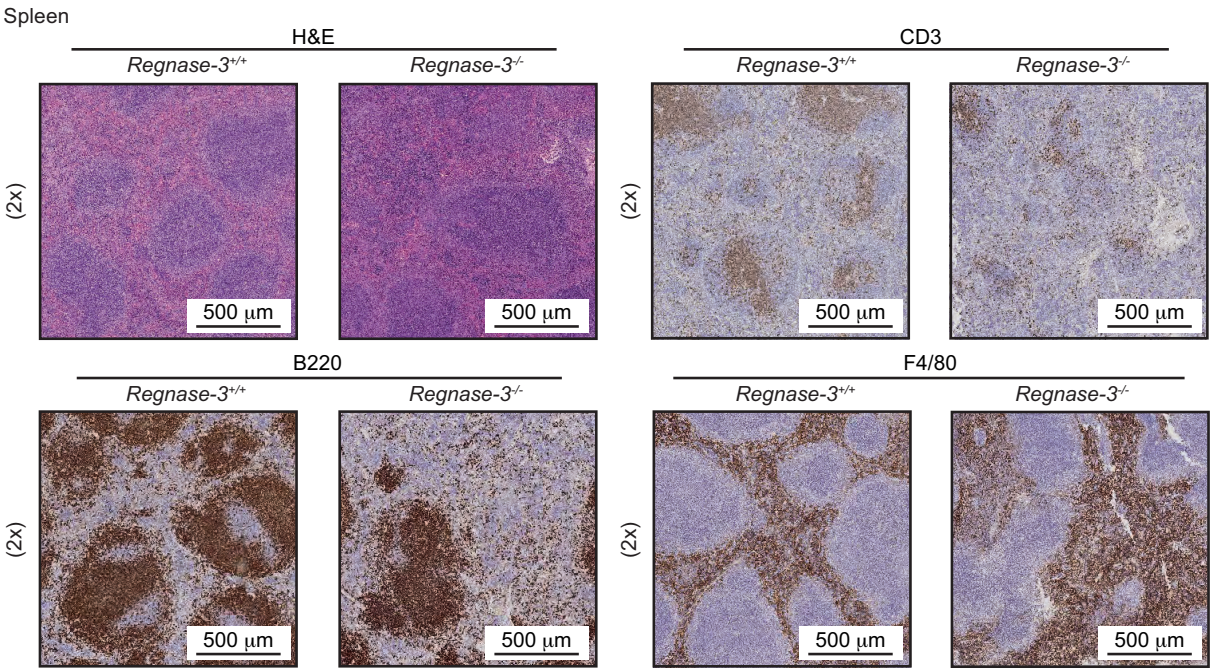


**Figure 24 Immunohistochemical analysis for immune cells in the spleen of *Regnase-3*$^{-/-}$ mice (von Gamm *et al.*, 2019).**

Histological sections of the spleen from *Regnase-3*$^{-/-}$ mice and *Regnase-3*$^{+/+}$ control mice were stained for B cells (B220), T cells (CD3) and macrophages (F4/80). Representative images from n = 3 *Regnase-3*$^{-/-}$ mice with lymphadenopathy and 3 *Regnase-3*$^{+/+}$ littermate controls at 8 months of age are shown. Magnification of images in brackets.

The proportions of germinal center B cells were assessed by flow cytometry analysis. In contrast to an expected increased number of germinal center B cells in case of autoimmunity, the proportion of germinal center B cells ($CD3^-$, $CD19^+$, $CD38^{lo}$, $CD95^{hi}$) was rather decreased than increased in *Regnase-3*-deficient mice, both in spleen and lymph nodes (Figure 25). This indicates that in *Regnase-3*$^{-/-}$ mice the formation of B cell follicles was impaired and germinal center formation was suppressed.

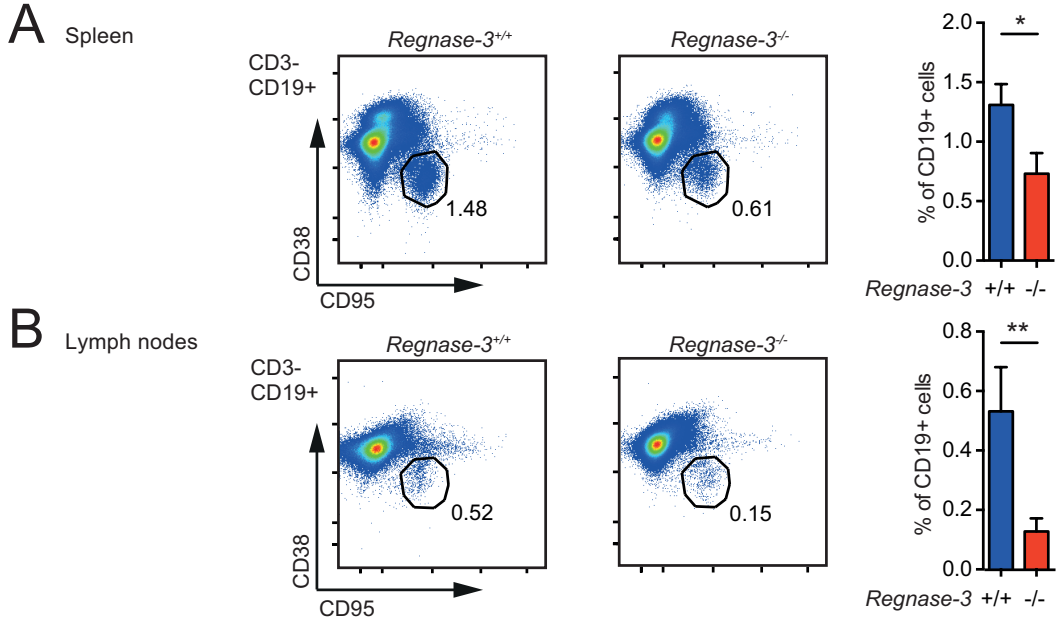


**Figure 25 Analysis of germinal center B cells in *Regnase-3*$^{-/-}$ mice (von Gamm *et al.*, 2019).**

Flow cytometry analysis for germinal center B cells (CD3$^-$, CD19$^+$, CD38$^-$/CD95$^+$) in (A) spleen and (B) lymph nodes. *Regnase-3*$^{-/-}$ mice with lymphadenopathy and their *Regnase-3*$^{+/+}$ littermate controls were assessed at 8 months of age (spleen: n = 11/11; lymph nodes n = 5/5). *Left*: Representative flow cytometry plots. *Right*: Statistical analysis. Data are represented as mean +/- SEM and were compared by the Mann-Whitney U test (* $p \leq 0.05$, ** $p \leq 0.01$).

Taken together, the measurements of immunoglobulins, the absence of splenomegaly in *Regnase-3*$^{-/-}$ mice, insignificant differences in two autoimmunity tests, unchanged peripheral blood counts, no infiltration of immune cells into tissues as well as reduced numbers of germinal center B cells in the knockout strongly indicate that autoimmunity is not driving lymphadenopathy in *Regnase-3*-deficient mice. Though the stated data do not provide any evidence for systemic or tissue specific autoimmunity, the existence of any type of auto-reactive antibodies in *Regnase-3*-deficient mice cannot be fully excluded since a variety of highly specific forms of autoimmunity have been described.

## 2.4 Enhanced interferon signaling in *Regnase-3*$^{-/-}$ mice

Immunohistochemistry as well as flow cytometric analysis revealed that B cells were the predominating cell type in hypertrophic lymph nodes in *Regnase-3*$^{-/-}$ mice. Thus, it was of high interest to further analyze these B cells in more detail. B cells (CD19$^{+}$) were therefore isolated from hypertrophic and from physiological sized lymph nodes of the same *Regnase-3*$^{-/-}$ mice as well as from wildtype littermate controls. The isolated B cells were then subjected to RNA sequencing and evaluated by principal component analysis (PCA). B cells from *Regnase-3*-deficient hypertrophic lymph nodes cluster together in the PCA plot, distinct from wildtype B cells and B cells from small lymph nodes (Figure 26). Two out of three B cell samples, which were derived from small lymph nodes of mice with lymphadenopathy, clustered together with wildtype B cells (Figure 26). This indicates strong local effects for B cells in hypertrophic lymph nodes, which are not fully reflected in all B cells within an individual *Regnase-3*-deficient mouse.

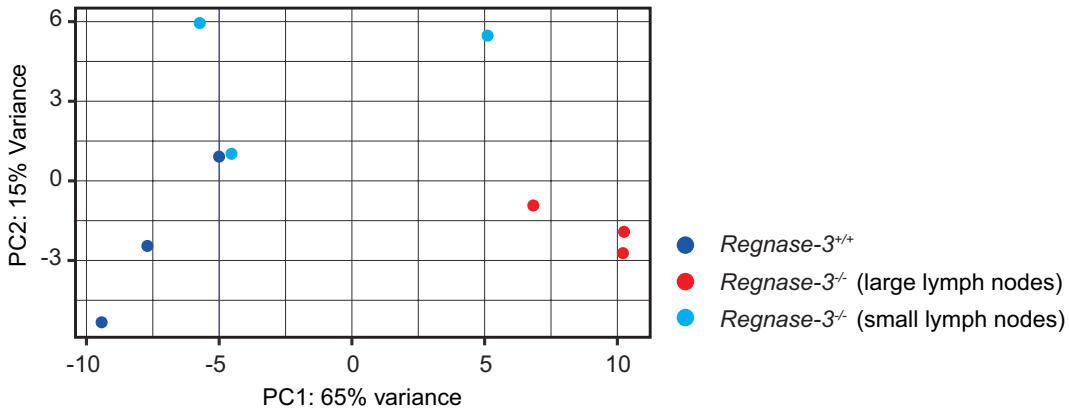


**Figure 26 RNA sequencing analysis for B cells from lymph nodes of *Regnase-3*$^{-/-}$ mice, PCA (von Gamm *et al.*, 2019).**

CD19$^{+}$ B cells were isolated from hypertrophic lymph nodes of *Regnase-3*$^{-/-}$ mice and from small lymph nodes of the same individuals as well as from *Regnase-3*$^{+/+}$ littermate controls (n = 3/3). Isolated RNA was subjected to sequencing analysis. B cell samples were plotted based on principal component analysis (PCA) and groups were highlighted by colors.

RNA sequencing data were further analyzed to get information on specific deregulated genes and pathways within B cells of hypertrophic lymph nodes derived B cells in *Regnase-3*-deficient mice. Thus, genes were determined, which are significantly upregulated ($\geq$ 2 log2-fold) within hypertrophic lymph nodes of *Regnase-3*-deficient mice compared to wildtype B cells. Strikingly, 12 out of 21 significantly enriched genes were recognized to be genes that respond either to IFNβ or IFNγ or both (Figure 27).

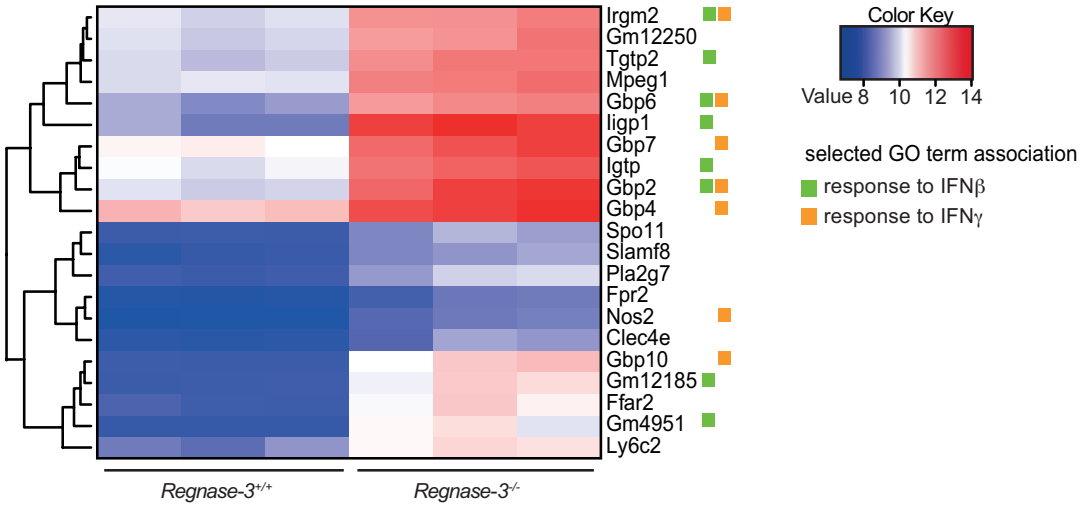


**Figure 27 RNA sequencing analysis for B cells from lymph nodes of *Regnase-3*$^{-/-}$ mice, heatmap (von Gamm *et al.*, 2019).**

B cells were isolated and processed as described in Figure 26. Samples from hypertrophic lymph nodes in *Regnase-3*$^{-/-}$ mice were compared to wildtype B cells by computational analysis. A heatmap of RNAseq data displays all significantly (⩾ 2 log2-fold) upregulated genes in *Regnase-3*$^{-/-}$ mice. Green and orange boxes highlight gene ontology (GO) term associations to 'response to interferone-beta' and 'response to interferone-gamma'.

Significantly upregulated genes (⩾ 2 log2-fold) in B cells from hypertrophic lymph nodes compared to wildtype B cells were calculated and further analyzed by enriched gene ontology (GO) terms. Gene ontology enables to cluster genes into groups within a specific umbrella topic, such as their biological processes. This helps to elucidate regulatory pathways that might be shifted in specific samples. The previously observed strong indication of a deregulation within the interferon pathway was also reflected in the GO term analysis with the GO term 'cellular response to IFNβ' as second position (p-value <0.05) (Figure 28).

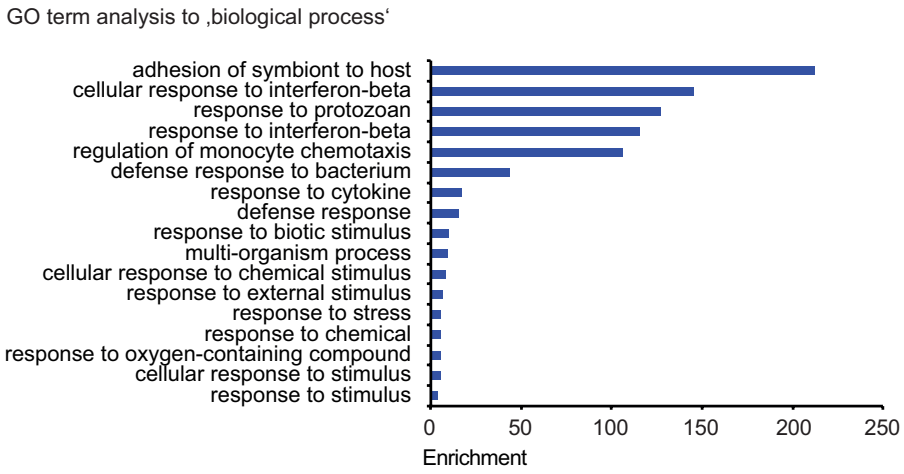


**Figure 28 RNA sequencing analysis for B cells from lymph nodes of *Regnase-3*$^{-/-}$ mice, GO term analysis (von Gamm *et al.*, 2019).**

B cells were isolated and processed as described in Figure 26. All upregulated genes (⩾ 2 log2-fold) from Figure 27 were clustered by their gene ontology (GO) terms (p-value < 0.05). Enriched GO terms are ordered according to their enrichment values.

We aimed to understand whether a specific systemic cytokine signature within *Regnase-3*$^{-/-}$ mice could explain the particular response in sequencing data for B cells of *Regnase-3*-deficient mice. Therefore, a variety of inflammatory cytokines was analyzed in the blood sera of *Regnase-3*-deficient mice and their littermate controls. Among the analyzed cytokines (IL-1α, IL-1β, IL-6, IL-10, IL-12p70, IL-17A, IL-23, IL-27, IFNβ, IFNγ, TNFα and GM-CSF), only IFNγ was seen to be systemically upregulated in *Regnase-3*$^{-/-}$ mice (Figure 29).

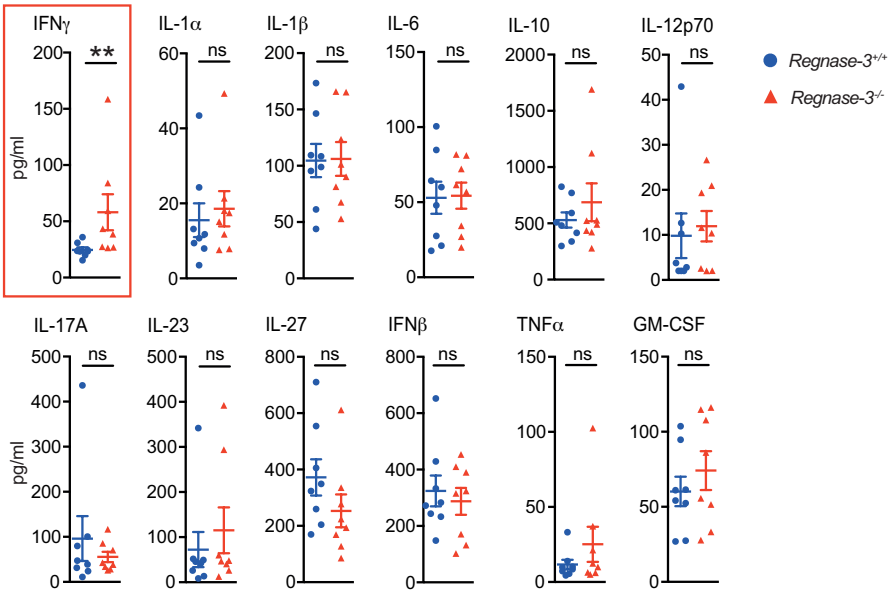


**Figure 29 Serum cytokine concentrations in *Regnase-3*$^{-/-}$ mice (von Gamm *et al.*, 2019).**

Blood serum was taken from *Regnase-3*$^{-/-}$ mice and *Regnase-3*$^{+/+}$ littermates at 6 months of age (n = 8/8). Several inflammatory cytokines were measured in a multiplex assay. Data are represented as mean +/- SEM and were compared by the Mann-Whitney U test (** $p \leq 0.01$, ns = not significant).

Binding of IFNγ to cellular receptors induces in particular downstream phosphorylation of the transcription factor signal transducer and activator of transcription 1 (STAT1) (Meissl *et al.*, 2017). Phosphorylated STAT1 molecules translocate to the nucleus and cause the transcriptional activation of different genes, leading to direct or indirect induction of interferon-regulated genes, including *Stat1* mRNA itself as well as Major histocompatibility complex class-II (MHC-II) (Giroux *et al.*, 2003; Lee *et al.*, 1999; Meissl *et al.*, 2017). Therefore, we aimed to analyze, whether these secondary interferon responses are also reflected in tissues of *Regnase-3*-deficient mice and determined *Stat1* mRNA levels. In line with sequencing results and cytokine measurements, also *Stat1* mRNA was significantly upregulated in lymph node, spleen, kidney, lung and liver tissue of *Regnase-3*-deficient mice with hypertrophic lymph nodes (Figure 30).

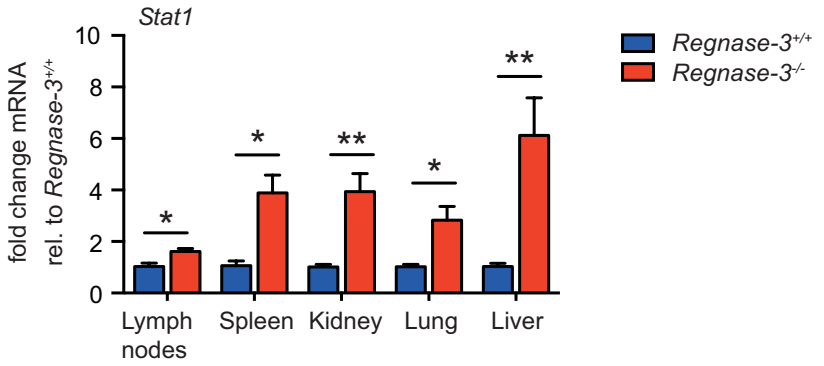


**Figure 30 Stat1 mRNA expression levels in *Regnase-3*$^{-/-}$ mice (von Gamm *et al.*, 2019).**

Lymph nodes, spleen, kidney, lung and liver were isolated from *Regnase-3*$^{+/+}$ and Regnase-3$^{-/-}$ mice at 8 months of age (n = 5/5). Isolated RNA was analyzed by RT-PCR, normalized to *Hprt1* and are displayed in relativity to the respective expression in *Regnase-3*$^{+/+}$ mice. Data are represented as mean +/- SEM and were compared by the Mann-Whitney U test (* $p \leq 0.05$, ** $p \leq 0.01$).

In addition to measurements of *Stat1* mRNA levels, STAT signaling was also investigated on the protein level. Phosphorylation and thus activation of STAT1 (pSTAT1) was analyzed by histology in lymph nodes of *Regnase-3*$^{-/-}$ mice. STAT1 phosphorylation was visibly increased in *Regnase-3*-deficient mice (Figure 31, *left*). Also computational analysis of the positively stained pixels revealed a significant increase of STAT1 phosphorylation within hypertrophic lymph nodes of *Regnase-3*$^{-/-}$ mice (Figure 31, *right*).

Thus, systemic interferon signaling was observed both on the mRNA level as well as on the protein level. Moreover, this was reflected not only in immunological, but also in non-lymphoid tissues, such as kidney or liver from *Regnase-3*-deficient mice.

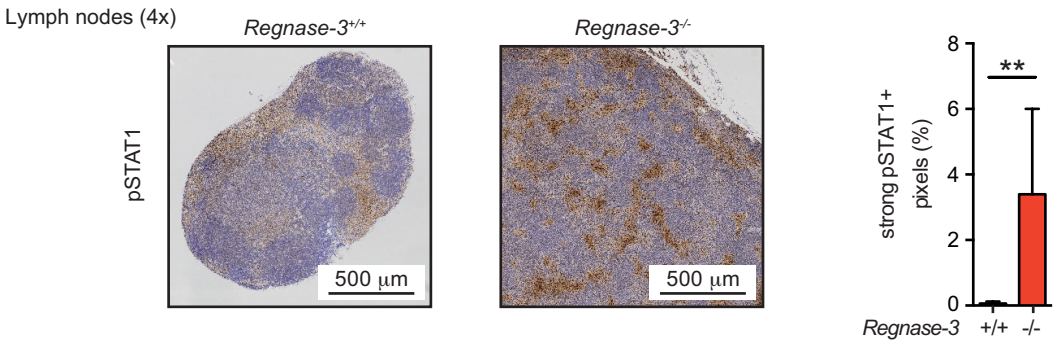


**Figure 31 Immunohistochemical analysis of pSTAT1 in *Regnase-3*$^{-/-}$ mice (von Gamm *et al.*, 2019).**

*Left*: Representative images for immunohistochemical analysis of phosphorylated STAT1 in sections of skin draining lymph nodes from *Regnase-3*$^{-/-}$ mice with lymphadenopathy and their *Regnase-3*$^{+/+}$ littermate controls (n = 6/6). *Right*: Percentage of strong positive pixels in pSTAT1 immunohistochemical sections, determined by computational analysis with the Definiens software (n = 6/6). Data are represented as mean +/- SEM and were compared by the Mann-Whitney U test (** $p \leq 0.01$).

Also MHC-II is induced upon interferon signaling and was thus used as marker for peripheral interferon responses. MHC-II protein expression was analyzed by immunohistochemistry in tissue sections of liver, kidney and lung with subsequent computational analysis of the positively stained area. MHC-II stain for liver and kidney sections were visibly darker in *Regnase-3*$^{-/-}$ mice with hypertrophic lymph nodes (Figure 32 A, B, *left*). This observation of significantly upregulated MHC-II expression in *Regnase-3*-deficient mice was verified by computational analysis of the positively stained pixel area (Figure 32 A, B, *right*). Also lung tissue of *Regnase-3*$^{-/-}$ mice seemed to have increased MHC-II expression (Figure 32 C, *left*). Further, computational analysis revealed that the average MHC-II positively stained area in lung tissues of *Regnase-3*$^{-/-}$ mice was approximately two fold increased compared to wildtype mice. However, the increase was statistically not significant, likely due to high standard deviation caused by the inhomogeneous tissue structure of lung samples (Figure 32 C, *right*). Of note, MHC-II expression in lymph nodes and spleen could not be evaluated as MHC-II is also expressed on B cells, which are changed in total numbers and percentages in *Regnase-3*-deficient mice.

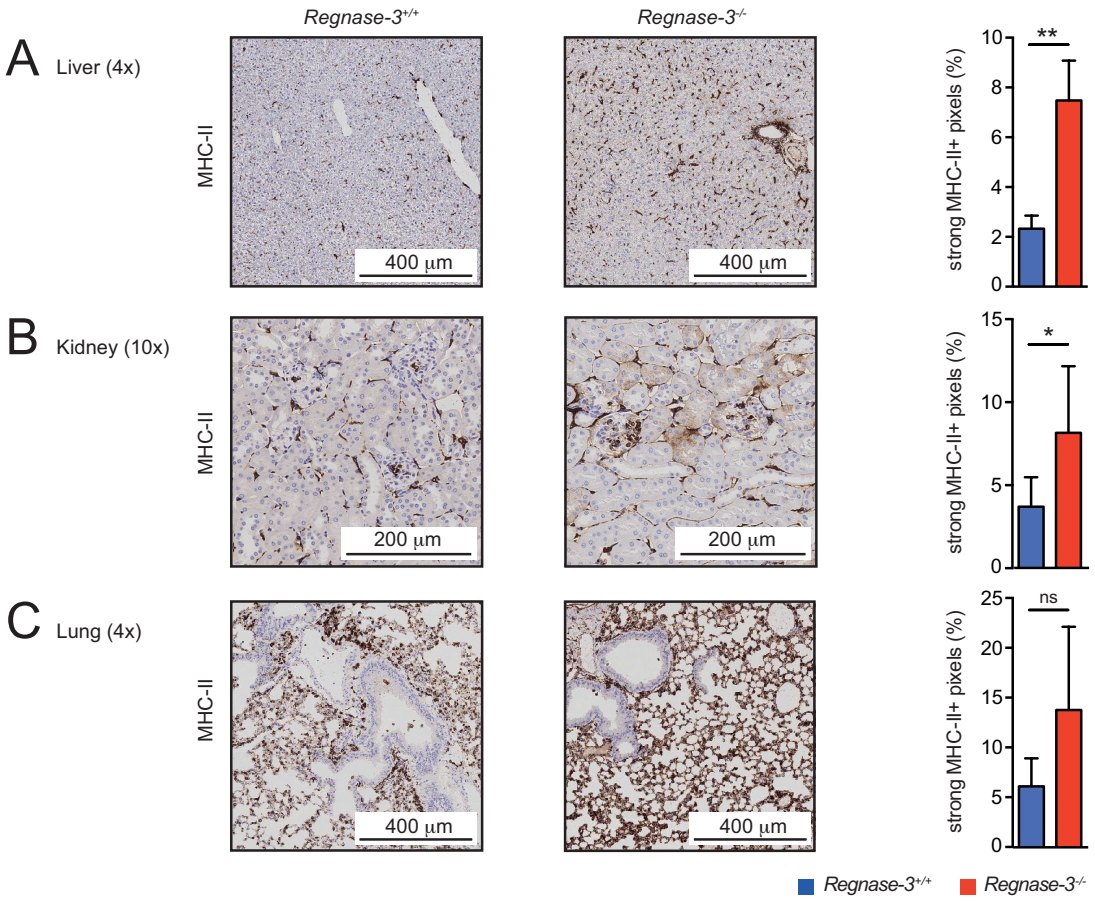


**Figure 32 Immunohistochemical analysis of MHC-II in *Regnase-3*$^{-/-}$ mice (von Gamm *et al.*, 2019).**

Tissues were isolated from *Regnase-3*$^{-/-}$ mice with lymphadenopathy and from their *Regnase-3*$^{+/+}$ littermate controls (n = 6/6). (A) Liver, (B) kidney and (C) lung sections were stained for MHC-II, magnification as indicated. *Left*: Representative images (n = 6/6). *Right*: Percentages of strong positive pixels in MHC-II immunohistochemical sections of indicated organs, determined by computational analysis with the Definiens software (n = 6/6). Data are represented as mean +/- SEM and were compared by the Mann-Whitney U test (* $p \leq 0.05$, ** $p \leq 0.01$, ns = not significant).

To further specify, whether MHC-II is not only increased in total tissue, but to get information on MHC-II expression on macrophages, consecutive histology sections were taken from lung samples and stained for the macrophage marker CD68 and MHC-II. Numbers of MHC-II positive macrophages in relation to total numbers of macrophages within specified areas were calculated. Also the number of MHC-II positive macrophages in lung tissues was increased in *Regnase-3*$^{-/-}$ mice (Figure 33).

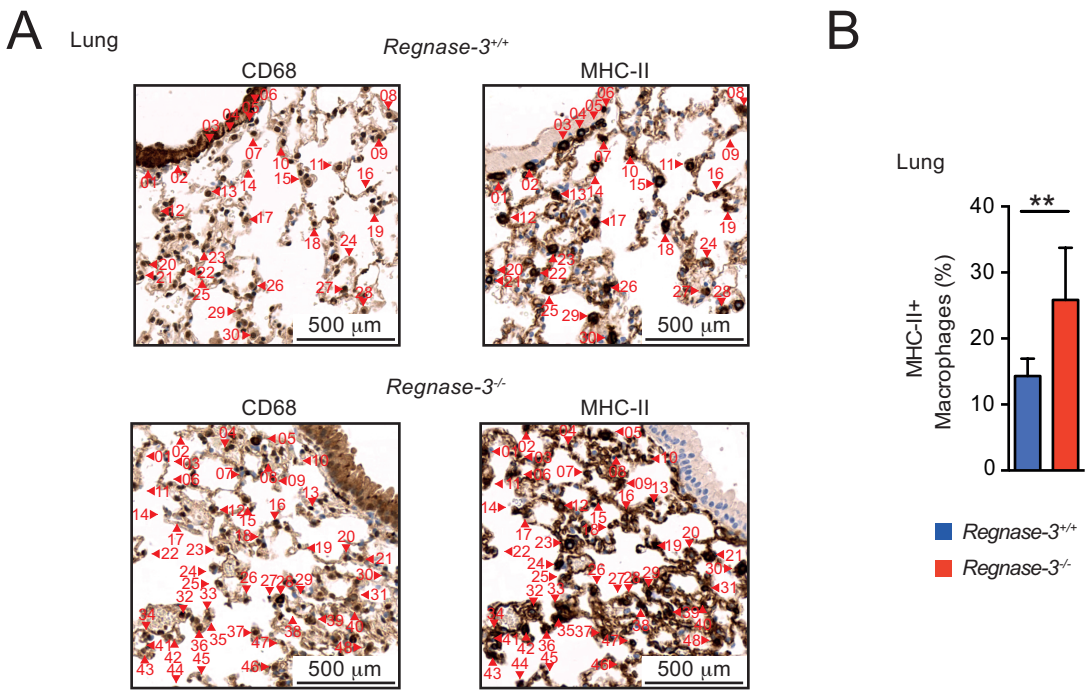


**Figure 33 MHC-II positive macrophages in the lung of *Regnase-3*$^{-/-}$ mice (von Gamm *et al.*, 2019).**

(A) Consecutive histological sections of lung tissue from *Regnase-3*$^{-/-}$ mice with lymphadenopathy and their *Regnase-3*$^{+/+}$ littermate controls were stained for macrophages (CD68) or MHC-II. CD68$^{+}$ macrophages, which are also positive for MHC-II were indicated with numbers (representative images of n = 5/6).
(B) Calculation of the percentages of MHC-II positive macrophages relative to the total number of macrophages within histological lung sections (n = 5/6). Data are represented as mean +/- SEM and were compared by the Mann-Whitney U test (** $p \leq 0.01$).

Sequencing analysis of B cells, blood cytokine measurements, evaluation of STAT1 and MHC-II by RT-PCR and histology as well as analyses of lung macrophages showed molecular consequences of strong interferon signaling. Altogether, our data indicate that *Regnase-3* deficiency in mice causes upregulated interferon signaling, both systemically as well as local within hypertrophic lymph nodes.

## 2.5 Analysis of the *in vivo* relevance of Regnase-3 in T cells

As we have found significant deregulation in *Regnase-3*$^{-/-}$ mice regarding IFNγ secretion and interferon response, we were now wondering whether absence of Regnase-3 particularly in T cells might have caused hypertrophic lymph nodes in *Regnase-3*$^{-/-}$ mice. This idea was emphasized by a publication from Uehata *et al*. demonstrating that *Regnase-1* deficiency specifically in T cells (*Regnase-1*$^{fl/fl}$ +CD4-Cre) developed a similar strong phenotype including splenomegaly, autoimmunity and premature death as compared to globally deficient mice (Uehata *et al.*, 2013).

Thus we aimed to analyze differences in T cell biology in *Regnase-3*-deficient mice, but also the role of Regnase-3 specifically for T cell function.

### 2.5.1 Characterization of T cell subsets in *Regnase-3*$^{-/-}$ mice

T cell development in the thymus was analyzed using flow cytometry to identify the proportions of T cells in the main developmental stages comprising the CD4/CD8 double negative, CD4/CD8 double positive and CD4 or CD8 single positive stages (see also introduction for more detailed description). Flow cytometric analysis found no significant changes in thymic T cell development for *Regnase-3*-deficient mice (Figure 34).

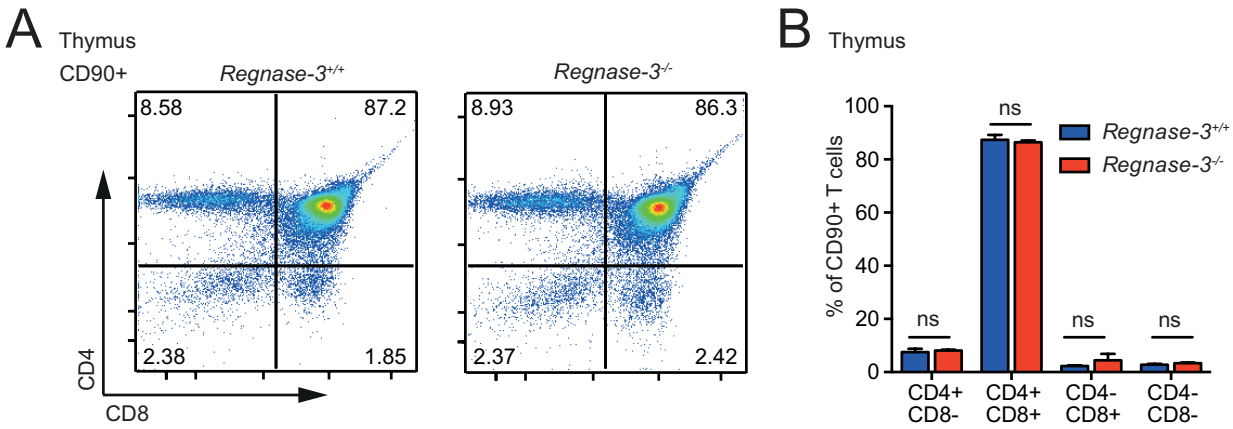


**Figure 34 Development of thymic T cells in *Regnase-3*$^{-/-}$ mice (von Gamm *et al*., 2019).**

Flow cytometric analysis of double negative, double positive and CD4 and CD8 single positive T cells in the thymus of *Regnase-3*$^{-/-}$ mice and their *Regnase-3*$^{+/+}$ littermate controls at 6 months of age (n = 8/8). (A) Representative plots. (B) Statistical analysis: Data are represented as mean +/- SEM and were compared by the Mann-Whitney U test (ns = not significant).

Despite normal thymic T cell development, some T cell populations were altered in spleen and lymph nodes of *Regnase-3*$^{-/-}$ mice. First, splenic T cells were shifted to higher percentages of CD4$^{+}$ T cells and reduced proportions of CD8$^{+}$ T cells in *Regnase-3*-deficient mice with hypertrophic lymph nodes (Figure 35).

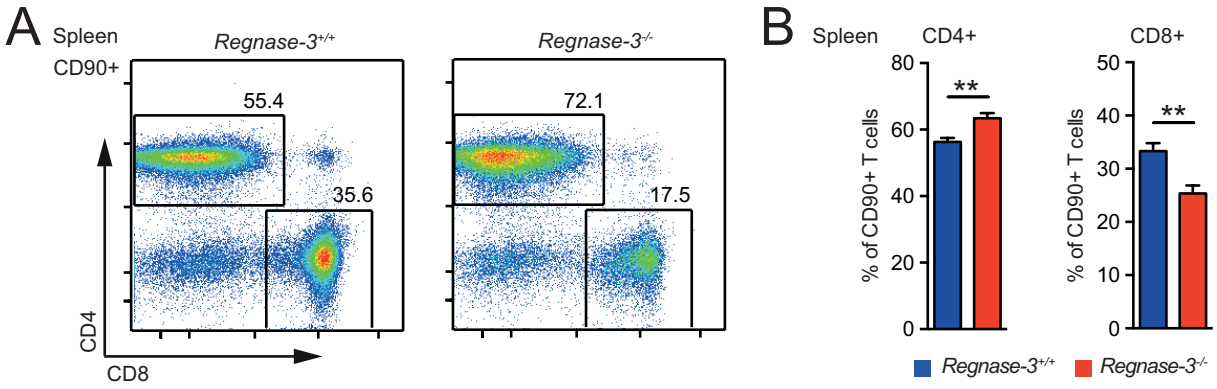


**Figure 35 Analysis of splenic CD4⁺ and CD8⁺ T cells in *Regnase-3*$^{-/-}$ mice (von Gamm *et al.*, 2019).**

Flow cytometric analysis of splenic CD4⁺ and CD8⁺ T cells, given as percentage of all T cells (CD90⁺). Splenic T cells were analyzed in *Regnase-3*$^{-/-}$ mice and their *Regnase-3*$^{+/+}$ littermate controls at 6 months (n = 9/9). (A) Representative plots and (B) Statistical analysis: Data are represented as mean +/- SEM and were compared by the Mann-Whitney U test (** p ≤ 0.01).

Also proportions of CD4⁺ effector T cells (CD90⁺, CD4⁺, CD62L⁻, CD44$^{hi}$) in lymph nodes as well as splenic CD8⁺ effector memory T cells (CD90⁺, CD8a⁺, CD62L⁻, CD44$^{hi}$) were elevated in *Regnase-3*-deficient mice (Figure 36).

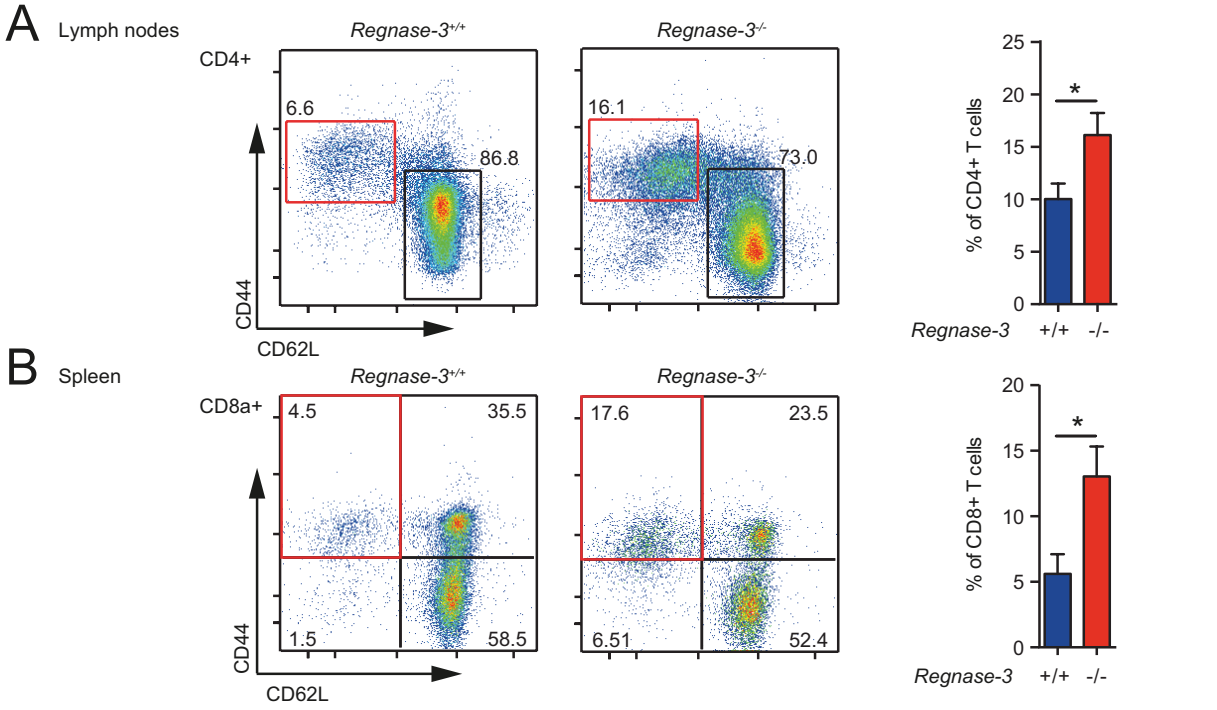


**Figure 36 Analysis of effector T cells in *Regnase-3*$^{-/-}$ mice (von Gamm *et al.*, 2019).**

(A) Flow cytometric analysis of CD4⁺ effector T cells (CD19⁻, CD90⁺, CD4⁺, CD62L⁻/CD44$^{hi}$) in lymph nodes of *Regnase-3*$^{-/-}$ mice and their *Regnase-3*$^{+/+}$ littermate controls, assessed at 6 months of age (n = 6/6). *Left*: Representative plots. *Right*: Statistical analysis.
(B) Flow cytometric analysis of splenic CD8⁺ effector memory T cells (CD19⁻, CD90⁺, CD8a⁺, CD62L⁻/CD44$^{hi}$) of *Regnase-3*$^{-/-}$ mice and their *Regnase-3*$^{+/+}$ littermate controls, assessed at 6 months of age (n = 6/6). *Left*: Representative plots. *Right*: Statistical analysis.
Data are represented as mean +/- SEM and were compared by the Mann-Whitney U test (* p ≤ 0.05).

However, CD4$^+$ effector T cells in the spleen as well as CD8$^+$ effector memory T cells in lymph nodes were not significantly changed (Figure 37).

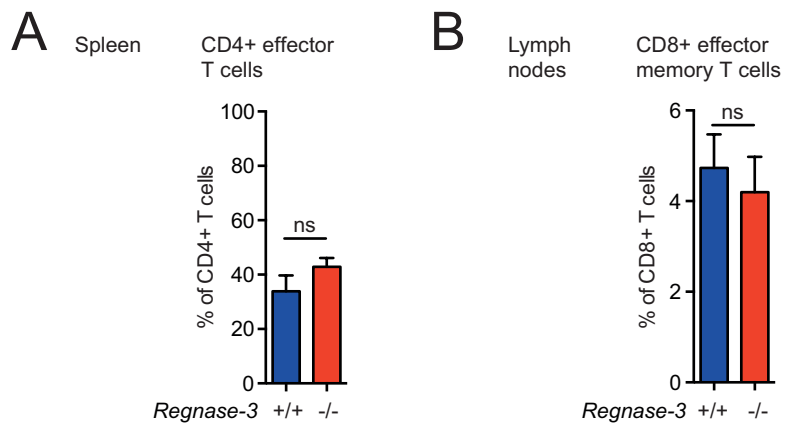


**Figure 37 Analysis of effector T cells in *Regnase-3*$^{-/-}$ mice (von Gamm *et al.*, 2019).**

(A) Flow cytometric analysis of splenic CD4$^+$ effector T cells (CD19$^-$, CD90$^+$, CD4$^+$, CD62L$^-$/CD44$^{hi}$) in *Regnase-3*$^{-/-}$ mice and their *Regnase-3*$^{+/+}$ littermate controls, assessed at 6 months of age. Statistical analysis of n = 6/6.

(B) Flow cytometric analysis of CD8$^+$ effector memory T cells (CD19$^-$, CD90$^+$, CD8$^+$, CD62L$^-$/CD44$^{hi}$) in lymph nodes of *Regnase-3*$^{-/-}$ mice and their *Regnase-3*$^{+/+}$ littermate controls, assessed at 6 months of age. Statistical analysis of n = 6/6.

Data are represented as mean +/- SEM and were compared by the Mann-Whitney U test (ns = not significant).

### 2.5.2 Conditional *Regnase-3* ablation in T cells

We next wanted to evaluate if lymphadenopathy and deregulated T cell activation were caused by a T cell intrinsic malfunction in *Regnase-3*$^{-/-}$ mice similar to the described role for Regnase-1 in T cells. Thus, we used the 'knockout-first' deficient mouse model to generate mice with a floxed allele for *Regnase-3* by crossbreeding with ROSA26 promotor driven FLPe deleter mice with global FLPe recombinase activity (see results section 1 and material and methods). The generated *Regnase-3*$^{fl/fl}$ mice were further bred to CD4 promotor driven Cre recombinase expressing mice to obtain animals with conditional *Regnase-3* deficiency in T cells. Of note, CD4-Cre deletes in both CD4$^+$ as well as CD8$^+$ T cells, since both T cell subsets originate from a CD4/CD8 double positive state during thymic development.

None of the 16 analyzed *Regnase-3*$^{fl/fl}$ +CD4-Cre mice developed hypertrophic lymph nodes (Figure 38 A). And also calculated total numbers of B cells and T cells were comparable in CD4-Cre positive and negative mice (Figure 38 B).

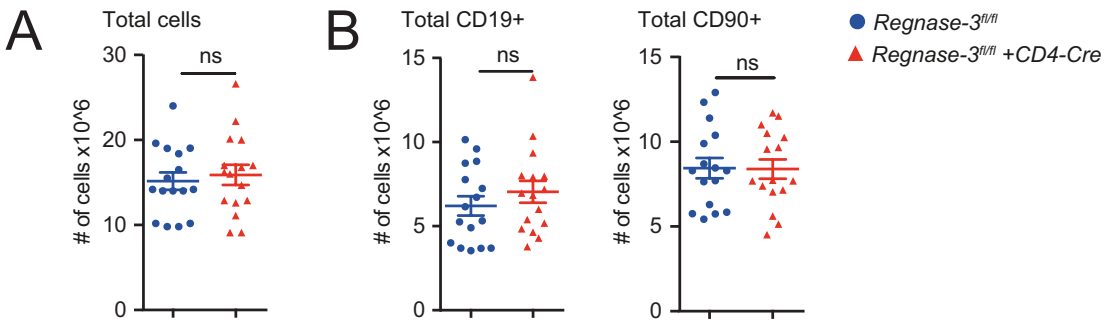


**Figure 38 Conditional *Regnase-3* deficiency in T cells (*Regnase-3*$^{fl/fl}$ + CD4-Cre mice): T and B cell analysis of lymph nodes (von Gamm *et al.*, 2019).**

(A) Total cell numbers in lymph nodes of *Regnase-3*$^{fl/fl}$ +CD4-Cre mice and their *Regnase-3*$^{fl/fl}$ littermates at 5 months of age (n = 16/16).
(B) Flow cytometric analysis of T and B cells: Numbers of calculated total B (CD19$^+$) and total T cells (CD90$^+$) in lymph nodes of *Regnase-3*$^{fl/fl}$ +CD4-Cre mice and their *Regnase-3*$^{fl/fl}$ littermates at 5 months of age (n = 16/16).
Data are represented as mean +/- SEM and were compared by the Mann-Whitney U test (ns = not significant).

We were also interested to analyze a subpopulation of T cells, the regulatory T cells. These cells modulate immune responses and enhance tolerance of the organism to self-antigens (Murphy and Weaver, 2018). Therefore, regulatory T cells counter regulate immune responses and prevent autoimmune diseases.
However, also proportions of regulatory T cells (CD4$^+$, FoxP3$^+$) were unchanged in thymus and lymph nodes of *Regnase-3*$^{fl/fl}$ +CD4-Cre mice (Figure 39).

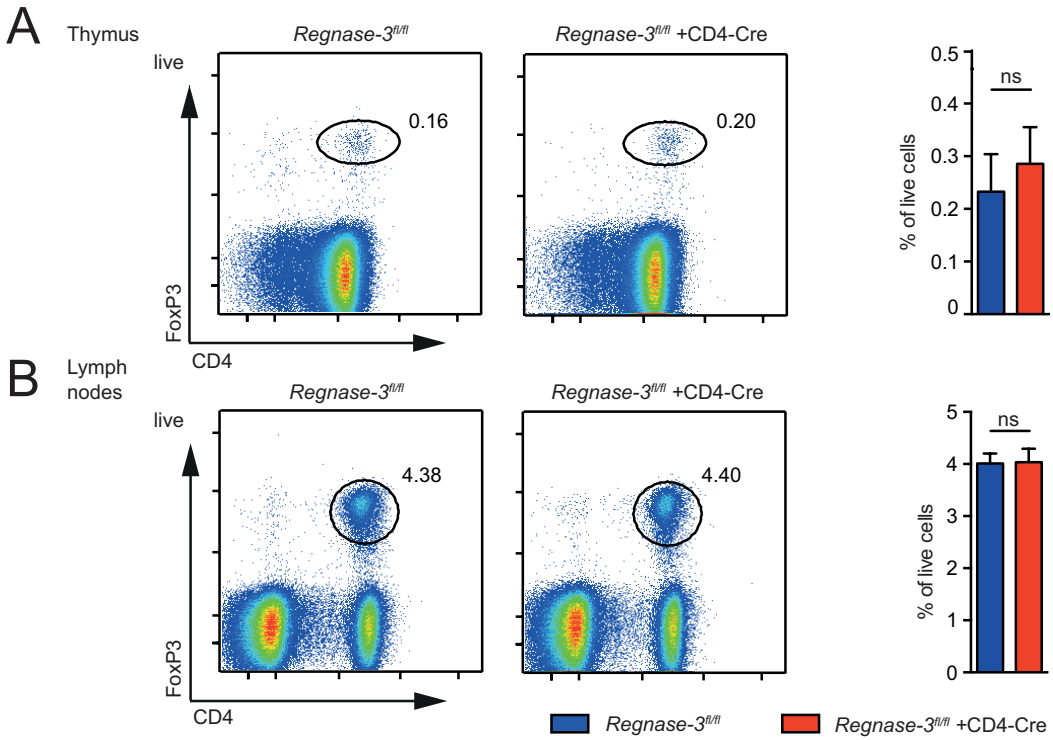


**Figure 39 Conditional *Regnase-3* deficiency in T cells (*Regnase-3*$^{fl/fl}$ + CD4-Cre mice): Analysis of regulatory T cells (von Gamm *et al.*, 2019).**

Flow cytometric analysis of thymic regulatory T cells (CD4$^+$, FoxP3$^+$) in *Regnase-3*$^{fl/fl}$ + CD4-Cre mice and *Regnase-3*$^{fl/fl}$ littermate controls, assessed at 5 months of age (n = 9/9). *Left*: Representative plots. *Right*: Statistical analysis. (A) From thymus. (B) From lymph. Data are represented as mean +/- SEM and were compared by the Mann-Whitney U test (ns = not significant).

These data demonstrate that subsets within the T cell linage are altered in *Regnase-3*$^{-/-}$ mice, but also strongly indicate that lymphadenopathy in globally *Regnase-3*-deficient mice is not caused by a CD4$^{+}$ or CD8$^{+}$ T cell intrinsic lack of *Regnase-3*.

## 2.6 Analysis of the *in vivo* relevance of Regnase-3 in B cells

As previously mentioned, *Regnase-3* deficiency in mice caused lymphadenopathy with significantly increased numbers of B cells. Thus, we aimed to further analyze B cells in *Regnase-3*$^{-/-}$ mice and aimed to understand whether hypertrophic lymph nodes were caused by a B cell intrinsic malfunction such as the formation of a B cell lymphoma.

### 2.6.1 Characterization of B cell subsets in *Regnase-3*$^{-/-}$ mice

Flow cytometry revealed that in the spleen, proportions of immature B cells (CD19$^{+}$, IgM$^{hi}$, IgD$^{lo}$) as well as marginal zone B cells (CD19$^{+}$, AA4.1$^{lo}$, CD21$^{+}$, IgM$^{hi}$) were increased significantly in *Regnase-3*$^{-/-}$ mice (Figure 40).

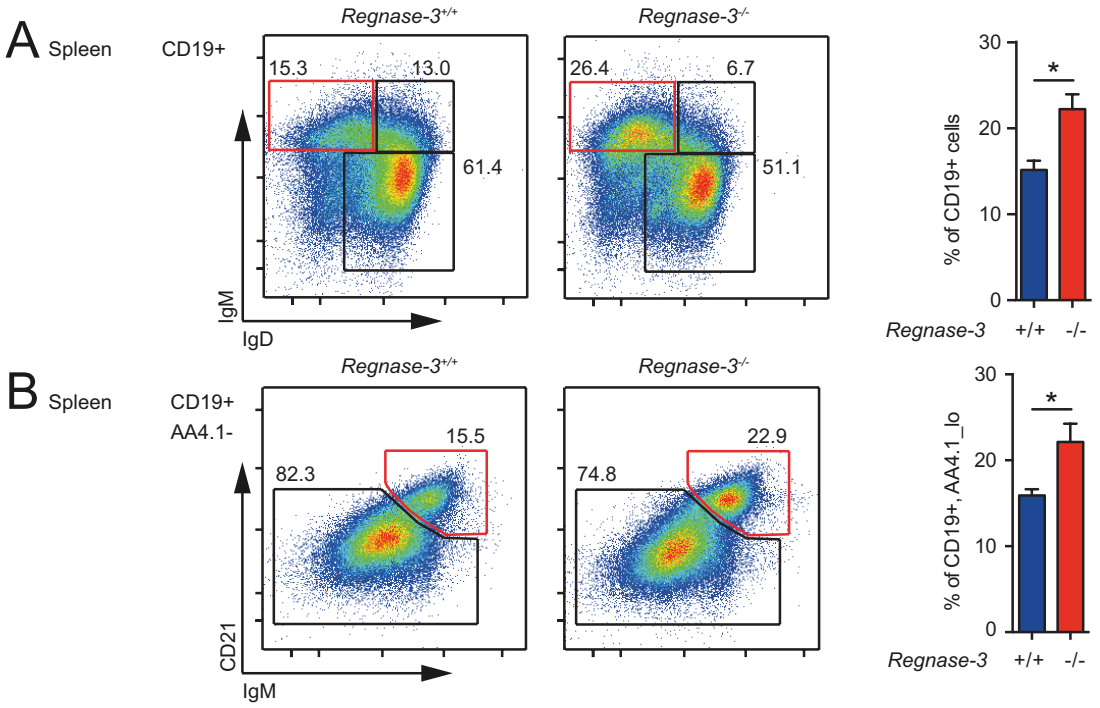


**Figure 40 Analysis of immature B cells and marginal zone B cells in the spleen of *Regnase-3*$^{-/-}$ mice (von Gamm *et al.*, 2019).**

(A) Flow cytometric analysis of splenic immature B cells (CD19$^{+}$, IgD$^{lo}$/IgM$^{hi}$), transitional B cells (CD19$^{+}$, IgD$^{int}$/IgM$^{int}$) and mature B cells (CD19$^{+}$, IgD$^{hi}$/IgM$^{lo}$) in *Regnase-3*$^{-/-}$ mice and their *Regnase-3*$^{+/+}$ littermate controls, assessed at 6 months of age (n = 6/6). *Left*: Representative plots. *Right*: Statistical analysis.
(B) Flow cytometric analysis of splenic marginal zone B cells (CD19$^{+}$, AA4.1$^{lo}$, CD21$^{+}$/IgM$^{hi}$) in *Regnase-3*$^{-/-}$ mice and their *Regnase-3*$^{+/+}$ littermate controls, assessed at 6 months of age (n = 6/6). *Left*: Representative plots. *Right*: Statistical analysis.
Data are represented as mean +/- SEM and were compared by the Mann-Whitney U test (* $p \leq 0.05$).

Within splenic immature B cells, the transitional stages (T1, T2, T3) were similar between *Regnase-3*$^{+/+}$ and *Regnase-3*$^{-/-}$ mice, indicating that transition from one to another transitional step is not blocked due to *Regnase-3* deficiency and B cell maturation is possible (Figure 41). In contrast, the percentage of germinal center B cells was reduced both in lymph nodes and spleen (see autoimmunity section).

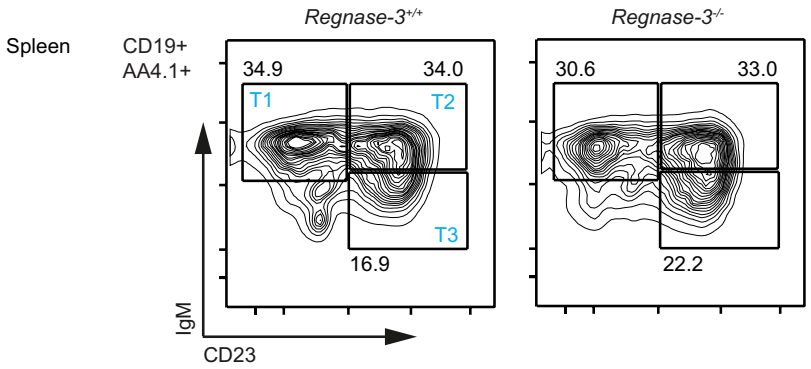


**Figure 41 Analysis for stages of transitional B cell subsets in the spleen of *Regnase-3*$^{-/-}$ mice (von Gamm *et al.*, 2019).**

Flow cytometric analysis for stages of transitional B cell subsets in the spleen of *Regnase-3*$^{-/-}$ mice and their *Regnase-3*$^{+/+}$ littermate controls, assessed at 6 months of age: Cells were pre-gated on life$^{+}$, CD19$^{+}$, AA4.1$^{hi}$ (= CD93) and classified using the Allman scheme (T1, T2, T3 as indicated). Representative plots of n = 6/6.

B cells within hypertrophic lymph nodes had similar low numbers of B plasma cells (CD19$^{+}$, CD138$^{+}$), demonstrating that the increased number of B cells in hypertrophic lymph nodes is not caused by a B plasma cell lymphoma (Figure 42).

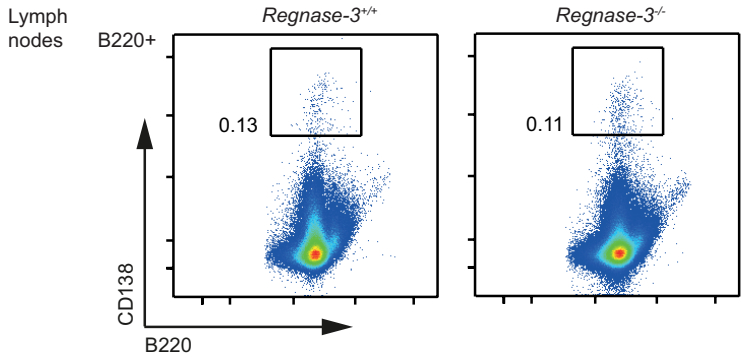


**Figure 42 Analysis of plasma B cells in lymph nodes of *Regnase-3*$^{-/-}$ mice (von Gamm *et al.*, 2019).**

Flow cytometric analysis of plasma B cells (B220$^{+}$, CD138$^{+}$) in lymph nodes of *Regnase-3*$^{-/-}$ mice and their *Regnase-3*$^{+/+}$ littermate controls, assessed at 6 months of age (representative plots of n = 3/3).

Similar IgM/IgD patterns on wildtype B cells and on B cells from hypertrophic lymph nodes in *Regnase-3*$^{-/-}$ mice indicate that B cells in hypertrophic lymph nodes are of follicular origin (Figure 43).

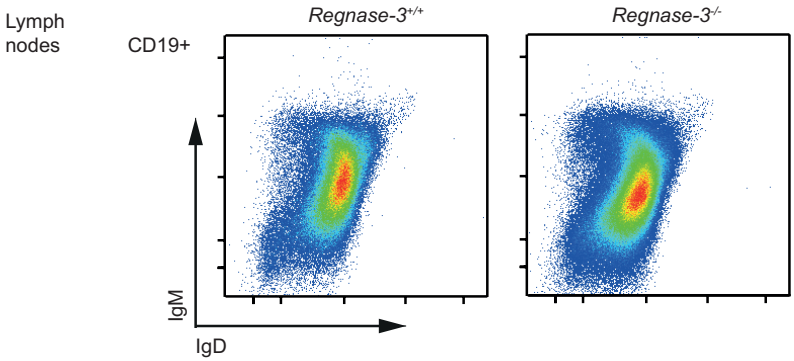


**Figure 43 Analysis of IgD/IgM patterns on B cells in lymph nodes of *Regnase-3*$^{-/-}$ mice (von Gamm *et al.*, 2019)**

Flow cytometric analysis of IgM and IgD expression on B cells (CD19$^{+}$) in lymph nodes of *Regnase-3*$^{-/-}$ mice and their *Regnase-3*$^{+/+}$ littermate controls, assessed at 6 months of age (representative plots of n = 6/6).

## 2.6.2 Proliferation characteristics of *Regnase-3*$^{-/-}$ B cells in *in vivo* and *in vitro*

As previously described, *Regnase-3*$^{-/-}$ mice develop a phenotype with significantly changed B cell subsets in the spleen and highly increased B cell counts in hypertrophic lymph nodes. Thus, we aimed to further analyze the proliferative behavior of B cells from *Regnase-3*-deficient mice, which could provide evidence whether *Regnase-3*$^{-/-}$ mice suffer from a B cell lymphoma. First, the proliferation velocity of splenic B cells from *Regnase-3*$^{+/+}$ and *Regnase-3*$^{-/-}$ mice was evaluated by carboxyfluorescein succinimidyl ester (CFSE) labeling after stimulation with CpG oligodeoxynucleotides (ODN) or LPS. B cells from wildtype and *Regnase-3*$^{-/-}$ mice proliferated equally (Figure 44).

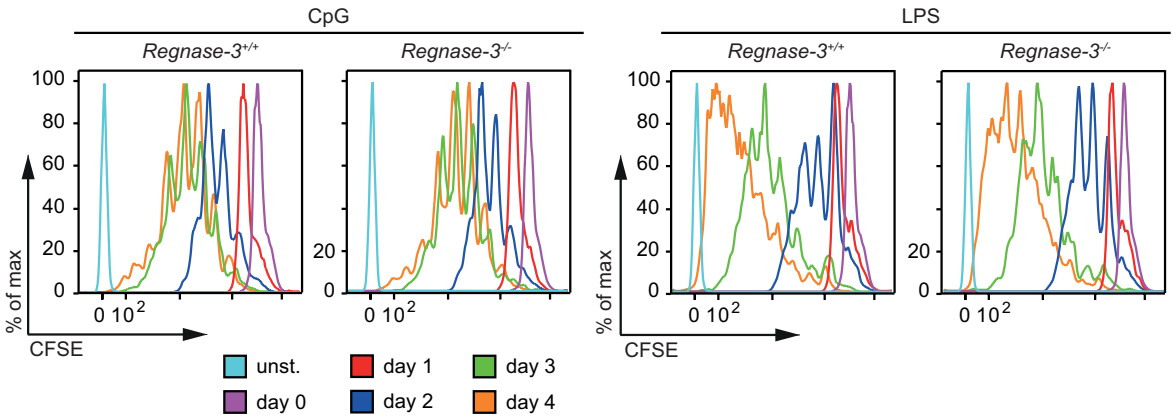


**Figure 44 B cell proliferation assay in *Regnase-3*$^{-/-}$ mice (von Gamm *et al.*, 2019).**

CFSE proliferation assay: Splenic CD19$^{+}$ B cells were isolated from *Regnase-3*$^{-/-}$ and *Regnase-3*$^{+/+}$ mice, using magnetic beads. Cells were labeled with CFSE and stimulated either with LPS (20 µg/ml) or CpG ODN2395 (1 µM) for four days and analyzed every 24h by flow cytometry. (representative plots from n = 3/3 individual animals).

Next, we aimed to get further insights into the *in vivo* proliferation status of B cells within hypertrophic lymph nodes. Thus, immunohistochemistry was used to evaluate the expression levels of the proliferation marker ki67. The ki67 protein is expressed in dividing cells, particularly in the S-phase and disappears from post-mitotic cells (Bruno and Darzynkiewicz, 1992). The number of positively stained cells within hypertrophic lymph nodes of *Regnase-3*$^{-/-}$ mice was comparable to that within wildtype lymph nodes (Figure 45). This further indicated that hypertrophic lymph nodes with increased B cell numbers in *Regnase-3*$^{-/-}$ mice were not caused by a B cell lymphoma.

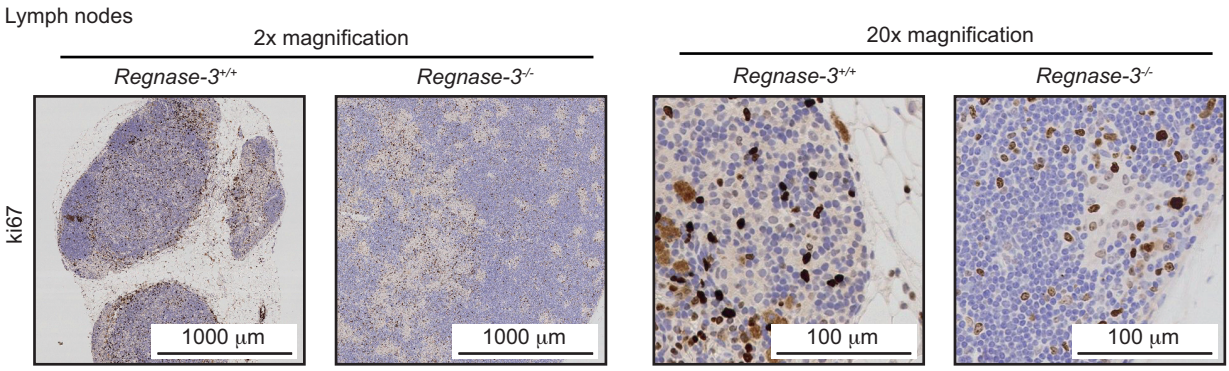


**Figure 45 Analysis of the proliferation marker ki67 in *Regnase-3*$^{-/-}$ mice (von Gamm *et al.*, 2019).**

Immunohistochemical analysis of ki67 in sections from skin draining lymph nodes from *Regnase-3*$^{-/-}$ mice and *Regnase-3*$^{+/+}$ controls. Representative images from n = 3 *Regnase-3*$^{-/-}$ mice with lymphadenopathy and 3 *Regnase-3*$^{+/+}$ controls at 8 months of age, magnifications as indicated.

### 2.6.3 Conditional *Regnase-3* ablation in B cells

To finally depict the role of Regnase-3 in B cells, we generated mice with conditional *Regnase-3* ablation in B cells by crossbreeding *Regnase-3*$^{fl/fl}$ to mice with CD19 promotor driven Cre expression (*Regnase-3*$^{fl/fl}$ +CD19-Cre). None of the 13 analyzed *Regnase-3*$^{fl/fl}$ +CD19-Cre mice developed lymphadenopathy (Figure 46).

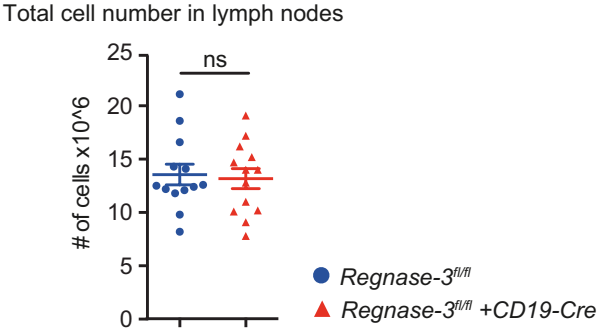


**Figure 46 Conditional *Regnase-3* deficiency in B cells (*Regnase-3*$^{fl/fl}$ +CD19-Cre mice): Cell numbers of lymph nodes (von Gamm *et al.*, 2019).**

Total cell numbers in lymph nodes of *Regnase-3*$^{fl/fl}$ +CD19-Cre mice and their *Regnase-3*$^{fl/fl}$ littermates at 5 months of age (n = 13/13).
Data are represented as mean +/- SEM and were compared by the Mann-Whitney U test (ns = not significant).

Cre positive and Cre negative mice had also similar proportions of T and B cells in their lymph nodes (Figure 47, *left*). Further, the calculated total numbers of B cells and T cells were consequently not significantly altered in mice with conditional deletion of *Regnase-3* in B lymphocytes (Figure 47, *right*).

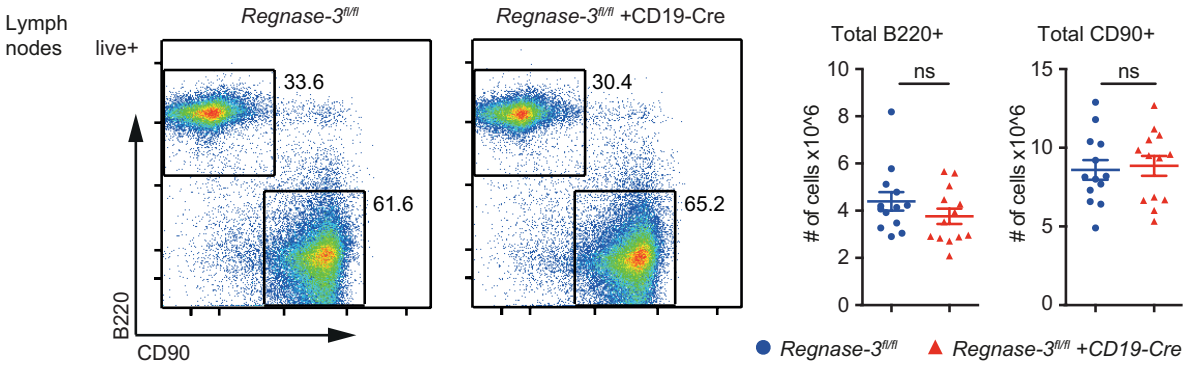


**Figure 47 Conditional *Regnase-3* deficiency in B cells (*Regnase-3*$^{fl/fl}$ +CD19-Cre mice): T and B cell analysis in lymph nodes (von Gamm *et al.*, 2019).**

Flow cytometric analysis of T and B cells: Numbers of calculated total B (B220$^+$) and total T cells (CD90$^+$) in lymph nodes of *Regnase-3*$^{fl/fl}$ +CD19-Cre mice and their *Regnase-3*$^{fl/fl}$ littermates at 5 months of age (n = 13/13). Data are represented as mean +/- SEM and were compared by the Mann-Whitney U test (ns = not significant).

Also splenic B cells subsets, which were altered in globally *Regnase-3*$^{-/-}$ mice, were not significantly changed, when *Regnase-3* was conditionally deleted in B cells. *Regnase-3*$^{fl/fl}$ +CD19-Cre mice had similar numbers of marginal zone B cells as compared to floxed mice (Figure 48).

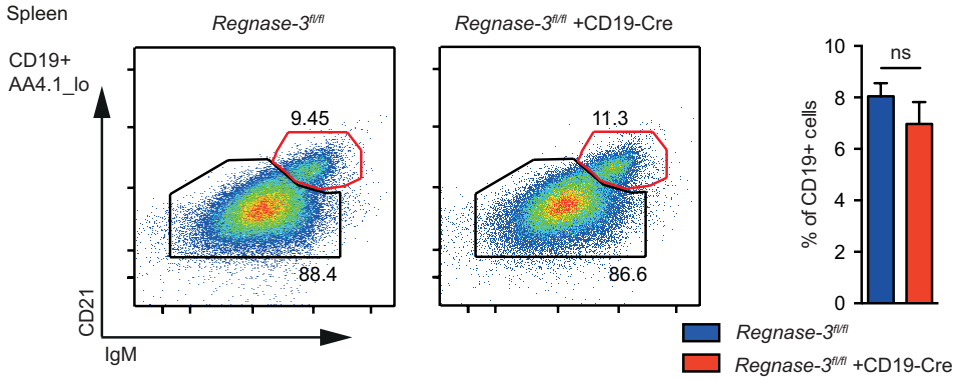


**Figure 48 Conditional *Regnase-3* deficiency in B cells (*Regnase-3*$^{fl/fl}$ +CD19-Cre mice): Analysis of splenic marginal zone B cells (von Gamm *et al.*, 2019).**

Flow cytometric analysis of splenic marginal zone B cells (CD19$^+$, AA4.1$^{lo}$, CD21$^+$/IgM$^{hi}$) in *Regnase-3*$^{fl/fl}$ +CD19-Cre mice and their *Regnase-3*$^{fl/fl}$ littermate controls, assessed at 6 months of age. *Left*: Representative plots (n = 13/13). *Right*: Statistical analysis (n = 13/13).
Data are represented as mean +/- SEM and were compared by the Mann-Whitney U test (ns = not significant).

In summary, the data indicate that altered B cell subsets were not caused by a B cell intrinsic function of Regnase-3 and that in particular hypertrophic lymph nodes seem to be not caused by a B cell lymphoma.

## 2.7 *Regnase-3* expression patterns indicate its significance in the myeloid linage

Data from previous sections demonstrated that major shifts of lymphocyte subsets in *Regnase-3*$^{-/-}$ mice were not caused by an intrinsic function of Regnase-3 in B and T cells. This led to the conclusion that Regnase-3 might be of high relevance in non-immunological cells, such as fibroblast or alternatively in the myeloid linage.

We now aimed to further depict the expression of Regnase-3 and its family members to make suggestions in which tissues, cell types and regulatory conditions Regnase-3 might be important.

### 2.7.1 *Regnase* mRNA steady state expression in tissues and immune cells

Expression analysis of mRNA levels for the four Regnase family members (*Regnase-1*, *-2*, *-3*, *-4*, or *Zc3h12a*, *-b*, *-c*, *-d*) revealed that the 4 *Regnase* family members had quite different and unique expression patterns. *Regnase-1* was broadly expressed in several tissues except the brain with highest expression values in spleen and lymph nodes, supporting published data describing its significant role in T cells (Figure 49). *Regnase-2* was seen to be exclusively high expressed in the intestine, while *Regnase-4* was particularly high expressed in spleen and lymph nodes compared to all other tested tissues (Figure 49). *Regnase-3* revealed to be highest expressed in kidney samples, but very low in thymus, intestine and bone marrow, while its expression was similar high in the non-immunological tissues heart, lung, brain and liver as in the lymphoid tissues spleen and lymph nodes (Figure 49). These expression patterns indicate that different family members seem to be uniquely high expressed in tissues in which other family members have low expression levels.

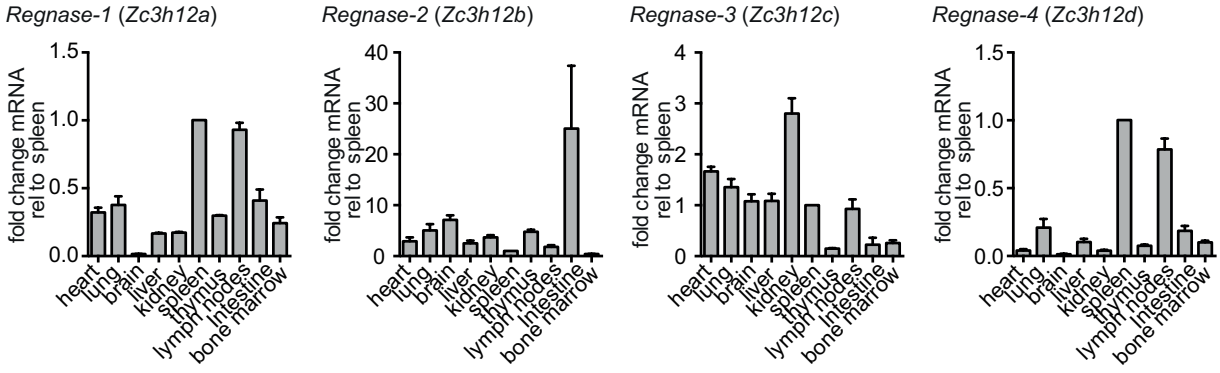


**Figure 49 RNA expression analysis of *Regnase* family members in tissues (von Gamm *et al.*, 2019).**

Tissues were taken from *C57BL/6J* mice and mRNA levels for *Regnase-1* (*Zc3h12a)*, *Regnase-2 (Zc3h12b)*, *Regnase-3* (*Zc3h12c*) and *Regnase-4 (Zc3h12d)* were determined by quantitative RT-PCR. Ct values were normalized to *Hprt1* and are displayed in relativity to their expression in the spleen. Mean +/- SEM from 3 *C57BL/6J* mice.

### 2.7.2 *Regnase* mRNA expression patterns upon immune cell stimulation

Different primary immune cell types were isolated or differentiated from mice and activated via T and B cell receptor stimulation or were treated with various Toll-like receptor agonists and mRNA expression patterns of *Regnase* family members were determined over time. This assay should suggest immune cell types and conditions under which Regnase-3 might be of high or unique relevance and could help to explain the *in vivo* relevance of Regnase-3. Bone marrow derived macrophages and dendritic cells were activated with the TLR4 agonist LPS, the TLR3 agonist polyinosinic-polycytidylic acid (poly-I:C / p-I:C) and the TLR9 agonist CpG ODN oligonucleotide. B cells were activated with anti IgM antibodies, LPS or CpG and T cells were activated with anti-CD3 and anti-CD28 antibodies or with poly-I:C. Overall, the regulation of *Regnase-3* mRNA expression upon stimulation under several conditions was comparable to that of *Regnase-1* and could not fully predict conditions in which Regnase-3 fulfills a unique function (Figure 50).

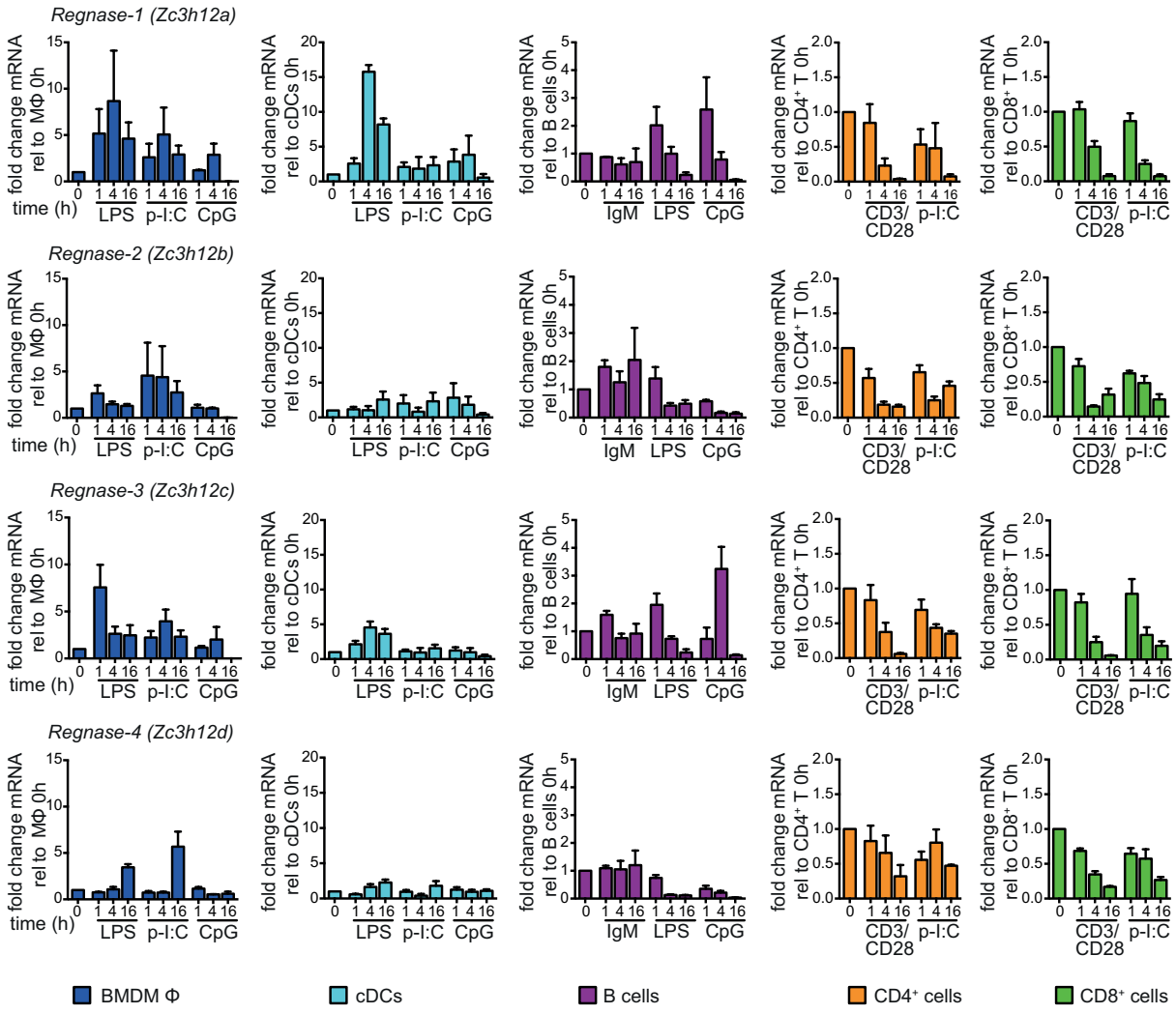

**Figure 50 RNA expression analysis of *Regnase* family members in immune cells (von Gamm *et al.*, 2019).**

Cells were isolated or differentiated as described in material and methods. *In vitro* differentiated bone marrow derived macrophages (BMDM Φ) and *in vitro* differentiated conventional dendritic cells (cDCs) were treated with LPS (100 ng/ml), low molecular weight poly-I:C (20 μg/ml), C-type CpG ODN 2395 (1 μM) for 1, 4 or 16 hours or were left untreated. B cells were positively selected from the spleen ($B220^+$ cells) and were then stimulated with anti-IgM (10 μg/ml), LPS (20 μg/ml) or C-Type CpG ODN 2395 (1 μM) for 1, 4 or 16 hours or were left untreated. $CD4^+$ and $CD8^+$ T cells were positively selected from the spleen (*via* CD4 and CD8 antigens) and were then stimulated with plate bound anti-CD3 and anti-CD28 or low molecular weight poly-I:C (20 μg/ml) for 1, 4 or 16 hours or were left untreated. RNA was isolated and mRNA expression levels for *Regnase-1* (*Zc3h12a*), *Regnase-2* (*Zc3h12b*), *Regnase-3* (*Zc3h12c*) and *Regnase-4* (*Zc3h12d*) were determined by RT-PCR. Ct values were normalized to *Hprt1* and are displayed in relativity to untreated cells. Mean +/- SEM from 3 independent experiments.

## 2.7.3 Development of a novel Regnase-3-specific monoclonal antibody

Commercially available anti-Regnase-3-specific antibodies were tested, but revealed to generate high background and unspecific binding in immunoblots of tissues and immune cell types. Thus, we generated a novel Regnase-3-specific antibody. Therefore, recombinant full length Regnase-3 protein with point mutation in the RNase domain and N-terminal GST-tag was derived and purified from bacteria. The Regnase-3 protein was used to immunize mice and rats from which hybridoma cell lines were derived. Several hundred cell culture supernatants were tested in consecutive steps first by ELISA and further in immunoblot assays on samples with overexpressed Regnase-3 protein and on murine tissues with *Regnase-3*-deficient tissue as control and revealed clone #4D3 as promising candidate. As schematically displayed in the protein alignment, the different family members share highly conserved domains for RNase and zinc finger domains (Figure 51). Regnase-3 shares higher sequence homology with Regnase-2 as compared to its other family members.

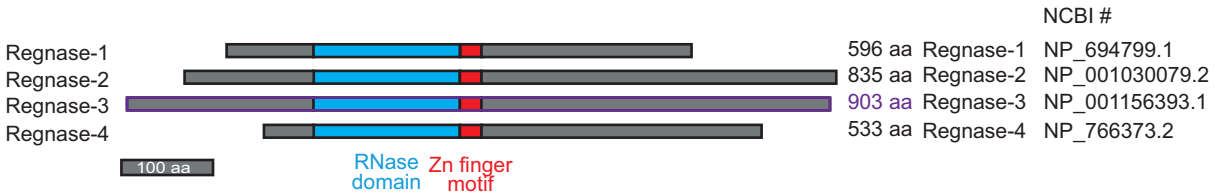


**Figure 51 Protein sequence alignment of *Regnase* family members (von Gamm *et al.*, 2019).**

Protein sequences were acquired from NCBI, accession numbers as indicated. Sequences were aligned using T coffee (http://tcoffee.crg.cat) with 'M-Coffee' algorithm. Aligned RNase domains and Zn finger motifs are highlighted.

Immunoblot analysis with overexpression of all Regnase family members with N-terminal GFP-tag revealed that antibody clone #4D3 strongly recognizes Regnase-3, but not Regnase-1 or Regnase-4. Overexpressed Regnase-2 was also recognized by clone #4D3, but to a lower extent as Regnase-3 (Figure 52). Since *Regnase-2* mRNA was expressed particularly in the intestine, but not in high levels in tissues with high *Regnase-3* expression, we considered the antibody as suitable for further evaluation of Regnase-3 protein (Figure 49). In addition, Regnase-2 and -3 differ in their calculated molecular weights, which would help to further discriminate the family members.

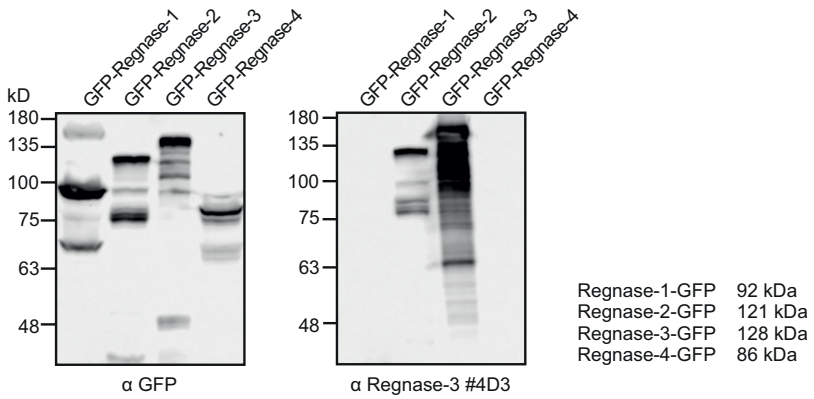


**Figure 52 Verification of the newly developed anti Regnase-3 antibody (von Gamm *et al.*, 2019).**

GFP-tagged Regnase-1, -2, -3 and -4 were overexpressed in 293T and analyzed by immunoblot. Predicted protein weights are indicated. *Left*: Anti-GFP as loading control, *Right*: anti-Regnase-3 (clone #4D3).

### 2.7.4 Regnase protein expression in tissues and immune cells

Immunoblot analysis of different murine tissues with our newly developed Regnase-3-specific antibody revealed that Regnase-3 is highly expressed in the non-lymphoid tissues lung, brain and particularly in the kidney. In clear contrast, Regnase-1 expression was highest in the lymphoid tissues spleen, thymus and lymph nodes as well as in the intestine (Figure 53). Additionally, it was recognized that Regnase-3 protein migrates at least in two versions in SDS-PAGE gels. The lower migrating band is in the range of the predicted molecular weight of 101 kD, while the upper one is approximately 7 to 15 kD larger. Tissue and immune cell samples from *Regnase-3*$^{-/-}$ mice revealed that both bands are specific, as they do not appear in the knockout samples (Figure 53 and Figure 54).

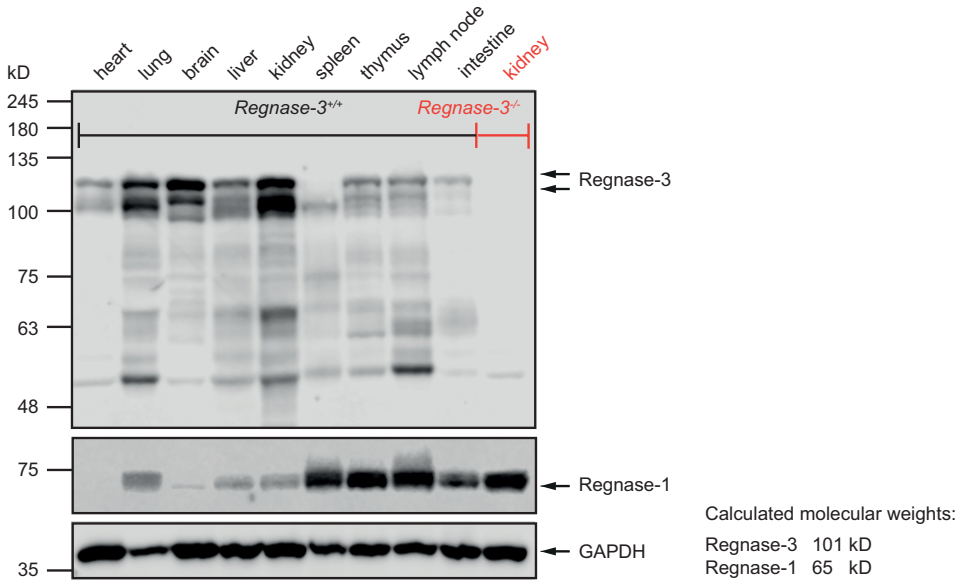


**Figure 53 Regnase-3 protein steady state expression in tissues (von Gamm *et al.*, 2019).**

Tissues were taken from *C57BL/6J* mice and processed to generate protein lysates. 400 µg total wet tissue was loaded per lane. Kidney lysate of a *Regnase-3*$^{-/-}$ mouse was loaded as negative control to prove specificity of the newly generated anti-Regnase-3 antibody (#4D3). Shown is one representative blot from 3 independent experiments.

In addition, several immune cells were isolated or differentiated from murine tissue and analyzed for Regnase-1 and -3 protein expression. While Regnase-1 was ubiquitously expressed in all immune cell types with lowest expression in macrophages, the Regnase-3 expression pattern was completely different. Regnase-3 was not expressed in $CD4^+$ and $CD8^+$ T cells, very low or almost undetectable expression was observed for B cells and Neutrophils, while high expression levels were seen in bone marrow derived conventional dendritic cells (cDCs) and in particular in bone marrow derived macrophages (BMDM).

Both in tissues as well as in immune cell subsets, Regnase-1 and -3 had expression levels with inverse correlation (Figure 53 and Figure 54). Of note, Regnase-1 expression was massively upregulated in *Regnase-3*-deficient kidney samples and macrophages as compared to their wildtype counterpart, suggesting a direct or indirect counter regulation of these two family members (Figure 53 and Figure 54).

In summary, we generated a novel Regnase-3 specific antibody, which has some cross-reactivity to Regnase-2 and found highest Regnase-3 protein expression in non-lymphoid tissues and macrophages.

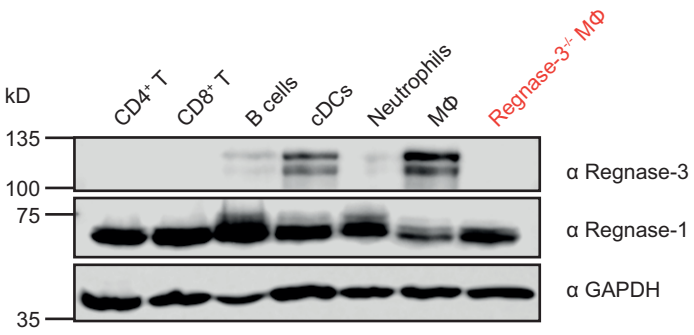


**Figure 54 Regnase-3 protein expression in immune cells (von Gamm *et al.*, 2019).**

Splenic $CD4^+$ T cells, splenic $CD8^+$ T cells, B cells ($CD19^+$), conventional dendritic cells (cDCs), bone marrow neutrophils and bone marrow derived macrophages (BMDM Φ) were isolated or differentiated as described in materials and methods. Macrophage lysate of a *Regnase-3*$^{-/-}$ mouse was loaded as negative control to prove specificity of the newly generated anti-Regnase-3 antibody (#4D3). Shown is one representative blot from 3 independent experiments.

## 2.8 Hypertrophic lymph nodes are caused by myeloid cells

Conditional mouse models demonstrated that T and B cells are not responsible to provoke hypertrophic lymph nodes in *Regnase-3*-deficient mice. Further, Regnase-3 protein expression suggested an important role for Regnase-3 in non-llymphoid tissues as well as in macrophages. Thus, we aimed to further understand Regnase-3 *in vivo* functions and generated mice with conditional *Regnase-3* ablation in the myeloid linage. For this, *Regnase-3*$^{fl/fl}$ mice were crossed to mice expressing Cre under the LysM promotor to generate *Regnase-3*$^{fl/fl}$ +LysM-Cre mice. LysM-Cre deletes floxed alleles in a broad range of myeloid cells, with an efficiency of almost 100% in tissue-resident macrophages, but only about 40%

efficiency in splenic macrophages. With 60% – 80% success rate, Cre activity is also high in neutrophils, but rather low (10% or less) in other myeloid subsets, such as dendritic cells, eosinophils, natural killer cells or mast cells (Abram *et al.*, 2014).

### 2.8.1 Analysis of lymph nodes in myeloid-specific *Regnase-3*-deficient mice

Conditional deletion of *Regnase-3* in the myeloid linage caused a very similar phenotype as it was observed in globally *Regnase-3*-deficient mice. Similar to globally *Regnase-3*-deficient mice, also *Regnase-3*$^{fl/fl}$ +LysM-Cre mice developed hypertrophic skin-draining lymph nodes, which could contain several hundred million of cells in some individuals (Figure 55 and Figure 56 A).

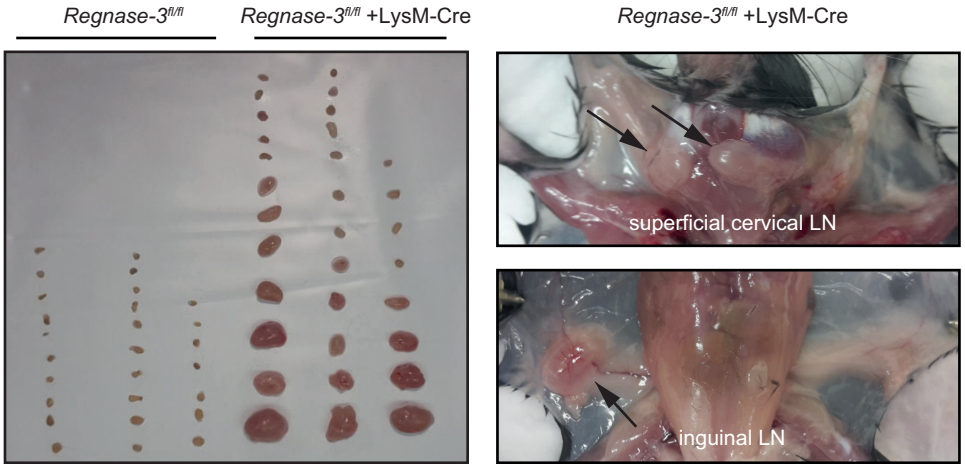


**Figure 55 Conditional *Regnase-3* deficiency in the myeloid linage (*Regnase-3*$^{fl/fl}$ +LysM-Cre): Lymphadenopathy (von Gamm *et al.*, 2019).**

*Left*: Photograph of skin draining lymph nodes (superficial cervical, axillary, brachial and inguinal) of 3 *Regnase-3*$^{fl/fl}$ +LysM-Cre mice and their *Regnase-3*$^{fl/fl}$ littermates at 5 months of age. *Right*: Representative images for hypertrophic superficial cervical and inguinal lymph nodes in a *Regnase-3*$^{fl/fl}$ +LysM-Cre mouse at 5 months of age.

As previously observed for globally *Regnase-3* deficiency, also hypertrophic lymph nodes in *Regnase-3*$^{fl/fl}$ +LysM-Cre mice contained increased numbers of both B cells as well as T cells. Flow cytometric analysis revealed that the total calculated proportions of B cells (CD19$^+$) as well as CD4$^+$ and CD8$^+$ T cells were significantly increased (Figure 56 B).

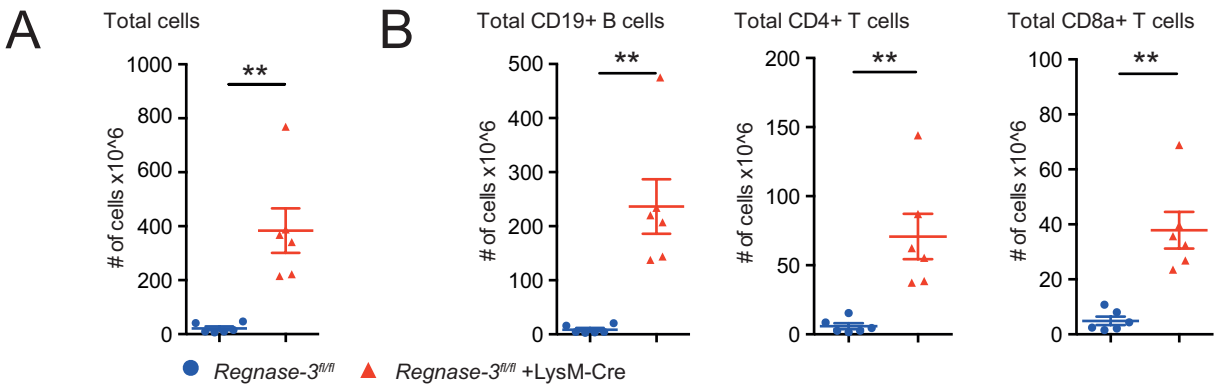


**Figure 56 Conditional *Regnase-3* deficiency in the myeloid linage (*Regnase-3*$^{fl/fl}$ +LysM-Cre mice): T and B cell analysis in lymph nodes, total numbers (von Gamm *et al.*, 2019).**

(A) Total cell numbers in lymph nodes of *Regnase-3*$^{fl/fl}$ +LysM-Cre mice and their *Regnase-3*$^{fl/fl}$ littermates at 5 months of age (n = 6/6).
(B) Flow cytometric analysis of T and B cells: Numbers of calculated total B (CD19$^+$) and total CD4$^+$ and CD8$^+$ T cells in lymph nodes of *Regnase-3*$^{fl/fl}$ +LysM-Cre mice and their *Regnase-3*$^{fl/fl}$ controls at 5 months of age (n = 6/6). Data are represented as mean +/- SEM and were compared by the Mann-Whitney U test (** p ⩽ 0.01).

Moreover, flow cytometric analysis demonstrated that several immune cell subsets in *Regnase-3*$^{fl/fl}$ +LysM-Cre mice with hypertrophic lymph nodes showed similar shifts as compared to *Regnase-3*$^{-/-}$ mice. The proportion of B cells (CD19$^+$) was increased and T cells (CD90$^+$) were decreased in lymph nodes of myeloid *Regnase-3*-deficient mice (Figure 57). Among T lymphocytes, the proportion of CD4$^+$ T cells was increased, while CD8$^+$ T cells were decreased (Figure 57). These effects are similar to those in globally deficient mice. CD4$^+$ effector T cells, which were slightly increased in globally deficient mice, as well as CD8$^+$ effector memory T cells were not significantly changed in *Regnase-3*$^{fl/fl}$ +LysM-Cre mice (Figure 57).

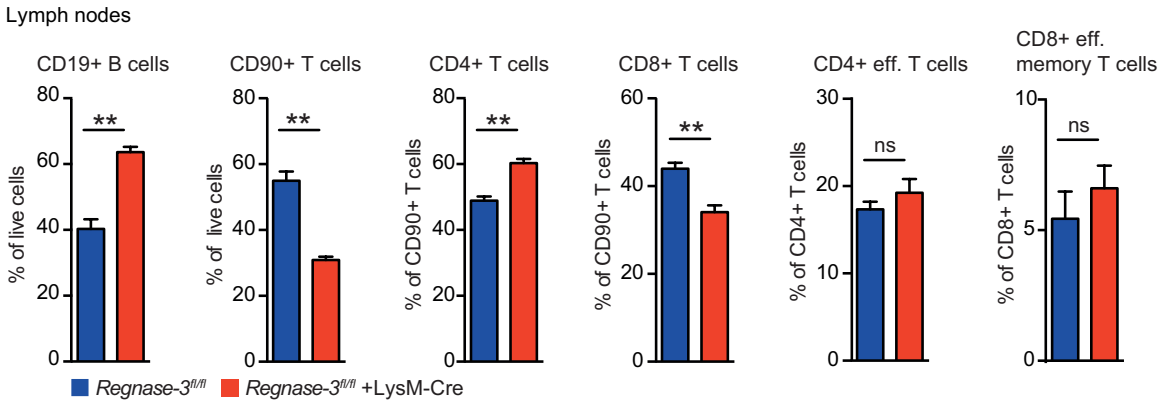


**Figure 57 Conditional *Regnase-3* deficiency in the myeloid linage (*Regnase-3*$^{fl/fl}$ +LysM-Cre mice): T and B cell analysis in lymph nodes, proportions (von Gamm *et al.*, 2019).**

Flow cytometric analysis of T and B cell subsets in lymph nodes of *Regnase-3*$^{fl/fl}$ +LysM-Cre mice and their *Regnase-3*$^{fl/fl}$ littermate controls, assessed at 6 months of age (n = 6/6): Percentages for B cells (CD19$^+$), T cells (CD90$^+$), CD4$^+$ and CD8$^+$ T cells, CD4$^+$ effector (CD19$^-$, CD90$^+$, CD4$^+$, CD62L$^-$/CD44$^{hi}$) and CD8$^+$ effector memory T cells (CD19$^-$, CD90$^+$, CD8a$^+$, CD62L$^-$/CD44$^{hi}$).
Data are represented as mean +/- SEM and were compared by the Mann-Whitney U test (** p ⩽ 0.01, ns = not significant).

### 2.8.2 Splenic lymphocyte populations in myeloid-specific *Regnase-3*-deficient mice

Also splenic lymphocyte populations were analyzed in *Regnase-3*$^{fl/fl}$ +LysM-Cre mice in order to determine whether the phenotypic observations in globally deficient mice were also reflected in mice with a myeloid-specific ablation. Indeed, similar shifts in lymphocyte populations were also seen in the spleen. The percentages of CD8$^+$ effector memory T cells, as well as marginal zone B cells and immature B cells were increased in *Regnase-3*$^{fl/fl}$ +LysM-Cre mice (Figure 58).

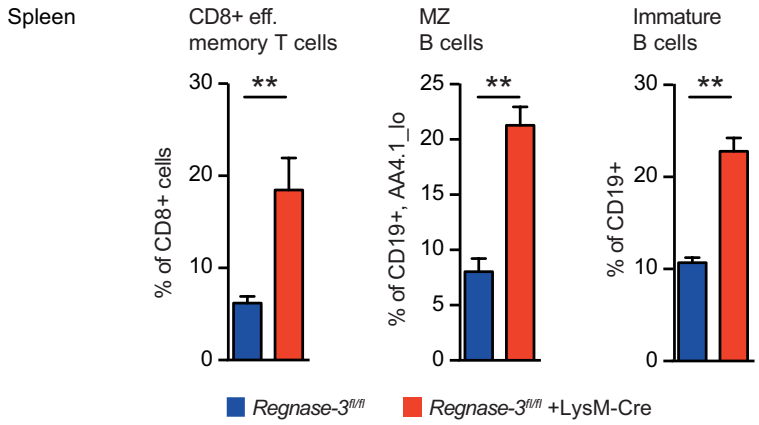


**Figure 58 Conditional *Regnase-3* deficiency in the myeloid linage (*Regnase-3*$^{fl/fl}$ +LysM-Cre mice): Splenic T and B cell subsets (von Gamm *et al.*, 2019).**

Flow cytometric analysis of splenic T and B cell subsets in *Regnase-3*$^{fl/fl}$ +LysM-Cre mice and their *Regnase-3*$^{fl/fl}$ littermate controls, assessed at 6 months of age (n = 6/6): Percentages of splenic CD8$^+$ effector memory T cells (CD19$^-$, CD90$^+$, CD8$^+$, CD62L$^-$/CD44$^{hi}$), marginal zone (MZ) B cells (CD19$^+$, AA4.1$^{lo}$, CD21$^+$/IgM$^{hi}$) and immature B cells (CD19$^+$, IgD$^{lo}$/IgM$^{hi}$).
Data are represented as mean +/- SEM and were compared by the Mann-Whitney U test (** $p \leq 0.01$).

In summary, *Regnase-3*$^{fl/fl}$ +LysM-Cre mice were seen to develop pathophysiological manifestations within the immune system that were comparable to that in globally *Regnase-3*-deficient mice with respect to its characteristics and magnitude. In particular, the incidence of hypertrophic lymph nodes with several million cells and a shift towards increased proportion of B cells were reflected in conditional myeloid deficient mice. These data strongly indicate that Regnase-3 is highly important in the myeloid linage and that its ablation in myeloid cells causes lymphadenopathy *in vivo*. Taking in account that Regnase-3 is very low expressed in neutrophils and in the bone marrow, which contains high numbers of neutrophils, it is rather unlikely that Regnase-3 fulfills major functions within this cell type. Thus, macrophages and in particular tissue macrophages, in which LysM-Cre deletes with almost 100% efficiency, are likely the most relevant cell type for Regnase-3 function *in vivo*.

### 2.8.3 Analysis of IFNγ source in myeloid-specific *Regnase-3*-deficient mice

Pro-inflammatory cytokines were also analyzed in blood sera of *Regnase-3*$^{fl/fl}$ +LysM-Cre mice and their *Regnase-3*$^{fl/fl}$ littermate controls. Again, IFNγ serum concentrations were significantly increased in *Regnase-3*$^{fl/fl}$ +LysM-Cre mice, while other pro-inflammatory cytokines appeared unchanged (Figure 59). This indicated that indeed deregulated interferons might be involved in the pathogenicity caused by *Regnase-3* deficiency *in vivo*.
Although macrophages are capable to secrete large amounts of IFNγ under certain stimulatory conditions, sources of systemic IFNγ are classically assigned to activated T cells, in particular cytotoxic T cells and CD4$^+$ $T_h$1 cells as well as natural killer cells (Munder *et al.*, 1998). Thus, it remains unclear, whether *Regnase-3* deficiency in the myeloid linage causes an intrinsic defect with increased IFNγ secretion by macrophages or if elevated serum IFNγ levels are of secondary origin.

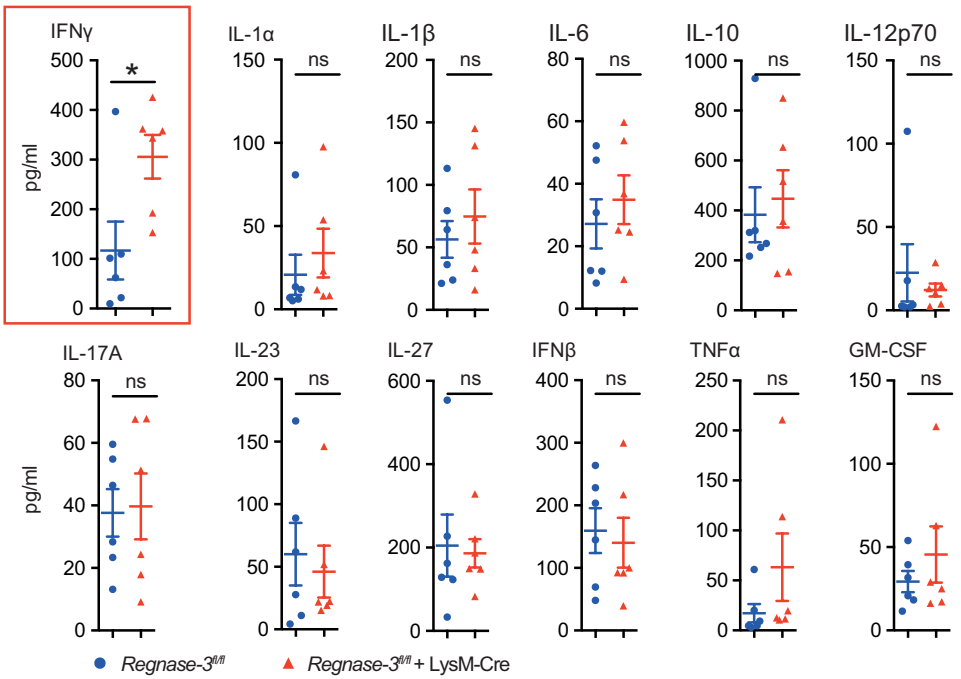


**Figure 59 Serum cytokine concentrations in *Regnase-3*$^{fl/fl}$ +LysM Cre mice.**

Blood serum was taken from *Regnase-3*$^{fl/fl}$ +LysM-Cre mice and their *Regnase-3*$^{fl/fl}$ littermate controls, assessed at 5 months of age (n = 6/6). Inflammatory cytokines were measured in a multiplex assay. Data are represented as mean +/- SEM and were compared by the Mann-Whitney U test (* $p \leq 0.05$, ns = not significant).

To more precisely localize the origin of IFNγ secretion, cells from lymph nodes and spleen of *Regnase-3*$^{fl/fl}$ +LysM-Cre mice and their floxed littermates were isolated and analyzed regarding their IFNγ production *ex vivo*. Therefore, extracted cells were activated with a combination of Inomycin and Phorbol-12-myristat-13-acetat (PMA). Ionomycin is a ionophore that causes $Ca^{2+}$ signaling and induces the serine/threonine protein phosphatase Calcineurin, which in turn activates the transcription factor Nuclear factor of activated

T cells cytoplasmic (NFATc) (Brignall *et al.*, 2017; Macian *et al.*, 2002). Thus, Ionomycin strongly activates T cell receptor downstream signaling, without the necessity of a direct stimulatory signal (Brignall *et al.*, 2017; Gaud *et al.*, 2018). PMA is an activator of the protein kinase C, which further promotes signal transduction *via* the NF-κB pathway and activation of the T cell co-receptor CD28 (Brignall *et al.*, 2017; Macian *et al.*, 2002; Gaud *et al.*, 2018). Together, PMA and Ionomycin mimic CD3/CD28 activation on T cells and induce cytokine production. Then, cells were supplemented with Brefeldin A, which is used as protein transport inhibitor to prevent cytokine secretion (Fujiwara *et al.*, 1988; Rajamahanty *et al.*, 2010). T cell activation with PMA and Ionomycin combined with secretion inhibition results in massive accumulation of cytokines within the cell. Subsequent flow cytometric analysis with surface stain for immune cell markers, together with intracellular immunostain for IFNγ allows determining the amount of activated cell subsets, such as cytotoxic effector T cells, which are capable of strong IFNγ production.

In particular, the proportion of IFNγ positive cells within the subset of $CD4^+$ helper T cells was increased in lymph nodes of *Regnase-3*$^{fl/fl}$ +LysM-Cre mice with lymphadenopathy (Figure 60, *top center*).

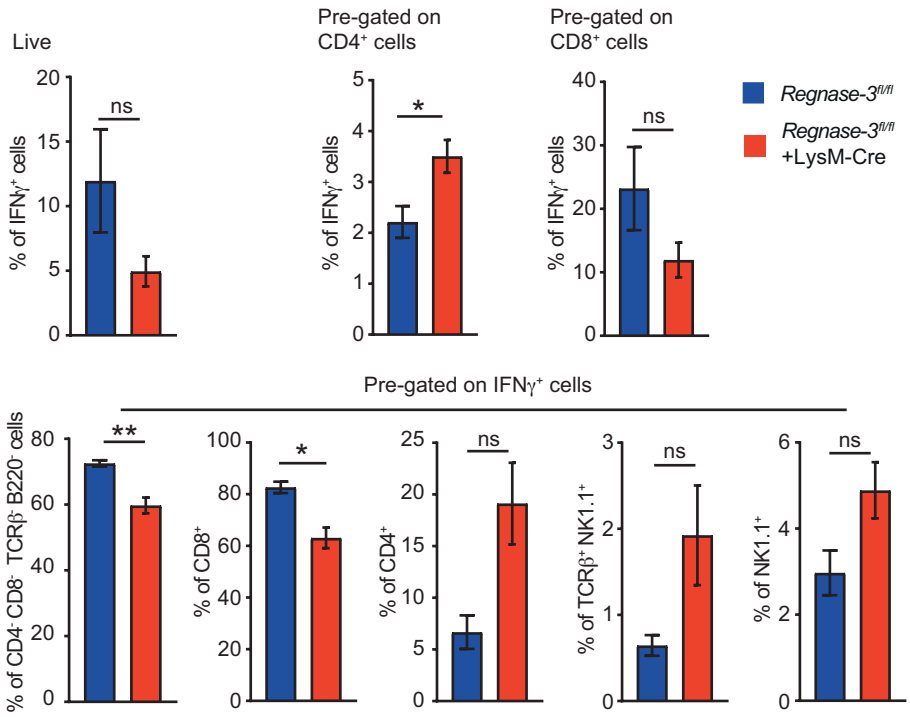


**Figure 60 Analysis of intracellular IFNγ production in *Regnase-3*$^{fl/fl}$ +LysM-Cre mice (von Gamm *et al.*, 2019).**

Cells from lymph nodes were isolated from lymph nodes of *Regnase-3*$^{fl/fl}$ +LysM-Cre mice with lymphadenopathy and their *Regnase-3*$^{fl/fl}$ littermate controls at 8 months of age (n = 4/3). Cells were subsequently treated with Phorbol-12-myristat-13-acetat (PMA; 20 nM) and ionomycin (1 μM) for 4h. For the second 2h, Brefeldin A (5 μg/ml) was added. Cells were first surface stained for CD4, CD8, B220, TCRβ, NK1.1 and life/dead marker and then intracellular stained for IFNγ. Cells were analyzed by flow cytometry and pre-gated as indicated. Data are represented as mean +/- SEM and were compared by the unpaired two-tailed students t-test (* $p \leq 0.05$, ** $p \leq 0.01$, ns = not significant).

## 2.9 Regnase-3 regulation in macrophages

We could verify that *Regnase-3* ablation within the myeloid linage caused hypertrophic lymph nodes *in vivo* and predicted macrophages in particular to be the relevant cell type. Thus, we aimed to further reveal the molecular role of Regnase-3 protein in macrophages.

### 2.9.1 Regnase-3 expression during macrophage maturation

An *in vitro* system was used to study differentiation of macrophages over time. In this system, a monocyte progenitor cell line is maintained by estrogen receptor (ER) driven overexpression of the transcription factor Homeobox protein B8 (Hoxb8) and supplementation of stem cell factor (SCF) to the growth medium (Wang *et al.*, 2006). Estrogen and SCF withdrawal in combination with recombinant M-CSF supplementation to the growth medium drives the cells into macrophage differentiation.
Cells were differentiated over eight days and samples were taken every day to analyze Regnase-1 and -3 protein expression over time. Surprisingly, Regnase-3 was highly expressed only at the very late phase of macrophage differentiation from day 6 to day 8, while in contrast Regnase-1 was ubiquitous expressed in all samples from the very beginning of differentiation (Figure 61).
In addition, protein expression of several transcription factors, which participate in macrophage differentiation were also studied over time. Regnase-3 expression highly correlated with the occurrence of the transcription factor Early growth response 2 (EGR2) (Figure 61). Nevertheless, these data do not give any evidence, whether Regnase-3 might be transcriptionally regulated by EGR2, or if the expression solely correlates with terminally differentiated macrophages.

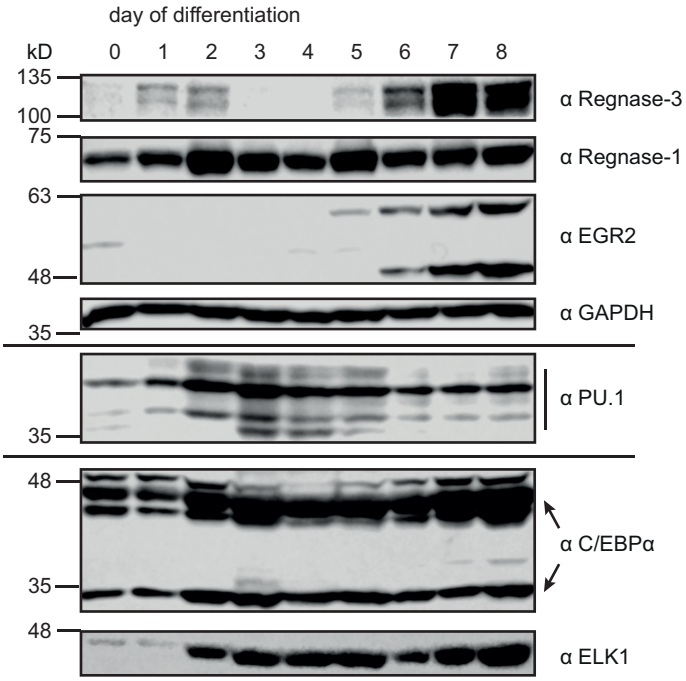


**Figure 61 Differentiation of myeloid progenitor cells into macrophages (von Gamm *et al*., 2019).**

A bone marrow derived myeloid progenitors cell line with estrogen receptor controlled overexpression of the transcription factor Hoxb8 was differentiated into mature macrophages by withdrawal of estrogen and supplementation of recombinant GM-CSF (20 ng/ml) to the cell culture medium. During maturation, cells were harvested every day and protein lysates were generated. Regnase-1 and Regnase-3 expression over time was then observed by immunoblot analysis. Shown is one representative immunoblot of n = 2 independent experiments.

Macrophage populations in human and mice were traditionally subdivided into two major branches, the pro-inflammatory M1 and anti-inflamatory M2 populations. Further information regarding nomenclature, origin and complexity of the M1-M2 paradigm are found in the introduction. Thus, we aimed to compare Regnase-3 expression under M1 or M2 priming conditions. Bone marrow derived macrophages were classically activated under M1 condition with LPS and IFNγ or were alternatively activated under M2 condition with IL-4 or were left untreated (M0 condition). Regnase-3 expression was slightly increased under M1 priming conditions as compared to M0 or M2 conditions (Figure 62, *left*). Successful priming was checked by flow cytometry analysis of markers that are either upregulated under M1 conditions (CD38) or M2 conditions (CD206) (Figure 62, *right*) (Jablonski *et al.*, 2015).

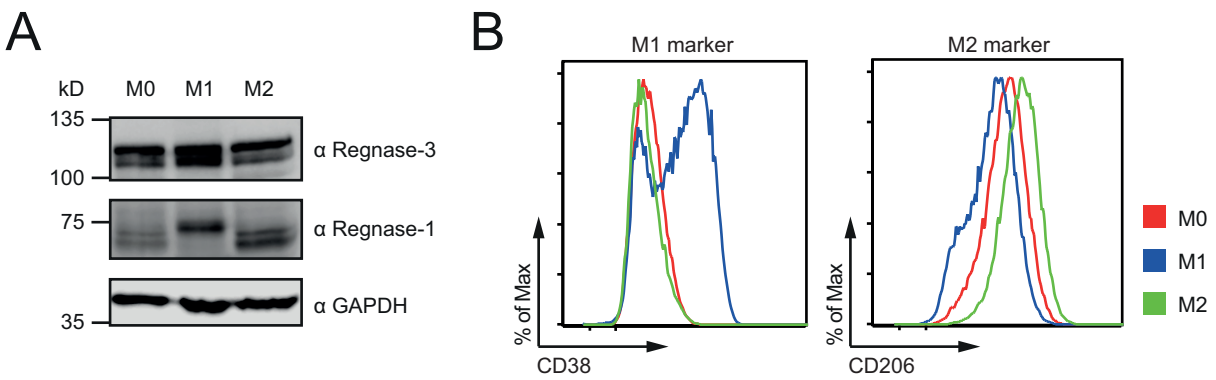


**Figure 62 Classical (M1) and alternative (M2) activation of macrophages (von Gamm *et al.*, 2019).**

(A) BMDM were differentiated from bone marrow of *C57BL/6J* mice and then classically activated by treatment with LPS (100 ng/ml) plus IFNγ (20 ng/ml) for 24h (M1 condition) or were alternatively activated by treatment with IL-4 (20 ng/ml) for 24h (M2 condition) or were left untreated (M0 condition). Regnase-1 and Regnase-3 expression in protein lysates was analyzed by immunoblot. A representative blot of n = 3 experiments is shown. (B) BMDM were activated as described in (A) and shifts towards M1 and M2 conditions were verified by flow cytometric analysis of markers, which were reported to be upregulated in M1-like macrophages (CD38) or M2-like macrophages (CD206).

### 2.9.2 Regnase-3 protein is like Regnase-1 regulated by the IKK complex

Regnase-1 has been described to be phosphorylated by the IKK complex, consisting of IKKα, IKKβ and NF-κB essential modulator (NEMO) (Iwasaki *et al.*, 2011). The IKK complex is activated upon induction of the NF-κB pathway, such as stimulation with the TLR4 agonist LPS, which causes Regnase-1 phosphorylation and subsequent polyubiquitination and degradation via the proteasome (see introduction). NEMO is indispensible for sufficient phosphorylation by the IKK complex and Regnase-1 degradation is thus inhibited in *NEMO*-deficient cells (Iwasaki *et al.*, 2011). Also treatment with the proteasome inhibitor MG132 prevented LPS induced degradation of Regnase-1 in HeLa cells (Iwasaki *et al.*, 2011).

Iwasaki *et al.* identified the DSGxxS motif to be targeted by the IKK complex, which is present as DSGIGS sequence in the Regnase-1 protein. In particular, the two serine residues (Ser435 and Ser439) within this sequence are phosphorylated by the IKK complex (see also in introduction).

Detailed sequence analysis of Regnase family members revealed that Regnase-3 contains a similar, but not identical motif. Also Regnase-3 has a motif in which two serine residues (Ser622 and Ser626) are spaced by three amino acids. In contrast to the described DSGxxS motif, Regnase-3 has an amino acid sequence of ISGPRS and thus aspartic acid is replaced by isoleucine (Figure 63). Different to Regnase-1 and -3, family members Regnase-2 and -4 had not such a motif.

Regnase-1 (Zc3h12a)

MSDPCGTKPVQESNPTMSLWSLEDRHSSQGRPQPDQDPVAKEAPTSELQMKVDFFRKLGYSSSEIHSVLQ
KLGVQADTNTVLGELVKHGSATERECQALTAPSPQPPLVPRGGSTPKPSTLEPSLPEEDREGSDLRPVVI
DGSNVAMSHGNKEVFSCRGILLAVNWFLERGHTDITVFVPSWRKEQPRPDVPITDQHILRELEKKKILVF
TPSRRVGGKRVVCYDDRFIVKLAFESDGVVVSNDTYRDLQGERQEWKRFIEERLLMYSFVNDKFMPPDDP
LGRHGPSLDNFLRKKPLPSEHRKQPCPYGKKCTYGIKCRFFHPERPSRPQRSVADELRANALLSPPRTPV
KDKSSQRPSPASQSSSVSLEAEPGSLDGKKLGARSSPGPHREGSPQTCAPAGRSLPVSGGSFGPTEWLAH
TQDSLPYTSQECLDSGIGSLESQMSELWGVRGGSPGESGPTRGPYAGYHSYGSKVPAAPSFSPFRPAMGA
GHFSVPTDYVPPPPTYPSREYWSEPYPLPPPTPVLQEPQRPSPGAGGGPWGRVGDLAKERAGVYTKLCGV
FPPHLVEAVMRRFPQLLDPQQLAAEILSYKSQHLSE

DSGIGS Ser435 Ser439

Regnase-3 (Zc3h12c)

MEAGPGAAEGNGPTAVILPLGPSRARGEYGVLCIQEYRKSSKVESSARNSFMGLKDHLGHDLGHLYMEST
DPQMSAAVPWPMVEKPTMDTVNSGKEGKGVSEENVSSGDSEGSTSSDHESEQLSSLSVEPCSLTKTHRQL
CRSPCLEPRLLKHSDILQDFKPEESQTPSKEVKKPPDVVREYQTKLEFALKLGYSEEQVQLVLNKLGTDA
LINDILGELVKLGNKSEADQTVSTINSVMRETSSLESQRSESPMQEVVVDDGENLRPVVIDGSNVAMSHG
NKEVFSCRGIKLAVDWFLERGHKDITVFVPAWRKEQSRPDALITDQEILRKLEKEKILVFTPSRRVQGRR
VVCYDDRFIVKLAFESDGIIVSNDNYRDLANEKPEWKKFIDERLLMYSFVNDKFMPPDDPLGRHGPSLDN
FLRKKPIVPEHKKQPCPYGKKCTYGHKCKYYHPERGSQPQRSVADELRAMSRNTAAKTTNEGGLVKSNSV
PCSTKADSTSDVKRGAPKRQSDPSIRTHVYQDIEEKLPTKNKLETRSVPSLVSIPATSTAKPQSTTPLSN
GLPSGVHFPPQDQRPQGQYPPMMMATKNHGTPMPYEQYPKCDSPVDVGYYSMLNAYSNLSISGPRSPERR
FSLDTDYRVNSVASDCSSEGSMSCGSSDSYVGYNDRSYVSSPDPQLEESLKCQHMHPHSRLNSQPFLQNF
HDPLTRVQSYSHEEPKFHPKRPLPHLAMHLQHPAVGARSSCPGDYPSPPSSAHSKAPHLGRSLVATRIDS
ISDSRLYDSSPSRQRKPYSRQEGLGSWGRPSYGLEAYGYRQTYSLPDNSTPPCYESITFQSLPEQQEPTW
RIPYCGMPHDPPRYQDNREKIFINLCNIFPPDLVRLVMKRNPHMTDAQQLAAAILVEKSQLGY

ISGPRS Ser622 Ser626

Comparison

| Motif | DSGXXS |
|---|---|
| Regnase-1 (Ser435 + Ser439) | DSGIGS |
| Regnase-3 (Ser622 + Ser626) | ISGPRS |

**Figure 63 Protein sequence analysis for a DSGxxS phosphorylation motif in Regnase-1 and -3.**

The protein sequence of Regnase-3 (NCBI accession number NP_001156393.1) was compared with Regnase-1 (NCBI accession number 694799.1) regarding the presence of a published DSGxxS motif in Regnase-1. The DSGxxS motif is in particular characterized by 2 serine residues, which are spaced by 3 amino acids.

Thus, we predicted that Regnase-3, but not -2 and -4 might be regulated in a similar way via phosphorylation of the IKK complex. This was tested by immunoblot analysis in macrophages and mouse embryonic fibroblasts (MEF) cells.

Macrophages were pre-treated with MG132 to block proteasomal degradation or were treated with solvent as control and further stimulated with LPS in a time course. Regnase-3 and Regnase-1 had rather similar kinetics with significantly reduced expression after 10 to 30 minutes post LPS stimulation and recovery after four hours in form of a higher migrating species (Figure 64). Treatment with MG132 inhibited LPS-mediated degradation of Regnase-3 as well as Regnase-1 (Figure 64). This indicated that Regnase-3 is similarly regulated as Regnase-1 via phosphorylation and proteasomal degradation.

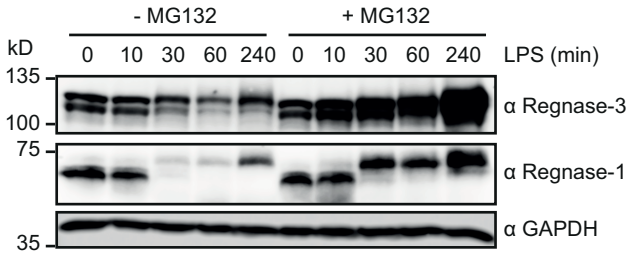


**Figure 64 Proteasome inhibition in LPS treated BMDM (von Gamm *et al.*, 2019).**

BMDM were differentiated from bone marrow of *C57BL/6J* mice and were first pre-treated with the proteasome inhibitor MG132 (10 μM) or with DMSO (vehicle) for 30 min. Cells were then stimulated with the TLR4 agonist LPS (100 ng/ml) for indicated times and protein lysates were made. Regnase-1 and Regnase-3 expression was analyzed by immunoblot. Shown is one representative blot of 3 independent experiments.

To further evaluate the involvement of the IKK complex in LPS-mediated degradation of Regnase family members, *NEMO*-deficient mouse embryonic fibroblast were obtained and modified. *NEMO*-deficient and *NEMO* reconstituted MEF cells were transduced with retroviruses carrying GFP-tagged Regnase family members and stimulated with LPS in a time course. Regnase-1 and -3 were degraded upon LPS stimulation, but in contrast to previous observations in macrophages for endogenous protein, GFP-tagged Regnase-1 and -3 were not re-expressed after four hours of stimulation (Figure 65). This can be likely explained by the absence of an endogenous promotor in overexpressed MEF cells. In contrast to family members Regnase-1 and -3, Regnase-2 and -4 did not disappear upon LPS treatment (Figure 65). This is in line with the missing DSGxxS motif in Regnase-2 and -4 sequences. LPS-mediated degradation of GFP-tagged Regnase-1 and -3 in *NEMO*$^{+/+}$ cells was inhibited in *NEMO*-deficient cells, indicating that IKK phosphorylation indeed caused the protein breakdown (Figure 65).

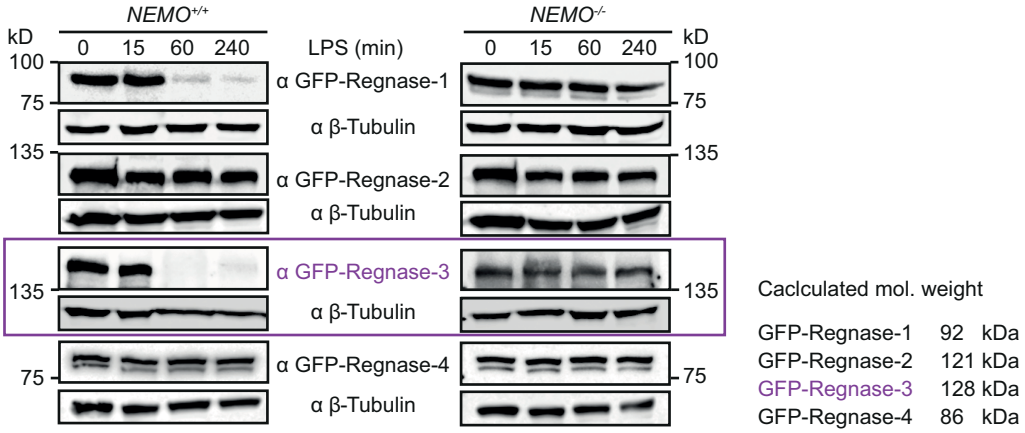


**Figure 65 Involvement of the IKK complex and LPS treatment on protein degradation of overexpressed Regnase family members (von Gamm *et al*., 2019).**

*NEMO*-deficient mouse embryonic fibroblasts (MEF) and *NEMO* reconstituted MEF were transduced with GFP-tagged Regnase family members. Cells were then treated with LPS (1 μg/ml) for indicated time points and Regnase expression levels were determined by immunoblot analysis with an anti-GFP antibody. Calculated molecular weights of GFP-tagged Regnase family members are displayed on the *right*. Shown is one representative blot of 3 independent experiments.

Endogenous Regnase-1 and Regnase-3 expression was further analyzed in *NEMO*$^{-/-}$ and *NEMO*$^{+/+}$ cells in response to TLR4 signaling. Four hours post LPS treatment, the same strong recovery of the Regnase-1 signal was observed in MEF cells, as previously described in macrophages (Figure 66). In contrast, Regnase-3 was also degraded but four hours after TLR4 induction, the Regnase-3 was still absent (Figure 66). Nevertheless, a strong inhibition in LPS-mediated degradation was in particular observed for Regnase-3, while the effect was less pronounced for Regnase-1 (Figure 66).

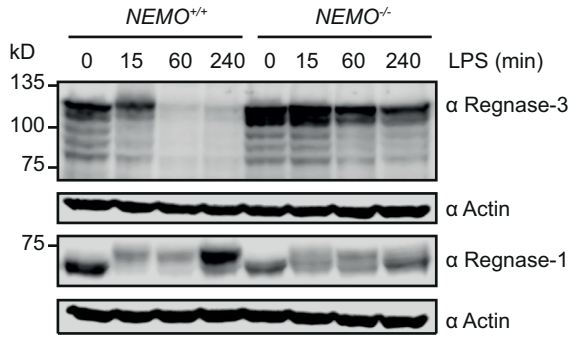


**Figure 66 Involvement of the IKK complex and LPS treatment on protein degradation of endogenous Regnase-1 and -3 protein (von Gamm *et al.*, 2019).**

*NEMO*-deficient mouse embryonic fibroblasts (MEF) and *NEMO* reconstituted MEF cells were treated with LPS (1 μg/ml) for indicated time points and endogenous Regnase-1 and -3 expression levels were determined by immunoblot. Shown is one representative blot of 3 independent experiments.

Taken together, these data provide strong evidence that in response to TLR4 activation Regnase-3 is similarly to Regnase-1 phosphorylate by the IKK complex and degraded via the proteasome. Unlike Regnase-1 expression patterns, Regnase-3 was not as strongly induced upon TLR4 activation.

### 2.9.3 Regnase-3 shows unique response patterns upon TLR3 induction

We further aimed to analyze the regulation of Regnase-3 protein in macrophages in response to several activated innate immune sensors. Therefore, bone marrow derived macrophages were generated and activated with a broad range of different receptor agonists. In particular, cells were treated with selective agonists for most Toll-like receptors (TLRs) as well as with several cytokines at two time points (see introduction for further details). Protein expression of Regnase-1 and -3 was then analyzed by immunoblot. LPS was used as TLR4 agonist, lipoteichoic acid (LTA) was used to stimulate TLR2, R848 was used for TLR7 and TLR8 activation and Flagellin is the natural ligand for TLR5 (Schwandner *et al.*, 1999; Hayashi *et al.*, 2001) (Figure 67, *top left*). High molecular weight poly-I:C was used to activate TLR3 (Figure 67, *top center*). Oligodeoxynucleotides (ODN) with unmethylated deoxycytidyl-deoxyguanosine (CpG) dinucleotides (CpG ODN) mimic specific patterns of bacterial DNA and activate TLR9. Several CpG ODNs are divided into classes, regarding their specificity to either stimulate plasmacytoid dendritic cells (A-class) or to activate B cells (B-class) (Vollmer *et al.*, 2004). Here, macrophages were stimulated with C-class ODN 2395, that combines features of both A- and B-class ODNs (Vollmer *et al.*, 2004) (Figure 67, *top center*). Nucleotide-binding oligomerization domain-containing protein 2 (NOD2) was activated with the peptidoglycan analog Murabutide (Geddes *et al.*, 2009) (Figure 67 *bottom left*). PMA activates protein kinase C, which is a second messenger that is involved in a wide range of signaling cascades (Niedel *et al.*, 1983). Furthermore, macrophages were stimulated

with several cytokines, including TNFα, IL-1β, IL-4, IL-6, IL-10, IL-15, IFNγ and a combination of IFNγ and LPS (Figure 67, *top right* and *bottom*). Several agonists caused both Regnase-1 and -3 to be degraded, likely due to above described IKK induced phosphorylation and degradation via the proteasome. In total, both Regnase-1 and -3 reacted overall very similar to the agonists (Figure 67). Nevertheless, one remarkable exception was seen for stimulation with the TLR3 agonist poly-I:C. While Regnase-1 barely reacted to poly-I:C, Regnase-3 was significantly upregulated after four hours of treatment (Figure 67, *top center*). Of note, TLR3 is the only Toll-like receptor that is only activated independently of the adaptor protein MyD88 (Takeuchi and Akira, 2010).

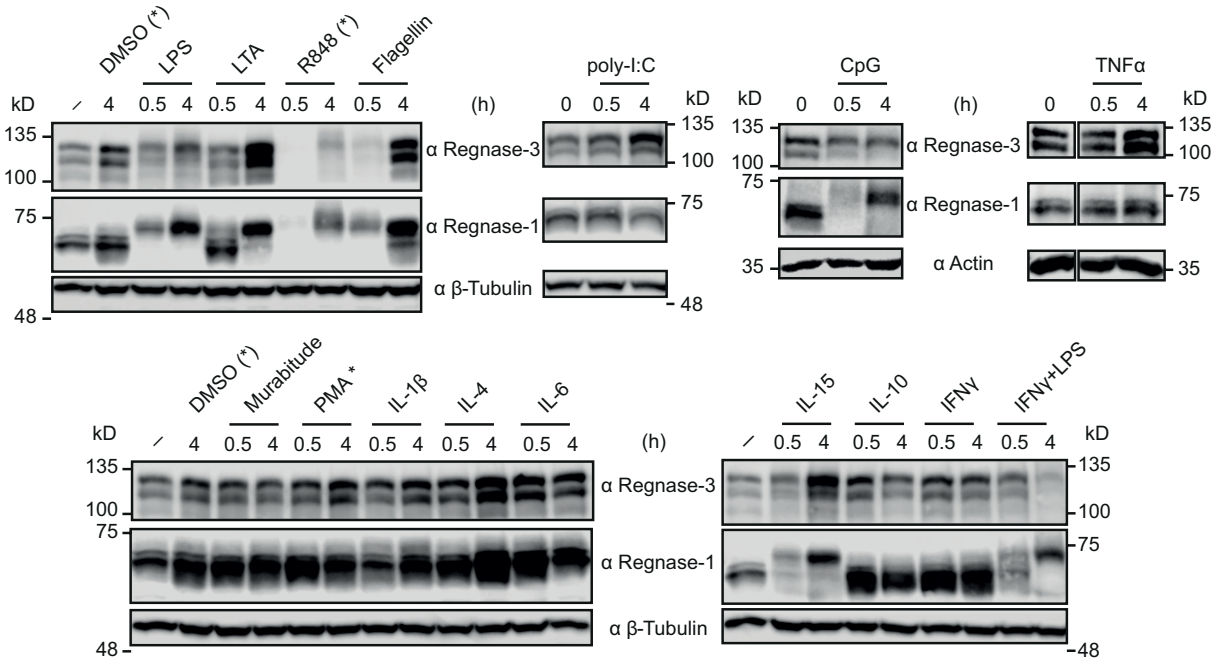


**Figure 67 Regnase-1 and -3 protein expression in activated BMDM (von Gamm *et al*., 2019).**

BMDM were differentiated from the bone marrow of *C57BL/6J* mice and were left untreated or were stimulated for 0.5 h and 4 h as follows: LPS (100 ng/ml), lipoteichoic acid (LTA, 1 μg/ml), R848 (Resiquimod, 1 μg/ml), Flagellin (100 ng/ml), high molecular weight poly-I:C (10 μg/ml), C-type CpG ODN2395 (1 μg/ml), TNFα (50 ng/ml), Murabutide (100 ng/ml), Phorbol-12-myristat-13-acetat (PMA, 25 ng/ml), IL-1β (50 ng/ml), IL-4 (50 ng/ml), IL-6 (50 ng/ml), IL-15 (50 ng/ml), IL-10 (50 ng/ml), IFNγ (50 ng/ml) or IFNγ plus LPS (50 ng/ml and 100 ng/ml). Controls were treated with vehicle (PBS or DMSO). Reagents dissolved in DMSO are marked with asterisk. Stimulated cells were analyzed by immunoblot. Representative blots from 3 experiments are shown.

Due to the unique expression profile of Regnase-3 in response to TLR3-mediated signaling, this pathway was analyzed in more detailed time series. Regnase-3 protein expression was not induced before about 1 hour of poly-I:C stimulation, but clearly upregulated four hours post treatment. Poly-I:C-mediated protein upregulation was again only seen for Regnase-3 but not for Regnase-1. Treatment with MG132 already upregulated Regnase-1 and -3 expression by itself, so that the effect of poly-I:C was not seen. In contrast, Regnase-1 and -3 expression was strongly decreased after 4 h of combi-treatment. This is likely

explained by cytotoxic effects that were caused by this combined treatment with poly-I:C and MG132 (Figure 68).

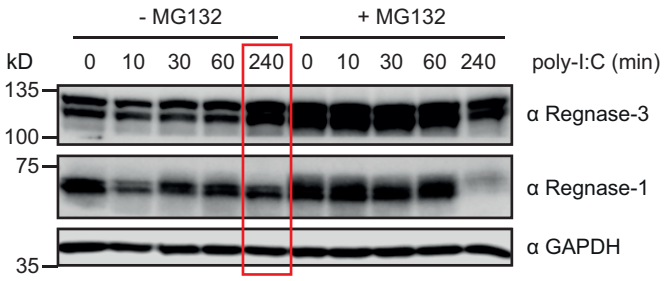


**Figure 68 Proteasome inhibition in poly-I:C treated BMDM (von Gamm *et al.*, 2019).**

BMDM were differentiated from bone marrow of *C57BL/6J* mice and were first pre-treated with the proteasome inhibitor MG132 (10 μM) or with DMSO (vehicle) for 30 min. Cells were then stimulated with the TLR3 agonist poly-I:C (10 μg/ml) for indicated times and Regnase-1 and Regnase-3 expression were analyzed in protein lysates by immunoblot. Representative blot of 3 independent experiments.

### 2.9.4 Regnase-3 is regulated via the transcription factor IRF7

Due to unique response patterns of Regnase-3 compared to Regnase-1 upon stimulation of TLR3, we aimed to further analyze the interferon pathway. TLR3 stimulation induces a cascade in which the signal is transferred *via* several adaptor proteins to a complex that contains the TANK-binding kinase (TBK1) (Chau *et al.*, 2008). This complex then phosphorylates and activates the transcription factors IRF3 and IRF7 with subsequent nuclear translocation (See introduction for more detailed description) (Chau *et al.*, 2008). The specific TBK1/IKKε inhibitor MRT67307 was used to block TLR3 downstream signaling to receive information on the involvement of transcriptional *Regnase-3* induction. Indeed, poly-I:C-mediated upregulation of Regnase-3 protein was blocked when cells were treated with the TBK1 inhibitor (Figure 69).

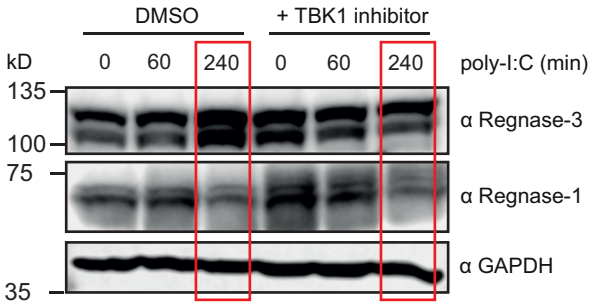


**Figure 69 Consequence of Ikkε/TBK1 inhibition for Regnase-1 and -3 protein expression in poly-I:C treated BMDM (von Gamm *et al.*, 2019).**

BMDM were differentiated from bone marrow of *C57BL/6J* mice and were first pre-treated with the Ikkε/TBKI inhibitor MRT67307 (20 μM) or with DMSO (vehicle) for a total of 5 h in all samples. Cells were subsequently treated with high molecular weight poly-I:C (10 μg/ml) for indicated times. Protein lysates were analyzed for Regnase-1 and -3 expression by immunoblot. Representative blot of 3 independent experiments.

Also poly-I:C induced upregulation of *Regnase-3* mRNA was blocked by MRT67307 (Figure 70). In contrast, *Regnase-1* mRNA was upregulated under TBK1 inhibitor treatment,

irrespective of poly-I:C addition. Expression of *Ifnβ* mRNA is shown to proof successful TLR3 induction and the inhibitory effect of MRT67307 (Figure 70).

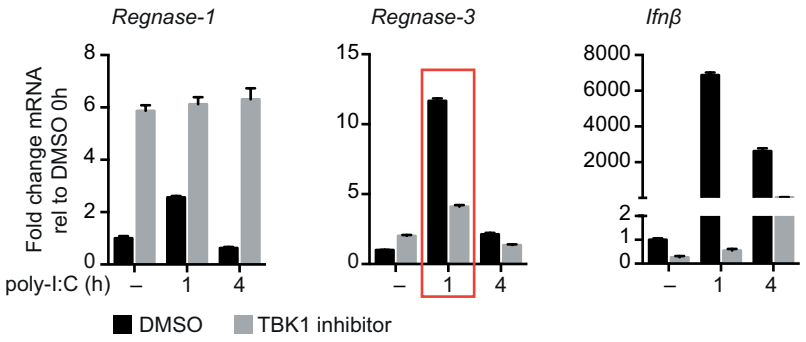


**Figure 70 Consequence of Ikkε/TBK1 inhibition for *Regnase-1* and *-3* mRNA expression in poly-I:C treated BMDM (von Gamm *et al.*, 2019).**

BMDM were differentiated from bone marrow of *C57BL/6J* mice and were first pre-treated with the Ikkε/TBKI inhibitor MRT67307 (20 μM) or with DMSO (vehicle) for a total of 5 h in all samples. Cells were subsequently treated with high molecular weight poly-I:C (10 mg/ml) for indicated times. *Regnase-1* (*Zc3h12a*), *Regnase-3* (*Zc3h12c*) and *Ifnβ* mRNA expression levels were determined by quantitative RT-PCR and normalized to *Hprt1*. Indicated mRNA levels are displayed in relativity to their expression values in untreated BMDM. Data are represented as mean +/- SEM from 3 biological replicates.

To further pin down the transcription factor that is responsible for Regnase-3 upregulation in response to TLR3 receptor stimulation, we obtained RAW macrophage cell lines with deficiency for either IRF3 or IRF7 and stimulated the cells under the same conditions. Upregulated Regnase-3 protein expression 4 hours post poly-I:C treatment was very slightly reduced in *Irf3*$^{-/-}$ RAW cells as compared to *Irf3*$^{+/+}$ cells (Figure 71 A). In contrast, Regnase-3 expression was almost not induced in *Irf7*-deficient RAW cells upon TLR3 induction (Figure 71 B). Regnase-1 was again unaltered upon stimulation with poly-I:C and also *Irf3* or *Irf7* deficiency did not influence Regnase-1 protein expression (Figure 71 A, B).
This indicates that either IRF7 homodimers or IRF3/IRF7 heterodimers with mandatory IRF7 contribution are responsible for TLR3-mediated upregulation of Regnase-3 in macrophages.

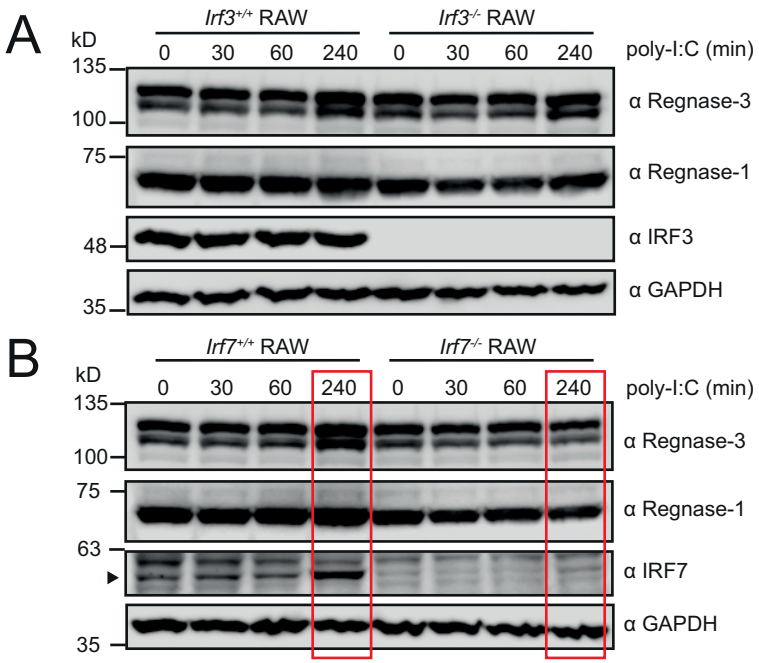


**Figure 71 Role of transcription factors IRF3 and IRF7 on Regnase-1 and -3 expression in TLR3 activated RAW cells (von Gamm *et al.*, 2019).**

Wildtype RAW cells (a murine macrophage cell line) as well as (A) *Irf3*$^{-/-}$ and (B) *Irf7*$^{-/-}$ RAW cells were treated with the TLR3 agonist poly-I:C (10 μg/ml) for indicated times. Regnase-1 and -3 expression was analyzed in protein lysates by immunoblot. Representative blots of 3 independent experiments are shown.

In addition to the interferon pathway, we also aimed to analyze the second important pathway in immune cell regulation, the NF-κB signaling cascade. The group of NF-κB transcription factors consists of the five members p65 (Rel A), Rel B, c-Rel, p105/p50 (NF-κB1) and p100/52 (NF-κB2), which can form hetero- or homodimers (Oeckinghaus and Ghosh, 2009). While up to 15 different dimers are possible, the p50/p65 heterodimer is the most abundant dimer and found in most cell types (see also introduction for NF-κB signaling) (Oeckinghaus and Ghosh, 2009). Thus, we used macrophages derived from *p50*-deficient mice to study NF-κB signaling. The NF-κB signaling pathways was activated in macrophages by TLR4 activation with LPS for up to 4 hours. As expected and previously observed, Regnase-1 was degraded within 30 minutes of activation and reappeared after four hours in wildtype cells (Figure 72, *left*). In *NF-κB p50*$^{-/-}$ macrophages, Regnase-1 degradation was also observed, but the recovery of the protein expression four hours later was almost fully abolished (Figure 72, *right*). Regnase-3 in contrast had rather low signal recovery after four hours of LPS stimulation as compared to Regnase-1 in wildtype macrophages (Figure 72, *left*). In *NF-κB p50*$^{-/-}$ cells, Regnase-3 expression four hours post LPS treatment was much higher as compared to *NF-κB p50*$^{+/+}$ macrophages (Figure 72, *right*).

These results indicate that Regnase-1 is regulated via the NF-κB signaling complex on two levels: First, Regnase-1 protein is degraded on the post-translational level in response to IKK activation. Second, Regnase-1 is transcriptionally upregulated via the transcription factor NF-κB with participation of p50 subunits. Similar to Regnase-1, but different to

family members -2 and -4, also Regnase-3 was observed to be post-translationally degraded in response to IKK activation. Nevertheless, Regnase-3 expression was not transcriptionally induced via NF-κB signaling. In contrast, its expression was even upregulated in *NF-κB p50*$^{-/-}$ macrophages. This might be explained by counter regulation of Reganse-1 and -3 as observed in *Regnase-3*-deficient tissues. Due to decreased Regnase-1 protein expression, *Regnase-3* mRNA might be less degraded, which could explain its increased expression.

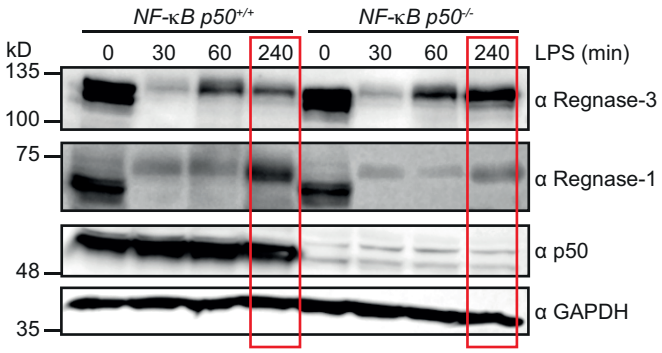


**Figure 72 Role of the transcription factor NF-κB on Regnase-1 and -3 expression in LPS treated BMDM (von Gamm *et al.*, 2019).**

BMDM were differentiated from *NF-κB p50*$^{+/+}$ and *NF-κB p50*$^{-/-}$ mice and were treated with lipopolysaccharide (LPS) (100 ng/ml) for indicated time points. Regnase-1 and Regnase-3 expression was analyzed by immunoblot. Representative blot from 3 *NF-κB p50*$^{+/+}$ and 3 *NF-κB p50*$^{-/-}$ mice.

## 2.10 Regnase-3 target identification

### 2.10.1 Regnase-3 protein alignment for conserved domains

Comprehensive research was done to describe the molecular function of Regnase-1 and is described in more detail in the introduction. In short, Regnase-1 has been found to directly bind at certain stem loop structures within the 3'UTRs of specific target mRNAs and degrades those mRNAs by its intrinsic RNase domain (Matsushita *et al.*, 2009; Mino *et al.*, 2015). Protein alignment of the RNase and Zn finger domains of Regnase family members using the alignment program 'T-coffee' with 'M-coffee' algorithm revealed a homology score of 97,1% (Figure 73) (Di Tommaso *et al.*, 2011; Moretti *et al.*, 2007). Thus, all family members might potentially act as ribonuclease.

A

```
T-COFFEE, Version_11.00.d625267 (2016-01-11 15:25:41 - Revision d625267 - Build 507)
Cedric Notredame
SCORE=971
*
 BAD AVG GOOD
*
gi|24233519|ref    :  97
gi|110347404|re    :  94
gi|242332574|re    :  93
gi|226423912|re    :  93
cons               :  97

gi|24233519|ref    GGS---TPKPSTLEPSLPEE-DREGSDLRPVVIDGSNVAMSHGNKEVFSCRGILLAVNWFLER
gi|110347404|re    GAS---SREIASPELSLEDE-IDNSDNLRPIVIDGSNVAMSHGNKEEFSCRGIQLAVDWFLDK
gi|242332574|re    ETS---SLESORSESPMOEVVVDDGENLRPVVIDGSNVAMSHGNKEVFSCRGIKLAVDWFLER
gi|226423912|re    GCCGVQDSAQQGLGPGLEEAGGDPARFLRPIVIDGSNVAMSHGNKEAFSCRGIRLAVDWFRDR

cons               .      : :  .  ***:*************** ****** ***:** ::


gi|24233519|ref    GHTDITVFVPSWRKEQPRPDVPITDQHILRELEKKKILVFTPSRRVGGKRVVCYDDRFIVKLA
gi|110347404|re    GHKDITVFVPAWRKEQSRPDAPITDQDILRKLEKEKILVFTPSRRVQGRRVVCYDDRFIVKLA
gi|242332574|re    GHKDITVFVPAWRKEQSRPDALITDQEILRKLEKEKILVFTPSRRVQGRRVVCYDDRFIVKLA
gi|226423912|re    GHTYIKVFVPSWRKEPSRSDTPIREQHVLEELERQAVLVYTPSRKVNGKRVVCYDDRYIVKVA

cons               **. *.****:**** .*.*. * :*.:*.:**:: :**:****:* *:********:***:*


gi|24233519|ref    FESDGVVVSNDTYRDLQGERQEWKRFIEERLLMYSFVNDKFMPPDDPLGRHGPSLDNFLRKKP
gi|110347404|re    FDSDGIIVSNDNYRDLQVEKPEWKKFIEERLLMYSFVNDKFMPPDDPLGRHGPSLENFLRKRP
gi|242332574|re    FESDGIIVSNDNYRDLANEKPEWKKFIDERLLMYSFVNDKFMPPDDPLGRHGPSLDNFLRKKP
gi|226423912|re    YEKDGIIVSNDNYRDLQNENPEWKWFIEQRLLMFSFVNDRFMPPDDPLGRRGPTLSNFLSKKP

cons               ::.**::****.****  *. *** **::****:*****:**********:**:*.*** *:*


gi|24233519|ref    L
gi|110347404|re    V
gi|242332574|re    I
gi|226423912|re    R

cons               
```

RNase domains:

| | | |
|---|---|---|
| Regnase-1 | aa112 | – aa297 |
| Regnase-2 | aa166 | – aa351 |
| Regnase-3 | aa241 | – aa427 |
| Regnase-4 | aa65 | – aa254 |

B

```
T-COFFEE, Version_11.00.d625267 (2016-01-11 15:25:41 - Revision d625267 - Build 507)
Cedric Notredame
SCORE=1000
*
 BAD AVG GOOD
*
gi|24233519|ref    : 100
gi|110347404|re    : 100
gi|242332574|re    : 100
gi|226423912|re    : 100
cons               : 100

gi|24233519|ref    EHRKQPCPYGKKCTYGIKCRFFHPER
gi|110347404|re    EHKKQPCPYGKKCTYGHKCKYYHPER
gi|242332574|re    EHKKQPCPYGKKCTYGHKCKYYHPER
gi|226423912|re    EPSWQHCPYGKKCTYGVKCRFYHPER

cons               *   * ********** **:::****
```

Zn finger motifs:

| | | |
|---|---|---|
| Regnase-1 | aa300 | – aa325 |
| Regnase-2 | aa354 | – aa379 |
| Regnase-3 | aa430 | – aa455 |
| Regnase-4 | aa257 | – aa282 |

**Figure 73 Protein alignment of Regnase family members.**

Analogous sequences for the annotated RNase domain (A) and Zn finger motif (B) in Regnase-1 were manually searched in Regnase-2, -3 and -4. Sequences were then aligned using T coffee (http://tcoffee.crg.cat) with 'M-Coffee' algorithm. Selected sequences for RNase domains and Zn finger motifs in Regnase family members are displayed in green boxes. NCBI accession numbers were as follows: Regnase-1 (24233519 / NP_694799.1), Regnase-2 (110347404 / NP_001030079.2), Regnase-3 (242332574 / NP_001156393.1), Regnase-4 (226423912 / NP_766373.2).

### 2.10.2 RNA sequencing in peritoneal macrophages for target identification

Our findings demonstrated that Regnase-3 plays a substantial role *in vivo* and that its loss in the myeloid linage results in hypertrophic lymph nodes. Moreover, we have found together with cooperation partners, that Regnase-3 recognizes and degrades various RNA species including poly-I:C *in vitro*, however without apparent specificity (von Gamm *et al.*, 2019). Further, we have observed at least some sequence specificity in a cell-based reporter gene assay. In this assay, Regnase-3 preferentially down regulated the 3'UTR of *Regnase-1*, but not that of *Hprt1* or *Ifnγ* (von Gamm *et al.*, 2019). However, *Regnase-1* mRNA was the only identified target so far. Therefore, we aimed to identify deregulated mRNA target genes in *Regnase-3*-deficient macrophages in a global and unbiased way.

Thus, alveolar macrophages ($CD11c^+$) were isolated from the lung of *Regnase-3*$^{-/-}$ mice with lymphadenopathy and from their wildtype littermate controls and subjected to RNA sequencing analysis. Unexpectedly, the number of significantly upregulated genes in *Regnase-3*$^{-/-}$ macrophage was with only six genes quite low (adj. p-value ⩽ 0.05) (Figure 74).

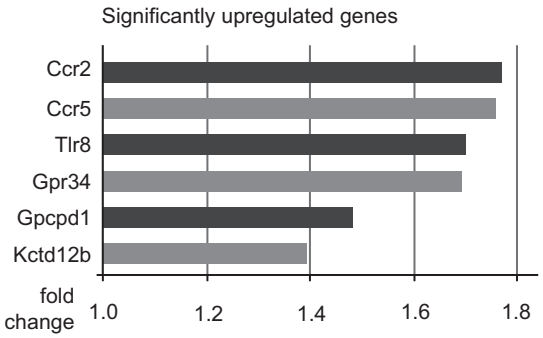


**Figure 74 Sequencing analysis for alveolar macrophages, *Regnase-3*$^{+/+}$ vs. from *Regnase-3*$^{-/-}$ mice: Upregulated genes (von Gamm *et al.*, 2019).**

Alveolar macrophages were positively selected via CD11c from the bronchoalveolar lavage (BAL) of *Regnase-3*$^{-/-}$ mice with lymphadenopathy and their *Regnase-3*$^{+/+}$ controls at 7 months of age (n = 3/3). Isolated RNA was subjected to RNA sequencing and computationally analyzed. Displayed are all significantly upregulated genes (adj. p-value ⩽ 0.05) in *Regnase-3*$^{-/-}$ mice together with their fold changes.

Among the significantly downregulated genes, gene ontology (GO) term enrichment clustered many of these genes into the 'oxidative stress' response pathway (Figure 75).

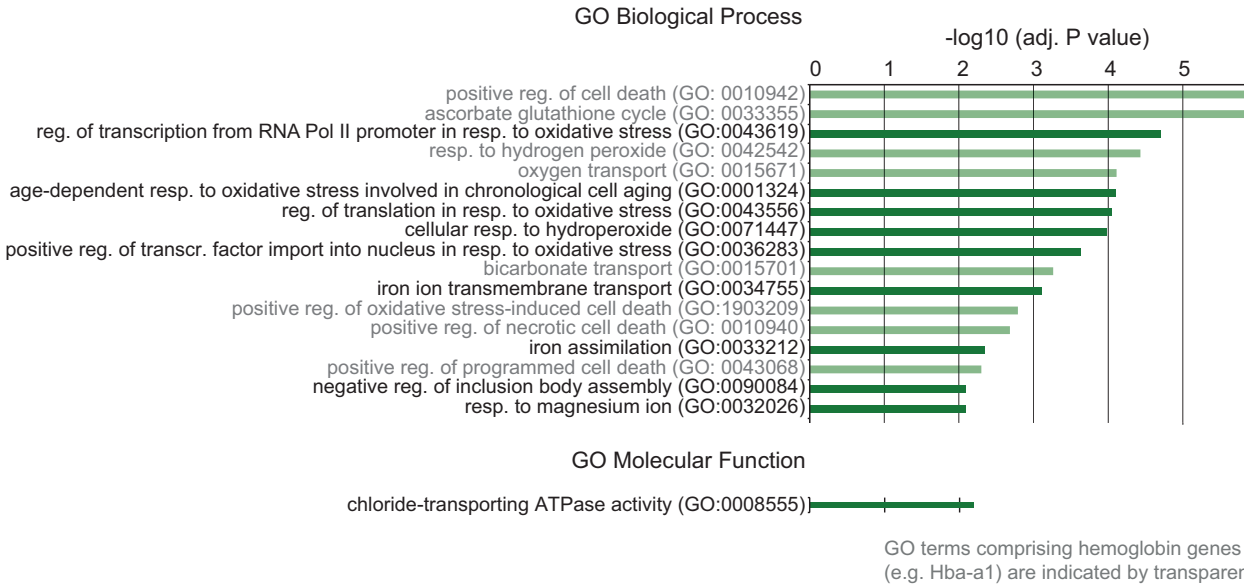


**Figure 75 Sequencing analysis for alveolar macrophages, *Regnase-3*$^{+/+}$ *Regnase-3*$^{-/-}$ mice: GO term analysis for downregulated genes (von Gamm *et al.*, 2019).**

All significantly downregulated genes (adj. p-value ⩽ 0.05) in *Regnase-3*$^{-/-}$ alveolar macrophages were determined in RNA sequencing data from Figure 74. GO term analysis on downregulated genes was performed and GO terms with an adj. p-value (-log10) ⩾ 2 are displayed and listed according to their p-values. GO terms covering hemoglobin genes (e.g. Hbba-a1) are indicated in light gray.

Upregulated genes, such as chemokine receptors *Ccr2* and *Ccr5* could indicate a pro-inflammatory response within these cells. When also taking in account that the number of downregulated genes was higher than the number of upregulated genes, it is likely that the deregulation in *Regnase-3*$^{-/-}$ macrophages was rather caused by a secondary immune response, than by direct degradation of target genes.

### 2.10.3 RNA sequencing analysis of *in vitro* treated macrophages

With the perspective to identify potential Regnase-3 target genes, we also aimed to mimic an immunological response in a controlled cell-based assay *ex vivo*. Therefore, bone marrow derived macrophages were generated from *Regnase-3*-deficient and wildtype mice, stimulated under a variety of conditions and subjected to RNA sequencing analysis. In a pre-test, 10 treatment conditions were tested on *Regnase-3*$^{+/+}$ and *Regnase-3*$^{-/-}$ macrophages with only one sample for every setup with the aim to find settings under which *Regnase-3* deficiency leads to significant differential gene expression. Macrophages were left untreated or were stimulated with poly-I:C, lipoteichoic acid, lipopolysaccharide, Flagellin or TNFα for either 3 or 12 hours. Some samples were first stimulated with TNFα, lipoteichoic acid or poly-I:C for a total of 6 hours and were additionally treated with Actinomycin D for the last two hours of activation. Actinomycin D blocks mRNA *de novo* synthesis by RNA polymerases. Thus, effects of RNA degradation are enhanced in the total RNA composition in sequencing samples and regulatory properties of Regnase-3 might be emphasized.

Unexpectedly, almost no genes were identified, which were deregulated more than 2 $\log_2$ fold in *Regnase-3*-deficient macrophages under any of the stated treatments (Figure 76). Only incubation with poly-I:C for 12 h revealed a single deregulated gene, which we assessed to be of minor relevance. Since almost no genes were deregulated under the tested conditions in the pre-experiment, the RNA sequencing assays were not repeated and the experimental setup consequently misses replicates. Nevertheless, it was still remarkable that RNA expression patterns appeared highly uniform in *Regnase-3*-deficient and wildtype macrophages under a variety of activation conditions.

In summary, luciferase and EMSA assays indicate that *Regnase-1* mRNA might be regulated by Regnase-3 protein either directly or indirectly (von Gamm *et al.*, 2019). However, sequencing analysis for activated bone marrow derived macrophages from wildtype and *Regnase-3*-deficient macrophages revealed almost no differentially expressed genes. Thus, further target genes still remain illusive.

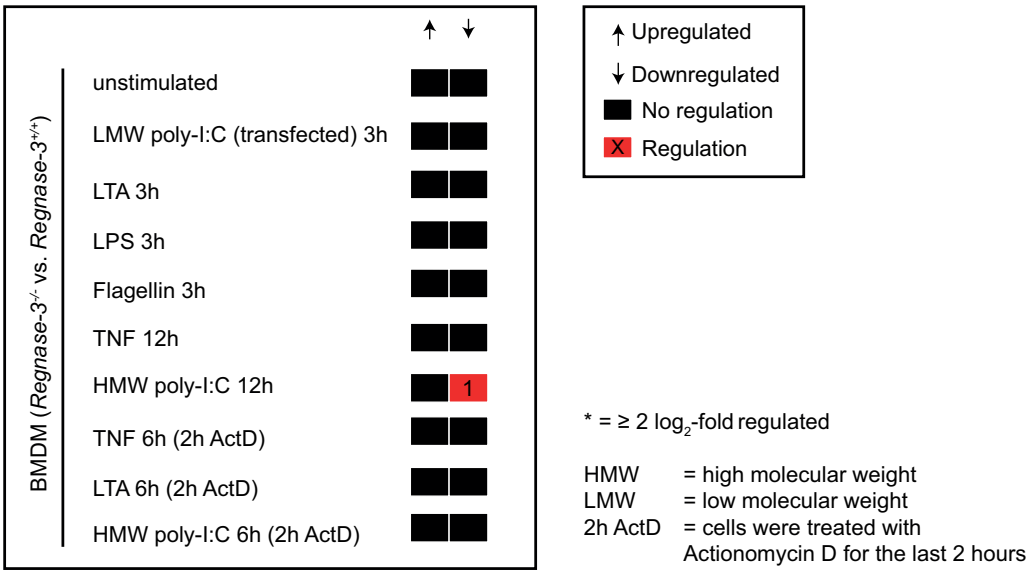


**Figure 76 RNA sequencing analysis in activated BMDM from *Regnase-3*$^{-/-}$ mice.**

BMDM were differentiated from bone marrow of *Regnase-3*$^{-/-}$ mice and *Regnase-3*$^{+/+}$ controls. Cells were left untreated or were treated under various conditions: Cells were either transfected with low molecular weight poly-I:C (100 μg/ml) complexed to JetPei and incubated for 3 hours. Alternatively, macrophages were stimulated with lipoteichoic acid (LTA, 1 μg/ml), lipopolysaccharide (LPS, 100 ng/ml) or Flagellin (100 ng/ml) for 3 h or were treated with TNFα (50 ng/ml) or high molecular weight poly-I:C (10 μg/ml) for 12 h. Or cells were first stimulated with TNFα (50 ng/ml), lipoteichoic acid (LTA, 1 μg/ml) or high molecular weight poly-I:C (10 μg/ml) for a total of 6 h and then Actinomacin D (ActD, 2 μg/ml) was added for the last 2 h of stimulation. RNA was isolated from activated BMDM and subjected to RNA sequencing (n = 1/1 for each condition). Differentially regulated genes in *Regnase-3*$^{-/-}$ macrophages (≥ 2 $\log_2$ fold) were determined. Black boxes indicated that no genes were differentially expressed in *Regnase-3*-deficient macrophages compared to wildtype macrophages under the respective treatment condition. The red box indicates differential expression and the number specifies the number of differentially expressed genes.

## 2.11 Endosomal localization of Regnase-3 does not influence phagocytosis

Together with colleagues, we could further demonstrate that Regnase-3 had a different subcellular localization than its family member Regnase-1 (von Gamm *et al.*, 2019). Regnase-3 is expressed in dot-like cytoplasmic structures, but in contrast to Regnase-1 does not co-localize with the P-body marker DDX6. While Regnase-3 partially localized to late and recycling endosomes, a very high staining overlay was observed with phagocytized Dextran (von Gamm *et al.*, 2019).
The high degree of co-localization of Regnase-3 with phagocytized Dextrane molecules suggested a participation of Regnase-3 in the phagocytosis pathway. Therefore, we were wondering if Regnase-3 might affect phagocytosis in an *in vitro* assay.

Bone marrow derived macrophages were differentiated from wildtype mice and *Regnase-3*-deficient mice and used to analyze their phagocytic potential. Therefore, bioparticles from *Staphylococcus aureus* coupled to the pH sensitive pHrodo green fluorophore were applied to macrophages. The increase in fluorescence due to acidification of the incorporated bioparticles was then measured over time. Phagocytosis in macrophages was also measured under different conditions by pretreating cells with LPS, LTA, poly-I:C and TNFα. While all agonists decreased the phagocytic activity, we did not observe any differences between wildtype and *Regnase-3*-deficient macrophages (Figure 77).

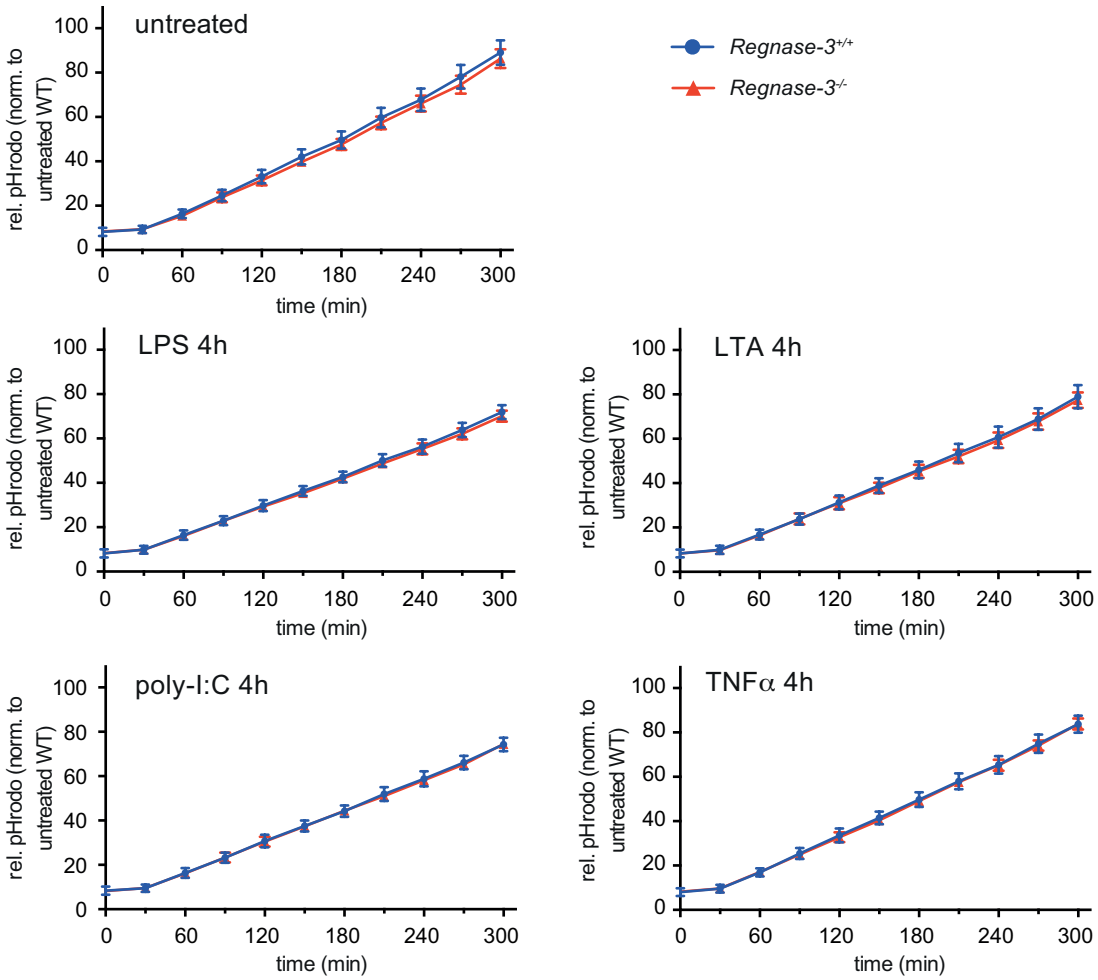


**Figure 77 *In vitro* phagocytosis assay in *Regnase-3*$^{-/-}$ macrophages (von Gamm *et al.*, 2019).**

BMDM were generated from *Regnase-3*$^{+/+}$ and *Regnase-3*$^{-/-}$ mice and were left untreated or were pre-stimulated for 4 h with LPS (100 ng/ml), lipoteichoic acid (LTA, 1 μg/ml), high molecular weight poly-I:C (10 μg/ml) or TNFα (50 ng/ml). Cells were then probed with *Staphylococcus aureus* bioparticles coupled to a pH sensitive fluorophore (pHrodo) and increased fluorescence was acquired over time on a microplate reader. Maximal fluorescence intensity of unstimulated wildtype BMDM in each assay was set to 100% and all other values were calculated in relativity to unstimulated wildtype BMDM. Data are represented as mean +/- SEM from 4 independent assays with BMDM from 2 mice in each assay (total n = 8/8).

Of note, together with cooperation partners we have also investigated, if *Regnase-3* deficiency might instead alter phagocytosis *in vivo*. Therefore, *Regnase-3*$^{fl/fl}$ +LysM-Cre mice and their *Regnase-3*$^{fl/fl}$ littermates were infected intranasally with Methicillin-resistant *Staphyloccocus aureus* (MRSA). 24 hours post infection, lung tissue was examined for analysis of the bacterial load and the capacity of lung-resident macrophages to phagocytose the infected bacteria. However, no significant differences were seen in the knockout (von Gamm *et al.*, 2019). In summary, Regnase-3 expression correlated with phagocytized dextrane molecules, but this did not change the capacity of *Regnase-3*-deficient macrophages to phagocytose *Staphylococcus aureus in vitro* or *in vivo*.

# 3 Discussion

## 3.1 Regnase-3 as an important mediator of immune homeostasis *in vivo*

### 3.1.1 Importance of RNA binding proteins in immune homeostasis

Post-transcriptional gene regulation gained growing interest by the research society within the last two decades. For the search term 'RNA binding protein(s)', PubMed reports 1180 publications for the year 1988, while ten and twenty years later the number increased about 6-times to 8293 and 7228 novel publications in the years 2008 and 2018, respectively. Gerstberger *et al*. predicted that among all protein-coding genes in humans, more than 7.5% (1542 genes) could be assigned to the group of potential RNA binding proteins (RBPs) (Gerstberger *et al.*, 2014). In particular rapidly responding immune cells came into the focus of research projects. This is emphasized by major discoveries implicating fundamental roles of RNA binding proteins for immune cell maturation, activation, inactivation and even for sensing of pathogens. For example, Hodson *et al*. reported that mice deficient for the RBPs *ZFP36L1* and *ZFP36L2* were impaired in their thymic T cell maturation (Hodson *et al.*, 2010). The Eukaryotic elongation factor 2 (eEF2) is important for the induction of an immune response by promoting translation of the pro-inflammatory cytokine TNFα (Gonzalez-Teran *et al.*, 2013). In contrast, several RNA binding proteins cause mRNA breakdown of inflammatory mRNAs and thus initiate the resolution phase of an immune response. For example, AU-rich element RNA-binding protein 1 (AUF1) is involved in the degradation of *Tnfα* and *Il-1β* mRNAs in macrophages and in line with this, induced septic shocks caused increased mortality in *Auf*-deficient mice (Lu *et al.*, 2006). An entirely different function has been reported for the Retinoic acid–inducible gene I (RIG-I), which senses viral RNA species within infected cells (Hornung *et al.*, 2006; Pichlmair *et al.*, 2006).

Moreover, a significant publication by the lab of Shizuo Akira in 2009 highlighted the significant impact of the RNase Regnase-1 (*Zc3h12a* gene) as negative regulator for inflammatory RNAs and its relevance to promote resolution of immune responses (Matsushita *et al.*, 2009). At brief intervals, several high impact studies have then been published, investigating the role of Regnase-1 *in vivo* together with its molecular mode of action (see introduction for a detailed description). However, other Regnase family members received little attention and rather few studies have been published so far. While *Regnase-4*-deficient mice were first described in 2014 (Minagawa *et al.*, 2014), phenotypic characterizations of mice deficient for *Regnase-2* or *Regnase-3* were missing in literature.

This study and its associated publication in '*The Journal of Experimental Medicine'*, provide the first in-depth characterization of mice deficient for *Regnase-3*. In addition, conditional deletion of *Regnase-3* in B lymphocytes, in T lymphocytes and in the myeloid linage could further specify cell types in which Regnase-3 fulfills indispensible biological functions.

Moreover, *in vitro* experiments helped to understand its molecular properties and biological, regulatory pathways. Thus, these data deliver novel insights into the role of an RNA sensing and processing protein in immune cells.
In the following sections, I will first set *Regnase-3*$^{-/-}$ mice into context with mice, which either develop similar symptoms or have related genetic modifications. Thereafter, Regnase-3 will be discussed on the cellular level and finally molecular properties will be connected to potential modes of action.

### 3.1.2 *Regnase-3* deficiency causes a unique profile of disease symptoms

We have obtained and thoroughly analyzed mice deficient for the putative RNase *Regnase-3*. These mice were born in mendelian ratios, developed well overall and premature death was rarely seen (Figure 12). However, starting at an age of approximately 3 months, the majority of *Regnase-3*$^{-/-}$ mice developed hypertrophic skin-draining lymph nodes (Figure 13 ff.). Apparently, the immunologic homeostasis in *Regnase-3*$^{-/-}$ mice lost its balance under certain conditions without further external interference, such as triggering the immune response with an infection. This demonstrates that biological functions of Regnase-3 are mandatory to maintain the balance in the highly orchestrated immune system *in vivo* under steady state conditions. Several publications with phenotypic descriptions of genetically modified mice reported lymphadenopathy and might be used to correlate cellular and systemic malfunctions, which were caused by *Regnase-3* deficiency. These studies comprise proteins with a wide range of molecular functions. Most relevant for comparative analysis were previous studies, covering its family member Regnase-1. Mice deficient for *Regnase-1* have been separately generated and described by the group of Shizuo Akira in 2009 and short after by the group of Mingui Fu (Matsushita *et al.*, 2009; Liang *et al.*, 2010). Similar to *Regnase-3*$^{-/-}$ mice, also *Regnase-1*$^{-/-}$ mice developed hypertrophic lymph nodes (Matsushita *et al.*, 2009; Liang *et al.*, 2010).
In addition, malfunctions of proteins with completely different functionality can cause lymphadenopathy. The Fas receptor belongs to the TNF receptor family and induces programmed cell death, when activated by its endogenous Fas ligand (Ishiwatari-Hayasaka *et al.*, 1997; Oshimi *et al.*, 1996). A specific mutation within the Fas receptor gene was found in a patient with the Canale-Smith syndrome, which is an autoimmune disease characterized by increased lymphocyte proliferation and the development of hypertrophic lymph nodes (Orlinick *et al.*, 1997). Also *MRL/lpr* mice with the spontaneous *lpr* mutation within the Fas receptor gene develop strong lymphadenopathy (Watanabe-Fukunaga *et al.*, 1992; Singer *et al.*, 1994). Similarly, mice with the *sanroque* mutation within the *Rc3h1* gene, encoding for the RNA binding protein Roquin-1 develop lymphadenopathy (Vinuesa *et al.*, 2005). Also mice deficient for the *C9orf72* gene developed a lupus erythematosus like phenotype including hypertrophic lymph nodes (Atanasio *et al.*, 2016). The exact underlying

molecular functions of the C9orf72 protein are still not clear, but functions in endocytosis or autophagy have been suggested (Babic Leko *et al.*, 2019; Farg *et al.*, 2014).

In summary, mice that have genetic variations in genes with very different functionality suffer from lymphadenopathy. The publications not only reported hypertrophic lymph nodes for the respective mouse models, but also described further rather similar phenotypic manifestations. *Regnase-1*$^{-/-}$, *MRL/lpr*, *Roquin*$^{san/san}$ and *C9orf72*$^{-/-}$ mice also developed symptoms of autoimmunity, including splenomegaly, enhanced germinal center reactions and the formation of autoantibodies (Matsushita *et al.*, 2009; Yang *et al.*, 2013; Watanabe-Fukunaga *et al.*, 1992; Vinuesa *et al.*, 2005; Atanasio *et al.*, 2016).

Due to this apparently high correlation of hypertrophic lymph nodes with autoimmunity, also *Regnase-3*-deficient mice were analyzed regarding possible signs for auto-reactive immune cells. However, no signs for autoimmunity could be observed in the knockout. First, hardly any *Regnase-3*$^{-/-}$ mouse developed splenomegaly, even when skin-draining lymph nodes were severely increased (Figure 19). Second, anti-nuclear antibodies and auto-tissue reactive antibody species were also not significantly increased in *Regnase-3*$^{-/-}$ mice (Figure 20 & Figure 21). And third, the number of germinal center B cells was also rather decreased than increased in spleen and lymph nodes of *Regnase-3*-deficient mice (Figure 25).

Thus, hypertrophic lymph nodes have been associated with a variety of genetic modifications, both in human and mice. Nevertheless, symptoms in *Regnase-3*$^{-/-}$ mice only partly resemble the phenotype of the previously mentioned mouse models, which all develope splenomegaly and autoimmunity. Thus, *Regnase-3*$^{-/-}$ mice have a unique combination of symptoms that occurred reproducibly in high numbers of analyzed mice, even though some individuals never developed hypertrophic lymph nodes (Figure 13). Of note, symptoms in *Regnase-3*$^{-/-}$ mice were also distinct compared to mice deficient for its family members *Regnase-1* and *-4* (Matsushita *et al.*, 2009; Liang *et al.*, 2010; Minagawa *et al.*, 2014). *Regnase-1*$^{-/-}$ mice develop severe autoimmunity symptoms and the majority died within the first 12 weeks of age (Matsushita *et al.*, 2009). This is in clear contrast to mice deficient for *Regnase-4*, in which no significant differences were observed under steady-state conditions (Minagawa *et al.*, 2014). Yet, in experimental autoimmune encephalomyelitis, an animal model that mimics human multiple sclerosis, *Regnase-4*-deficient mice developed stronger symptoms than their wildtype counterparts (Minagawa *et al.*, 2014).

Taken together, *Regnase-3* ablation in mice caused unique pathologic patterns that were weaker compared to mice deficient for the family member Regnase-1, but significantly stronger than that in *Regnase-4*-deficient mice. A brief summary of key symptoms that are associated with *Regnase-3* deficiency is given in Figure 78.

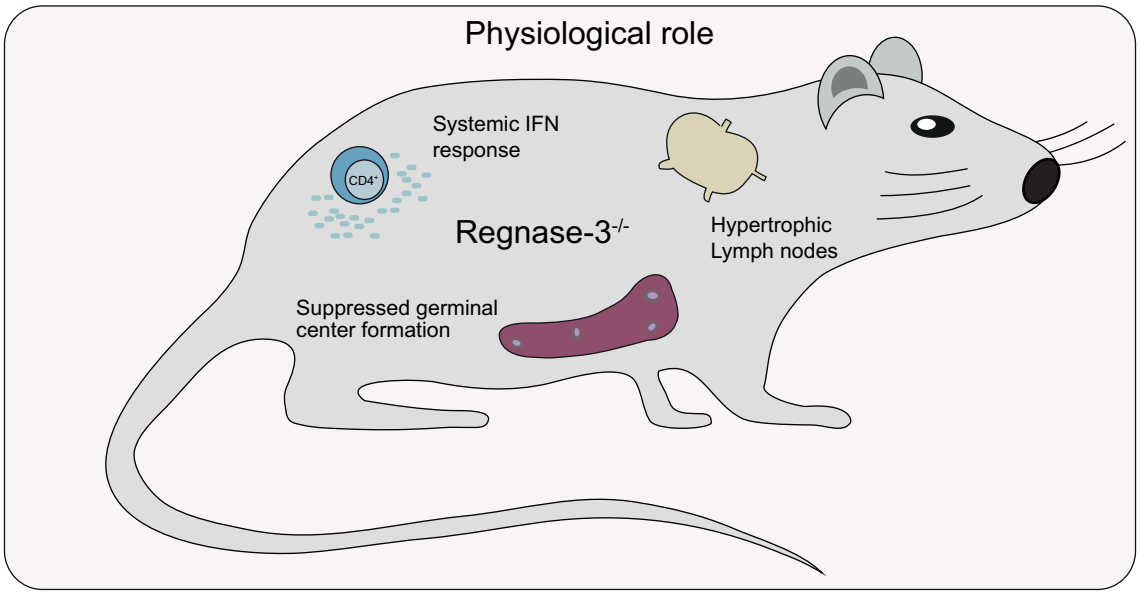


**Figure 78 Schematic representation of characteristic symptoms in Regnase-3-deficient mice.**
Deficiency of *Regnase-3* caused hypertrophic lymph nodes, suppressed the formation of germinal centers and induced local and systemic interferon responses. Figure adopted from von Gamm *et al.*, 2019.

## *3.2* Relevant immune cell types for Regnase-3 function *in vivo*

In the following sections, relevant immune cell shifts in *Regnase-3*$^{-/-}$ mice will be summarized. Further, it will be demonstrated and discussed for which immune cells Regnase-3 expression is mandatory to prevent lymphadenopathy and for which cell types Regnase-3 might be dispensable *in vivo*.

### 3.2.1 Lymphadenopathy in *Regnase-3*$^{-/-}$ mice is not caused by dysfunctional B cells

Hypertrophic lymph nodes in *Regnase-3*$^{-/-}$ mice were seen to contain significantly increased proportions of B cells (Figure 14 & Figure 16). In addition, further shifts in different splenic B cell subsets have been observed in *Regnase-3*-deficient mice. For example, the percentages for immature B cells and marginal zone B cells in the spleen of *Regnase-3*$^{-/-}$ mice were elevated (Figure 40). Due to several shifts in B cell subsets, we postulated that Regnase-3 may fulfill a major B cell intrinsic function and could be relevant for correct maturation or responses within these cells. In particular we were debating, whether the underlying disease that causes hypertrophic lymph nodes in *Regnase-3*-deficient mice represents a B cell lymphoma, in particular because no evidence for autoimmunity was found.
It has been reported that RNA binding proteins are indeed relevant for cell fate decisions during lymphocyte maturation and that malfunctions are even associated with the development of cancer. Galloway *et al.* found that mice deficient for the two RNA binding proteins *ZFP36L1* and *ZFP36L2* specifically in B cells (Mb1-Cre) were impaired in their B cell maturation (Galloway *et al.*, 2016). Cell cycle progression within B cells of these *ZFP36L1*

and *ZFP36L2* double knockout mice was accelerated and cell quiescence was skipped, which prevented correct rearrangement of the VDJ antigen receptor genes (Galloway *et al.*, 2016). Thus, B cells in the bone marrow could not mature and were stuck in the pro- and pre-B cell stadium (Galloway *et al.*, 2016).

Similarly, RNA binding proteins also influence T cell maturation. UPF1 is an RNA helicase that is involved in nonsense-mediated decay mechanisms (Fiorini *et al.*, 2015). Mice that express a dominant-negative form of UPF1 showed developmental arrest of thymocytes and had reduced cell numbers in the fetal thymus (Frischmeyer-Guerrerio *et al.*, 2011). This was explained by perturbed V to DJ arrangements of the T cell receptor genes caused by missing clearance of out-of-frame alleles by nonsense-mediated mRNA decay pathways (Frischmeyer-Guerrerio *et al.*, 2011). Deletion of the mentioned RNA binding proteins *ZFP36L1* and *ZFP36L2* specifically in T cells during thymic development (CD2-Cre) caused the emergence of T cell acute lymphoblastic leukemia (Hodson *et al.*, 2010). Leukemia in these mice was explained by elevated levels of the oncogenic transcription factor Notch1 (Hodson *et al.*, 2010).

In summary, it is known that RNA binding proteins are relevant for determining cell fate decisions and defects can cause malignancies. In this study, we therefore analyzed, if *Regnase-3*$^{-/-}$ mice developed a B cell lymphoma. However, several observations conflicted with this hypothesis. First, the proliferation marker ki67, which is frequently used as diagnostic cancer marker also in human B cell lymphomas (Broyde *et al.*, 2009), was unchanged (Figure 45). Second, also *in vitro* proliferation assays refuted generalized accelerated proliferation rates of *Regnase-3*$^{-/-}$ B cells (Figure 44). Third, and most importantly, conditional *Regnase-3* deficiency in B cells failed to provoke lymphadenopathy (Figure 46).

Conditional *Regnase-3* ablation in B cells was realized with the CD19-Cre, which becomes active within the B cell linage during B cell maturation in the bone marrow and has a deletion efficiency of a 90 – 95% (Rickert *et al.*, 1997). This strongly indicates, that accumulation of B cells in hypertrophic lymph nodes was induced indirectly by another cell type. However, it is noteworthy to mention that although the CD19-Cre is already active during B cell maturation in the bone marrow, the CD19-Cre is not yet activated during the very first developmental step. The B cell co-receptor CD19 is expressed on B cells from late pro-B cells onwards and remains expressed in pre-B cells, immature B cells and most subtypes of matured B cells (Murphy and Weaver, 2018). Thus, if one would also include the very first steps of B cell maturation, the Mb1-Cre should be favored over the CD19-Cre line (Hobeika *et al.*, 2006). *Mb1* encodes for the Ig-$\alpha$ subunit of the B cell receptor and the *Mb1* gene has the advantage to be exclusively expressed within B cells and is present already in the very early pro-B cell stage (Hobeika *et al.*, 2006).

### 3.2.2 Lymphadenopathy in *Regnase-3*$^{-/-}$ mice is not caused by dysfunctional T cells

In addition to B cells, T cells also came into our focus as the potential cause of lymphadenopathy in *Regnase-3*-deficient mice. First, *Regnase-3*$^{-/-}$ mice had also relevant changes in T cell subsets, such as increased proportions of CD4$^{+}$ effector T cells within their lymph nodes or elevated proportions of splenic CD8$^{+}$ effector T cells (Figure 36). But even more importantly, hypertrophic lymph nodes also co-occur with symptoms of autoimmunity, which frequently involves over-responsive T cells. Even though indications for autoimmunity were low in *Regnase-3*-deficient mice, related proteins were shown to have major functions particularly in T cells.

Expression of some RNA binding proteins specifically in T cells prevents autoimmunity. For example, conditional *Regnase-1* deletion in T cells (CD4-Cre) provokes serve autoimmunity symptoms, including splenomegaly and hyperimmunoglobulinemia in a magnitude similar to globally deficient mice (Uehata *et al.*, 2013). Of note, initial *Regnase-1* publications were focused on its role in macrophages (Matsushita *et al.*, 2009; Liang *et al.*, 2010; Iwasaki *et al.*, 2011; Huang *et al.*, 2013). However, later publications found Regnase-1 to be primarily relevant in T cells (Uehata *et al.*, 2013; Jeltsch *et al.*, 2014; Cui *et al.*, 2017). Therefore, mice were also generated with conditional ablation of *Regnase-3* in T cells, using the CD4-Cre. Of note, CD4-Cre does not only delete in CD4$^{+}$ T cells, but also in CD8$^{+}$ T cells, as both of them experience a CD4/CD8 double-positive step during thymic development. However, *Regnase-3*$^{fl/fl}$+CD4-Cre mice did not develop hypertrophic lymph nodes and also the proportions of different immune cell subsets that were changed in globally *Regnase-3*-deficient mice appeared similar (Figure 38). Even though there were no strong indications for autoimmunity in *Regnase-3*-deficient mice, it was still remarkable that deletion of its family member *Regnase-1* in T cells caused premature death, while T cell-specific *Regnase-3* deletion causes no obvious phenotype at all, indicating quite unique roles for the two family members.

However, it might be possible that those *Regnase-3*$^{fl/fl}$+CD4-Cre mice develop mild defects or that malfunctions are only apparent under certain triggers. For example, mice deficient for *Regnase-4* did not develop changes in lymphocyte populations under steady-state conditions, however they had stronger symptoms in a model of experimental autoimmune encephalitis (Minagawa *et al.*, 2014).

In summary, Regnase-3 expression in B or T lymphocytes is not required to prevent lymphadenopathy *in vivo*.

### 3.2.3 Lymphadenopathy in *Regnase-3*$^{-/-}$ mice originates from dysfunctional myeloid cells

The observation that Regnase-3 was dispensable for the two major cell types of the adaptive immunity, however, suggested a potential role within the myeloid linage. Thus, *Regnase-3*$^{fl/fl}$ mice were crossed to mice expressing the Cre transgene under the LysM promotor to generate *Regnase-3*$^{fl/fl}$+LysM-Cre mice. LysM-Cre causes deletion of floxed alleles in a broad range of myeloid cells with high efficiency in tissue-resident macrophages (almost 100%), but only to approximately 40% in splenic macrophages. In addition, LysM-Cre deletes strongly in neutrophils (60 – 80%), but to a low amount (10% or less) in other myeloid cells such as different dendritic cell subsets, eosinophils, basophils, natural killer cells and mast cells (Abram *et al.*, 2014).

Interestingly, *Regnase-3*$^{fl/fl}$+LysM-Cre mice developed phenotypic manifestations that were both in characteristics and in magnitude similar to those observed in globally deficient mice. In particular, conditional deletion of *Regnase-3* within the myeloid linage also caused the development of severely increased skin-draining lymph nodes (Figure 55). Similarly, these hypertrophic lymph nodes could exceed numbers of up to several hundred million cells, while lymph nodes in wildtype mice have usually less then 20 million (Figure 56). And again, even though mice were deficient for *Regnase-3* in the myeloid linage, the dominant cell types were B cells and T cells, as described for the full knockout (Figure 56). Major changes in proportions of lymphocyte populations in spleen and lymph nodes were also revealed to be quite similar (Figure 56, Figure 57 & Figure 58). Thus, massively increased B cell numbers in hypertrophic lymph nodes of *Regnase-3*$^{-/-}$ mice with elevated B cell numbers do not originate from B or T cell intrinsic malignancy or maturation defects, but were instead the result of a secondary response to malfunctions within cells of the myeloid linage.

In sum, Regnase-3 expression within myeloid cells was shown to be mandatory to maintain lymphocyte homeostasis under steady-state conditions and to protect mice from lymphadenopathy. LysM-Cre deletes strongly not only in macrophages, but also in neutrophils. However, it is likely that Regnase-3 functions primarily in macrophages, since protein expression in neutrophils was rarely detectable (Figure 54).

Although one can assume that pathophysiological manifestations in both globally and myeloid-specific *Regnase-3* deficiency were caused by defects in macrophages, it is rather challenging to analyze specifically all macrophages with Cre lines. So far, suitable Cre mice that target exclusively all macrophages are not available. Difficulties in the generation of general macrophage-specific Cre lines with high deletion efficiency is likely explained by the inhomogeneity of macrophage populations. A mouse line that expressed Cre under the promotor of the chemokine receptor *$CX_3CR1$* has been shown to be quite effective in tissue-resident macrophages, but also targets monocytes and few other cell types (Yona *et al.*, 2013). Cre under the promotor of the *Tnfrsf11a* cytokine receptor is active within a high

proportion of tissue-resident macrophages, however 10 – 15% of B and T cells are also targeted (Mass *et al.*, 2016). Cre under the Integrin subunit alpha X (CD11c) promotor perfectly target alveolar macrophages, but also dendritic cells (Abram *et al.*, 2014). A Cre line that was designed for the pan macrophage marker EGF-like module-containing mucin-like hormone receptor-like 1 (better know as F4/80 antigen) was shown to be surprisingly ineffective (Abram *et al.*, 2014). In summary, it would be necessary to use several macrophage-specific Cre lines to exactly define the responsible myeloid cell subset.
A profound comparison can be also drawn to mice with myeloid conditional ablation of the family member *Regnase-1* (*Regnase-1*$^{fl/fl}$ +LysM-Cre mice), which were described in 2017 (Li *et al.*, 2017). These mice developed symptoms that were much weaker compared to mice with global or T cell-specific *Regnase-1* deficiency. Myeloid conditional deletion did not cause premature death before 5 months of age and splenomegaly or lymphadenopathy was not observed up to 3 months of age (Li *et al.*, 2017). Nevertheless starting from 5 months of age, *Regnase-1*$^{fl/fl}$ +LysM-Cre mice developed cachexia, splenomegaly, lymphadenopathy and multi-organ inflammation. Like globally *Regnase-1*-deficient mice, mice with myeloid *Regnase-1* deletion were also highly sensible to LPS induced inflammation and responded with severe lung injury (Li *et al.*, 2017). Of note, also myeloid *Regnase-1* ablation led to splenomegaly, which was not observed in *Regnase-3*-deficient mice.
Overall, conditional deletion of *Regnase-3* in T cell, B cells and in the myeloid linage demonstrated that Regnase-3 expression, particularly within macrophages, is mandatory to maintain a balanced immune system and to prevent lymphadenopathy.

## 3.3 Regnase-1 and -3 fulfill complementary functions in the innate immune response

In the following two sections, specific and common molecular expression patterns for Regnase-1 and -3 in response to activation of PRRs in macrophages will be outlined. Further, unique characteristics for Regnase-1 and -3 within the NF-κB and interferon signaling cascades will be emphasized.

### 3.3.1 Regnase-1 is a key actor in the NF-κB pathway

Regnase-1 is significantly regulated by the NF-κB signaling cascade and also controls the NF-κB pathway by itself on multiple levels. First, Regnase-1 is directly phosphorylated by the I-κB kinase (IKK) complex in response to TLR4 stimulation (see also introduction for a more detailed description). Phosphorylated Regnase-1 is then poly-ubiquinated by the E3 ligase β-TrCP and degraded via the proteasome (Iwasaki *et al.*, 2011). Second, Regnase-1 protein is also strongly expressed several hours post activation with agonists that strongly induce NF-κB signaling such as lipopolysaccharide or IL-1β (Iwasaki *et al.*, 2011). In line with this observation, intronic regions of the Regnase-1 gene contain NF-κB binding sites

(Skalniak *et al.*, 2009). Third, Regnase-1 itself also regulates the NF-κB signaling cascade by targeting the mRNA of *NF-κB inhibitor zeta* (*Nfkbiz* gene) and the mRNA of the *NF-κB* subunit *c-Rel* (Jeltsch *et al.*, 2014; Uehata *et al.*, 2013). And fourth, several NF-κB response genes, such as *Il6* mRNA are degraded by Regnase-1 (Matsushita *et al.*, 2009; Mino *et al.*, 2015).

Herein, we confirmed NF-κB-mediated transcriptional control of *Regnase-1*. Unlike wildtype macrophages, cells deficient for the NF-κB subunit *p50* failed to induce Regnase-1 protein expression four hours post Toll-like receptor 4 induction (Figure 72). In contrast, Regnase-3 expression was even stronger in *p50*-deficient macrophages, when macrophages were treated with lipopolysaccharide (Figure 72).

Nevertheless, Regnase-3 has overlapping regulatory pathways with its family member Regnase-1 and is also to some extent involved in NF-κB signaling. For example, we have found that Regnase-3, like Regnase-1 responds similarly to activation of different pattern recognition receptors (Figure 67) and in particular it is, like Regnase-1, degraded via the IKK complex (Figure 65 & Figure 66). Further, Regnase-3 overexpression was previously reported to inhibit TNFα-induced IKKα/β phosphorylation and was therefore suggested to function as negative feedback-loop in NF-κB signaling pathways (Liu *et al.*, 2013).

### 3.3.2 Regnase-3 is a key mediator in interferon responses

Despite some overlapping characteristics with Regnase-1 in the NF-κB pathway, we have found major and unique contributions for Regnase-3 in interferon responses on multiple levels.

First of all, *Regnase-3*$^{-/-}$ mice had significant pathophysiological changes, which were associated with the interferon pathway. RNA sequencing analysis of B cells from hypertrophic lymph in *Regnase-3*$^{-/-}$ mice revealed significant upregulation of interferon response genes (Figure 27). In contrast, B cells from small lymph nodes of sick *Regnase-3*$^{-/-}$ mice had no interferon signature, speaking for a distinct local prevalence (Figure 26). Nonetheless, interferon responses were also seen systemically. IFNγ serum levels are increased both in globally as well as in myeloid-deficient mice, while other tested pro-inflammatory cytokines were unchanged (Figure 29 & Figure 59). IFNγ does likely not originate from macrophages, but is most likely secreted by $CD4^+$ T cells (Figure 60). In addition, diverse interferon response factors, such as STAT1 and MHC-II were enhanced both locally within hypertrophic lymph nodes as well as systemically (Figure 30 – Figure 33). In addition to the stated interferon responses in *Regnase-3*$^{-/-}$ mice, we also found Regnase-3 to be involved in the interferon signaling cascades on a molecular level.

Regnase-1 and -3 were overall similarly regulated by an overlapping set of receptor agonist. An exception, however, was found for TLR3 activation (Figure 67 & Figure 68). Only Regnase-3, but not -1 was induced upon treatment with the double stranded RNA analog

poly-I:C. Double stranded RNA is found in some viruses and is the natural ligand for TLR3. We have found that Regnase-3 was induced transcriptionally by activation of the TLR3 downstream signaling cascade involving TBK1 and interferon regulatory receptors (IRFs) (Figure 69 & Figure 70). IRF7 was identified to be the responsible transcription factor, since an *Irf7*-deficient macrophage cell line failed to induce poly-I:C-mediated upregulation of Regnase-3 (Figure 71).

Together, these results implicate that Regnase-3 is mandatory to protect mice from overwhelming interferon responses *in vivo* and further that *Regnase-3*, but not its family member *Regnase-1* is controlled by the transcription factor IRF7 in response to innate viral immune triggers. By contrast, Regnase-1 is particularly important in the NF-κB signaling cascade. A simplified model on how Regnase-1 and -3 could be controlled in macrophages upon viral or bacterial infections is shown in Figure 79.

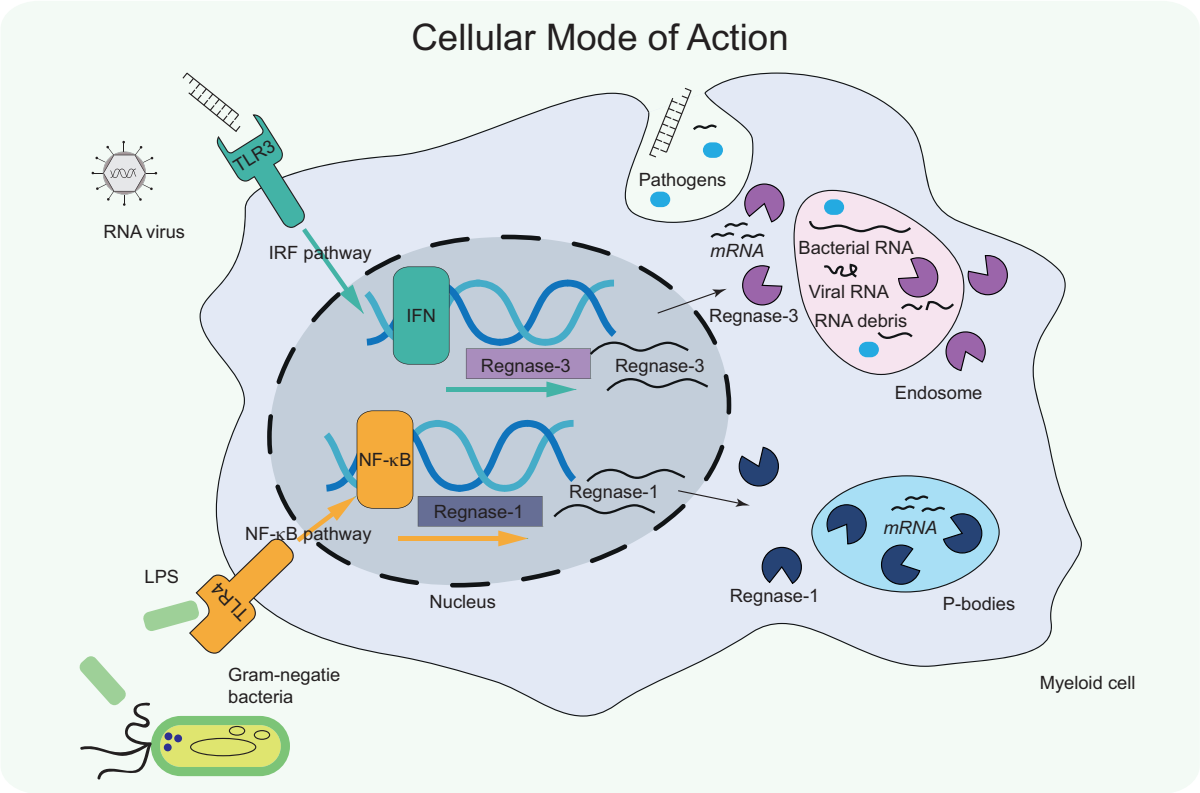


**Figure 79 Schematic representation for the proposed molecular activation pathways for Regnase-1 and Regnase-3 in macrophages.**

*Top*: TLR3 is activated by viral double stranded RNA, which induces the interferon signaling pathway, resulting in activation of the transcription factor IRF7, which causes transcription of *Regnase-3*. Translated Regnase-3 protein might cause breakdown of mRNAs, but could be also involved in recognition of phagocytized external RNA species.

*Bottom*: Bacterial cell wall components activate TLR4, which initiates NF-κB downstream signaling, resulting in NF-κB-mediated *Regnase-1* transcription. Translated Regnase-1 protein accumulates in P-bodies, where it degrades specific mRNAs. Figure adopted from von Gamm *et al.*, 2019.

Future experiments could answer if elevated interferon levels in *Regnase-3*$^{-/-}$ mice might also have a protective impact against infections. Transgenic Yeti mice have a stabilized *Ifnγ* 3'UTR leading to elevated IFNγ production (Reinhardt *et al.*, 2015). Homozygote Yeti mice develop poorly overall, however they are protected against infection with *Listeria monocytogenes* (Reinhardt *et al.*, 2015). *L. monocytogenes* is an intracellular bacterium and its clearance requires IFNγ (Buchmeier and Schreiber, 1985). Another useful experiment would be to crossbreed *Regnase-3*$^{-/-}$ mice with mice deficient for *Interferon γ* or the *Interferon γ receptor*. This approach could reveal, if hypertrophic lymph nodes with increased numbers of interferon responsive B cells originate from permanent IFNγ signaling.

## 3.4 Regnase-3 as functional complement to Regnase-1

Having demonstrated that Regnase-1 and -3 differ substantially in how they are activated in macrophages, we further wanted to evaluate if differences in Regnase expression patterns among tissues and immune cell types could indicate relevant sites of action for the respective family members. Findings regarding their expression characteristics and how this might imply their relevance for specific biological functions will be discussed in the following sections.

### 3.4.1 Regnase-1 and Regnase-3 are counter expressed

First, mRNA levels for all *Regnase* family members have been analyzed in several organs. Interestingly, the mRNA expression profiles are revealed to be quite unique. While *Regnase-1* was particularly high in the lymphoid tissues spleen and lymph nodes, *Regnase-2* was exclusively highly expressed in the intestine (Figure 49). Of note, the only publication that focuses particularly on Regnase-2 found that the mRNA of *Regnase-2* is highest expressed in human brain tissue. However, neither intestine nor lymphoid tissues were included in their analysis (Wawro *et al.*, 2019). Like *Regnase-1*, also *Regnase-4* showed an expression pattern that is focused on spleen and lymph nodes (Figure 49). In clear contrast, *Regnase-3* has low expression in thymus, bone marrow and intestine. *Regnase-3* expression in heart, lung, brain, liver and particular kidney is similar or even higher than that in spleen or lymph nodes. However, mRNA expression patterns often do not fully resemble the protein expression, not even under steady-state conditions and thus only provide an incomplete picture (Edfors *et al.*, 2016).

Unfortunately, no reliable Regnase-3-specific antibody was available at the beginning of the project. Thus, a novel monoclonal Regnase-3-specific antibody was developed in cooperation with the Helmholtz antibody core facility. This novel antibody highly recognized overexpressed Regnase-3, but unfortunately detected with reduced sensitivity also its closest family member Regnase-2 (Figure 52). Nevertheless, we estimated the antibody to be sufficient for molecular analyses. First, *Regnase-3* and *Regnase-2* showed

quite unique mRNA expression profiles and also have different calculated molecular weights. Also no relevant signal was detected in *Regnase-3*-deficient kidney tissue or macrophages.

On the level of protein, differences between Regnase-1 and -3 expression were even more pronounced. Those family members were actually counter expressed. In tissues with high Regnase-3 expression, Regnase-1 was low and *vice versa* (Figure 53). While Regnase-3 was expressed the highest in kidney, lung, brain and liver, Regnase-1 protein was barely detectable in these organs. In contrast, Regnase-1 had strong signals in spleen and lymph nodes and interestingly also in the thymus, in which *Regnase-1* mRNA levels were rather low – demonstrating that mRNA and protein abundance not necessarily correlate. In lymphoid tissues, Regnase-3 was however very lowly expressed. Data regarding Regnase-1 tissue expression, but not Regnase-3, have been already published and were revealed to be quite similar to our results (Iwasaki *et al.*, 2011).

Regnase-3 protein expression was revealed to be also quite unique in immune cells (Figure 54). Regnase-1 was ubiquitously expressed in all tested immune cells ($CD4^+$ and $CD8^+$ T cells, B cells, neutrophils, dendritic cells and macrophages). However, its expression was lowest in macrophages. In contrast, Regnase-3 was strongly expressed in macrophages and dendritic cells and weakly in B cells, while almost no signal was detectable in T cells or neutrophils.

The dominant Regnase-3 expression in antigen presenting cells, in particular in macrophages, strongly correlates with analysis for mice with conditional *Regnase-3* deficiencies. While *Regnase-3* ablation in B cells (CD19-Cre) and T cells (CD4-Cre) did not provoke lymphadenopathy, *Regnase-3* deficiency in myeloid cells (LysM-Cre) caused severe symptoms, as discussed above. Lymphadenopathy combined with almost absent Regnase-3 protein expression in neutrophils led to the conclusion that Regnase-3 has its most important function in macrophages. When also considering low abundance in lymphoid tissues and high expression in non-lymphoid tissues such as kidney, lung, liver and brain one could assume, that Regnase-3 might be important for tissue-resident macrophages.

Counter expression of Regnase-1 and -3 was also emphasized by the observation that the two members could influence the expression of their counterparts. Regnase-1 protein was significantly increased in kidney tissue as well as in macrophages deficient for *Regnase-3* (Figure 53 & Figure 54). Further, Regnase-1 has been previously reported to target its own mRNA transcript (see introduction for more details). Together with partners, we have now also performed a cell-based reporter gene assay, which demonstrated that Regnase-3 protein down regulates *Regnase-1* mRNA and that this depends on a functional RNase PIN domain in Regnase-3 (von Gamm *et al.*, 2019).

### 3.4.2 Regnase-3 might function in tissue-resident macrophages

Here, we could also emphasize particular relevance for Regnase-3 in matured macrophages with an *in vitro* experiment in which monocyte progenitor cells were differentiated into mature macrophages. While Regnase-1 was ubiquitously present throughout all days of maturation, Regnase-3 was almost absent during the first 5 days of differentiation and then occurred strongly upon the final differentiation (Figure 61). This highlights that Regnase-3 expression must be induced by factors that are part of the macrophage signature.

During this differentiation, we found a correlation of Regnase-3 expression with that of the transcription factor EGR2 (Figure 61). EGR2 is relevant for monocyte differentiation and particularly associated with anti-inflammatory M2-like macrophages (Pham *et al.*, 2012; Veremeyko *et al.*, 2018; Jablonski *et al.*, 2015). If *Regnase-3* is directly transcriptionally controlled by EGR2, or if protein expressions only correlate, remains unclear so far, but could be revealed by Chromatin Immunoprecipitation DNA-sequencing experiments (ChIP-Seq).

As described, several of our results indicated that Regnase-3 could be particularly relevant within tissue-resident macrophages. Such signs include high expression in macrophages and non-lymphoid tissues, strong protein regulation upon Toll-like receptor activation in macrophages and most importantly pathophysiologic manifestations upon its myeloid-specific deletion in mice.

Tissue-resident macrophages are very heterogeneous and have extremely tissue-specific properties, such as bone resorption in osteoclast. Therefore, failures in the functions of tissue-resident macrophages are often connected to pathologies in the normal tissue homeostasis and are difficult to predict. For example, mice deficient for granulocyte-macrophage colony-stimulating factor (GM-CSF) have unexpectedly unimpaired steady-state hematopoiesis, but instead develop progressive accumulation of surfactant lipids and proteins in the alveolar space (Dranoff *et al.*, 1994). Thus, evaluating tissue-specific functions of Regnase-3 will be interesting, though challenging.

### 3.4.3 Regnase-3 in non-lymphoid tissues

Although we have found multiple indications that suggest a role for Regnase-3 in tissue-resident macrophages, high Regnase-3 tissue-expression may also originate from non-immune cells, such as endothelial cells. First, Liu *et al.* analyzed the role of Regnase-3 in endothelial cells and found deregulated adhesion of monocytes to those cells (Liu *et al.*, 2013). Next, endogenous Regnase-3 expression in mouse embryonic fibroblast was also high enough to be easily detected in immunoblot assays and was also regulated upon LPS stimulation in those fibroblasts (Figure 66). Further, Regnase-3 expression was particularly high in kidney cells. Some tissue-resident macrophages indeed reside within the kidney,

which are believed to settle the organ during embryonic development (Schulz *et al.*, 2012; Sheng *et al.*, 2015). However, the amount of total immune cells is rather low in healthy, adult kidney tissue, while injury significantly enhances recruitment of macrophages (Kawakami *et al.*, 2013; Bolisetty *et al.*, 2015). Consequently, it might also be plausible that high Regnase-3 expression in non-lymphoid tissues originates from non-immune cells.
Of note, together with our cooperation partner Mathias Heikenwälder, we have tried to use our newly developed Regnase-3-specific antibody in histologic tissue sections, but failed to obtain reliable results. In addition to high Regnase-3 expression in the kidney, *Regnase-3*$^{-/-}$ mice also had higher prevalence to suffer from hydronephrosis (data not shown). However, since those observations varied significantly and were very inconsistent over time, data were not included into the study. Interestingly, the occurrence of nephropathy did not correlate well with lymphadenopathy. Thus, Regnase-3 might also impacts renal function and disease.

### 3.4.4 Regnase-3 as evolutionary counterpart to Regnase-1

In summary, our data as well as published studies imply, that Regnase-1 contributes significantly to the NF-κB signaling cascade and is required to protect mice from autoimmunity by controlling T cell responses. In clear distinction, Regnase-3 is profoundly involved in the regulation of interferon responses *in vivo*, is controlled by interferon response factors and is mandatory in myeloid cells.
On the level of protein and mRNA, those two family members seem to be counter expressed and reporter gene assays assume that Regnase family members do not only possess an intrinsic feedback loop, but are further mutually controlled. This suggests that Regnase-3 evolved as an evolutionary counterpart to Regnase-1 and acts in myeloid cells in response to interferon signaling.
Figure 80 displays a schematic model that should visualize how Regnase-1 and -3 contribute to a balanced immune homeostasis. Counter regulation of Regnase-1 and -3 is indicated with a double-scale on the right hand site. Their activation by pro-inflammatory NF-κB or interferon pathways is shown on the left, while Regnase-1 and -3 themselves act as anti-inflammatory factors (*right* site).

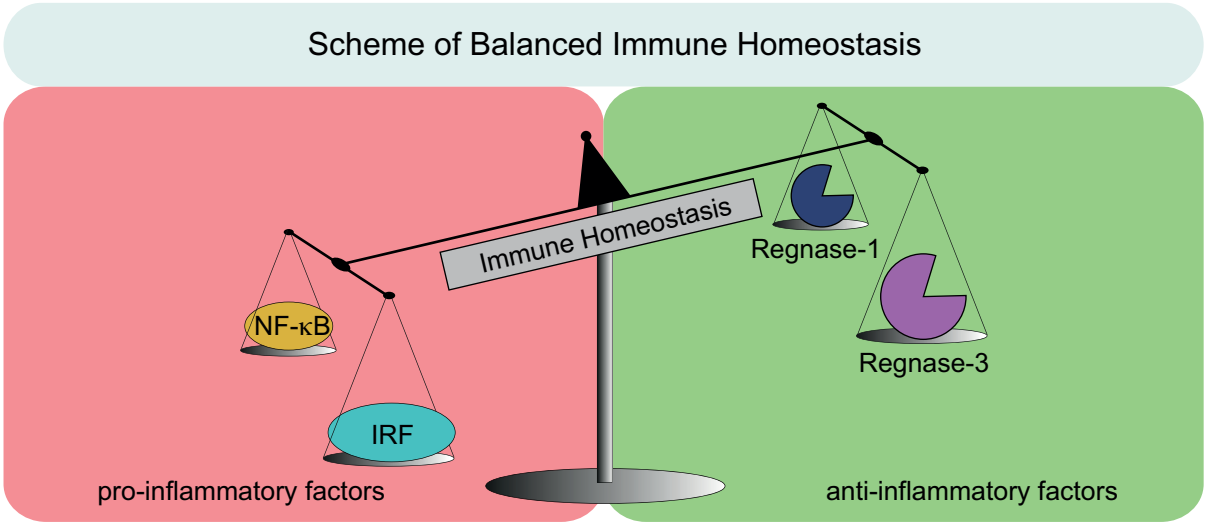


**Figure 80 Schematic representation for balanced immune homeostasis regulated by Regnase-1 and -3.**

*Left*: Activation of transcription factors of the NF-κB and IRF signaling cascades induce pro-inflammatory factors. *Right*: Regnase-1 and Regnase-3 are also induced by NF-κB and IRFs, respectively, but act as anti-inflammatory factors. In addition, Regnase-1 and -3 seem to affect each other and appear counter-expressed. This provides a complex homeostasis, which is be visualized by the double-scales. Figure modified from (von Gamm *et al.*, 2019)

## 3.5 Molecular properties and predicted functions

So far, the physiological significance for Regnase-3 has been discussed and thereafter its specificity for organs and cell types. Now, subcellular attributes and molecular functions of Regnase-3 will be reviewed to suggest potential modes of action.

### 3.5.1 Regnase-3 can bind and degrade RNA

All Regnase family members possess a specific CCCH zinc finger motif for nucleic acid binding (Liang *et al.*, 2008). This active site is highly conserved among the family members and contains 3 cysteines and one histidine in close proximity. In all four proteins, the zinc finger is composed as $C(X)_5C(X)_5C(X)_3H$ type, meaning that each of the 3 cysteines is spaced by 5 amino acids from another cysteine and that cysteine and histidine are spaced by 3 amino acids (Liang *et al.*, 2008). Regnase-3 has highest sequence homology with Regnase-2, so that all spacing amino acids of the CCCH domain are identical in these two family members, but slightly differ from Regnase-1 and -4 (Liang *et al.*, 2008).

The origin of the name for this group of RBPs is the $Zn^{2+}$ ion, which is harbored in a pocket formed by the CCCH motif (Yokogawa *et al.*, 2016). Although some of the 59 known rodent CCCH Zn finger proteins may bind DNA, most of them primarily bind RNA and have diverse molecular functionality including RNA deadenylation, mRNA splicing, translation, RNA decay and several more (Fu and Blackshear, 2017).

Direct binding of the CCCH Zn finger domain in *Regnase-1* to mRNA has been demonstrated by crystal structure analysis (Yokogawa *et al.*, 2016). In our publication associated to this

work, we could also demonstrate that Regnase-3 binds to different RNA species in an RNA electrophoretic mobility shift assays (EMSA) (von Gamm *et al.*, 2019).

Further, all Regnase family members share the PilT N-terminus like (PIN) domain, which contains an RNase catalytic center (Matsushita *et al.*, 2009; Yokogawa *et al.*, 2016). The PIN domain forms a negatively charged catalytic pocket that harbors a $Mg^{2+}$ ion and is important for the catalytic activity of the protein (Matsushita *et al.*, 2009). The potential of Regnase-1 to degrade RNA has been shown in multiple assays and the catalytic activity of the PIN domain has been verified by generation of the D141N mutant in which the negatively charged aspartic acid is mutated to the positively charged asparagine and therefore lacks RNase activity (Matsushita *et al.*, 2009).

Regnase-1 was seen to specifically recognize AU rich elements, primarily in the 3'UTR of target mRNAs (Mino *et al.*, 2015) (also see introduction for more detailed description). Consequently, Regnase-1 does not randomly degrade all kinds of RNA *in vivo*, but in contrast has strong sequence specificity. For example, *Il6* mRNA is a Regnase-1 target gene, but *Tnfα* mRNA is not (Matsushita *et al.*, 2009).

Our publication also showed that Regnase-3 degrades several RNA species *in vitro*, however without apparent sequence specificity (von Gamm *et al.*, 2019). This observation does not necessarily reflect the *in vivo* situation, since also Regnase-1 lacked sequence specificity in a pure *in vitro* assay (Matsushita *et al.*, 2009). Thus, it has been proposed that Regnase-1 provides the nuclease activity, while sequence specificity comes from further interacting RNA binding proteins, such as Roquin-1 (Jeltsch *et al.*, 2014).

Although unspecific RNA degradation by Regnase-3 was seen in a pure *in vitro* assay, a cell-based reporter gene assay demonstrated that the 3'UTR of the barely regulated control gene *Hprt1* and also that of *Ifnγ* were not regulated by Regnase-3 protein, while the 3'UTR of *Regnase-1* was destabilized when Regnase-3 protein was overexpressed (von Gamm *et al.*, 2019). The observed down regulation was dependent on the Regnase-3 PIN domain, since the effect was abolished when cells were transfected with a Regnase-3 D271N mutant form, reflecting the D141N mutation in Regnase-1 (von Gamm *et al.*, 2019). This indicates that Regnase-3 also possesses specificity under cellular conditions and might also promote a negative feedback loop in immune responses by initiating mRNA breakdown of defined mRNAs.

### 3.5.2 Regnase-3 as a potential RNA sensor

Regnase-3 protein is highly expressed in macrophages and most likely acts primarily in myeloid cells *in vivo*. Thus, it was reasonable to reveal differentially expressed genes in *Regnase-3*$^{-/-}$ macrophages in a global approach with the perspective to explain pathophysiologic manifestations in *Regnase-3*$^{-/-}$ mice.

Therefore, *Regnase-3*$^{+/+}$ and *Regnase-3*$^{-/-}$ macrophages were differentiated from bone marrow and treated under a variety of conditions and were analyzed by RNA sequencing (Figure 76).

Macrophages were treated for example with high molecular weight poly-I:C, which was seen to particularly activate Regnase-3 expression, but not that of its family member Regnase-1 (see discussion above). In some samples, subsequent to receptor activation, cells were treated with Actinomycin D, which blocks mRNA *de novo* synthesis. Thus, effects caused by mRNA breakdown are emphasized in the sequencing counts.
Surprisingly, almost no gene was differentially expressed in the knockout cells under any of the nine tested treatment conditions (Figure 76). This unexpected result opens space for debate and three possible explanations, which are related to RNA sensing properties in related proteins, will be discussed below.

One explanation could be that bone marrow derived macrophages lack co-expressed proteins needed for sufficient activation and that those cells therefore might be not suitable. It could be possible that activation of Regnase-3 is similarly complex like that of the antiviral endoribonuclease RNase L. The "L" in RNase L originates from "latent", since the endoribonuclease is inactive, when synthesized (Payne, 2017). This protein needs activation by 2'-5' oligo A synthase (OAS). OAS is also produced as an inactive form, but gets activated when bound to double stranded RNA, which occurs during some viral infections (Payne, 2017). Activated OAS then metabolizes ATP to 2'-5'oligoadenylate, which acts as second messenger that causes dimerization and thus activation of RNase L (Chakrabarti *et al.*, 2011). The functional RNase L dimers then degrade viral RNA and therefore execute an efficient antiviral defense mechanism (Payne, 2017). However, RNase L has low specificity and also degrades host RNA species, such as ribosomal RNA and causes autophagy (Chakrabarti *et al.*, 2012). Apparently, activated RNase L can be very harmful for the cell and thus its expression and activation is controlled on multiple levels, including transcriptional activation by interferons (Chakrabarti *et al.*, 2011).
Up to now, molecular functions of Regnase-3 are far from being understood and thus it is quite conceivable that Regnase-3 might be involved in a complex regulatory activation pathway like that of RNase L, which similarly acts in the interferon response.

A second explanation for barely differentially expressed genes in Regnase-3$^{-/-}$ macrophages could be given by assuming that Regnase-3 does not primarily target mRNAs. Certain observations support a functional model, in which Regnase-3 would be responsible for processing of incoming pathogens or cellular components rather than regulating post-transcriptional gene expression. In our associated publication, we demonstrated that Regnase-3 shows a distinct subcellular localization profile that differs from that for Regnase-1 (von Gamm *et al.*, 2019). Regnase-3 was localized within small subcellular granules, which however did not co-localize with Regnase-1 or with processing bodies, in which mRNA turnover takes place (von Gamm *et al.*, 2019). In contrast, endogenous Regnase-3 partially localized to endosomes, in which extracellular matrix is internalized and

strongly co-localized with phagocytized Dextrane molecules (von Gamm *et al.*, 2019). Thus, Regnase-3 might work as an RNase that degrades viral or resorbed cytosolic RNA molecules, and consequently suppresses viral infections. Of note, among all tested immune cells, Regnase-3 protein expression was only observed in macrophages, dendritic cells and B cells, which all belong to the group of antigen presenting cells (Figure 54). Thus, Regnase-3 may play a role in processing phagocytized components for antigen presentation. However, uptake of *Staphylococcus aureus* particles was unchanged in *Regnase-3*$^{-/-}$ macrophages *in vitro* (Figure 77). Also an *in vivo* infection model with *Staphylococcus aureus*, which was performed together with our cooperation partners revealed no differences in bacterial clearance or defects in phagocytic uptake (von Gamm *et al.*, 2019).

A third, however, closely related function for Regnase-3 would be RIG-I-like RNA sensing properties. Like Retinoic acid-inducible gene I (RIG-I), Regnase-1 might also function as viral RNA sensing molecule and initiate viral response programs. RIG-I is a cytoplasmic protein, can be induced by interferons and is able to recognize viral, double stranded RNA molecules (see also introduction for more detailed description) (Theofilopoulos *et al.*, 2011; Takeuchi and Akira, 2010). RIG-I specifically recognizes viral 5' tri-phosphorylated RNA (Hornung *et al.*, 2006). The downstream signaling cascade of RIG-I results in the activation of key innate immune transcription factors, including IRF3 & 7 as well as NF-κB, consequently causing enhanced expression of type I and III interferons and other pro-inflammatory factors (Chow *et al.*, 2018).

## 3.6 Disease association and perspective for Regnase-3 as potential drug target

### 3.6.1 GWAS associate Regnase-3 with psoriasis and Alzheimer's disease

Though only very few publications cover Regnase-3 so far, the gene has already been correlated to human diseases. One publication associated Regnase-3 with late onset Alzheimer's disease (Chaudhry *et al.*, 2015). In line with that observation, we have also observed rather high Regnase-3 protein expression in the brain. Future evaluations as to whether this expression is related to the microglia, a brain-resident macrophage population or to neuronal and other cells might help to clarify brain-associated functions of Regnase-3.
Further, *Regnase-3* has been also identified as a psoriasis susceptibility gene in a genome wide association study (GWAS) for single-nucleotide polymorphisms (SNPs) in a Caucasian cohort (Tsoi *et al.*, 2012). In addition, *Regnase-3* was also found to be associated with the disease in a genome wide association study in a cohort of 533 Pakistani psoriasis patients and 373 controls (Munir *et al.*, 2015). Whether malfunctioning Regnase-3 indeed provokes psoriasis remains enigmatic up to now. Significant skin irritations have not been observed in *Regnase-3*$^{-/-}$ mice, although we noticed that hypertrophy was frequently observed in skin-

draining lymph nodes, but only rarely in mesenteric lymph nodes, which are located in close proximity to the intestine.

Etiology of psoriasis is still incompletely understood and several immune cell types are affected in skin lesions, among those is a specific type of myeloid cells, the Langerhans cells. Langerhans cells from psoriasis skin did not migrate in response to TNFα or IL-1β like cells from healthy tissue did (Cumberbatch *et al.*, 2006). In line with this, overexpression of Regnase-3 impaired migration of tumor cells (Suk *et al.*, 2018), which could provide a potential explanation for psoriasis susceptibility upon altered *Regnase-3* genes in humans.

### 3.6.2 Targeting Regnase-3 in cancer therapies

In addition to dementia and psoriasis, Regnase-3 could be also evaluated regarding its potential to be targeted in novel cancer treatment regimens, which aim to activate endogenous immune cells to fight tumor cells. Those targeting strategies block mechanisms that inhibit activation pathways and thus indirectly enhance the immune response. Since Regnase-3 acts as an anti-inflammatory molecule *in vivo*, it could be potentially used as drug target in such cancer treatments.

The treatments have been initially developed for $CD8^+$ T cells, because they are highly important to fight virus infected or cancerous endogenous cells. Under specific conditions, such as constant antigen encounter in chronic viral infections or within the tumor microenvironment, $CD8^+$ T cells however might convert into a status of unresponsiveness, also known as exhaustion (Gallimore *et al.*, 1998; Ahmadzadeh *et al.*, 2009). Activation of exhausted T cells is impeded due to upregulation of inhibitory receptors, which reduce signal transduction. The Nobel laureate James P. Allison demonstrated that increased surface expression of the Cytotoxic T-lymphocyte-associated protein 4 (CTLA-4) on $CD8^+$ T cells reduces their activation responses (Krummel and Allison, 1995). CTLA-4 shows sequence homology to the T cell co-receptor CD28 and can outcompete its binding to co-stimulatory receptors CD80 and CD86 on antigen presenting cells (Linsley *et al.*, 1994; Linsley *et al.*, 1991). This reduced signal transduction is initiated by activation programs and is known as immune checkpoint to prevent overwhelming immune responses, which could otherwise cause tissue damage.

However, unresponsiveness in T cells may impede sufficient tumor cell eradication and thus pharmaceutical checkpoint inhibitors have been developed to release the brake in immune cell activation. The monoclonal antibody Ipilimumab inhibits CTLA-4 and has been approved by the US food and drug administration (FDA) for the treatment of melanoma and other malignancies (Phan *et al.*, 2003; Park *et al.*, 2016).

Meanwhile, therapeutic interference of checkpoint blockade drugs is not restricted to T cells alone anymore. Also tumor and stromal cells have been identified as potent drug targets in checkpoint inhibition therapies. For example, Programmed death-ligand 1 (PD-L1) is found

on tumor cells and antigen presenting cells such as macrophages and inhibits $CD8^+$ T cells via binding to their Programmed cell death protein 1 (PD-1) receptors (Ishida *et al.*, 1992; Karwacz *et al.*, 2011).

Several clinical trials are currently testing different PD-L1-specific antibodies such as Atezolizumab to target tumor-infiltrating macrophages and other cells of the tumor microenvironment (Seidel *et al.*, 2018; Balar *et al.*, 2017). Tumor infiltrating macrophages are believed to have immune suppressive functions on cytotoxic T cells and abundance of some macrophage subtypes is a negative prognostic marker for tumor growth and survival in humans (Mitchem *et al.*, 2013; Lundgren *et al.*, 2017). Therefore, releasing inhibitory functions in macrophages might be beneficial to improve treatment regimes in cancer patients. Thus, one could speculate that inhibition of Regnase-3 as a potential negative regulator of immune responses could also improve tumor cell eradication by enhancing cytotoxicity of T cells.

# 4 Conclusion

Several RNA binding proteins, such as Regnase-1, are fundamental for maturation, activation, inactivation and pathogen recognition processes in immune cells. Though Regnase-1 has been thoroughly studied in the past, functions of its family member Regnase-3 remained widely unknown so far.

Data presented herein provide the first in-depth characterization of mice deficient for the RNase *Regnase-3* and demonstrate its fundamental role in myeloid immune cells.
We have found that absence of *Regnase-3* destroys the homeostatic balance *in vivo*, causing lymphadenopathy and shifted immune cell populations in the mouse. Further, we excluded B cells and T cells as initially disease-causing cell types and found that defects in myeloid cells provoked hypertrophy in lymph nodes.
Furthermore, Regnase-3 expression in myeloid cells was identified to be pivotal for controlling the *in vivo* interferon response. In line with this, protein expression of Regnase-3, but not that of its family member Regnase-1, was induced by the transcription factor IRF7, when macrophages were treated with a viral, double stranded RNA analogue.
Regnase-1 is key for the NF-κB signaling cascade and highly relevant in T cell responses. Regnase-3, however, is involved in the interferon signaling pathway and is highly abundant in macrophages, but also in non-lymphoid tissues. This suggests that Regnase-3 evolved as key modulator in myeloid cells for the regulation of *in vivo* interferon responses and represents a functional counterpart to Regnase-1.

This study is the first to depict pathophysiological consequences of *Regnase-3* deficiency *in vivo* and describes cell-biological and molecular attributes of Regnase-3, which help to explain the pathogenesis. Although multiple aspects still remain elusive, we believe that our work provides a substantial contribution to the field. We hope these data will give an impetus to the scientific community for future research that may also tackle the predicted association of Regnase-3 with psoriasis susceptibility in humans.

# 5 Materials

## 5.1 Equipment

**Table 1 Equipment**

| *Device* | *Company* |
|---|---|
| 2100 Bioanalyzer instrument | Agilent |
| ABX Micros ES60, automated cell counter | Horiba Medical |
| AxioScan.Z1, digital slide scanner | Carl Zeiss |
| Beckman J2_MI centrifuge | Beckman |
| Bond Max, immunohistochemistry robot | Leica |
| BZ-9000, fluorescence microscope | Keyence |
| Centrifuge 5424 R and 5720 R cooling centrifuge | Eppendorf |
| DynaMag-2 and-5 Magnet (magnet for Dynabeads) | Life Technologies |
| FACS AriaIII Flow Cytometer (FACS Sorter) | BD Bioscience |
| GelDoc-It TS Imaging System (DNA gel imaging system) | Analytik Jena |
| HERA cell 150i $CO_2$ incubator (cell culture incubator) | Thermo Scientific |
| Herasafe KS biological safety cabinet | Thermo Scientific |
| Heratherm IGS180 microbiological incubator | Thermo Scientific |
| HiSeq 2500 | Illumina |
| HiSeq 4000 | Illumina |
| Infinite F200 Pro, microplate reader | Tecan |
| Innova shaker incubator (for bacterial cultures) | New Brunswick |
| MACS magnets for LM columns and LS columns | Miltenyi |
| Mastercycler nexus, thermal PCR cycler | Eppendorf |
| Mastercycler pro, thermal PCR cycler | Eppendorf |
| Milli-Q A10 Advantage lab water device | Merck-Millipore |
| Mini-PROTEAN II multiscreen apparatus, for immunoblots | Bio-Rad |
| Mini-PROTEAN Tetra Vertical Electrophoresis Cell (chamber for SDS-PAGE gels and protein transfer) | Bio-Rad |
| Multifuge X3 FR cooling centrifuge | Heraeus |
| Nanodrop 2000 (micro volume Spectrophotometer) | Thermo Scientific |
| Neubauer chamber (hemocytometer) | Carl Roth |
| PHERAstar, microplate reader | BMG Labtech |
| Quant Studio 6 Flex, real-time PCR system | Life Technologies |
| Qubit 2.0 Fluorometer | Thermo Scientific |
| Rolling mixing device RM5-1765 | Fröbel Labortechnik |
| SCN400, digital slide scanner | Leica |
| ThermoMixer C shaker incubator | Eppendorf |
| TissueLyser II, bead mill | Qiagen |
| Ultra-fine scale | Mettler Toledo |
| VarioSkan Lux, microplate reader | Thermo Scientific |
| Water bath WB7 | Memmert |

## 5.2 Mouse strains

**Table 2 Mouse strains**

| *Mouse strain* | *Origin* |
|---|---|
| *Zc3h12c*$^{tm2a(EUCOMM)Hmgu}$ (*Regnase-3*-deficient mice, knockout-first allele) | EUCOMM via Wolfgang Wurst (Helmholtz Center Munich) |
| *Gt(ROSA)26Sor*$^{tm1(FLP1)Dym}$ (ROSA26-Flp mice) | Kindly provided by Wolfgang Wurst (Helmholtz Center Munich) |
| *GT (ROSA) 26Sor Cre* (ROSA26-Cre mice) | Kindly provided by Wolfgang Wurst (Helmholtz Center Munich) |
| *B6.129P2-Lyz2*$^{tm1(cre)Ifo}$/J (LysM-Cre mice) | Kindly provided by Veit Buchholtz (TU Munich) |
| *STOCK Tg(Cd4-cre)1Cwi/BfluJ* (CD4-Cre mice) | Kindly provided by Daniel Krappmann |
| *C.Cg-Cd19*$^{tm1(cre)Cgn}$ *Igh*$^{b}$*/J* (CD19-Cre mice) | Kindly provided by Marc Schmidt-Supprian (TU Munich) |
| C57BL/6J | Jackson Laboratory via Charles River |
| *B6.Cg-Nfkb1*$^{tm1Bal}$/J (*p50*-deficient mice) | Kindly provided by Tobias Stöger (Helmholtz Center Munich) |

Mice with conditional deficiency for *Regnase-3* (*Zc3h12c*) were generated by mating strategies as described in the methods section.

## 5.3 Cell lines

**Table 3 Cell lines**

| *Cell line* | *Origin* |
|---|---|
| Estrogen receptor driven Hoxb8 expressing bone marrow progenitor cells (ER-Hoxb8 cells) | Generated and provided by Christian Schulz *et al.* (LMU Munich) with constructs provided by Hans Haecker (St. Jude Children's Research Hospital, Memphis, USA). |
| HEK293T cells | ATCC |
| J774.2 cells | ATCC |
| L929 cells (for M-CSF production) | Kindly provided by Prof. Henriette Uhlenhaut (Helmholtz Center Munich) |
| *NEMO*$^{-/-}$ mouse embryonic fibroblasts (MEFs) and *NEMO* reconstitutes MEFs. | Generated by Marc Schmidt-Supprian *et al.* (TU Munich) and provided by Daniel Krappmann (Helmholtz Center Munich) |
| Mouse embryonic fibroblasts (MEFs) with overexpression of Regnase family members | Self generated as described in material and methods. |
| RAW-Lucia ISG cells | Invivogen |
| RAW-Lucia ISG-KO-IRF3 cells | Invivogen |
| RAW-Lucia ISG-KO-IRF7 cells | Invivogen |
| Stem cell factor (SCF)–producing Chinese Hamster Ovary (CHO) cells | Kindly provided by Prof. Christian Schulz (LMU Munich) |

## 5.4 Antibodies and material for flow cytometry

**Table 4 Flow Cytometry antibodies and dyes**

| *Antigen / reagent* | *Clone* | *Fluorophore* | *Manufacturer* | *Dilution* |
|---|---|---|---|---|
| Carboxyfluorescein succinimidyl ester (CFSE) | – | CFSE | Invitrogen | 1:1000 |
| CD11b | M1/70 | FITC | Biolegend | 1:100 |
| CD11c | N418 | APC | Biolegend | 1:300 |
| CD138 | 281-2 | PE | Biolegend | 1:100 |
| CD16/32 (Fc block) | FCR3-4G8 | – | Core facility (R. Feederle) | 1:300 |
| CD19 | 6D5 | PerCP/Cy5.5 | Biolegend | 1:100 |
| CD206 | MMR | BV421 | Biolegend | 1:100 |
| CD21 | 8D9 | FITC | eBioscience | 1:100 |
| CD23 | B3B4 | PE | Biolegend | 1:100 |
| CD38 | 8D9 | FITC | Biolegend | 1:100 |
| CD3e | 145-2C11 | FITC | Biolegend | 1:100 |
| CD4 | GK1.5 | FITC | Biolegend | 1:100 |
| CD4 | RM4-5 | PE | BD Biosciences | 1:400 |
| CD44 | IM7 | PE | BD Pharmingen | 1:800 |
| CD45R/B220 | RA3-6B2 | PE | Biolegend | 1:100 |
| CD45R/B220 | RA3-6B2 | PerCP/Cy5.5 | Biolegend | 1:100 |
| CD45R/B220 | RA3-6B2 | PE/Cy7 | eBioscience | 1:200 |
| CD62L | MEL-14 | APC | Biolegend | 1:100 |
| CD8a | 53-6.7 | FITC | Biolegend | 1:200 |
| CD8a | 53-6.7 | PE/Cy7 | Biolegend | 1:300 |
| CD90.2/Thy1.2 | 53-2.1 | Pacific Blue | Biolegend | 1:200 |
| CD93/AA4.1 | AA4.1 | APC | eBioscience | 1:100 |
| CD95 (APO-1/Fas) | 15A7 | PE | eBioscience | 1:75 |
| F4/80 | BM8 | PE | Biolegend | 1:100 |
| Fixable viability dye | – | eFluor 780 | eBioscience | 1:2000 |
| Fixable viability dye | – | Zombie Aqua | Biolegend | 1:300 |
| FoxP3 | FJK-16s | APC | eBioscience | 1:100 |
| Gr1 | RB6-8C5 | APC | Biolegend | 1:800 |
| IFNγ | XMG1.2 | BV421 | eBioscience | 1:200 |
| IgD | 11-26c.2a | Pacific Blue | Biolegend | 1:100 |
| IgM | RMM-1 | AF647 | Biolegend | 1:100 |
| IgM | RMM-1 | PE/Cy7 | Biolegend | 1:100 |
| NK1.1 | PK136 | PerCP/Cy5.5 | eBioscience | 1:200 |
| TCRβ | H57-597 | APC | eBioscience | 1:200 |

## 5.5 Antibodies and material for immunoblotting

**Table 5 Immunoblot antibodies**

| *Antigen* | *Clone* | *Manufacturer/Origin* |
|---|---|---|
| Actin | C4 | Merck |
| C/EBPα | G-10 | Santa Cruz |
| Elk-1 | 9182 | Cell Signaling |
| GAPDH | 1A7 | Core facility (R. Feederle) |
| GFP | 3H9 | Core facility (R. Feederle) |
| HA | 12CA5 | Core facility (R. Feederle) |
| IRF3 | D83B9 | Cell Signaling |
| IRF7 | W16064A | Biolegend |
| p50 | sc-1190 | Santa Cruz |
| PU.1 | C-3 | Santa Cruz |
| Regnase-1 (Zc3h12a) | 15D11 | Core facility (R. Feederle) |
| Regnase-3 (Zc3h12c) | 4D3 | Core facility (R. Feederle) (newly established) |
| β-Tubulin | H-235 | Santa Cruz |

Horseradish peroxidase (HRP) conjugated secondary antibodies were all from Cell Signaling: goat anti-rabbit IgG (7074), horse anti-mouse IgG (7076) and goat anti-rat IgG (7077). Commercially purchased primary antibodies were diluted 1:1000 in 5% BSA in TBS-T with 0.01% sodium azide, except anti-IRF7, which was diluted 1:400. Antibodies from the core facility were delivered as cell culture supernatant, which was diluted 1:20 in 5% BSA plus 1% milk in TBS-T with 0.01% sodium azide.

## 5.6 Antibodies for immunohistochemistry

**Table 6 Immunohistochemistry antibodies**

| *Antigen* | *Clone* | *Species* | *Manufacturer/Origin* | *Dilution* |
|---|---|---|---|---|
| B220 | RA3-6B2 | Rat-IgG2a | Becton Dickinson | 1:3000 |
| CD3 | SP7 | Rabbit IgG | Zytomed | 1:250 |
| CD68 | Ab125212 | Rabbit IgG | Abcam | 1:100 |
| F4/80 | BM8 | Rat-IgG2a | Linaris | 1:200 |
| Ki67 | SP6 | Rabbit IgG | Thermo Scientific | 1:200 |
| MHC-II | M5/114.15.2 | Rat IgG | Novus Biologicals | 1:500 |
| Tyr701-pSTAT1 | 58D6 | Rabbit IgG | Cell Signaling | 1:100 |

Stainings were performed on the immunohistochemistry robot Bond Max (Leica). Detection reagents were from the 'Bond Polymer Refine Detection Kit' (DS9800), including peroxidase block, secondary-anti-rabbit-HRP antibody, 3,3'-Diaminobenzidine (DAB) reagent and haematoxylin/eosin (H&E) solutions. Primary antibodies from the rat were pre-incubated with an additional rabbit-anti-rat bridging antibody (Dianova, #312-005-045).

## 5.7 Antibodies, cytokines, agonists and inhibitors for cell culture

**Table 7 Cytokines, chemokines, agonists and inhibitors used in cell culture**

| *Cytokine, chemokine, agonist, inhibitor* | *Manufacturer* |
|---|---|
| (S)-MG132 | Cayman Chemical |
| Brefeldin A | Sigma-Aldrich |
| C-type CpG ODN2395 | Miltenyi |
| Chloroquine diphosphate salt | Sigma-Aldrich |
| Dimethyl sulfoxide (DMSO) | Carl Roth |
| Flagellin (utra-pure) | Invivogen |
| GM-CSF | Peprotech |
| IFNγ (murine, recombinant) | R&D Systems |
| IL-10 (murine, recombinant) | R&D Systems |
| IL-15 (murine, recombinant) | R&D Systems |
| IL-1β (murine, recombinant) | R&D Systems |
| IL-4 (murine, recombinant) | R&D Systems |
| IL-6 (murine, recombinant) | R&D Systems |
| Ionomycin | Santa Cruz Biotechnology |
| Lipopolysaccharides (LPS) from *Salmonella enterica* serotype *typhimurium* | Sigma-Aldrich |
| Lipoteichoic acid (LTA) from *Staphylococcus aureus* | Sigma-Aldrich |
| M-CSF | Peprotech |
| MRT67307 (Ikkε/TBKI inhibitor) | Merck |
| Murabutide | Invivogen |
| Phorbol-12-myristat-13-acetat (PMA) | Sigma-Aldrich |
| Polybrene (Hexadimethrine bromide) | Sigma-Aldrich |
| Polyinosinic:polycytidylic acid (poly-I:C), high molecular weight | Invivogen |
| Polyinosinic:polycytidylic acid (poly-I:C), low molecular weight | Merck |
| Proleukin S (IL2-analog) | Novartis |
| Puromycine · 2HCl | Merck |
| R848 (Resiquimod) | Cayman Chemical |
| *Staphylococcus aureus* bioparticles coupled to pH sensitive pHrodo green fluorophore | Invitrogen |
| TNFα (murine, recombinant) | Novus Biologicals |
| β-estradiol | Cayman Chemical |

**Table 8 Antibodies used for cell culture and Regnase-3 antibody ELISA**

| *Antigen* | *Clone* | *Species* | *Manufacturer/Origin* |
|---|---|---|---|
| CD11c-APC | N418 | Hamster monoclonal | Biolegend |
| CD11c-biotin | N418 | Hamster monoclonal | Biolegend |
| CD16/32 (Fc block) | FCR3-4G8 | – | Core facility (R. Feederle) |
| CD19-biotin | 6D5 | Rat monoclonal | Biolegend |
| CD28 | 37N | Hamster monoclonal | Core facility (R. Feederle) |
| CD3 | 145-2C11 | Hamster monoclonal | Core facility (R. Feederle) |
| Glutathion-S-Transferasen (GST) | 6G9 | Rat monoclonal | Core facility (R. Feederle) |
| Glutathion-S-Transferasen (GST) | 2C8 | Mouse monoclonal | Core facility (R. Feederle) |
| Goat-anti hamster IgG | # 55397 | Goat polyclonal | MP Biomedicals |
| IgM | RMM-1 | Rat monoclonal | Biolegend |

## 5.8 Media for cell culture

**Table 9 Compounds used for cell culture media**

| *Chemical / Kit* | *Manufacturer* |
|---|---|
| Accutase solution | Sigma Aldrich |
| Dulbecco's Modified Eagle's Medium (DMEM), high glucose | Life Technologies |
| Fetal bovine serum (FBS) (# F9665) | Sigma Aldrich (used for DCs, macrophages, RAW cells) |
| Fetal bovine serum (FBS) (# 10270) | Invitrogen (used for all cells except primary macrophages, DCs and RAW cells) |
| GlutaMAX | Life Technologies |
| HEPES buffer (1 M) | Life Technologies |
| Iscove's Modified Dulbecco's Medium (IMDM) | Life Technologies |
| MEM Vitamin Solution (100x) | Life Technologies |
| Non-essential amino acids (100x) | Life Technologies |
| Penicillin-streptomycin (10.000 U/ml) (P/S) | Life Technologies |
| Phosphate-buffered saline (PBS) | Life Technologies |
| RPMI 1640 | Life Technologies |
| Sodium pyruvate | Lonza |
| Trypsin/EDTA (0.05%) | Life Technologies |
| β-mercaptoethanol | Life Technologies |

**Table 10 Composition of cell culture media**

| *Cell culture Medium* | *Composition* |
|---|---|
| 293T medium | DMEM, supplemented with 10% FBS (Invitrogen), 100 U/ml penicillin/streptomycin and 10 mM HEPES pH 7.2 |
| BMDM differentiation medium | DMEM, supplemented with 10% FBS (Sigma), 30% L929 supernatant (sterile filtered) and 100 U/ml penicillin/streptomycin |
| Bone marrow isolation medium | DMEM, supplemented with 10% FBS (Sigma) and 100 U/ml penicillin/streptomycin |
| CHO, SCF-producing cells | RPMI, supplemented with 10 % FBS (Sigma) and 100 U/ml penicillin/streptomycin |
| Conventional dendritic cell (cDC) differentiation medium | IMDM, supplemented with 10% FBS (Sigma), 1% GlutaMax solution, 100 U/ml penicillin/streptomycin, 0.05 mM β-mercaptoethanol, 10 mM HEPES pH 7.2, 25 ng/ml GM-CSF and 25 ng/ml IL4 |
| ER-Hoxb8 progenitor differentiation medium | RPMI 1640, supplemented with 10% FBS (Sigma), 30 µM β-mercaptoethanol, 100 U/ml penicillin/streptomycin, 1% cell culture supernatant from a SCF–producing CHO cell line and 20 ng/ml M-CSF |
| ER-Hoxb8 progenitor maintance medium | RPMI, supplemented with 10% FBS (Sigma), 6% SCF-supernatant, 100 U/ml penicillin/streptomycin, 30 µM β-mercaptoethanol,1 µM β-estradiol |
| J774.2 medium | DMEM, supplemented with 10% FBS (Sigma), 100 U/ml penicillin/streptomycin and 10 mM HEPES pH 7.2 |
| L929 maintenance medium | DMEM, supplemented with 10% FBS (Sigma) and 100 U/ml penicillin/streptomycin |
| Lymphocyte medium (for T and B cells) | RPMI 1640, supplemented with 10% FBS (Invitrogen), 100 U/ml penicillin/streptomycin, 0.05 mM β-mercaptoethanol, 1mM sodium pyruvate, 1% GlutaMax solution, 1% nonessential amino acids solution, 1% MEM vitamin solution, 10 mM HEPES pH 7.2 |
| Macrophage-SFM | Macrophage-SFM (Serum-free medium from Life Technologies), supplemented with 100 U/ml penicillin/streptomycin |
| Mouse embryonic fibroblast (MEF) maintenance medium | DMEM, supplemented with 10% FBS (Invitrogen), 100 U/ml penicillin/streptomycin and 10 mM HEPES pH 7.2 |
| Phagocytosis assay medium | RPMI without phenol red, 1% Glutamax, 10% FBS (Sigma), 100 U/ml penicillin/streptomycin and 10 mM HEPES pH 7.2 |
| RAW cell medium | DMEM, supplemented with 10% FBS (Sigma), 1% Glutamax, 100 U/ml penicillin/streptomycin and 10 mM HEPES pH 7.2 |

## 5.9 RT-PCR primers and genotyping primers

**Table 11 RT-PCR primers**

| *Target* | *Direction (5'-3')* | *Sequence* |
|---|---|---|
| *Hprt1* | Fw | AGCAGTACAGCCCCAAAATG |
| | Rev | ATCCAACAAAGTCTGGCCTGT |
| *Zc3h12a (Regnase-1)* | Fw | GTCATCGACGGAAGCAATGT |
| | Rev | ATATCTGTGTGGCCTCGCTC |
| *Zc3h12b (Regnase-2)* | Fw | TGCTGAGCTGGACAGAGAGA |
| | Rev | CAGTCCATCATGGCAGTGAAT |
| *Zc3h12c (Regnase-3)* | Fw | GAACAGTCCCGCCCTGAC |
| | Rev | CATCATAGCACACCACTCGC |
| *Zc3h12d (Regnase-4)* | Fw | GAGCCATCAAGGTCTGATACTCC |
| | Rev | TCATCGTAGCAGACCACTCG |
| *Ifnβ* | Fw | TGGGAGATGTCCTCAACTGC |
| | Rev | CCAGGCGTAGCTGTTGTACT |
| *Stat1* | Fw | ACAACATGCTGGTGACAGAGCC |
| | Rev | TGAAAACTGCCAACTCAACACCTC |

**Table 12 Genotyping primers**

| *Target* | *Direction* | *Sequence (5'-3')* | *Product (bp)* |
|---|---|---|---|
| Targeting cassette in Zc3h12c$^{tm2a(EUCOMM)Hmgu}$ | Fw | GGAAGAAGTTCATAGATGAGCGG | 303 |
| | Rev | GAACTGATGGCGAGCTCAGAC | |
| *Zc3h12c* WT locus in Zc3h12c$^{tm2a(EUCOMM)Hmgu}$ | Fw | CTGGCTGACAGAAATATCTGTC | 401 |
| | Rev | GGTGCTCAGACTTCAACCTG | |
| *Zc3h12c* locus: Detection of deletion | Fw | GGAAACTGGGAAAGGCGATAACA | See below |
| | Rev | CTTCTTGTAACTTGTGCTTGTTTATG | |
| Cre transgene (CD19, CD4, LysM) | Fw | ATGCCCAAGAAGAAGAGGAAGGT | 447 |
| | Rev | GAAATCAGTGCGTTCGAACGCTAGA | |
| FLP transgene | Fw | ATAGGACCGGCAATTCTTCAAG | 377 |
| | Rev | GCTGCCACTCCTCAATTGGAT | |

Primers for the *Zc3h12c* locus to detect deletion efficiency of Cre and Flp transgenes give different product size depending on mouse line as shown below. The PCR product for the targeting cassette in *Zc3h12c$^{tm2a(EUCOMM)Hmgu}$* mice is only obtained under specific PCR conditions with polymerases that enable amplification of long products, such as LongAmp (NEB).

**Table 13 Genotyping PCR products for *Zc3h12c* locus in different mice strains**

| *Genetic modification of the Zc3h12c locus* | *PCR product (bp)* |
|---|---|
| Targeting cassette in *Zc3h12c*$^{tm2a(EUCOMM)Hmgu}$ | 8194 |
| *Zc3h12c$^{fl/fl}$* locus (in *Zc3h12c$^{tm2a(EUCOMM)Hmgu}$* after mated to FLPe ROSA26) | 1290 |
| *Zc3h12c* wildtype locus | 1097 |
| *Zc3h12c$^{-/-}$* locus (*Zc3h12c$^{fl/fl}$* locus after mating to (global) deleting Cre) | 358 |

## 5.10 Chemicals, reaction kits and consumables

**Table 14 Standard chemicals and reagents**

| *Chemical / Reagent* | *Manufacturer* |
|---|---|
| Acrylamide solution (30%) | AppliChem |
| Agarose | Biozym |
| Albumin Fraction V, bovine, protease free | Carl Roth |
| Ammonium chloride ($NH_4Cl$) | Sigma-Aldrich |
| Ammonium persulfate (APS) | Sigma-Aldrich |
| Ampicillin Na salt | Carl Roth |
| Bacto Brain Heart Infusion (BHI) medium, porcine | BD |
| Bromophenol blue | Sigma-Aldrich |
| Chloroform | Sigma-Aldrich |
| Deoxynucleotide (dNTP) solution mix | New England BioLabs |
| DETACHaBEAD | Thermo Scientific |
| Dithiothreitol (DTT) | Carl Roth |
| DNA gel loading dye, purple (6X) | New England BioLabs |
| DNA ladder 1 kb | Thermo Scientific |
| DNA ladder 100 bp | Thermo Scientific |
| DreamTaq Green DNA Polymerase | Thermo Scientific |
| Dynabeads Mouse CD4 | Thermo Scientific |
| ECL prime western blot detection reagent | GE Healthcare Life Sciences |
| ECL select western blot detection reagent | GE Healthcare Life Sciences |
| Ethanol | Merck |
| Ethylenediaminetetraacetic acid (EDTA) | VWR chemicals |
| Ethylenediaminetetraacetic acid (EDTA), UltraPure, 0.5M, pH 8.0 | Thermo Scientific |
| Glycerol | Sigma-Aldrich |
| Glycine | Sigma-Aldrich |
| GlycoBlue Coprecipitant | Thermo Scientific |
| HEPES buffer (1M) | Life Technologies |
| Histopaque-1077 | Sigma-Aldrich |
| Histopaque-1119 | Sigma-Aldrich |
| Hydrochloric acid (1M or 30%) | Merck |
| Isopropanol | Merck |
| KCl | Carl Roth |
| LB-Agar (Luria-Miller) | Carl Roth |
| LB-Medium (Luria-Miller) | Carl Roth |
| LR clonase II | Invitrogen |
| Methanol | Merck |
| $MgCl_2$ | Sigma-Aldrich |
| N,N,N,N-Tetramethylethan-1,2-diamin (TEMED) | AppliChem |
| NaCl | Sigma-Aldrich |
| NaOH pellets and 5M | Sigma-Aldrich |
| NP-40 detergent | Sigma-Aldrich |
| Nuclease-free $H_2O$ | Sigma-Aldrich |
| Nuclease-free Tris HCl (1M), pH 7.4 | Lonza |
| Paraformaldehyde (PFA), 4% in PBS | Santa Cruz |
| Phosphatase Inhibitor (PhosStop) | Roche |

| ***Chemical / Reagent*** | ***Manufacturer*** |
|---|---|
| Phosphate-buffered saline (PBS) tablet | Sigma-Aldrich |
| Phusion High-Fidelity DNA Polymerase | New England BioLabs |
| Power SYBRgreen Master mix | Life Technologies |
| Protease Inhibitor (cOmplete, EDTA-free) | Roche |
| Protease inhibitor cocktail powder with EDTA | Sigma-Aldrich |
| Proteinase K | Applichem |
| PVDF transfer membrane | Thermo Scientific |
| Qiagen RLT Buffer | Qiagen |
| QIAzol Lysis Reagent | Qiagen |
| Restriction enzymes (Xho-I, Bgl-II, Not-I, Cla-I and all others) | New England BioLabs |
| RNAse (DNase-free) | Roche |
| RNase A | New England BioLabs |
| RNase T1 | New England BioLabs |
| RNaseZap | Sigma-Aldrich |
| Roti Histofix (4%) | Carl Roth |
| Saponin | Fisher chemical |
| Skimmed milk powder | AppliChem |
| Sodium azide | Sigma-Aldrich |
| Sodium chloride solution | Braun |
| Sodium citrate | Sigma-Aldrich |
| Sodium deoxycholate | Sigma-Aldrich |
| Sodium dodecyl sulfate (SDS) | Sigma-Aldrich |
| Spectinomycin x 2 HCl x 5 $H_2O$ | Sigma-Aldrich |
| Sucrose | Carl Roth |
| SYBR Gold | Thermo Scientific |
| TMB ELISA substrate, 1-Step Ultra | Thermo Scientific |
| Tris base | Carl Roth |
| Tris Buffer (1.0 M) | Calbiochem |
| Tris-EDTA (TE) pH 8.0 | Sigma-Aldrich |
| Tris-HCl | Carl Roth |
| Tris-HCl (1 M, pH 7.4), (1 M, pH 8.0), (10 mM, pH 8.0) | Sigma-Aldrich |
| Triton X-100 | Sigma-Aldrich |
| Tween 20 | Sigma-Aldrich |
| β-mercaptoethanol | Sigma-Aldrich |

**Table 15 Reaction kits and specific chemicals**

| *Reaction kit / Chemical* | *Manufacturer* |
|---|---|
| Anti-Biotin MicroBeads | Miltenyi |
| Autoantibody test (IIFT:HEp-2) | Euroimmun |
| BCA protein assay kit | Pierce |
| CD45R (B220) Cell Isolation Kit, MicroBeads, mouse | Miltenyi |
| $CD8a^+$ T Cell Isolation Kit, MicroBeads, mouse | Miltenyi |
| FITC-coupled anti-mouse-IgG (sc-2010) for autoantibodies | Santa Cruz |
| FoxP3 staining buffer kit | eBioscience |
| GSTrap column trap | GE Healthcare Life Sciences |
| HiTrap Chelating trap | GE Healthcare Life Sciences |
| LEGENDplex 'mouse inflammation panel' (multiplex assay) | Biolegend |
| Mouse IgG total Ready-Set-Go (ELISA for serum IgG, IgM, IgA) | eBioscience |
| Nucleo Bond Xtra Maxi plasmid DNA preparation kit | Macherey-Nagel |
| NucleoSpin Gel and PCR Clean-up Kit | Macherey-Nagel |
| pCR8/GW/TOPO TA Cloning Kit with One Shot TOP10 *E. coli* | Invitrogen |
| QIAprep Spin Miniprep Kit | Qiagen |
| QuantiTect Reverse Transcription Kit | Qiagen |
| Qubit dsDNA HS Assay kit | Invitrogen |
| Qubit RNA HS assay kit | Invitrogen |
| Quick ligation kit | New England BioLabs |
| QuikChange II XL Site-Directed Mutagenesis Kit | Agilent Technologies |
| RNA 6000 Nano Kit | Agilent Technologies |
| RNA 6000 Pico Kit | Agilent Technologies |
| RNeasy Plus Micro Kit | Qiagen |
| TruSeq stranded total RNA library prep kit | Illumina |

Standard consumables, such as microcentrifugation tubes, 15 ml and 50 ml conical tubes, serological pipettes, cell culture dishes, cell culture plates, pipette tips, syringes and needles were purchased from Greiner Bio-One, Falcon, Eppendorf, BD and Braun. Specific products are depicted in Table 16.

**Table 16 Specific consumables**

| *Consumables* | *Manufacturer* |
|---|---|
| 10-kD molecular mass cutoff Amicon concentrator | Merck-Millipore |
| 21G catheter tubing | B. Braun |
| DNA low bind microcentrifuge tubes | Eppendorf |
| LS Columns, magnetic positive separation columns | Miltenyi |
| Luer connector for 21G catheter tubing | B. Braun |
| MS Columns, magnetic positive separation columns | Miltenyi |
| Petri dish 145x20, non tissue-treated (for macrophages culture) | Greiner Bio-One |
| Protein G Dynabeads | Invitrogen |

## 5.11 Buffer, solutions, media

**Table 17 Composition of buffers, solutions and media**

| *Buffer name* | *Composition* |
|---|---|
| 4x Laemmli buffer | 200 mM Tris/HCl pH 6.8, 8% SDS, 40% glycerol, 0.1% bromphenol blue, 10% β-mercaptoethanol |
| 8% SDS dissolving gel composition | Per 10 ml: 4.6 ml $H_2O$, 2.7 30% acrylamide mix (29:1), 2.5 ml 1.5 M Tris pH8.8, 0.1 ml 10% SDS, 0.1 ml ammonium persulfate solution, 0.006 ml TEMED |
| Bronchoalveolar lavage (BAL) rinsing buffer | PBS containing 2.5 mM EDTA and 2.5% FBS |
| FACS intracellular permeabilization staining buffer | PBS containing 1% BSA and 0.5% saponin buffer containing (Prepare always fresh at the day of use) |
| FACS surface staining buffer | PBS containing 0.5% BSA, 0.01% sodium azide and 2mM EDTA |
| Immunoblot transfer buffer | 25 mM Tris-Base, 192 mM glycin, 20 % methanol (pH 8.4) in H2O |
| Meisters lysis buffer | 20mM Tris-HCl pH 7.5, 0.25% NP-40, 150 mM NaCl, 1,5 mM $MgCl_2$, supplemented with 5 mM EDTA, 1 mM dithiothreitol, complete Mini EDTA free protease inhibitors (Roche), and protease inhibitor cocktail powder (Sigma) |
| RIPA protein lysis buffer | 20 mM Tris HCl pH 7.5, 250 mM NaCl, 10 mM MgCl2, 1% NP40, 0.1% sodium dodecyl sulfate (SDS), 0.5% sodium deoxycholate, supplemented with 5 mM EDTA, 1 mM dithiothreitol, complete Mini EDTA free protease inhibitors (Roche), and protease inhibitor cocktail powder (Sigma) |
| SDS stacking gel composition | Per 10 ml: 6.8 ml $H_2O$, 1.66 30% acrylamide mix (29:1), 1.26 ml 1.0 M Tris pH6.8, 0.1 ml 10% SDS, 0.1 ml ammonium persulfate solution, 0.01 ml TEMED |
| SDS-PAGE running buffer | 25 mM Tris, 250 mM Glycine, 0,1% SDS |
| Sera dilution buffer | TBS, 5% BSA, 0.01% sodium azide |
| TAE buffer (1x) | 2 M Tris-base, 1M acetic acid, 50mM Na EDTA |
| TBS (1x) | 10 mM Tris/HCl pH 8.0, 150 mM NaCl |
| TBS-T (1x) | TBS (1x), 0.05 % Tween 20 |
| Tris-ammonium-chloride buffer (TAC) | 2.06 g/l Tris, 7.47 g/l $NH_4Cl$, pH 7.2 |

## 5.12 Software

Softwares used for analysis of different data are depicted in Table 18.

**Table 18 Software**

| *Software* | *Version* |
|---|---|
| ApE-A, plasmid editor | V2.0.47 |
| Bioconductor packages for R | Diverse |
| DAVID | 6.8 |
| Definiens Tissue Studio (Definiens AG) | Version 4.4 |
| Enrichr | Online (November 2018 and July 2017) |
| FlowJo, flow cytometry data | Version 9.7.6 and 10.0 |
| GOrilla | Online (November 2018 and July 2017) |
| GraphPad Prism, statistical analysis software | Version 6 |
| ImageScope digital microscope imaging viewer (Leica) | V12.3.2.5030 |
| NetScope digital microscope imaging viewer (NetScope) | 1.0.6863.20841 |
| RStudio | 0.98.1091 and 1.0.136 |
| T coffee (http://tcoffee.crg.cat) with 'M-Coffee' algorithm | Online (March 2017) |

# 6 Methods

Parts of the methods section have been published in the associated publication in '*The Journal of Experimental Medicine*' under the title 'Immune homeostasis and regulation of the interferon pathway require myeloid-derived Regnase-3' (von Gamm *et al.*, 2019).

## 6.1 Mice: Genetic background, mouse strains and breeding strategies

*Zc3h12c*$^{tm2a(EUCOMM)Hmgu}$ mice were generated and provided by the European Conditional Mouse Mutagenesis Program (EUCOMM) via Wolfgang Wurst (Institute of Developmental Genetics, Helmholtz Centre Munich).

Mice with 'knockout-first allele' promoter-driven selection cassette for the *Zc3h12c* (*Regnase-3*) gene (*Zc3h12c*$^{tm2a(EUCOMM)Hmgu}$ mice) on *C57BL/6J* background were obtained from EUCOMM and are further described with a detailed scheme of the targeting cassette and the mating steps in the results section. EUCOMM generated *Zc3h12c*$^{tm2a(EUCOMM)Hmgu}$ mice through targeted gene disruption by electroporating the linearized L1L2_Bact_P vector with a promotor-driven selection cassette flanked by 5' and 3' arms of the *Zc3h12c* gene into blastocyst embryonic stem cells. A splice acceptor and a premature poly-A signal in the targeting cassette that is located within the intronic region between Exon 3 and 4 cause a destructed *Zc3h12c* gene product. Thus, the first generation of homozygous *Zc3h12c*$^{tm2a(EUCOMM)Hmgu}$ mice are globally deficient for *Regnase-3*, which is reflected in the term 'knockout-first allele' and are therefore termed *Regnase-3*$^{-/-}$ mice in this study (Coleman *et al.*, 2015). Mating these mice to mice expressing the FLP transgene under the global ROSA26 promotor (*Gt(ROSA)26Sor*$^{tm1(FLP1)Dym}$) removes major parts of the targeting cassette, resulting in mice with a floxed Exon 4 in the *Regnase-3* locus (*Regnase-3*$^{fl/fl}$ mice). The FLP transgene was eliminated in further breeding steps. To generate mice with conditional deletion of *Regnase-3* in specific cell types, *Regnase-3*$^{fl/fl}$ mice were further bred to mice expressing the Cre transgene under specific promotors. Removal of Exon 4 results in a frame shift of the resulting gene product. *Regnase-3* ablation in B cells was achieved by crossing *Regnase-3*$^{fl/fl}$ mice to *C.Cg-Cd19*$^{tm1(cre)Cgn}$ *Igh*$^{b}$*/J* mice, which express the Cre transgene under the CD19 promotor (*Regnase-3*$^{fl/fl}$ +CD19-Cre mice). *Regnase-3* ablation in T cells was achieved by crossing *Regnase-3*$^{fl/fl}$ mice to *STOCK Tg(Cd4-cre)1Cwi/BfluJ* mice, which express the Cre transgene under the CD4 promotor (*Regnase-3*$^{fl/fl}$ +CD4-Cre mice). *Regnase-3* ablation in the myeloid linage was achieved by crossing *Regnase-3*$^{fl/fl}$ mice to *B6.129P2-Lyz2*$^{tm1(cre)Ifo}$*/J* mice, which express the Cre transgene under the LysM promotor (*Regnase-3*$^{fl/fl}$ +LysM-Cre mice). *Regnase-3*$^{fl/fl}$ mice were also crossed to mice expressing the Cre transgene under the global ROSA26 promotor (*GT (ROSA) 26Sor Cre* mice). The Cre transgene was eliminated in further mating steps, resulting in mice globally deficient for *Regnase-3* caused by deletion of Exon 4.

These mice were used alternatively to mice with a 'knockout-first allele' for *Regnase-3* (*Zc3h12c*$^{tm2a(EUCOMM)Hmgu}$ mice) in some assays, particularly in *in vitro* experiments. *B6.Cg-Nfkb1*$^{tm1Bal}$*/J* mice are deficient for the NF-κB member *p50* (*p50*$^{-/-}$ mice) and were described elsewhere (Sha *et al.*, 1995).

The origin of the used mice is summarized in Table 2 in the material section. All mentioned strains as well as *C57BL/6J* mice were housed and bred in specific pathogen-free barrier animal facilities of the Helmholtz Center Munich in accordance to institutional and federal guidelines. Mouse colony maintenance and animal experimental protocols that were done for this study were approved by the regulations of the governmental district of Upper Bavaria under the following protocol number: ROB-55.2-2532.Vet_02-14-33.

Mice were euthanized using $CO_2$ or cervical dislocation according to the institutional and governmental guidelines.

## 6.2 Cloning and Vectors

For *in vitro* studies, *Regnase* family members (*Regnase-1–4* / *Zc3h12a–d*) were cloned with or without protein tags into different vector backbones. Coding sequences for the *Regnase* family members were obtained as customized order (Geneart by Life Technologies) or from image clones (Source BioScience). Coding sequences of *Regnase* family members were first inserted into the pCR8/GW/TOPO gateway vector according to the manufacturer's protocol. To further obtain vectors in which the *Regnase* family members are fused to an N-terminal GFP sequence, nucleotide overhangs containing restriction sites were added to the coding sequences by PCR. An overhang with restriction sites for Bgl-II and Xho-I upstream and Not-I and Cla-I downstream were added to the coding sequences of *Regnase-2*, *Regnase-3* and *Regnase-4* by PCR with primers extended at the 5' end. Similarly, *Regnase-1* was equipped upstream with restriction sites for Hind-III and Kpn-I and downstream with sites for Not-I and Cla-I. The PCR products were inserted into the pCR8/GW/TOPO gateway vector to obtain plasmids in which the Regnase family members are extended with restriction sites at the 5' end. Next, also the *GFP* sequence (obtained from Geneart) was extended upstream with sites for Bgl-II and Xho-I and downstream with Not-1 and Cla-1 for cloning it upstream of *Regnase-2, -3* and *-4*. Similarly, the *GFP* sequence was equipped upstream with Hind-III and downstream with Kpn-I sites to be cloned upstream of *Regnase-1*. *GFP* coding sequences with overhangs for restriction sites as well as *Regnase* family members in pCR8/GW/TOPO with upstream-added restriction sites were digested with the respective restriction enzymes according to the suggested protocols from New England Biolabs. Digested products were separated by agarose gel electrophoresis, the correct bands were excised from the gel and purified using the NucleoSpin Gel and PCR Clean-up kit. PCR products were then ligated using Quick ligation kit according to the manufacturer's protocol and were transformed into chemically competent DH5α *Escherichia coli* (*E. coli*). Positive colonies were picked, grown in small scale and purified on columns

with a DNA Mini preparation kit. Sanger sequencing verified integrity of the cloned coding sequences. For mammalian expression, *GFP*-tagged *Regnase* constructs were subcloned into pLNCX2 and pMSCV/Puro using the Gateway LR Clonase II enzyme kit according to the manufacturer's protocol. Gateway vectors on the pLNCX2 and pMSCV/Puro backbone were kindly provided by Vigo Heissmeyer. For generating the newly developed Regnase-3-specific antibody as well as for specific *in vitro* RNA binding assays, *Regnase-3* constructs for bacterial expression were needed. Therefore, the full length *Regnase-3* coding sequence as well as truncated versions of the protein were cloned via restriction sites as described above into the pGEX-6P-2 vector backbone. PCR products were extended upstream with sites for EcoR-I and downstream with a His-tag and a Not-I restriction site. Digested PCR products were then ligated into the digested pGEX-6P-2 vector with N-terminal Glutathione S-transferase (GST)-tag. Thus, the vectors contain full length or truncated Regnase-3 coding sequences with an N-terminal GST-tag and a C-terminal His-tag. The RNase domain of Regnase-1 and Regnase-3 was mutated in some of the constructs by site-directed mutagenesis using the QuickChange II XL site directed mutagenesis kit according to the manufacturer's protocol. A single point mutation from guanine to adenine formed the D141N *Regnase-1* mutant and the D271N *Regnase-3* mutant. The D141N mutant in *Regnase-1* has been published and is inactive to degrade RNA (Matsushita *et al.*, 2009), while the D272N mutant in *Regnase-3* was chosen through protein sequence alignment. Larger amounts of plasmid DNA were produced with the Nucleo Bond Xtra Maxi plasmid DNA preparation kit according to the manufacturer's protocol from 400 ml cultures.

## 6.3 Cell culture

The origin of the different cell lines is displayed in Table 3. Cell lines were kept in cell culture media composed as shown in Table 11. All cells were kept in incubators at 37°C, 5% $CO_2$ and saturated humidity.

### 6.3.1 Generation of Regnase overexpressing MEF

In order to analyze IKK dependent degradation of Regnase family members, *NEMO*-deficient and *NEMO* reconstituted MEFs were transduced with GFP-tagged *Regnase* family members to obtain constitutive overexpression. Therefore, HEK 293T cells were seeded at a density of 0.3 million cells per ml in 10 ml on 8 cm dishes the day before transfection. The next day, the medium was replaced with fresh culture medium, supplemented with 25 µM chloroquine and incubated for one hour. Then, 25 µg plasmid of GFP-tagged *Regnase* family members in pMSCV/Puro, together with 3 µg retroviral packaging plasmid EcoPack were complexed using the calcium phosphate method. Therefore, plasmid DNA was diluted to 450 µl $H_2O$ and 50 µl of 2.5 M $CaCl_2$ were added. This mixture was then vortexed at low speed while 500 µl 2xHSS was added drop by drop. This mixture was incubated for 15 min and carefully applied to 293T cells. 8 to 10 hours after transfection, culture medium was replaced with fresh

medium. The next day, the GFP fluorescent was checked in a fluorescence microscope to prove transfection efficiency. Two to three days post transfection, retrovirus-containing supernatant was collected and sterile filtered with 0.45 μm PVDF syringe filters. The supernatant was supplemented with 10 µg/ml Polybrene (Hexadimethrine bromide) and 25% fresh MEF cell culture medium. 7 ml of this mixture was added for 8 hours to *NEMO*-deficient or *NEMO* reconstituted MEF cells, which were seeded at 0.3 million cells per ml in 6-wells. Transduced cells were selected with 2 µg/ml Puromycin antibiotics. The retroviral transduction procedure was repeated for at least two more times.

### 6.3.2 Differentiation of Hoxb8 cells

Estrogen receptor (ER) driven Hoxb8 expressing bone marrow progenitor cells (ER-Hoxb8 cells), are cells that originate from mouse hematopoietic stem cells and maintain their pluripotent status by estrogen dependent overexpression of the transcription factor Hoxb8. These cells were generated from the bone marrow of *C57BL/6* mice in the lab of Christian Schulz (LMU Munich) according to a protocol from Redecke *et al.* and an ER-Hoxb8 construct provided by Hans Häcker (St. Jude Children's Research Hospital, Tennessee, USA) (Redecke *et al.*, 2013).

For the ER-Hoxb8 progenitor differentiation assay, cells were kept in ER-Hoxb8 maintenance medium and split every second day. For differentiation, cells were washed 3 times to remove al residual estradiol, counted and seeded at 0.2 million cells per ml onto non-tissue culture treated 8 cm dishes in ER-Hoxb8 differentiation medium. At least 9 dishes were seeded at the same day and after each day of differentiation, cells of one dish were counted and lysed in 2 x concentrated, boiling Laemmli buffer and processed as described in the section ‘Immunoblotting’.

### 6.3.3 Generation of primary BMDM and cDCs

Bone marrow single cell suspensions for differentiation of bone marrow derived macrophages (BMDM) and bone marrow derived conventional dendritic cells (cCDs) were generated by the same procedure. Femur and tibia were isolated from the mouse and muscle and cartilage was removed using paper tissue. Then, bones were sterilized with tissues soaked in 70% ethanol. Bones were opened at the epiphysis at both ends with sterile scissors and the marrow was flushed out with a syringe and 25G needle using cold bone marrow isolation medium. The bone marrow was carefully strained through a 70 μm mesh, collected by centrifugation (300xg, 5 min, 4°C) and erythrocytes were lysed in Tris-ammonium-chloride (TAC) buffer. Erythrocyte lysis was performed with 4 ml TAC buffer for 4 min and stopped with 25 ml cold bone marrow isolation medium.

For generation of bone marrow derived macrophages, bone marrow cells of one mouse were suspended in 75 ml of BMDM differentiation medium and distributed to three 14 cm non-tissue culture-treated 14 cm dishes (day 0). On day 3, 50% of the differentiation medium was

removed and 20 ml fresh BMDM differentiation medium was added. Cells were differentiated for 3 more days. On day 6, cells were washed with warm PBS and dislodged with Accutase, collected in Macrophage SFM and counted. Cells were collected (150 x g, RT, 5 min), suspended in Macrophage SFM and plated onto non tissue culture-treated 6-well plates for immunoblot and RT-PCR assays (1.5 million cells per well in 1.5 to 2 ml medium) or onto 96-well plates for phagocytosis assay.

For generation of bone marrow derived conventional dendritic cells, bone marrow cells were counted after red blood cell lysis and cells were seeded at a density of 1 million cells per ml in 10 ml cDC differentiation medium onto 8 cm tissue culture-treated dishes (day 0). On day 3, 50% of the medium was replaced by fresh differentiation medium and differentiated for 3 more days. On day 6, cells were washed with PBS and dislodged using Accutase. Cells were then plated onto tissue culture-treated 6-well plates in cDC differentiation medium without supplemented recombinant cytokines (1.0 to 1.5 million cells per well in 1.5 to 2 ml medium).

M-CSF containing L929 cell supernatant was generated as follows: L929 cells were expanded and plated onto 14 cm dishes and grown to 80% confluence. Then, medium was replaced by 25 ml fresh L929 medium and cells were kept in the cell culture incubator for 4 days. Then, the supernatant was removed from the cells, collected, sterile filtered through 45 μm PVDF membrane filters and stored for few days at 4°C. L929 cells were covered with 25 ml fresh medium and kept for 4 more days. The medium was again collected and filtered as described and mixed with the supernatant from the first round. Aliquots of the supernatant were stored at -80°C until needed. Differentiation of bone marrow cells with a new L929 supernatant batch was compared to the differentiation of the previous batch.

### 6.3.4 Classical and alternative activation of BMDM (M1/M2)

BMDM were differentiated from C57BL/6 bone marrow cells as described in the section ‘Generation of primary BMDM and cDCs’.

Treatment with 100 ng/ml lipopolysaccharide (LPS) from *Salmonella enterica serotype typhimurium* together with 20 ng/ml IFNγ for 24 h produced classically activated (M1-like) macrophages and 20 ng/ml IL-4 generated alternatively activated (M2-like) macrophages. A control was left untreated (M0 condition). Cells were lysed in 2 x concentrated boiling Laemmli buffer and processed as described the section ‘Immunoblotting’. Shifts towards the classical M1-like and alternative M2-like macrophage conditions were verified by flow cytometry, using markers that were described to be upregulated under these conditions. CD38 is upregulated under M1 conditions and CD206 is induced under M2 conditions (Jablonski *et al.*, 2015).

### 6.3.5 Isolation of primary B cells

B cells were either isolated from the spleen or from lymph nodes. The tissue was cut into smaller pieces with sterile scissors and carefully pressed through a 70 μm cell strainer mesh with the plunger of a syringe, thereby avoiding to much friction. Cells were flushed with lymphocyte medium and collected by centrifugation. Erythrocyte lysis was only done in splenic samples as described in the section 'Generation of primary BMDM and cDCs'. For analysis of Regnase mRNA expression levels in immune cell subsets, B cells were isolated using positive selection MicroBeads (Miltenyi) for B220 according to the manufacturer's protocol. For all other assays, in particular for Regnase-3 protein expression analysis in immune cell types, for the CFSE proliferation assay and for sequencing analysis of B cells from lymph nodes, B cells were isolated via the CD19 surface marker. Therefore, cells were first incubated with biotinylated anti-CD19 (15 μg in 300 μl lymphocyte medium per spleen) for 15 min and washed with lymphocyte medium (300 x g, 5 min, 4°C). Biotinylated cells were then isolated with anti-Biotin positive selection MicroBeads (Miltenyi) according to the manufacturer's protocol. B cells were either directly lysed in 2 x concentrated boiling Laemmli buffer for immunobloting or Trizol reagent for RNA isolation or were maintained in lymphocyte medium.

### 6.3.6 Isolation and expansion of primary $CD4^+$ T cells

The spleen was taken from *C57BL/6* mice, cut into smaller pieces strained through a 70 μm mesh as described for B cell isolation. Erythrocytes were lysed as described in section 'Generation of primary BMDM and cDCs'. $CD4^+$ T cells were isolated using anti-CD4 labeled Dynabeads and subsequently treated with the corresponding DETACHaBEAD reagent to free cells from the beads, according to the manufacturer's protocol. $CD4^+$ T cells were either directly lysed in 2 x concentrated boiling Laemmli buffer for immunobloting or Trizol reagent for RNA isolation or were were maintained in lymphocyte medium. $CD4^+$ T cells were expanded by activating T cell receptor signaling with plate-bound anti-CD3/CD28. Cell culture plates were first pre-incubated with goat anti-hamster IgG (20 μg/ml in PBS) at 4°C over night and then washed with PBS. Pre-incubation with anti-hamster IgG enables soluble anti-CD3 and anti-CD28 (both from hamster) to bind in the correct orientation to the plate surface. T cells were suspended in lymphocyte medium containing 1 μg/ml anti-CD3 and 2,5 μg/ml anti-CD28 in a density of 1 million cells per ml and placed onto anti-hamster coated cell culture plates. After two days, when T cells have started to form cell clusters, cells were removed from the surface by intensive pipetting and suspended in lymphocyte expansion medium containing 200 IE/ml Proleukin S (IL2-analog), but no further addition of antibodies. Cells were expanded for 2 – 3 more days. If cells were stimulated, cells were counted and 1 – 2 million cells were placed in fresh lymphocyte medium onto 6-well plates.

### 6.3.7 Isolation and expansion of primary CD8⁺ T cells

CD8⁺ T cells were isolated from the spleen of *C57BL/6* mice. Therefore, the spleen was cut into smaller parts and processed as described in the section 'Isolation of primary B cells' to obtain a splenocyte suspension. For analysis of Regnase mRNA expression levels in immune cell subsets, CD8⁺ T cells were isolated using positive selection MicroBeads (Miltenyi) for CD8 according to the manufacturer's protocol. For Regnase-3 protein expression analysis in immune cell types, splenic cells were depleted from CD19⁺ B cells and CD4⁺ T cells as described in the respective sections and then expanded as described for CD4⁺ T cells. Cells were treated as described in the relevant sections and either lysed in 2 x concentrated boiling Laemmli buffer for immunobloting or Trizol reagent for RNA isolation.

### 6.3.8 Isolation of primary Neutrophils

To obtain Neutrophils from the bone marrow, bones were taken from *C57BL/6* mice and a bone marrow suspension was prepared as described in the section 'Generation of primary BMDM and cDCs', but without TAC erythrocyte lysis. Neutrophils were then isolated using density centrifugation with HistoPaque as described elsewhere (Swamydas *et al.*, 2015). In brief: Erythrocytes were lysed in hypotonic NaCl buffer, washed and resuspended in isotonic NaCl buffer. Then, three solutions with different densities were overlayed on top of each other in a 15 ml conical centrifuge tube. Bottom layer: Histopaque 1119 (density, 1.119 g/ml); second layer: Histopaque 1077 (density, 1.077 g/ml); Top layer: bone marrow cells in isotonic NaCl solution. Cells were centrifuged for 30 minutes at 872 x g at room temperature without brake. Neutrophils were collected at the interface of the Histopaque 1119 and Histopaque 1077 layers and were washed. Neutrophils were lysed in 2 x concentrated boiling Laemmli buffer for immunobloting.

## 6.4 Proliferation assay in B cells

Splenic CD19⁺ B cells were isolated from *Regnase-3*$^{-/-}$ mice and *Regnase-3*$^{+/+}$ littermates as described in section 'Isolation of primary B cells'. B cells were counted and one million cells per condition were used in the experiment. Cells from the same mouse under different condition were labeled together and distributed afterwards. Cells from different animals were labeled simultaneously, while working quickly to guaranty similar labeling efficiency. A CFSE stock solution of 5 mM in DMSO was prepared directly prior to the experiment. Then, B cells were labeled with diluted CFSE solution (5 μM in PBS) for 5 min in the dark at room temperature. Labeling was stopped by addition of 10 ml lymphocyte medium. Cells were collected (300 x g, 4°C, 5 min) and washed once more. Labeled cells were brought to the cell culture incubator for 15 min to allow the cell to decarboxylate CFSE. An aliquot of day 0 labeled cells as well as unstained B cells were fixed with 4% PFA in PBS for 10 min and then stored in extracellular FACS buffer at 4°C in the dark. The rest of the labeled B cells was

distributed to 48-well plates and treated with either 20 μg/ml LPS or with 1 μM CpG ODN2395. Over four days, an aliquot of B cells was taken every 24 h, fixed with PFA and stored at 4°C. Then, all samples were analyzed together by flow cytometry.

### 6.5 Flow cytometry

Lymphoid organs (spleen, thymus, lymph nodes) were dissected from the mice and cut into smaller pieces. In *Regnase-3*-deficient mice, increased lymph nodes and normal sized lymph nodes were frequently divided and processed separately. Then, cells were strained through a 70 μm mesh, using the plunger of a 5 ml syringe and 5 to 10 ml lymphocyte medium. Cells were collected (300 x g, 5 min, 4°C) and erythrocytes in splenic samples were lysed as described in the section 'Generation of primary BMDM and cDCs' and subsequently washed and counted. Then, cells were stained with fluorophore labeled antibodies. Buffers, antibodies and reagents for flow cytometry are found in the material section. All steps were performed at 4°C, if not stated otherwise and protected from light. Depending on the expected proportions of the cells of interest, one to five million cells per organ were used for each staining and distributed into V-bottom 96-well plates. In addition, excess cells were distributed to 96-well plates for single-staining compensation controls.

Surface staining of primary immune cells and cultured cells was performed as follows: First, cells were stained with a fixable life/dead marker in pure PBS for 20 min. Cells were washed once with PBS (350 x g, 4°C, 5 min) and suspended in 50 μl Fc Block (anti-CD16/32) containing FACS surface staining buffer and incubated for 10 min. Then, 50 μl of 2 x concentrated master mix containing all staining antibodies was added to the Fc block suspension, mixed and incubated for 15 min. Cells were collected, washed once with FACS surface staining buffer (350 x g, 4°C, 5 min) and fixed with 4% PFA in PBS for 10 min at room temperature. Cells were collected, washed again with FACS surface staining buffer and stored in the same buffer at 4°C, protected from light until analyzed by flow cytometry. Samples stained for the transcription factor FoxP3 were first surface stained as described above, but not fixed with PFA. Instead, samples were further processed with the commercial FoxP3 staining buffer set according to the manufacturer's protocol.

For analysis of intracellular IFNγ cytokine expression, the cells were taken up in lymphocyte medium and stimulated with 20 nM PMA and 1 μM Ionomycin for 4 hours to induce T cell responses and then additionally treated with 5 μg/ml Brefeldin A for the last 2 hours. Then, cells were washed and stained with a fixable viability dye and surface staining antibodies as described above and fixed with 4% PFA in PBS. Cells were then washed and permeabilized in FACS intracellular permeabilization staining buffer. Anti-IFNγ in intracellular permeabilization staining buffer was added and cells were incubated for 30 min. Cells were washed with intracellular staining buffer twice and transferred into surface staining buffer until measured. Samples were analyzed on a FACS Aria III flow cytometer and data were analyzed and calculated with FlowJo software (version 9 and 10).

## 6.6 Immunohistochemistry

Processing of samples for immunohistochemistry was performed at the DKFZ (see acknowledgements).

Organs were dissected from *Regnase-3*$^{-/-}$ and *Regnase-3*$^{+/+}$ littermate controls and placed into 4% Roti-Histo-Fix solution for 30 min. Then, the fixative was replaced by fresh 4% Roti-Histo-Fix and tissues were fixed for an additional 48 h. Samples were transferred into 70% ethanol and stored at 4°C until further processed. Tissues were dehydrated and embedded into paraffin and 2 μm sections were cut. Dewaxing and unmasking of antigens was performed on the immunohistochemistry robot Bond Max (Leica) according to the program displayed in Table 19. Antigen retrieval was done with EDTA solution for B220, CD3, ki67, CD206 and phospho-STAT1 antigens, with citrate buffer for the CD64 antigen and with proteolytic solution (AR9551, Leica) for MHC-II and F4/80 antigens.

**Table 19 Dewaxing and unmasking program used on Bond Max robot**

| *Replicates* | *Reagent* | *Time* |
|---|---|---|
| 3x | Bond Dewax Solution | 00:30 |
| 3x | Ethanol | |
| 3x | Bond Wash Solution | 05:00 |
| 4x | Bond ER Solution | Antibody dependent |
| 3x | Bond Wash Solution | |

Haematoxylin & eosin as well as antibody stainings were also performed on the immunohistochemistry robot Bond Max (Leica) with the antibodies listed in Table 6 of the material section. Staining and visualization of the antibodies were done using the 'Bond Polymer Refine Detection Kit' (including peroxidase block, secondary-HRP antibody, 3,3'-Diaminobenzidine (DAB) reagent and haematoxylin/eosin, DS9800) according to the protocol displayed in Table 20. If the primary antibody was from rat, an additional bridging antibody from rabbit, reactive against rat IgG (Dianova, # 312-005-045) was used prior to incubation with the secondary anti-rabbit-HRP antibody.

**Table 20 Staining protocol on Bond Max robot**

| *Replicates* | *Reagent* | *Time* |
|---|---|---|
| 1x | Peroxidase Block | 05:00 |
| 3x | Bond Wash Solution | |
| 1x | Primary antibody | Antibody dependent |
| 3x | Bond Wash Solution | |
| 1x | Bridging antibody (if primary antibody is not from rabbit) | 20:00 |
| 3x | Bond Wash Solution | |
| 1x | Polymer (anti-rabbit-HRP) | 20:00 |
| 2x | Bond Wash Solution | |
| 1x | $H_2O$ | |

| | | |
|---|---|---|
| 2x | Mixed-DAB-Solution | 06:00 |
| 3x | $H_2O$ | |
| 1x | Hematoxylin | 05:00 |
| 1x | $H_2O$ | |
| 1x | Bond Wash Solution | |
| 1x | $H_2O$ | |

Immunohistochemistry sections were then dehydrated on the Bond Max robot according to protocol displayed in Table 21 and sections were mounted. If the primary antibody was from rat, an additional bridging antibody rabbit-anti-rat (Dianova, # 312-005-045) was used prior to anti-rabbit-HRP incubation.

**Table 21 Dehydration for mounting**

| ***Step*** | ***Reagent*** | ***Time*** |
|---|---|---|
| 1x | $H_2O$ | 01:00 |
| 1x | 70% Ethanol | 01:00 |
| 2x | 100% Ethanol | 01:00 |
| 2x | Xylol | 01:00 |

Stained tissue sections were acquired as whole digital slides on the SCN400 (Leica) or on the AxioScan.Z1 (Zeiss) digital slide scanner. Representative images were captured with either Aperio ImageScope software or with the NetScope viewer software. Images were further analyzed with Definiens Tissue Studio software to obtain percentages for highly positive stained pixels in specific tissues. The analysis of positive pixel counts was performed in cooperation with Annette Feuchtinger (Research Unit Analytical Pathology of the Helmholtz Center Munich) according to a published procedure (Feuchtinger *et al.*, 2015).
To determine the percentage of strong MHC-II positive macrophages in the lung, consecutive immunohistochemical sections stained for CD64 and MHC-II were analyzed. In representative lung sections of ca. 73 000 $\mu m^2$ size, the total number of CD64 positive macrophages was determined as well as all macrophages ($CD64^+$) which were additionally positive for MHC-II in the consecutive section were counted. From these numbers the percentages of strong MHC-II positive macrophages were calculated.

## 6.7 RT-PCR

### 6.7.1 Isolation of RNA

Cells were lysed in Trizol lysis reagent through extensive pipetting and whole murine tissue samples were disrupted in the TissueLyser bead mill. Trizol samples were then incubated for 5 min and stored at -80°C until further processed. Samples were thawed at room temperature and 200 µl chloroform were added per one ml of Trizol lysis reagent. The samples were then mixed intensively through manual shaking, incubated for 2 min at room temperature and centrifuged (12 000 x g, 15 min, 4°C). The upper, aqueous phase was

transferred to a fresh 1.5 ml tube and supplemented with 500 µl isopropanol and 1 µl of the co-precipitant GylcoBlue for RNA precipitation. The samples were mixed and centrifuged (12 000 x g, 10 min, 4°C). RNA pellets were washed with 1 ml 75 % ethanol and centrifuged (7 600 x g, 5 min, 4°C). The supernatant was fully removed from the pellets and tubes were left open for 5 to 10 min to allow air-drying. Nuclease-free water was added and samples were incubated at 60°C for 5 min to enable full dissolution of the RNA.
Alternatively, lung alveolar macrophages for RNA sequencing analysis were lysed in RLT lysis buffer and RNA was extracted using the RNeasy Plus Micro Kit according to the manufacturer's instructions. If RNA should be used for RT-PCR, concentration and quality was checked with the NanoDrop micro-volume spectral photometer. If RNA should be used for RNA sequencing experiments, concentration and quality was checked by RNA-electrophoresis on the Bioanalyzer system.

### 6.7.2 cDNA synthesis and RT-PCR

For RT-PCR, cDNA was generated with the QuantiTect Reverse Transcription Kit. Genomic wipeout and reverse transcriptase reactions were done according to the manufacturer's protocol. RT-PCR was performed on a QuantStudio 6 real-time PCR system and the SYBR green dye for quantification. Primer pairs are given Table 11 of the material section. The amplification efficiencies for the *Hprt1*, *Zc3h12a*, *Zc3h12b*, *Zc3h12c* and *Zc3h12d* genes were calculated with the slope of the standard curves and were determined to be in the range of 90% – 100%. Differential expression was calculated using the $\Delta C_t$ method for quantification.

## 6.8 Expression analysis for *Regnase* mRNA in immune cell types and tissues

To analyze the mRNA expression levels for *Regnase* family members in immune cells upon response to an activation with receptor agonists, bone marrow derived macrophages (BMDM), conventional dendritic cells (cDCs), B cells, $CD4^+$ and $CD8^+$ T cells were isolated or differentiated as described in sections 6.3.3, 6.3.5, 6.3.6 and 6.3.7.
BMDM and cDCs were treated for 1, 4 and 16 hours with 100 ng/ml LPS, 20 µg/ml low molecular weight poly-I:C or 1 µM C-type CpG ODN 2395 or were left untreated.
B cells were stimulated for 1, 4 and 16 hours with 10 µg/ml anti-IgM antibody or 20 µg/ml LPS or with 1 µM C-type CpG ODN 2395 or were left untreated.
$CD4^+$ and $CD8^+$ T cells were activated via their T cell receptors with plate-bound anti-CD3/CD28 as described in more detail in section 'Isolation and expansion of primary $CD4^+$ T cells'. In short, plates were coated with goat-anti hamster IgG to enable soluble anti-CD3 and anti-CD28 to bind in the correct orientation to the surface of the plate. Then, the cell suspension containing 1 µg/ml anti-CD3 and 2,5 µg/ml anti-CD28 was added. $CD4^+$ and $CD8^+$

T cells were also treated with 20 μg/ml low molecular weight poly-I:C. T cells were stimulated for 1, 4 and 16 hours or were left untreated. After the respective time points, immune cells were collected and lyzed with Trizol lysis reagent and further processed as described in the section 'RT-PCR'.

## 6.9 RNA sequencing analysis of B cells and alveolar macrophages

Lymph nodes were taken from *Regnase-3*$^{+/+}$ mice and from *Regnase-3*$^{-/-}$ mice. In *Regnase-3*-deficient mice, the lymph nodes of each mouse were divided into hypertrophic ones and lymph nodes of physiological size. B cells were isolated as described in the section 'Isolation of primary B cells'.

Alveolar lung macrophages were isolated as follows: Mice were euthanized using $CO_2$, the trachea was carefully exposed using dissection tools and a small incision was made using the tip of a 20G needle. 21G catheter tubing was attached to a Luer connector, allowing a tight connection of a syringe to the catheter tubing. The tubing was inserted few mm into the trachea of the mouse and tightly fixed using suture. One ml of cold (4°C) bronchoalveolar lavage (BAL) rinsing buffer was slowly pressed into the lung of the mouse using a syringe connected to the tubing. The liquid was kept in the lung for 1 min and the thorax was slightly massaged. Then, the liquid was slowly removed from the lung with the syringe and collected into tubes and kept on ice. This procedure was repeated 5 times and the rinsing suspensions from one mouse were pooled.

Cells were collected (300 x g, 5 min, 4°C) and Fc receptors were blocked by pre-incubation in 100 μl anti-CD16/32 for 15 min. A mix of 1 μg anti-CD11c-biotin and 0,2 μg anti-CD11c-APC were added to the lavage suspension of one mouse and incubated on ice for 10 min. Biotinylated CD11c is necessary for the subsequent isolation of macrophages, while the CD11c-APC is used to verify the isolation efficiency by flow cytometry. Cells were washed with 5 ml BAL rinsing buffer (300 x g, 5 min, 4°C) and incubated with 20 μl anti-biotin microbeads (Miltenyi) in 200 μl rinsing buffer for 15 min on ice and washed again. Positive cells were then isolated on a MS column according to the manufacturers protocol. Cells were lysed in buffer RLT Plus lysis buffer of the RNeasy Plus Micro Kit according to manufacturer's instructions.

RNA from B cells as well from alveolar macrophages was then used for RNA sequencing analysis. The 'TruSeq Stranded Total RNA Library Prep Kit' (Illumina) was used for library preparation and rRNA depletion. Barcoded libraries from the B cell samples were sequenced on a HiSeq 2500 (Illumina) with paired-end, 100 bp reads. Barcoded libraries from alveolar macrophages were sequenced on a HiSeq 4000 (Illumina) with paired-end, 150 bp reads. The sequencing reads of B cell samples were mapped against the mouse genome mm9 (UCSC version mm9, NCBI37) with STAR. Quantification of reads mapped to annotated genes was performed with the featureCounts software from the subread package (v1.6.0) (Liao *et al.*,

2014). Differentially expressed genes were quantified using the DESeq2 software (Varet *et al.*, 2016). Gorilla software was applied to determine gene ontology (GO) term analysis (Eden *et al.*, 2009). RNA sequencing reads from alveolar macrophages were mapped against the mouse genome mm10 (GRCm38) with HISAT2. Quantification of reads mapped to annotated genes was also performed with the featureCounts software from the subread package. Differentially expressed genes were quantified with the edgeR software (Robinson *et al.*, 2010). Enrichr software was applied to determine gene ontology (GO) term analysis and redundant GO terms were removed with REViGO (Kuleshov *et al.*, 2016; Supek *et al.*, 2011). The RNA sequencing data from B cells and alveolar macrophages were deposited at the Gene Expression Omnibus (GEO) database and can be found under the accession number GSE129325.

### 6.10 Immunoblotting

For immunoblot analysis of murine tissue, organs were dissected from mice and immediately snap frozen in liquid nitrogen. Tissues were then powdered by grinding with mortar and pestle under liquid nitrogen cooling. The powdered tissues were weighed and lysed by adding boiling (95°C) 2 x concentrated Laemmli buffer for 5 min. Addition of boiling Laemmli buffer inhibits rapid degradation of the Regnase-3 protein, which was observed under other lysis conditions. Isolated or differentiated cell types, such as bone marrow derived macrophages as well as cell lines were first counted and then lysed similarly by addition of boiling 2 x Laemmli buffer and boiling for 5 min under vigorous shaking. Material lysed in Laemmli buffer, was directly applied to SDS-PAGE without further processing. Alternatively, cell lines were also lysed by incubation for 5 min in RIPA buffer, supplemented with 5 mM EDTA, 1 mM dithiothreitol, complete Mini EDTA free protease inhibitors (Roche), and protease inhibitor cocktail powder (Sigma). Here, presence of EDTA was observed to be highly relevant to prevent rapid degradation of Regnase-3. RIPA samples were snap frozen in liquid nitrogen, thawed on ice and debris was pelleted by centrifugation (10000 x g, 15 min, 4°C). An aliquot of the supernatant was transferred to fresh tubes, 4 x Laemmli buffer with 10% β-mercaptoethanol was added and boiled for 5 min at 95°C. The protein concentration was measured with the bicinchoninic acid (BCA) assay.

Gels for the sodium dodecyl sulfate–polyacrylamide gel electrophoresis (SDS-PAGE) were prepared according to recipe in Table 17 of the material section. Equal amounts of tissue, cells or protein were loaded and proteins were separated on 8% SDS-PAGE gels. Proteins were blotted to PVDF membranes in transfer buffer for 2 hours at 50 V or over night at 30 V in a cold room (4°C). PVDF membranes were blocked with 5% milk in TBS for one hour at room temperature on a shaker and membranes were washed with TBS-T. Primary antibodies from Table 5 were applied to the membranes and incubated over night under constant staking or rotation. Membranes were washed three times with TBS-T for 5, 10 and 15 min. Secondary horseradish peroxidase (HRP) coupled secondary antibodies were diluted in 1%

milk and applied to the washed membranes. After 90 min incubation, membranes were washed twice with TBS-T for 5 and 10 min and once with TBS for 5 min. ECL reagent was applied to membranes and chemiluminescence was detected on the LI-COR Odyssey imaging system.

### 6.11 Development of the novel Regnase-3-specific antibody

The Regnase-3-specific antibody was developed in cooperation with the Protein Expression and Purification facility at the Institute of Structural Biology and the Monoclonal Antibody Core Facility from the Helmholtz Centre Munich (see a acknowledgement).

Commercially available anti-Regnase-3 antibodies were tested, but identified to generate insufficient or unspecific signals in the immunoblot when tested against *Regnase-3*-deficient tissue. Therefore, a novel recombinant antibody was generated. The full-length Regnase-3 protein sequence (aa 1–903) was cloned with an N-terminal Glutathione S-transferase (GST) tag and a C-terminal His-tag into the pGEX-6P-2 vector backbone and expressed in *E. coli*. The Regnase-3 protein was purified in two consecutive steps on a HiTrap Chelating column and a GSTrap column. The purified Regnase-3 protein and five short peptides of 15 – 20 aa length corresponding Regnase-3 unique sequences were used to immunize Lou/C rats and *C57BL/6* mice and hybridoma clones were generated as published elsewhere (Feederle *et al.*, 2016). Supernatants from hybridoma clones were first screened by an enzyme-linked immunoassay as follows: 96-well plates were coated with 5 μg/ml mouse anti-GST antibody from Table 8 in carbonate buffer (pH 9.5) at 4°C over night. The next day, the plate was washed with PBS and blocked for 15 min with 2% FBS. Then, purified Regnase-3 protein or peptide was applied to the plates in a 1:200 dilution and incubated for 30 min. Plates were washed once with PBS and incubated with HRP-labeled anti-rat antibodies for 30 min. Then, plates were washed five times with PBS, visualized with the 1-Step Ultra TMB ELISA substrate and read on a Tecan Infinite F200 Pro at 650 nm. The hybridoma cells of Regnase-3-reactive supernatants were cloned at least twice by limiting dilution.

All positively selected clones from the ELISA secreening (about 600 clones from peptides or the full length protein) were then individually tested by immunoblot analysis in lysates with GFP-Regnase-3 overexpression using the Mini-PROTEAN II apparatus. Antibodies, which were positive in the second screening, were then tested in tissues from *Regnase-3*$^{+/+}$ and *Regnase-3*$^{-/-}$ mice. Finally, best antibody clones were then checked against overexpressed protein of all Regnase family members by immunoblot.

Rat monoclonal antibody 4D3 (IgG2a) was obtained and used in this study.

## 6.12 Expression analysis for Regnase-3 protein in immune cell types and tissues

Murine tissues were isolated and processed as described in 'Immunohistochemistry'.
B cells were isolated as described in the section 'Isolation of primary B cells'. $CD4^+$ and $CD8^+$ T cells were isolated and expanded as described in sections 'Isolation and expansion of primary $CD4^+$ T cells' and 'Isolation and expansion of primary $CD8^+$ T cells'. Bone marrow derived macrophages and bone marrow derived conventional dendritic cells were differentiated as described in the section 'Generation of primary BMDM and cDCs'. Neutrophils were isolated as described in the section 'Isolation of primary Neutrophils'.
The purity of cell types used for immunoblot analysis was evaluated by flow cytometry and was between 85% and 98%. B cells were stained with anti-B220, $CD4^+$ and $CD8^+$ T cells were labeled with anti-CD4 and anti-CD8, respectively. Anti-F4/80 was used for macrophrages and anti-CD11c for dendritic cells. Cells were counted and lysed in 2 x concentrated, boiling Laemmli buffer. Lysed tissue samples and immune cells were further processed as described in the section 'Immunoblotting'.

## 6.13 Treatment of BMDM for immunoblot and RT-PCR analysis

Bone marrow cells from *C57BL/6J*, *Regnase-3*$^{+/+}$, *Regnase-3*$^{-/-}$ and *NF-κB p50*$^{-/-}$ mice were differentiated into macrophages as described in the section 'Generation of primary BMDM and cDCs'. 1.0 x $10^6$ cells per 6-well were seeded onto non-tissue culture-treated 6-well plates in 1.5 ml SFM medium the day before treatment. For some assays, cells were pre-treated with 10 μM (S)-MG132 or DMSO as vehicle, if indicated in the figure legend. Different receptor agonists were then added and cells were incubated for indicated time points. The used concentrations were as follows: 100 ng/ml lipopolysaccharides (LPS) from *Salmonella enterica* serotype typhimurium, 1 μg/ml lipoteichoic acid (LTA) from *Staphylococcus aureus*, 1 μg/ml R848 (Resiquimod), 100 ng/ml utra-pure Flagellin, 10 μg/ml high molecular weight poly-I:C, 1 μg/ml C-type CpG ODN2395, 100 ng/ml Murabutide, 25 ng/ml Phorbol-12-myristat-13-acetat (PMA), 50 ng/ml TNFα, 50 ng/ml IL-1β, 50 ng/ml IL-4, 50 ng/ml IL-6, 50 ng/ml IL-10, 50 ng/ml IL-15, 50 ng/ml IFNγ and 50 ng/ml IFNγ plus 100 ng/ml LPS. For the TBK1 assay, in which downstream signaling of the TLR3 receptor was analyzed, cells were first pre-treated with 20 μM IKKε/TBK1 inhibitor MRT67307 or with DMSO (vehicle) for 5 hours and then incubated with 10 μg/ml high molecular weight poly-I:C for indicted times or were left untreated.
For protein analysis, cells were scraped off the plate in macrophage SFM medium and transferred to 1.5 ml tubes. Cells were collected (300 x g, 4°C, 3 min) and lyzed in 2 x concentrated Laemmli as described in the section 'Immunoblotting'. For RNA analysis, supernatant was aspirated and 1 ml Trizol reagent was added directly to the plates. Cells were lysed by thorough pipetting and further processed as described under 'RT-PCR'.

## 6.14 Analysis of blood and serum in *Regnase-3*$^{-/-}$ mice

### 6.14.1 Peripheral blood counts

Blood was taken from $CO_2$ euthanized *Regnase-3*$^{-/-}$ mice and *Regnase-3*$^{+/+}$ littermates and anti-coagulated with EDTA. Peripheral blood counts were measured on the automated cell counter ABX Micros ES60.

### 6.14.2 ELISA for serum IgG, IgM, IgA

*Regnase-3*$^{+/+}$ and *Regnase-3*$^{-/-}$ mice were euthanized by $CO_2$ and heart blood was collected. The blood samples were turned up and down for several minutes and then kept on ice. Next, coagulated blood was centrifuged (2000 x g, 15 min, 4°C) to obtain blood serum.
Immunoglobulin levels for IgG, IgM and IgA were analyzed by plate bound enzyme-linked immunosorbent assays according to the manufacturer's instructions and measured on the PHERAstar microplate reader.

### 6.14.3 Multiplex assay for serum cytokines

Serum from *Regnase-3*$^{-/-}$ mice and *Regnase-3*$^{+/+}$ littermates as well as from *Regnase-3*$^{fl/fl}$ and *Regnase-3*$^{fl/fl}$ +LysM-Cre mice was obtained as described for 'ELISA for serum IgG, IgM, IgA'. The multiplex assay LEGENDplex 'mouse inflammation panel' was used to determine IL-1α, IL-1β, IL-6, IL-10, IL-12p70, IL-17A, IL-23, IL-27, IFNβ, IFNγ, TNFα and GM-CSF in the sera. The assay was used according to the manufacturer's protocol and measured on the FACS Aria III flow cytometer. Concentrations were calculated using the provided LEGENDplex Data Analysis Software.

## 6.15 Auto reactive antibody tests

### 6.15.1 Auto reactive antibodies against tissue

Serum from *Regnase-3*$^{-/-}$ mice and *Regnase-3*$^{+/+}$ littermates was collected as described for 'ELISA for serum IgG, IgM, IgA'. Protein lysates from the liver of immunodeficient NOD scid gamma mice were kindly provided by Prof. Vigo Heissmeyer (LMU Munich). 400 µg NSG liver lysate was applied to one big pocket covering the whole width of a 10% SDS-PAGE gel, except a small pocket for the marker, then separated and blotted to PVDF membranes as described in the section 'Immunoblotting'. Membranes were blocked in 5% BSA in TBS for one hour. Mouse sera were diluted 1:200 in sera dilution buffer and applied to the PVDF membranes using the Mini-PROTEAN II apparatus, which allows incubating several antibodies in stripes next to each other on one membrane. Sera of *Rc3h1*$^{san/san}$ and *MRL/lpr* mice were kindly provided by Prof. Vigo Heissmeyer (LMU Munich) and Prof. Ari Waisman (University of Mainz) and served as positive controls. The Mini-PROTEAN II apparatus was placed into a humid chamber on a plate shaker and incubated over night. Sera were then

aspirated from the apparatus and membranes were washed twice with 1% milk in TBS-T, when still placed in the apparatus to remove residual traces of sera. Then, membranes were removed from the apparatus and were washed two more times in 1% milk in TBS-T. Secondary HRP-coupled anti-mouse IgG was diluted 1:2000 in 1% milk in TBS-T and membranes were incubated for one hour. Membranes were washed three times in 1% milk in TBS-T for 5, 10 and 15 min. Chemiluminescence of the Amersham ECL prime reagent was detected by photosensitive films. Intensities for each mouse were scored as 0 = negative, 1 = weak positive, 2 = strong positive.

### 6.15.2 Anti-nuclear antibodies

Serum from *Regnase-3*$^{-/-}$ mice and *Regnase-3*$^{+/+}$ littermates was collected as described in the section 'ELISA for serum IgG, IgM, IgA' and diluted 1:50 in sera dilution buffer. Then, immobilized HEp-2 human epithelial cells were probed with the diluted sera and indirect immunofluorescence was analyzed according to the manufacturer's instruction with small modifications. In particular, FITC coupled goat anti-mouse IgG (Santa Cruz, # sc-2010) was used instead of anti-human IgG antibodies of the Kit. Sera from *MRL/lpr* mice served as positive controls. Images were captured with a Keyence BZ-9000 fluorescence microscope. Fluorescence images were scored as negative, 1 = weak positive, 2 = strong positive.

## 6.16 Phagocytosis in BMDM

BMDM were differentiated from *Regnase-3*$^{+/+}$ and *Regnase-3*$^{-/-}$ mice as described in the section 'Generation of primary BMDM and cDCs'. 150,000 macrophages per well were seeded onto 96-well plates in Macrophage SFM medium the day prior the assay. The next day, the medium was replaced by phagocytosis assay medium and cells were pre-treated for 4 hours with 100 ng/ml lipopolysaccharides (LPS) from *Salmonella enterica* serotype typhimurium, 1 μg/ml lipoteichoic acid (LTA) from *Staphylococcus aureus*, 10 μg/ml high molecular weight poly-I:C or 50 ng/ml TNFα or were left untreated. Each condition was pipetted in quadruplicates. *Staphylococcus aureus* bioparticles coupled to pH sensitive pHrodo green fluorophore were diluted in phagocytosis assay medium so that one vial of bioparticles was distributed to 80 wells. When cells were probed with the pHrodo bioparticles, 96-well plates were centrifuged (300 x g, 1 min, room temperature) to accelerate particle sedimentation. Fluorescence was then immediately measured on the VarioSkan Lux microplate reader with excitation at 509 nm and emission at 533 nm in order to receive a time zero value. Plates were brought back into a cell culture incubator and increase in fluorescence was measured every 30 min over a time frame of 5 hours. To calculate the increase in fluorescence intensities, time zero values of the respective wells were subtracted from their measurement values at a specific time. The fluorescence intensity of untreated *Regnase-3*$^{+/+}$ macrophages after 5 hours of incubation was set to 100% and all other conditions were calculated in relativity to this value.

## 6.17 Statistical analysis

Specific statistical or bioinformatical analyses are described in the respective sections. Other data were analyzed using Prism software (GraphPad) with statistical tests as indicated. Significance is indicated as follows: * $p \leqslant 0.05$, ** $p \leqslant 0.01$, *** $p \leqslant 0.001$, **** $p \leqslant 0.0001$, ns = not significant.

# 7 Contribution & Acknowledgment

My doctoral thesis as well as our associated publication 'Immune homeostasis and regulation of the interferon pathway require myeloid-derived Regnase-3' in '*The Journal of Experimental Medicine'* (von Gamm *et al.*, 2019) contains substantial data that has been generated in cooperation with colleagues and external partners. I highly appreciate their contributions and efforts to make this project possible.
Here, I would like to sum up all the people who supported me and I would like to acknowledge their main contributions or assistances.

**Dr. Elke Glasmacher** is the principal investigator behind this study. She conceived the research project on which my doctoral thesis and our publication in '*The Journal of Experimental Medicine*' are based on.

Special thanks go to **Dr. Elke Glasmacher** for her ideas, her strong commitment for the project and her passion that ensured constant scientific progress. In addition, I thank her for her engagement to acquire fruitful collaborators. I also appreciate her support in my personal and professional development. She also helped me with immune cell isolations for RNA expression studies (Figure 50).

I would also like to thank **Prof. Matthias H. Tschöp** and **Prof. Martin Hrabě de Angelis** for supporting me as 1st and 2nd examiner of my doctoral thesis and their suggestions from our thesis committee meetings.

I thank **Prof. Mathias Heikenwälder** (DKFZ, Heidelberg) and his team members **Danijela Heide** and **Jenny Hetzer**, who greatly supported us throughout the whole study with histological analyses of *Regnase-3*-deficient mice. All tissue sections were processed and stained in the lab of Mathias Heikenwälder. Slides were scanned either at the DKFZ or at the Helmholtz Center Munich.
Myself, together with **Elke Glasmacher** and **Anna Macht** performed manual evaluation of the data. **Anna Macht** and myself analyzed positive pixel counts. **Dr. Annette Feuchtinger** (core facility 'Pathology & Tissue analytics') kindly provided a computational algorithm for positive pixel counts. Many thanks for your contributions.
Histo: Figure 14, Figure 15, Figure 23, Figure 24, Figure 31, Figure 32, Figure 33, Figure 45

I thank my former colleague **Christine Wolf**, who supported me throughout the years in multiple ways, in particular with professional contributions for immunoblot analyses. She helped me greatly with preparations of cells, cell lysates and western blot for immunoblot analysis and with tissue preparations for FACS analysis.
The following Figures contain data from immunoblot analyses, which were mainly done by Christine Wolf. Immune cells were in part isolated/generated by myself as well as some of the treatments:
Western Blots: Figure 53, Figure 54, Figure 61, Figure 64, Figure 67, Figure 68, Figure 69, Figure 72.
The following Western Blots contain data, which were acquired together by Christine Wolf and myself: Figure 52, Figure 65, Figure 66.

I thank my former colleague **Dr. Johannes Lichti**, who performed RNA library preparations and essential parts of the sequencing data analyses. Immune cells, which were used for RNA sequencing, were isolated and treated by myself.
**Dr. Elisabeth Graf** and **Sandy Lösecke** from our core facility sequenced the samples. **Prof. Caroline Friedel** (LMU Munich) further supported sequencing data analysis. Many thanks also for your contributions.
Sequencing data: Figure 26, Figure 27, Figure 28, Figure 74, Figure 75, Figure 76
Johannes Lichti and myself performed together the *in vitro* phagocytosis assay in Figure 77 and the qPCR analysis in Figure 30. He also supported me strongly during the publishing process of our article in '*The Journal of Experimental Medicine*'.

I thank my former colleague **Anna Macht**, who greatly supported me in many ways. In particular I would like to point out her help in the analysis of histology sections and with tissue preparation for flow cytometry experiments. Further she helped me with the anti-nuclear antibody test in Figure 20 and with mouse colony maintenance.

I thank my former colleague **Annalisa Schaub**, who performed and analyzed confocal staining to unravel Regnase-3 subcellular localization (not presented herein, but in our publication in '*The Journal of Experimental Medicine*'). She supported me further in multiple ways, such as with cloning and during the publishing process of our manuscript.

Many thanks also go to **Dr. Arie Geerlof**, who purified Regnase-3 protein for rat and mouse immunizations, necessary for antibody generation and the RNA degradation assay (not presented herein but in our publication in '*The Journal of Experimental Medicine*').

I thank the members of the Monoclonal Antibody Core Facility, which was previously managed by **Dr. Elisabeth Kremmer** and is now by **Dr. Regina Feederle**. In particular I want to acknowledge the work of **Andrew Flatley**, who generated the hybridoma clones for our novel Regnase-3-specific antibody and did the ELISA tests for the antibody clones. Validation of the antibody by immunoblot was done by myself together with Christine Wolf.

Many thanks also go to **Dr. Katharina Essig** (Roche Pharma Research)**,** who determined together with me intracellular interferon gamma levels in *Regnase-3*-deficient mice by flow cytometry as shown in Figure 60. She also helped me with my analysis of *Irf3*- and *Irf7*-deficient RAW cells (Figure 72).

I thank **Dr. Joachim Pircher** (LMU Munich), who analyzed together we me peripheral blood counts in *Regnase-3*-deficient mice as shown in Figure 22.

I thank **Prof. Wolfgang Wurst**, who provided *Regnase-3*-deficient mice via EUCOMM.

I thank my former colleague **Dr. Kathrin Davari**, who initiated the TBK1 inhibitor studies.

I thank **Betty Haderlein** and **Marlene Kilian**, who helped me with mouse colony maintenance.

I also appreciate the engagement of **Sandra Schneid** and **Melanie Kienzl**, who did internships and in particular helped me with cloning of expression constructs.

I thank my former colleague **Christian Gallus** for providing me plasmids.

I thank **Prof. Marc Schmidt-Supprian**, (TU München), who provided his *NEMO*$^{-/-}$ mouse embryonic fibroblasts to us via **Prof. Daniel Krappmann**.

I thank **Prof. Wolfgang Wurst**, **Dr. Veit Buchholz**, **Prof. Daniel Krappmann**, **Dr. Tobias Stöger**, and **Prof. Marc Schmidt-Supprian** for providing mouse lines (as listed in the material section).

I thank **Prof. Henriette Uhlenhaut** for providing L929 cells and **Prof. Christian Schulz** for providing ER-Hoxb8 cells and SCF-CHO cells.

Special thanks also goes to **Dr. Elke Glasmacher**, **Dr. Sara Brandt** and **Dr. Johannes Lichti** for critically proofreading my thesis.

Further I would like also to express my sincere gratitude to colleagues, who have contributed valuable data and scientific input, which is not particularly presented herein, but was very important for our associated publication:

I thank **Prof. Christian Schulz** (LMU Munich), who conceived the *in vivo* infection study and supported us with his expertise in macrophage biology. I also thank his team members **Dr. Joachim Pircher** and **Andreas Ehrlich,** who performed the experiments. I also thank **Dr. Benjamin Busch** (LMU Munich), who contributed to the *in vivo* study.

Many thanks also go to the lab of **Prof. Michael Sattler**. In particular, I would like to appreciate the help of **Dr. Arie Geerlof**, who also purified Regnase-3 protein for RNA binding studies. I also thank **Dr. Alisha N. Jones**, who performed RNA EMSA experiments.

Many thanks go to the lab of **Prof. Vigo Heissmeyer** (LMU Munich). I thank him for his critical review of our publication. In particular I would like to acknowledge the help of **Dr. Gesine Behrens**, who performed reporter gene assays.

Many thanks also go to the lab of **Prof. Veit Hornung** (LMU Munich). I thank him for his critical review of our publication. I further thank **Dr. Dhruv Chauhan** for ELISA analysis of the supernatants from *Regnase-3*-deficient macrophages.

I thank **Dr. Stefanie M. Hauck** for her commitment to provide mass spectrometry data, although the data sadly did not make it into the final publication.

I thank **Dr. Nadine Hövelmeyer**, **Dr. Sonja Reissig** and **Prof. Ari Waisman** from the University of Mainz, who helped me to establish flow cytometry analyses for immune cells.

Further, I would like to express my gratitude also **to many people** who provided material or scientific advice or supported me in any other way throughout the years and is not specifically mentioned. It was a pleasure to experience so much support from multiple sites.

And finally I express my sincere gratitude to my **family and friends** for their mental support and believe in my perseverance. Many Thanks for that!

# 8 Literature

ABRAM, C. L., ROBERGE, G. L., HU, Y. & LOWELL, C. A. 2014. Comparative analysis of the efficiency and specificity of myeloid-Cre deleting strains using ROSA-EYFP reporter mice. *J Immunol Methods,* 408**,** 89-100.

ACTOR, J. K. 2014. *Introductory Immunology : Basic Concepts for Interdisciplinary Applications,* San Diego, UNITED STATES, Elsevier Science & Technology.

AHMADZADEH, M., JOHNSON, L. A., HEEMSKERK, B., WUNDERLICH, J. R., DUDLEY, M. E., WHITE, D. E.*, et al.* 2009. Tumor antigen-specific CD8 T cells infiltrating the tumor express high levels of PD-1 and are functionally impaired. *Blood,* 114**,** 1537-44.

AKIRA, S. 2013. Regnase-1, a ribonuclease involved in the regulation of immune responses. *Cold Spring Harb Symp Quant Biol,* 78**,** 51-60.

ANDREWS, B. S., EISENBERG, R. A., THEOFILOPOULOS, A. N., IZUI, S., WILSON, C. B., MCCONAHEY, P. J.*, et al.* 1978. Spontaneous murine lupus-like syndromes. Clinical and immunopathological manifestations in several strains. *J Exp Med,* 148**,** 1198-215.

ATANASIO, A., DECMAN, V., WHITE, D., RAMOS, M., IKIZ, B., LEE, H. C.*, et al.* 2016. C9orf72 ablation causes immune dysregulation characterized by leukocyte expansion, autoantibody production, and glomerulonephropathy in mice. *Sci Rep,* 6**,** 23204.

BABIC LEKO, M., ZUPUNSKI, V., KIRINCICH, J., SMILOVIC, D., HORTOBAGYI, T., HOF, P. R.*, et al.* 2019. Molecular Mechanisms of Neurodegeneration Related to C9orf72 Hexanucleotide Repeat Expansion. *Behav Neurol,* 2019**,** 2909168.

BACCALA, R., GONZALEZ-QUINTIAL, R., LAWSON, B. R., STERN, M. E., KONO, D. H., BEUTLER, B.*, et al.* 2009. Sensors of the innate immune system: their mode of action. *Nat Rev Rheumatol,* 5**,** 448-56.

BALAR, A. V., GALSKY, M. D., ROSENBERG, J. E., POWLES, T., PETRYLAK, D. P., BELLMUNT, J.*, et al.* 2017. Atezolizumab as first-line treatment in cisplatin-ineligible patients with locally advanced and metastatic urothelial carcinoma: a single-arm, multicentre, phase 2 trial. *Lancet,* 389**,** 67-76.

BEUTLER, B. 2009a. Microbe sensing, positive feedback loops, and the pathogenesis of inflammatory diseases. *Immunol Rev,* 227**,** 248-63.

BEUTLER, B. A. 2009b. TLRs and innate immunity. *Blood,* 113**,** 1399-407.

BOLISETTY, S., ZARJOU, A., HULL, T. D., TRAYLOR, A. M., PERIANAYAGAM, A., JOSEPH, R.*, et al.* 2015. Macrophage and epithelial cell H-ferritin expression regulates renal inflammation. *Kidney Int,* 88**,** 95-108.

BRIGNALL, R., CAUCHY, P., BEVINGTON, S. L., GORMAN, B., PISCO, A. O., BAGNALL, J.*, et al.* 2017. Integration of Kinase and Calcium Signaling at the Level of Chromatin Underlies Inducible Gene Activation in T Cells. *J Immunol,* 199**,** 2652-2667.

BROYDE, A., BOYCOV, O., STRENOV, Y., OKON, E., SHPILBERG, O. & BAIREY, O. 2009. Role and prognostic significance of the Ki-67 index in non-Hodgkin's lymphoma. *Am J Hematol,* 84**,** 338-43.

BRUNO, S. & DARZYNKIEWICZ, Z. 1992. Cell cycle dependent expression and stability of the nuclear protein detected by Ki-67 antibody in HL-60 cells. *Cell Prolif,* 25**,** 31-40.

BUCHMEIER, N. A. & SCHREIBER, R. D. 1985. Requirement of endogenous interferon-gamma production for resolution of Listeria monocytogenes infection. *Proc Natl Acad Sci U S A,* 82**,** 7404-8.

CARBALLO, E., GILKESON, G. S. & BLACKSHEAR, P. J. 1997. Bone marrow transplantation reproduces the tristetraprolin-deficiency syndrome in recombination activating

gene-2 (-/-) mice. Evidence that monocyte/macrophage progenitors may be responsible for TNFalpha overproduction. *J Clin Invest,* 100**,** 986-95.
CHAKRABARTI, A., GHOSH, P. K., BANERJEE, S., GAUGHAN, C. & SILVERMAN, R. H. 2012. RNase L triggers autophagy in response to viral infections. *J Virol,* 86**,** 11311-21.
CHAKRABARTI, A., JHA, B. K. & SILVERMAN, R. H. 2011. New insights into the role of RNase L in innate immunity. *J Interferon Cytokine Res,* 31**,** 49-57.
CHAU, T. L., GIOIA, R., GATOT, J. S., PATRASCU, F., CARPENTIER, I., CHAPELLE, J. P.*, et al.* 2008. Are the IKKs and IKK-related kinases TBK1 and IKK-epsilon similarly activated? *Trends in Biochemical Sciences,* 33**,** 171-180.
CHAUDHRY, M., WANG, X., BAMNE, M. N., HASNAIN, S., DEMIRCI, F. Y., LOPEZ, O. L.*, et al.* 2015. Genetic variation in imprinted genes is associated with risk of late-onset Alzheimer's disease. *J Alzheimers Dis,* 44**,** 989-94.
CHERWINSKI, H. M., SCHUMACHER, J. H., BROWN, K. D. & MOSMANN, T. R. 1987. Two types of mouse helper T cell clone. III. Further differences in lymphokine synthesis between Th1 and Th2 clones revealed by RNA hybridization, functionally monospecific bioassays, and monoclonal antibodies. *J Exp Med,* 166**,** 1229-44.
CHOW, K. T., GALE, M., JR. & LOO, Y. M. 2018. RIG-I and Other RNA Sensors in Antiviral Immunity. *Annu Rev Immunol,* 36**,** 667-694.
COFFMAN, R. L. 2006. Origins of the T(H)1-T(H)2 model: a personal perspective. *Nat Immunol,* 7**,** 539-41.
COLEMAN, J. L., BRENNAN, K., NGO, T., BALAJI, P., GRAHAM, R. M. & SMITH, N. J. 2015. Rapid Knockout and Reporter Mouse Line Generation and Breeding Colony Establishment Using EUCOMM Conditional-Ready Embryonic Stem Cells: A Case Study. *Front Endocrinol (Lausanne),* 6**,** 105.
CUI, X., MINO, T., YOSHINAGA, M., NAKATSUKA, Y., HIA, F., YAMASOBA, D.*, et al.* 2017. Regnase-1 and Roquin Nonredundantly Regulate Th1 Differentiation Causing Cardiac Inflammation and Fibrosis. *J Immunol,* 199**,** 4066-4077.
CUMBERBATCH, M., SINGH, M., DEARMAN, R. J., YOUNG, H. S., KIMBER, I. & GRIFFITHS, C. E. 2006. Impaired Langerhans cell migration in psoriasis. *J Exp Med,* 203**,** 953-60.
DAVIES, L. C., JENKINS, S. J., ALLEN, J. E. & TAYLOR, P. R. 2013. Tissue-resident macrophages. *Nat Immunol,* 14**,** 986-95.
DI TOMMASO, P., MORETTI, S., XENARIOS, I., OROBITG, M., MONTANYOLA, A., CHANG, J. M.*, et al.* 2011. T-Coffee: a web server for the multiple sequence alignment of protein and RNA sequences using structural information and homology extension. *Nucleic Acids Res,* 39**,** W13-7.
DRANOFF, G. 2004. Cytokines in cancer pathogenesis and cancer therapy. *Nat Rev Cancer,* 4**,** 11-22.
DRANOFF, G., CRAWFORD, A. D., SADELAIN, M., REAM, B., RASHID, A., BRONSON, R. T.*, et al.* 1994. Involvement of granulocyte-macrophage colony-stimulating factor in pulmonary homeostasis. *Science,* 264**,** 713-6.
EDEN, E., NAVON, R., STEINFELD, I., LIPSON, D. & YAKHINI, Z. 2009. GOrilla: a tool for discovery and visualization of enriched GO terms in ranked gene lists. *BMC Bioinformatics,* 10**,** 48.
EDFORS, F., DANIELSSON, F., HALLSTROM, B. M., KALL, L., LUNDBERG, E., PONTEN, F.*, et al.* 2016. Gene-specific correlation of RNA and protein levels in human cells and tissues. *Mol Syst Biol,* 12**,** 883.
FARG, M. A., SUNDARAMOORTHY, V., SULTANA, J. M., YANG, S., ATKINSON, R. A., LEVINA, V.*, et al.* 2014. C9ORF72, implicated in amytrophic lateral sclerosis and frontotemporal dementia, regulates endosomal trafficking. *Hum Mol Genet,* 23**,** 3579-95.

FEEDERLE, R., GERBER, J. K., MIDDLETON, A., NORTHRUP, E., KIST, R., KREMMER, E., *et al.* 2016. Generation of Pax1/PAX1-Specific Monoclonal Antibodies. *Monoclon Antib Immunodiagn Immunother,* 35**,** 259-262.

FEUCHTINGER, A., STIEHLER, T., JUTTING, U., MARJANOVIC, G., LUBER, B., LANGER, R., *et al.* 2015. Image analysis of immunohistochemistry is superior to visual scoring as shown for patient outcome of esophageal adenocarcinoma. *Histochem Cell Biol,* 143**,** 1-9.

FIORINI, F., BAGCHI, D., LE HIR, H. & CROQUETTE, V. 2015. Human Upf1 is a highly processive RNA helicase and translocase with RNP remodelling activities. *Nat Commun,* 6**,** 7581.

FRISCHMEYER-GUERRERIO, P. A., MONTGOMERY, R. A., WARREN, D. S., COOKE, S. K., LUTZ, J., SONNENDAY, C. J., *et al.* 2011. Perturbation of thymocyte development in nonsense-mediated decay (NMD)-deficient mice. *Proc Natl Acad Sci U S A,* 108**,** 10638-43.

FU, M. & BLACKSHEAR, P. J. 2017. RNA-binding proteins in immune regulation: a focus on CCCH zinc finger proteins. *Nat Rev Immunol,* 17**,** 130-143.

FUJIWARA, T., ODA, K., YOKOTA, S., TAKATSUKI, A. & IKEHARA, Y. 1988. Brefeldin A causes disassembly of the Golgi complex and accumulation of secretory proteins in the endoplasmic reticulum. *J Biol Chem,* 263**,** 18545-52.

GALLIMORE, A., GLITHERO, A., GODKIN, A., TISSOT, A. C., PLUCKTHUN, A., ELLIOTT, T., *et al.* 1998. Induction and exhaustion of lymphocytic choriomeningitis virus-specific cytotoxic T lymphocytes visualized using soluble tetrameric major histocompatibility complex class I-peptide complexes. *J Exp Med,* 187**,** 1383-93.

GALLOWAY, A., SAVELIEV, A., LUKASIAK, S., HODSON, D. J., BOLLAND, D., BALMANNO, K., *et al.* 2016. RNA-binding proteins ZFP36L1 and ZFP36L2 promote cell quiescence. *Science,* 352**,** 453-9.

GAUD, G., LESOURNE, R. & LOVE, P. E. 2018. Regulatory mechanisms in T cell receptor signalling. *Nat Rev Immunol,* 18**,** 485-497.

GEDDES, K., MAGALHAES, J. G. & GIRARDIN, S. E. 2009. Unleashing the therapeutic potential of NOD-like receptors. *Nat Rev Drug Discov,* 8**,** 465-79.

GEIJTENBEEK, T. B. & GRINGHUIS, S. I. 2009. Signalling through C-type lectin receptors: shaping immune responses. *Nat Rev Immunol,* 9**,** 465-79.

GERSTBERGER, S., HAFNER, M. & TUSCHL, T. 2014. A census of human RNA-binding proteins. *Nat Rev Genet,* 15**,** 829-45.

GIROUX, M., SCHMIDT, M. & DESCOTEAUX, A. 2003. IFN-gamma-induced MHC class II expression: transactivation of class II transactivator promoter IV by IFN regulatory factor-1 is regulated by protein kinase C-alpha. *J Immunol,* 171**,** 4187-94.

GLASMACHER, E., HOEFIG, K. P., VOGEL, K. U., RATH, N., DU, L., WOLF, C., *et al.* 2010. Roquin binds inducible costimulator mRNA and effectors of mRNA decay to induce microRNA-independent post-transcriptional repression. *Nat Immunol,* 11**,** 725-33.

GONZALEZ-TERAN, B., CORTES, J. R., MANIERI, E., MATESANZ, N., VERDUGO, A., RODRIGUEZ, M. E., *et al.* 2013. Eukaryotic elongation factor 2 controls TNF-alpha translation in LPS-induced hepatitis. *J Clin Invest,* 123**,** 164-78.

GUO, J., QU, H., CHEN, Y. & XIA, J. 2017. The role of RNA-binding protein tristetraprolin in cancer and immunity. *Med Oncol,* 34**,** 196.

HAYASHI, F., SMITH, K. D., OZINSKY, A., HAWN, T. R., YI, E. C., GOODLETT, D. R., *et al.* 2001. The innate immune response to bacterial flagellin is mediated by Toll-like receptor 5. *Nature,* 410**,** 1099-103.

HEINZEL, F. P., SADICK, M. D., HOLADAY, B. J., COFFMAN, R. L. & LOCKSLEY, R. M. 1989. Reciprocal expression of interferon gamma or interleukin 4 during the resolution or

progression of murine leishmaniasis. Evidence for expansion of distinct helper T cell subsets. *J Exp Med,* 169**,** 59-72.

HOBEIKA, E., THIEMANN, S., STORCH, B., JUMAA, H., NIELSEN, P. J., PELANDA, R.*, et al.* 2006. Testing gene function early in the B cell lineage in mb1-cre mice. *Proc Natl Acad Sci U S A,* 103**,** 13789-94.

HODSON, D. J., JANAS, M. L., GALLOWAY, A., BELL, S. E., ANDREWS, S., LI, C. M.*, et al.* 2010. Deletion of the RNA-binding proteins ZFP36L1 and ZFP36L2 leads to perturbed thymic development and T lymphoblastic leukemia. *Nat Immunol,* 11**,** 717-24.

HONDA, K. & TANIGUCHI, T. 2006. IRFs: master regulators of signalling by Toll-like receptors and cytosolic pattern-recognition receptors. *Nat Rev Immunol,* 6**,** 644-58.

HORNUNG, V., ELLEGAST, J., KIM, S., BRZOZKA, K., JUNG, A., KATO, H.*, et al.* 2006. 5'-Triphosphate RNA is the ligand for RIG-I. *Science,* 314**,** 994-7.

HUANG, S., MIAO, R., ZHOU, Z., WANG, T., LIU, J., LIU, G.*, et al.* 2013. MCPIP1 negatively regulates toll-like receptor 4 signaling and protects mice from LPS-induced septic shock. *Cell Signal,* 25**,** 1228-34.

HUANG, S., QI, D., LIANG, J., MIAO, R., MINAGAWA, K., QUINN, T.*, et al.* 2012. The putative tumor suppressor Zc3h12d modulates toll-like receptor signaling in macrophages. *Cell Signal,* 24**,** 569-76.

ISHIDA, Y., AGATA, Y., SHIBAHARA, K. & HONJO, T. 1992. Induced expression of PD-1, a novel member of the immunoglobulin gene superfamily, upon programmed cell death. *EMBO J,* 11**,** 3887-95.

ISHIWATARI-HAYASAKA, H., KAWASHIMA, H., OSAWA, T., NAGATA, S. & MIYASAKA, M. 1997. Induction of cell death by chimeric L-selectin-Fas receptors. *Int Immunol,* 9**,** 627-35.

IWASAKI, H., TAKEUCHI, O., TERAGUCHI, S., MATSUSHITA, K., UEHATA, T., KUNIYOSHI, K.*, et al.* 2011. The IkappaB kinase complex regulates the stability of cytokine-encoding mRNA induced by TLR-IL-1R by controlling degradation of regnase-1. *Nat Immunol,* 12**,** 1167-75.

JABLONSKI, K. A., AMICI, S. A., WEBB, L. M., RUIZ-ROSADO JDE, D., POPOVICH, P. G., PARTIDA-SANCHEZ, S.*, et al.* 2015. Novel Markers to Delineate Murine M1 and M2 Macrophages. *PLoS One,* 10**,** e0145342.

JAWORSKI, M. & THOME, M. 2016. The paracaspase MALT1: biological function and potential for therapeutic inhibition. *Cell Mol Life Sci,* 73**,** 459-73.

JELTSCH, K. M., HU, D., BRENNER, S., ZOLLER, J., HEINZ, G. A., NAGEL, D.*, et al.* 2014. Cleavage of roquin and regnase-1 by the paracaspase MALT1 releases their cooperatively repressed targets to promote T(H)17 differentiation. *Nat Immunol,* 15**,** 1079-89.

KARWACZ, K., BRICOGNE, C., MACDONALD, D., ARCE, F., BENNETT, C. L., COLLINS, M.*, et al.* 2011. PD-L1 co-stimulation contributes to ligand-induced T cell receptor down-modulation on CD8+ T cells. *EMBO Mol Med,* 3**,** 581-92.

KASZA, A., WYRZYKOWSKA, P., HORWACIK, I., TYMOSZUK, P., MIZGALSKA, D., PALMER, K.*, et al.* 2010. Transcription factors Elk-1 and SRF are engaged in IL1-dependent regulation of ZC3H12A expression. *BMC Mol Biol,* 11**,** 14.

KAWAKAMI, T., LICHTNEKERT, J., THOMPSON, L. J., KARNA, P., BOUABE, H., HOHL, T. M.*, et al.* 2013. Resident renal mononuclear phagocytes comprise five discrete populations with distinct phenotypes and functions. *J Immunol,* 191**,** 3358-72.

KRUMMEL, M. F. & ALLISON, J. P. 1995. CD28 and CTLA-4 have opposing effects on the response of T cells to stimulation. *J Exp Med,* 182**,** 459-65.

KULESHOV, M. V., JONES, M. R., ROUILLARD, A. D., FERNANDEZ, N. F., DUAN, Q., WANG, Z.*, et al.* 2016. Enrichr: a comprehensive gene set enrichment analysis web server 2016 update. *Nucleic Acids Res,* 44**,** W90-7.

LAI, W. S., STUMPO, D. J. & BLACKSHEAR, P. J. 1990. Rapid insulin-stimulated accumulation of an mRNA encoding a proline-rich protein. *J Biol Chem,* 265**,** 16556-63.

LEE, K. Y., ANDERSON, E., MADANI, K. & ROSEN, G. D. 1999. Loss of STAT1 expression confers resistance to IFN-gamma-induced apoptosis in ME180 cells. *FEBS Lett,* 459**,** 323-6.

LI, M., CAO, W., LIU, H., ZHANG, W., LIU, X., CAI, Z.*, et al.* 2012. MCPIP1 down-regulates IL-2 expression through an ARE-independent pathway. *PLoS One,* 7**,** e49841.

LI, Y., HUANG, X., HUANG, S., HE, H., LEI, T., SAAOUD, F.*, et al.* 2017. Central role of myeloid MCPIP1 in protecting against LPS-induced inflammation and lung injury. *Signal Transduct Target Ther,* 2**,** 17066.

LIANG, J., SAAD, Y., LEI, T., WANG, J., QI, D., YANG, Q.*, et al.* 2010. MCP-induced protein 1 deubiquitinates TRAF proteins and negatively regulates JNK and NF-kappaB signaling. *J Exp Med,* 207**,** 2959-73.

LIANG, J., WANG, J., AZFER, A., SONG, W., TROMP, G., KOLATTUKUDY, P. E.*, et al.* 2008. A novel CCCH-zinc finger protein family regulates proinflammatory activation of macrophages. *J Biol Chem,* 283**,** 6337-46.

LIAO, Y., SMYTH, G. K. & SHI, W. 2014. featureCounts: an efficient general purpose program for assigning sequence reads to genomic features. *Bioinformatics,* 30**,** 923-30.

LINSLEY, P. S., BRADY, W., URNES, M., GROSMAIRE, L. S., DAMLE, N. K. & LEDBETTER, J. A. 1991. CTLA-4 is a second receptor for the B cell activation antigen B7. *J Exp Med,* 174**,** 561-9.

LINSLEY, P. S., GREENE, J. L., BRADY, W., BAJORATH, J., LEDBETTER, J. A. & PEACH, R. 1994. Human B7-1 (CD80) and B7-2 (CD86) bind with similar avidities but distinct kinetics to CD28 and CTLA-4 receptors. *Immunity,* 1**,** 793-801.

LIU, L., ZHOU, Z., HUANG, S., GUO, Y., FAN, Y., ZHANG, J.*, et al.* 2013. Zc3h12c inhibits vascular inflammation by repressing NF-kappaB activation and pro-inflammatory gene expression in endothelial cells. *Biochem J,* 451**,** 55-60.

LU, J. Y., SADRI, N. & SCHNEIDER, R. J. 2006. Endotoxic shock in AUF1 knockout mice mediated by failure to degrade proinflammatory cytokine mRNAs. *Genes Dev,* 20**,** 3174-84.

LU, Y. C., YEH, W. C. & OHASHI, P. S. 2008. LPS/TLR4 signal transduction pathway. *Cytokine,* 42**,** 145-151.

LUNDGREN, S., KARNEVI, E., ELEBRO, J., NODIN, B., KARLSSON, M. C. I., EBERHARD, J.*, et al.* 2017. The clinical importance of tumour-infiltrating macrophages and dendritic cells in periampullary adenocarcinoma differs by morphological subtype. *J Transl Med,* 15**,** 152.

LUZINA, I. G., ATAMAS, S. P., STORRER, C. E., DASILVA, L. C., KELSOE, G., PAPADIMITRIOU, J. C.*, et al.* 2001. Spontaneous formation of germinal centers in autoimmune mice. *J Leukoc Biol,* 70**,** 578-84.

MACIAN, F., GARCIA-COZAR, F., IM, S. H., HORTON, H. F., BYRNE, M. C. & RAO, A. 2002. Transcriptional mechanisms underlying lymphocyte tolerance. *Cell,* 109**,** 719-31.

MAO, R., YANG, R., CHEN, X., HARHAJ, E. W., WANG, X. & FAN, Y. 2017. Regnase-1, a rapid response ribonuclease regulating inflammation and stress responses. *Cell Mol Immunol,* 14**,** 412-422.

MARTINEZ, F. O. & GORDON, S. 2014. The M1 and M2 paradigm of macrophage activation: time for reassessment. *F1000Prime Rep,* 6**,** 13.

MASS, E., BALLESTEROS, I., FARLIK, M., HALBRITTER, F., GUNTHER, P., CROZET, L.*, et al.* 2016. Specification of tissue-resident macrophages during organogenesis. *Science,* 353.

MATSUSHITA, K., TAKEUCHI, O., STANDLEY, D. M., KUMAGAI, Y., KAWAGOE, T., MIYAKE, T., *et al.* 2009. Zc3h12a is an RNase essential for controlling immune responses by regulating mRNA decay. *Nature,* 458**,** 1185-90.

MEDZHITOV, R., PRESTON-HURLBURT, P. & JANEWAY, C. A., JR. 1997. A human homologue of the Drosophila Toll protein signals activation of adaptive immunity. *Nature,* 388**,** 394-7.

MEISSL, K., MACHO-MASCHLER, S., MULLER, M. & STROBL, B. 2017. The good and the bad faces of STAT1 in solid tumours. *Cytokine,* 89**,** 12-20.

MILLS, C. D. 2015. Anatomy of a discovery: m1 and m2 macrophages. *Front Immunol,* 6**,** 212.

MILLS, C. D., KINCAID, K., ALT, J. M., HEILMAN, M. J. & HILL, A. M. 2000. M-1/M-2 macrophages and the Th1/Th2 paradigm. *J Immunol,* 164**,** 6166-73.

MINAGAWA, K., WAKAHASHI, K., KAWANO, H., NISHIKAWA, S., FUKUI, C., KAWANO, Y., *et al.* 2014. Posttranscriptional modulation of cytokine production in T cells for the regulation of excessive inflammation by TFL. *J Immunol,* 192**,** 1512-24.

MINO, T., MURAKAWA, Y., FUKAO, A., VANDENBON, A., WESSELS, H. H., ORI, D., *et al.* 2015. Regnase-1 and Roquin Regulate a Common Element in Inflammatory mRNAs by Spatiotemporally Distinct Mechanisms. *Cell,* 161**,** 1058-1073.

MITCHEM, J. B., BRENNAN, D. J., KNOLHOFF, B. L., BELT, B. A., ZHU, Y., SANFORD, D. E., *et al.* 2013. Targeting tumor-infiltrating macrophages decreases tumor-initiating cells, relieves immunosuppression, and improves chemotherapeutic responses. *Cancer Res,* 73**,** 1128-41.

MORETTI, S., ARMOUGOM, F., WALLACE, I. M., HIGGINS, D. G., JONGENEEL, C. V. & NOTREDAME, C. 2007. The M-Coffee web server: a meta-method for computing multiple sequence alignments by combining alternative alignment methods. *Nucleic Acids Res,* 35**,** W645-8.

MUNDER, M., MALLO, M., EICHMANN, K. & MODOLELL, M. 1998. Murine macrophages secrete interferon gamma upon combined stimulation with interleukin (IL)-12 and IL-18: A novel pathway of autocrine macrophage activation. *J Exp Med,* 187**,** 2103-8.

MUNIR, S., BER RAHMAN, S., REHMAN, S., SABA, N., AHMAD, W., NILSSON, S., *et al.* 2015. Association analysis of GWAS and candidate gene loci in a Pakistani population with psoriasis. *Mol Immunol,* 64**,** 190-4.

MURPHY, K. M. & WEAVER, C. 2018. *Janeway Immunologie, 9. Auflage*, Springer Spektrum, Berlin, Heidelberg.

NAPETSCHNIG, J. & WU, H. 2013. Molecular basis of NF-kappaB signaling. *Annu Rev Biophys,* 42**,** 443-68.

NETEA, M. G., BALKWILL, F., CHONCHOL, M., COMINELLI, F., DONATH, M. Y., GIAMARELLOS-BOURBOULIS, E. J., *et al.* 2017. A guiding map for inflammation. *Nat Immunol,* 18**,** 826-831.

NIEDEL, J. E., KUHN, L. J. & VANDENBARK, G. R. 1983. Phorbol diester receptor copurifies with protein kinase C. *Proc Natl Acad Sci U S A,* 80**,** 36-40.

NIU, J., SHI, Y., XUE, J., MIAO, R., HUANG, S., WANG, T., *et al.* 2013. USP10 inhibits genotoxic NF-kappaB activation by MCPIP1-facilitated deubiquitination of NEMO. *EMBO J,* 32**,** 3206-19.

OECKINGHAUS, A. & GHOSH, S. 2009. The NF-kappaB family of transcription factors and its regulation. *Cold Spring Harb Perspect Biol,* 1**,** a000034.

OKABE, Y. & MEDZHITOV, R. 2016. Tissue biology perspective on macrophages. *Nat Immunol,* 17**,** 9-17.

ORLINICK, J. R., VAISHNAW, A., ELKON, K. B. & CHAO, M. V. 1997. Requirement of cysteine-rich repeats of the Fas receptor for binding by the Fas ligand. *J Biol Chem,* 272**,** 28889-94.

OSHIMI, Y., ODA, S., HONDA, Y., NAGATA, S. & MIYAZAKI, S. 1996. Involvement of Fas ligand and Fas-mediated pathway in the cytotoxicity of human natural killer cells. *J Immunol,* 157**,** 2909-15.

PARK, J., KWON, M. & SHIN, E. C. 2016. Immune checkpoint inhibitors for cancer treatment. *Arch Pharm Res,* 39**,** 1577-1587.

PAUL, W. E. 2013. *Fundamental immunology*.

PAYNE, S. 2017. Immunity and Resistance to Viruses.

PHAM, T. H., BENNER, C., LICHTINGER, M., SCHWARZFISCHER, L., HU, Y., ANDREESEN, R.*, et al.* 2012. Dynamic epigenetic enhancer signatures reveal key transcription factors associated with monocytic differentiation states. *Blood,* 119**,** e161-71.

PHAN, G. Q., YANG, J. C., SHERRY, R. M., HWU, P., TOPALIAN, S. L., SCHWARTZENTRUBER, D. J.*, et al.* 2003. Cancer regression and autoimmunity induced by cytotoxic T lymphocyte-associated antigen 4 blockade in patients with metastatic melanoma. *Proc Natl Acad Sci U S A,* 100**,** 8372-7.

PICCIRILLO, C. A., BJUR, E., TOPISIROVIC, I., SONENBERG, N. & LARSSON, O. 2014. Translational control of immune responses: from transcripts to translatomes. *Nat Immunol,* 15**,** 503-11.

PICHLMAIR, A., SCHULZ, O., TAN, C. P., NASLUND, T. I., LILJESTROM, P., WEBER, F.*, et al.* 2006. RIG-I-mediated antiviral responses to single-stranded RNA bearing 5'-phosphates. *Science,* 314**,** 997-1001.

PIEPER, K., GRIMBACHER, B. & EIBEL, H. 2013. B-cell biology and development. *J Allergy Clin Immunol,* 131**,** 959-71.

RAJAMAHANTY, S., ALONZO, C., AYNEHCHI, S., CHOUDHURY, M. & KONNO, S. 2010. Growth inhibition of androgen-responsive prostate cancer cells with brefeldin A targeting cell cycle and androgen receptor. *J Biomed Sci,* 17**,** 5.

REDECKE, V., WU, R., ZHOU, J., FINKELSTEIN, D., CHATURVEDI, V., HIGH, A. A.*, et al.* 2013. Hematopoietic progenitor cell lines with myeloid and lymphoid potential. *Nat Methods,* 10**,** 795-803.

REINHARDT, R. L., LIANG, H. E., BAO, K., PRICE, A. E., MOHRS, M., KELLY, B. L.*, et al.* 2015. A novel model for IFN-gamma-mediated autoinflammatory syndromes. *J Immunol,* 194**,** 2358-68.

RICKERT, R. C., ROES, J. & RAJEWSKY, K. 1997. B lymphocyte-specific, Cre-mediated mutagenesis in mice. *Nucleic Acids Res,* 25**,** 1317-8.

ROBINSON, M. D., MCCARTHY, D. J. & SMYTH, G. K. 2010. edgeR: a Bioconductor package for differential expression analysis of digital gene expression data. *Bioinformatics,* 26**,** 139-40.

SCHETT, G. & NEURATH, M. F. 2018. Resolution of chronic inflammatory disease: universal and tissue-specific concepts. *Nat Commun,* 9**,** 3261.

SCHULZ, C., GOMEZ PERDIGUERO, E., CHORRO, L., SZABO-ROGERS, H., CAGNARD, N., KIERDORF, K.*, et al.* 2012. A lineage of myeloid cells independent of Myb and hematopoietic stem cells. *Science,* 336**,** 86-90.

SCHWANDNER, R., DZIARSKI, R., WESCHE, H., ROTHE, M. & KIRSCHNING, C. J. 1999. Peptidoglycan- and lipoteichoic acid-induced cell activation is mediated by toll-like receptor 2. *J Biol Chem,* 274**,** 17406-9.

SEIDEL, J. A., OTSUKA, A. & KABASHIMA, K. 2018. Anti-PD-1 and Anti-CTLA-4 Therapies in Cancer: Mechanisms of Action, Efficacy, and Limitations. *Front Oncol,* 8**,** 86.

SEN, R. & BALTIMORE, D. 1986a. Inducibility of kappa immunoglobulin enhancer-binding protein Nf-kappa B by a posttranslational mechanism. *Cell,* 47**,** 921-8.

SEN, R. & BALTIMORE, D. 1986b. Multiple nuclear factors interact with the immunoglobulin enhancer sequences. *Cell,* 46**,** 705-16.

SHA, W. C., LIOU, H. C., TUOMANEN, E. I. & BALTIMORE, D. 1995. Targeted disruption of the p50 subunit of NF-kappa B leads to multifocal defects in immune responses. *Cell,* 80**,** 321-30.

SHENG, J., RUEDL, C. & KARJALAINEN, K. 2015. Most Tissue-Resident Macrophages Except Microglia Are Derived from Fetal Hematopoietic Stem Cells. *Immunity,* 43**,** 382-93.

SIGNORINO, G., MOHAMMADI, N., PATANE, F., BUSCETTA, M., VENZA, M., VENZA, I.*, et al.* 2014. Role of Toll-like receptor 13 in innate immune recognition of group B streptococci. *Infect Immun,* 82**,** 5013-22.

SINGER, G. G., CARRERA, A. C., MARSHAK-ROTHSTEIN, A., MARTINEZ, C. & ABBAS, A. K. 1994. Apoptosis, Fas and systemic autoimmunity: the MRL-lpr/lpr model. *Curr Opin Immunol,* 6**,** 913-20.

SKALNIAK, L., MIZGALSKA, D., ZAREBSKI, A., WYRZYKOWSKA, P., KOJ, A. & JURA, J. 2009. Regulatory feedback loop between NF-kappaB and MCP-1-induced protein 1 RNase. *FEBS J,* 276**,** 5892-905.

SUK, F. M., CHANG, C. C., LIN, R. J., LIN, S. Y., CHEN, Y. T. & LIANG, Y. C. 2018. MCPIP3 as a Potential Metastasis Suppressor Gene in Human Colorectal Cancer. *Int J Mol Sci,* 19.

SUPEK, F., BOSNJAK, M., SKUNCA, N. & SMUC, T. 2011. REVIGO summarizes and visualizes long lists of gene ontology terms. *PLoS One,* 6**,** e21800.

SUTHERLAND, J. M., SIDDALL, N. A., HIME, G. R. & MCLAUGHLIN, E. A. 2015. RNA binding proteins in spermatogenesis: an in depth focus on the Musashi family. *Asian J Androl,* 17**,** 529-36.

SUZUKI, H. I., ARASE, M., MATSUYAMA, H., CHOI, Y. L., UENO, T., MANO, H.*, et al.* 2011. MCPIP1 ribonuclease antagonizes dicer and terminates microRNA biogenesis through precursor microRNA degradation. *Mol Cell,* 44**,** 424-36.

SWAMYDAS, M., LUO, Y., DORF, M. E. & LIONAKIS, M. S. 2015. Isolation of Mouse Neutrophils. *Curr Protoc Immunol,* 110**,** 3 20 1-3 20 15.

TAKEUCHI, O. 2018. Endonuclease Regnase-1/Monocyte chemotactic protein-1-induced protein-1 (MCPIP1) in controlling immune responses and beyond. *Wiley Interdiscip Rev RNA,* 9.

TAKEUCHI, O. & AKIRA, S. 2010. Pattern recognition receptors and inflammation. *Cell,* 140**,** 805-20.

TAYLOR, G. A., CARBALLO, E., LEE, D. M., LAI, W. S., THOMPSON, M. J., PATEL, D. D.*, et al.* 1996. A pathogenetic role for TNF alpha in the syndrome of cachexia, arthritis, and autoimmunity resulting from tristetraprolin (TTP) deficiency. *Immunity,* 4**,** 445-54.

THEOFILOPOULOS, A. N., KONO, D. H., BEUTLER, B. & BACCALA, R. 2011. Intracellular nucleic acid sensors and autoimmunity. *J Interferon Cytokine Res,* 31**,** 867-86.

TSOI, L. C., SPAIN, S. L., KNIGHT, J., ELLINGHAUS, E., STUART, P. E., CAPON, F.*, et al.* 2012. Identification of 15 new psoriasis susceptibility loci highlights the role of innate immunity. *Nat Genet,* 44**,** 1341-8.

UEHATA, T., IWASAKI, H., VANDENBON, A., MATSUSHITA, K., HERNANDEZ-CUELLAR, E., KUNIYOSHI, K.*, et al.* 2013. Malt1-induced cleavage of regnase-1 in CD4(+) helper T cells regulates immune activation. *Cell,* 153**,** 1036-49.

VARET, H., BRILLET-GUEGUEN, L., COPPEE, J. Y. & DILLIES, M. A. 2016. SARTools: A DESeq2- and EdgeR-Based R Pipeline for Comprehensive Differential Analysis of RNA-Seq Data. *PLoS One,* 11**,** e0157022.

VAROL, C., MILDNER, A. & JUNG, S. 2015. Macrophages: development and tissue specialization. *Annu Rev Immunol,* 33**,** 643-75.

VEREMEYKO, T., YUNG, A. W. Y., ANTHONY, D. C., STREKALOVA, T. & PONOMAREV, E. D. 2018. Early Growth Response Gene-2 Is Essential for M1 and M2 Macrophage Activation and Plasticity by Modulation of the Transcription Factor CEBPbeta. *Front Immunol,* 9**,** 2515.

VINUESA, C. G., COOK, M. C., ANGELUCCI, C., ATHANASOPOULOS, V., RUI, L., HILL, K. M., *et al.* 2005. A RING-type ubiquitin ligase family member required to repress follicular helper T cells and autoimmunity. *Nature,* 435**,** 452-8.

VOLLMER, J., WEERATNA, R., PAYETTE, P., JURK, M., SCHETTER, C., LAUCHT, M., *et al.* 2004. Characterization of three CpG oligodeoxynucleotide classes with distinct immunostimulatory activities. *Eur J Immunol,* 34**,** 251-62.

VON GAMM, M., SCHAUB, A., JONES, A. N., WOLF, C., BEHRENS, G., LICHTI, J., *et al.* 2019. Immune homeostasis and regulation of the interferon pathway require myeloid-derived Regnase-3. *J Exp Med*.

WANG, G. G., CALVO, K. R., PASILLAS, M. P., SYKES, D. B., HACKER, H. & KAMPS, M. P. 2006. Quantitative production of macrophages or neutrophils ex vivo using conditional Hoxb8. *Nat Methods,* 3**,** 287-93.

WATANABE-FUKUNAGA, R., BRANNAN, C. I., COPELAND, N. G., JENKINS, N. A. & NAGATA, S. 1992. Lymphoproliferation disorder in mice explained by defects in Fas antigen that mediates apoptosis. *Nature,* 356**,** 314-7.

WAWRO, M., WAWRO, K., KOCHAN, J., SOLECKA, A., SOWINSKA, W., LICHAWSKA-CIESLAR, A., *et al.* 2019. ZC3H12B, a new active member of the ZC3H12 family. *RNA*.

YANG, X., YANG, J., CHU, Y., WANG, J., GUAN, M., ZHU, X., *et al.* 2013. T follicular helper cells mediate expansion of regulatory B cells via IL-21 in Lupus-prone MRL/lpr mice. *PLoS One,* 8**,** e62855.

YOKOGAWA, M., TSUSHIMA, T., NODA, N. N., KUMETA, H., ENOKIZONO, Y., YAMASHITA, K., *et al.* 2016. Structural basis for the regulation of enzymatic activity of Regnase-1 by domain-domain interactions. *Sci Rep,* 6**,** 22324.

YONA, S., KIM, K. W., WOLF, Y., MILDNER, A., VAROL, D., BREKER, M., *et al.* 2013. Fate mapping reveals origins and dynamics of monocytes and tissue macrophages under homeostasis. *Immunity,* 38**,** 79-91.

YU, D., TAN, A. H., HU, X., ATHANASOPOULOS, V., SIMPSON, N., SILVA, D. G., *et al.* 2007. Roquin represses autoimmunity by limiting inducible T-cell co-stimulator messenger RNA. *Nature,* 450**,** 299-303.

ZHANG, H., WANG, W. C., CHEN, J. K., ZHOU, L., WANG, M., WANG, Z. D., *et al.* 2015. ZC3H12D attenuated inflammation responses by reducing mRNA stability of proinflammatory genes. *Mol Immunol,* 67**,** 206-12.

ZHOU, L., AZFER, A., NIU, J., GRAHAM, S., CHOUDHURY, M., ADAMSKI, F. M., *et al.* 2006. Monocyte chemoattractant protein-1 induces a novel transcription factor that causes cardiac myocyte apoptosis and ventricular dysfunction. *Circ Res,* 98**,** 1177-85.

# 9 List of abbreviations

| | |
|---|---|
| 3'UTR | 3' untranslated region |
| aa | amino acids |
| ANA | anti-nuclear antibodies |
| ARE | AU-rich element |
| BMDM | bone marrow derived macrophages |
| CARD | caspase activation and recruitment domains |
| CD | cluster of differentiation |
| cDCs | conventional dendritic cells |
| CLIP–seq | crosslinking and immunoprecipitation followed by sequencing |
| CLRs | C-type lectin receptors |
| CpG | unmethylated deoxycytidyl-deoxyguanosine |
| CTD | C-terminal domain |
| CTLA-4 | Cytotoxic T-lymphocyte-associated protein 4 |
| DC | dendritic cell |
| DNA | deoxyribonucleic acid |
| *E. coli* | *Escherichia coli* |
| EAE | experimental autoimmune encephalitis |
| EGR2 | Early growth response 2 |
| ELK1 | ETS domain-containing protein |
| EMSA | electrophoretic mobility shift assays |
| ER | estrogen receptor |
| FITC | Fluorescein isothiocyanate |
| FRT | flippase recognition target |
| GM-CSF | granulocyte-macrophage colony-stimulating factor |
| GO | gene ontology |
| GST | Glutathione S-transferase |
| GWAS | genome wide association study |
| Hoxb8 | Homeobox protein B8 |
| HRP | horseradish peroxidase |
| HSC | hematopoietic stem cell |
| HUVEC | human umbilical vein endothelial cell |
| IFN | Interferon |
| Ig | immunoglobulin |
| IKK | IκB kinase |
| IKKε | IκB kinase ε |
| IL | Interleukin |
| $iT_{reg}$ | induced regulatory T cells |
| IκB | Inhibitor of κB |
| JNK | c-Jun N-terminal kinase |
| kb | kilobase |
| kD | kilodalton |
| lacZ | β-galactosidase |
| LGP2 | Laboratory of genetics and physiology 2 |
| LPS | lipopolysaccharide |
| LTA | lipoteichoic acid |
| LysM | lysozyme 2 |
| MALT1 | Mucosa-associated lymphoid tissue lymphoma translocation protein 1 |
| MCPIP1 | Monocyte Chemotactic Protein-Induced Protein 1 |
| MDA5 | Melanoma differentiation-associated protein 5 |
| MEF | mouse embryonic fibroblasts |

MHC ..... Major histocompatibility complex
mRNA ..... messenger RNA
MyD88 ..... myeloid differentiation factor 88
MZ ..... marginal zone
NAD ..... NACHT-associated domain
NEMO ..... NF-κB essential modulator
NFATc ..... Nuclear factor of activated T cells cytoplasmic
NF-κB ..... nuclear factor kappa-light-chain-enhancer of activated B-cells
NK ..... natural killer
NLRs ..... NOD-like receptors
NOD ..... nucleotide-binding oligomerization domain
NTD ..... N-terminal domain
$nT_{reg}$ ..... natural tolerogenic regulatory T cell
OAS ..... 2'-5' oligo A synthase
ODN ..... oligodeoxynucleotides
PAMPs ..... pathogen-associated molecular patterns
PCA ..... principal component analysis
PCR ..... polymerase chain reaction
PD-1 ..... Programmed cell death protein 1
PD-L1 ..... Programmed death-ligand 1
PIN ..... PilT N-terminus
PLT ..... platelets
PMA ..... Phorbol-12-myristat-13-acetat
poly-I:C ..... polyinosinic-polycytidylic acid
PRRs ..... pattern recognition receptors
PVDF ..... polyvinylidene difluoride
PYD ..... pyrin domain
RBC ..... red blood cells
RBP ..... RNA binding protein
RIG-I ..... Retinoic acid-inducible gene I
RIP-seq ..... RNA immunoprecipitation and sequencing
RLRs ..... Retinoic acid-inducible gene (RIG)-I-like receptors
RNA ..... ribonucleic acid
RT ..... reverse transcription
SA ..... splice acceptor
SCF ..... stem cell factor
SDS-PAGE ..... sodium dodecyl sulfate–polyacrylamide gel electrophoresis
SNPs ..... single-nucleotide polymorphisms
STAT1 ..... signal transducer and activator of transcription 1
TANK ..... TRAF-family member-associated NF-κB activator
TBK1 ..... TANK binding kinase
TCR ..... T cell receptor
$T_{fh}$ ..... follicular B helper T
TFL ..... transformed follicular lymphoma
TLRs ..... Toll-like receptors
TNFα ..... Tumor necrosis factor α
TRAF ..... TNF receptor-associated factor
TRIF ..... TIR-domain-containing adapter-inducing interferon-β
TTP ..... Tristetraprolin
WBC ..... white blood cells

## 10 Erklärung

Ich erkläre an Eides statt, dass ich die bei der promotionsführenden Einrichtung Fakultät für Medizin der TUM zur Promotionsprüfung vorgelegte Arbeit mit dem Titel: '***Myeloid cells require the ribonuclease Regnase-3 for immune homeostasis and balanced interferon responses in vivo***' am Helmholtz Zentrum München, Institute for Diabetes and Obesity unter der Anleitung und Betreuung durch Dr. Elke Glasmacher ohne sonstige Hilfe erstellt und bei der Abfassung nur die gemäß § 6 Ab. 6 und 7 Satz 2 angebotenen Hilfsmittel benutzt habe.

☒ Ich habe keine Organisation eingeschaltet, die gegen Entgelt Betreuerinnen und Betreuer für die Anfertigung von Dissertationen sucht, oder die mir obliegenden Pflichten hinsichtlich der Prüfungsleistungen für mich ganz oder teilweise erledigt.

☒ Ich habe die Dissertation in dieser oder ähnlicher Form in keinem anderen Prüfungsverfahren als Prüfungsleistung vorgelegt.

☐ Die vollständige Dissertation wurde in _____ veröffentlicht. Die promotionsführende Einrichtung _____hat der Veröffentlichung zugestimmt.

☒ Ich habe den angestrebten Doktorgrad noch nicht erworben und bin nicht in einem früheren Promotionsverfahren für den angestrebten Doktorgrad endgültig gescheitert.

☐ Ich habe bereits am _____ bei der Fakultät für _____der Hochschule_____ unter Vorlage einer Dissertation mit dem Thema_____ _____die Zulassung zur Promotion beantragt mit dem Ergebnis:_____

Die öffentlich zugängliche Promotionsordnung der TUM ist mir bekannt, insbesondere habe ich die Bedeutung von § 28 (Nichtigkeit der Promotion) und § 29 (Entzug des Doktorgrades) zur Kenntnis genommen. Ich bin mir der Konsequenzen einer falschen Eidesstattlichen Erklärung bewusst.

Mit der Aufnahme meiner personenbezogenen Daten in die Alumni-Datei bei der TUM bin ich
☒ einverstanden, ☐ nicht einverstanden.

_____ _____

Ort, Datum Matthias von Gamm

# 11 Publications

Major parts of data and figures presented in this dissertation have been published in the following publication:

**Matthias von Gamm**, Annalisa Schaub, Alisha N. Jones, Christine Wolf, Gesine Behrens, Johannes Lichti, Katharina Essig, Anna Macht, Joachim Pircher, Andreas Ehrlich, Kathrin Davari, Dhruv Chauhan, Benjamin Busch, Wolfgang Wurst, Regina Feederle, Annette Feuchtinger, Matthias H. Tschöp, Caroline C. Friedel, Stefanie M. Hauck, Michael Sattler, Arie Geerlof, Veit Hornung,Vigo Heissmeyer, Christian Schulz, Mathias Heikenwalder, and Elke Glasmacher

***'Immune homeostasis and regulation of the interferon pathway require myeloid-derived Regnase-3'***
*The Journal of Experimental Medicine*, 2019

Parts of the data have been presented as scientific poster at the following conferences:

| | |
|---|---|
| 27.09.2017 – 29.09.2017 | ***'Development of Tissue and Pathogen-specific Cellular Innate Immunity'*** |
| | In Freiburg, Germany<br>***Award for the best poster*** |
| 05.03.2017 – 10.03.2017 | ***'Immunology Spring School'*** |
| | In Ettal, Germany |
| 03.11.2016 – 04.11.2016 | ***'Interact'*** |
| | In Munich, Germany |
| 28.09.2015 – 30.09.2015 | ***'Control and Plasticity of Cell-Fate Decisions in the Immune System'*** |
| | In Grainau, Germany |

# 12 Curriculum vitae

AUSBILDUNG

| | |
|---|---|
| 05/2014 – aktuell | **Doktoranden Programm**: Helmholtz Zentrum München, Institute for Diabetes and Obesity, Arbeitsgruppe AG Glasmacher<br>**Thema**: Molekulare Immunologie |
| 04/2014 – 05/2014 | **Praktikum**: Helmholtz Zentrum München, Institute for Diabetes and Obesity, Arbeitsgruppe AG Glasmacher<br>**Thema**: Molekulare Immunologie |
| 10/2011 – 09/2013 | **Master Programm:** Pharmaceutical Sciences<br>**Universität**: Ludwig-Maximilians-Universität (LMU), München<br>**Abschlussarbeit:** "Pretubulysin and its Analogues: Tumor Cell Migration and Underlying Signal Transduction" (Pharmazeutische Biology, Prof. A. Vollmar)<br>**Abschluss**: Master of Science |
| 10/2008 – 10/2011 | **Bachelor Programm:** Pharmaceutical Sciences<br>**Universität**: Ludwig-Maximilians-Universität (LMU), München<br>**Abschlussarbeit:** „Protein-Protein Interaction Analysis of the CNGB1a Subunit of the Retinal CNG Channel" (Pharmakologie, Prof. M. Biel)<br>**Abschluss**: Bachelor of Science |
| 09/1998 – 06/2007 | Gymnasium Geretsried |
| 09/1994 – 07/1998 | Karl Lederer Grundschule Geretsried |

STUDIUM IM AUSLAND

| | |
|---|---|
| 08/2013 – 12/2013 | **Universität:** Uppsala Universitet (Uppsala, Schweden)<br>**Wissenschaftliche Arbeit:** "Stereoselective oxygenation of fatty acids by Lipoxygenases" (Biochemical Pharmacology, Prof. E. Oliw) |

ZIVILDIENST

| | |
|---|---|
| 06/20007 – 03/2008 | Oberlandwerkstätten Geretsried:<br>Einrichtung für Menschen mit Behinderung |